Development of environmental sensors based on MIP/graphene electrode allowing the detection of pesticides in waters

Imer Sadriu

ÉCOLE DOCTORALE **Energie, Matériaux, Sciences de la Terre et de l'Univers (EMSTU)**

ICMN **Interfaces, Confinement, Matériaux et Nanostructures**

THÈSE EN COTUTELLE INTERNATIONALE présentée par :

Imer SADRIU

soutenance le : 12 Juillet 2021

pour obtenir le grade de :
Docteur de l'Université d'Orléans
et Docteur de l'Université de Prishtina

Discipline/Spécialité : CHIMIE DES MATÉRIAUX

Development of environmental sensors based on MIP/graphene electrode allowing the detection of pesticides in waters

THÈSE dirigée par :

Pr Christine VAUTRIN-UL	Professeure, Université d'Orléans
Pr Fetah PODVORICA	Professeur, Université de Prishtina

THÈSE encadrant :

Dr Jimmy NICOLLE	Maître de Conférences, Université d'Orléans

RAPPORTEURS :

Pr Christine CACHET-VIVIER	Professeure, Université Paris-Est Créteil
Dr Catherine COMBELLAS	Directrice de Recherche au CNRS, ITODYS, Paris

---

JURY :

Pr Christine VAUTRIN-UL	Professeure, Université d'Orléans
Pr Fetah PODVORICA	Professeur, Université de Prishtina
Dr Jimmy NICOLLE	Maître de Conférences, Université d'Orléans
Pr Christine CACHET-VIVIER	Professeure, Université Paris-Est Créteil
Dr Catherine COMBELLAS	Directrice de Recherche au CNRS, ITODYS, Paris
Pr Ramë VATAJ (Président de jury)	Professeur, Université de Prishtina


université
de TOURS

UNIVERSITE D'ORLEANS

INSA
CENTRE VAL DE LOIRE

UNIVERSITETI I PRISHTINES
UNIVERSITAS STUDIORUM PRISHTINENSIS
1970 MCMLXX

DOCTORAL SCHOOL **Energy, Materials, Earth and Universe Sciences (EMEUS)**

ICMN **Interfaces, Confinement, Materials and Nanostructures**

THESIS IN COLLABORATION INTERNATIONAL presented by :

Imer SADRIU

public defense on : 12 July 2021

for the title of :

Doctor of the Orléans University
and Doctor of the University of Prishtina

Discipline/Speciality : CHEMISTRY OF MATERIALS

Development of environmental sensors based on MIP/graphene electrode allowing the detection of pesticides in waters

THESIS directors :

Pr Christine VAUTRIN-UL	Professor, Orléans University
Pr Fetah PODVORICA	Professor, University of Prishtina

THESIS supervisor :

Dr Jimmy NICOLLE	Professor asoc, Orléans University

RAPPORTEURS :

Pr Christine CACHET-VIVIER	Professor, Université Paris-Est Créteil
Dr Catherine COMBELLAS	Research director in CNRS, ITODYS, Paris

---

JURY :

Pr Christine VAUTRIN-UL	Professor, Orléans University
Pr Fetah PODVORICA	Professor, University of Prishtina
Dr Jimmy NICOLLE	Professor asoc, Orléans University
Pr Christine CACHET-VIVIER	Professor, Paris-Est Créteil University
Dr Catherine COMBELLAS	Research director in CNRS, ITODYS, Paris
Pr Ramë VATAJ (President of jury)	Professor, University of Prishtina


université
de TOURS

UNIVERSITE D'ORLEANS

INSA
CENTRE VAL DE LOIRE

UNIVERSITETI I PRISHTINES
UNIVERSITAS STUDIORUM PRISHTINENSIS
1970 MCMLXX

To my love Kaltrina,

for her patience, her support and her faith, because she always was with me.

Acknowledgements

First of all, with much respect and honor, I express my sincere gratitude to the director of my PhD thesis **Prof Christine VAUTRIN-UL**, from the Orléans University, for accepting me to her research group at ICMN-CNRS-OU Laboratory to collaborate and do my research work for my PhD. Her advices and suggestions, have made this work easier and more understandable during the entire time I have stayed at ICMN laboratory. Special thanks also go to the co-director of my PhD thesis **Prof Fetah PODVORICA** from the University of Prishtina, Kosovo, for the discussions, experiences he shared with me and his profitable advices which helped me to solve lots of problems I had during the experiments. I would like also to thank the supervisor of my PhD **Dr Jimmy NICOLLE**, who has always been supervising me during the experiments and has done an excellent job of introducing me to and learning many new techniques during my stay at ICMN. Without their guidance, this research would not have been possible.

I would like also to gratefully thank members of jury for the thesis defense **Prof Christine CACHET-VIVIER, Prof Catherine COMBELLAS, Prof Ramë VATAJ, Prof Christine VAUTRIN-UL, Prof Fetah PODVORICA, and Dr Jimmy NICOLLE**, for taking time out of their busy scheduled work, to read, evaluate and analyze my research work. Their suggestions and critical opinions will help me to improve quality of this work.

I would also like to express my sincere thanks to the other members of our group, such as **Prof Valerie BERTAGNA**, **Dr Emilie MATHIEU-SCHEERS**, **Celine GRILLOT** - engineering assistant, and **Oumayma LOURHZAL** - PhD student, who helped and advised me on many tasks during our work in the laboratory.

I also thank the permanent members of the ICMN laboratory, in particular the director **Prof Sylvie BONNAMY, Prof Caroline ANDREAZZA**, and **Prof Christophe SINTUREL** for the discussions, help and their support. Another special thanks go to not permanent members of the ICMN laboratory, my lab colleagues, postdoc researchers, PhD students, and other students in internship, who have made memorable my stay in the lab, with the jokes, activities, and lunches we have had together.

I express special thanks for the France Embassy in Kosovo and French Government for funding my PhD studies and Campus France Agency for managing me during my stay in France.

And last but not the least, I would like to thank entire family and friends. Especially my mother Qamile Sadriu, who has been supporting me with everything she had and helped me a lot to be where I am today. I would also like to thank so much my fiancée Kaltrina Rexha, for her love and her support, especially for her patience during the redaction time of this thesis.

Thank you all.

Imer SADRIU

Orléans, France

1. Table of Contents

List of Abbreviations 1
List of Figures 4
List of Tables 10
Summary 12
Résumé 14
Përmbledhje (Summary in Albanian) 16
General introduction 19
Hyrje e përgjithshme (General introduction in Albanian) 22
1. CHAPTER I: LITERATURE REVIEW 28
1.1. Pesticides and their effect on the environment 29
1.1.1. Water quality 29
1.1.2. The use of pesticides in agriculture 30
1.1.3. Isoproturon among other herbicides 32
1.1.3.1. Methods used for the determination of herbicides 33
1.2. Definition of the chemical and electrochemical sensors 34
1.3. Conducting polymers (CPs) 39
1.3.1. Generality about CPs 39
1.3.1.1. Introduction to conducting polymers 39
1.3.1.2. Preparation of CPs 40
1.3.1.3. Properties and applications of the conducting polymers 42
1.3.2. Conductivity of CPs 44
1.3.2.1. Conduction modes of CPs 44
1.3.2.2. Doping of CPs 45
1.3.3. Polypyrrole (PPy) as a conducting polymer (CPPy) 46
1.3.3.1. Presentation of PPy 46
1.3.3.2. Electrochemical polymerization of polypyrrole versus chemical polymerization 47
1.3.3.3. Mechanism of pyrrole electropolymerization 48
1.3.3.4. Electrical conductivity of PPy 51

1.3.3.5. Properties and applications of PPy 53
1.3.3.6. PPy for sensor applications 54
1.4. Molecularly imprinted polymers (MIPs) 57
1.4.1. Introduction to Molecularly Imprinted Polymers (MIPs) 57
1.4.2. General concepts of MIPs 58
1.4.3. The preparation methods of MIPs 60
1.5. Electrochemical MIP-sensors for environmental analysis 63
1.5.1. The main electrochemical MIP-based sensors 63
1.5.2. Volt-amperometric MIP-based sensors with PPy 65
2. CHAPTER II: EXPERIMENTAL SECTION 69
2.1. Chemicals 69
2.2. Electrodes and electrochemical apparatus 71
2.2.1. Reference electrode 71
2.2.2. Counter electrode 72
2.2.3. Working electrode 72
2.2.4. Electrochemical apparatus 73
2.3. Electrochemical techniques for analysis 74
2.3.1. Cyclic voltammetry (CV) 74
2.3.2. Chronoamperometry (CA) 76
2.3.3. Square wave voltammetry (SWV) 76
2.3.4. Electrochemical impedance spectroscopy (EIS) 77
2.3.5. Electrochemical Quartz Crystal Microbalance (EQCM) 78
2.4. Techniques used for the characterization of chemical, structural and morphology of the electrode materials 80
2.4.1. Infrared spectroscopy (IR) 80
2.4.2. Raman spectroscopy 81
2.4.3. Atomic force microscopy (AFM) 82
2.4.4. X-ray photoelectron spectroscopy (XPS) 83
2.4.5. Photolithography 84
3. CHAPTER III: Development of a molecularly imprinted polymer modified glassy carbon electrode for the electrochemical analysis of isoproturon in water 88

3.1. Introduction 88
3.2. The working procedure of the MIP-GC electrodes 89
3.3. Experimental conditions 91
3.3.1. Electrochemical behavior of isoproturon 91
3.3.2. Synthesis of NIP-GC and MIP-GC electrodes 92
3.3.3. Detection of isoproturon by MIP-GC electrodes 92
3.4. Elaboration of the MIP-GC electrode 93
3.4.1. Electropolymerization of pyrrole 93
3.4.2. Extraction of the template molecule 94
3.5. Optimization of the MIP-GC elaboration procedure 95
3.5.1. Influence of potential range in the CV extraction process of isoproturon 95
3.5.2. Preparation of isoproturon MIP-GC electrodes by cyclic voltammetry (CV): influence of the scan number 96
3.5.3. Preparation of isoproturon MIP-GC electrodes by chronoamperometry (CA) 97
3.5.3.1. Effect of solvent – the role of ethanol/water ratio 97
3.5.3.2. Influence of electropolymerization time 99
3.5.4. The influence of the electrodeposition substrate material: EQCM study of NIPs obtained by CA and CV onto gold and platinum electrodes 101
3.6. Electrochemical detection of isoproturon by the GC-MIP electrode: Optimization of incubation (rebinding) time 102
3.7. Electroanalytical performances of the GC-MIP electrodes 103
3.7.1. Calibration curve and determination of LOD/LOQ 103
3.7.2. Interference study 105
3.7.3. Application of the electrochemical sensors in real water samples 106
3.8. Conclusion and perspectives 108
4. CHAPTER IV: Optimization parameters of Molecularly Imprinted Polymer films for Isoproturon detection: impact of anodic potential on the overoxidation of polypyrrole 111
4.1. Introduction 111
4.2. Experimental conditions 112
4.2.1. Preparation of MIP and non-imprinted polymer (NIP) electrodes 112
4.2.2. Characterization of the MIP polypyrrole film 113
4.3. The influence of the electrodeposition method 114

4.3.1. Electrochemical synthesis of MIP and NIP polypyrrole films by CA 114
4.3.2. Electrochemical synthesis of MIP and NIP polypyrrole films by CV 115
4.3.2.1. Influence of the potential range 115
4.3.2.2. The influence of number of cycles 117
4.3.3. Influence of the overoxidation potential applied on the properties of MIP-PPy film 120
4.3.3.1. The effect of the overoxidation potential on the conductivity of the film: characterization by EIS 120
4.3.3.2. Effect of the overoxidation on the composition of the film: FT-IR and XPS characterization 123
4.4. Conclusion and perspectives 130
5. CHAPTER V: Electropolymerization of molecularly imprinted polymer (MIP) film onto pure graphene electrodes for isoproturon detection 133
5.1. Introduction 133
5.2. The fabrication process of graphene/polystyrene electrodes through electrochemical exfoliation of graphite rod 137
5.2.1. Electrochemical exfoliation of graphite rod into graphene flakes in aqueous liquid media 138
5.2.2. Electrochemical exfoliation of graphite rod into graphene flakes in organic media 142
5.2.3. The transfer process of graphene powder onto polystyrene plates 143
5.3. Characterization of different forms of graphene/polystyrene electrodes by using various spectroscopy techniques 146
5.3.1. XPS characterization 146
5.3.2. Raman characterization 151
5.3.3. IR characterization 154
5.3.4. Electrical conductivity measurements 156
5.4. Electrochemical characterization of graphene/polystyrene electrodes 157
5.4.1. Electrochemical window 157
5.4.2. Electrochemical probes characterization 158
5.4.2.1. Delamination study of the graphene electrodes 158
5.4.2.2. Evolution of the electrochemical active area 160
5.4.2.3. Calculation of the kinetic constant (k_0) 167

5.5. Correlation between crystallography structure of different graphene electrodes and their electrochemical behavior 170
5.6. Electrochemical preparation of MIP films onto graphene/polystyrene electrodes .. 172
5.6.1. Electrochemical behavior of isoproturon on graphene/polystyrene electrodes ... 172
5.6.2. Electropolymerization of isoproturon imprinted polypyrrole films onto graphene/polystyrene electrodes 173
5.6.3. Cyclic voltammetry extraction of isoproturon 175
5.6.4. Electrochemical detection of isoproturon by using graphene-MIP/polystyrene electrodes 176
5.6.4.1. Incubation (rebinding) step 176
5.6.4.2. Calibration curve and determination of LOD/LOQ 177
5.7. Conclusion and future perspectives 179
General conclusions and future perspectives 181
Appendices 186
Limit of detection (LOD) and limit of quantification (LOQ) 186
Response time and long-term stability 187
Application for real samples 187
References 194

List of Abbreviations

Chapter I

WHO	World health organization
WFD	Water framework directive
EU	European Union
ISO	Isoproturon
HPLC	High performance liquid chromatography
GC	Glassy carbon
UV	Ultra-violet
CNT	Carbon nanotubes
MWCNT	Multi walled carbon nanotubes
GCE	Glassy carbon electrode
FET	Field effect transistor
ISE	Ion selective electrode
CWE	Coated wire electrode
IS-FET	Ion selective-field effect transistor
CE	Counter electrode
RE	Reference electrode
WE	Working electrode
UME	Ultra micro-electrode
ME	Micro-electrode
CME	Chemical modified electrode
CP	Conducting polymer
PA	Polyacetylene
PP	Polyphenylene
PPy	Polypyrrole
PT	Polythiophene
PANI	Polyaniline
PPV	Poly (phenylene-vinylene)
CR	Cation radical
AC	Activated carbon
VB	Valence band
CB	Conduction band
SCE	Saturated calomel electrode
MIP	Molecularly imprinted polymer
NIP	Non-imprinted polymer
SPE	Solid phase extraction

SPME	Solid phase micro extraction
SBSE	Stir bar sorption extraction
CEC	Capillary electrochromatography
CLC	Capillary liquid chromatography
TLC	Thin layer chromatography
MMA	Methyl methacrylate
MAA	Methacrylic acid
EGDMA	Ethylene glycol dimethyl acrylate
AIBN	Azobisisobutyronitrile
DMF	Dimethyl formamide
QCM	Quartz crystal microbalance
MICP	Molecularly imprinted conducting polymer
MIP-PPy	Molecularly imprinted polypyrrole

Chapter II

NHE	Normal hydrogen electrode
EQCM	Electrochemical quartz crystal microbalance
CV	Cyclic voltammetry
CA	Chronoamperometry
SWV	Square wave voltammetry
DME	Dropping mercury electrode
EIS	Electrochemical impedance spectroscopy
IR	Infrared spectroscopy
AFM	Atomic force microscope
XPS	X-ray photoelectron spectroscopy
PC	Personal computer

Chapter III & Chapter I

MIP-PPy	Molecularly imprinted polypyrrole
NIP-PPy	Non-imprinted polypyrrole
MOF	Metal organic framework
MIP-ECL	Molecularly imprinted polyaminophenol
MIP-GC	Molecularly imprinted polymer-glassy carbon
NIP-GC	Non-imprinted polymer-glassy carbon
GC/MIPPy/ISO	Glassy carbon/molecularly imprinted polypyrrole/isoproturon
SD	Standard deviation

RSD	Relative standard deviation
LOD	Limit of detection
LOQ	Limit of quantification
EMI	Electromagnetic interference

Chapter V

ISO-MIPPy	Isoproturon-molecularly imprinted polypyrrole
GIC	Graphite intercalation complex
TBA	Tetrabutylammonium
CVD	Chemical vapor deposition
GOx	Graphene oxide
rGOx	Reduced graphene oxide
NMP	1-methyl-2-pyrrolidinone
LSV	Linear sweep voltammetry

List of Figures

Figure 1. Global use of pesticides in 2017 [5]. 30
Figure 2. The pesticides cycle in the environment [7]. 31
Figure 3. Isoproturon structure. 32
Figure 4. Classification of sensors in different types. 35
Figure 5. Schematically representation of a typical electrochemical sensor. 36
Figure 6. Schematic representation of a typical amperometric/voltammetric sensing system [58]. 37
Figure 7. Different π-conjugated structures of CPs [65]. 39
Figure 8. Electropolymerization of a conjugated monomer [69]. 41
Figure 9. Band structures for the three different categories of materials. 44
Figure 10. Conductivity (in S/cm) of CPs in their neutral states or doped compared to those of some insulating materials, semiconductors or conductors [69]. 45
Figure 11. A) Chemical polymerization of polypyrrole, B) Electrochemical polymerization of polypyrrole [74]. 48
Figure 12. Electropolymerization of pyrrole by Diaz, a radical coupling mechanism [107]. 50
Figure 13. Polypyrrole structure with π conjugated double bonds. 51
Figure 14. Electronic energy diagrams and structures for (a) neutral PPy, (b) polaron, (c) bipolaron, and (d) fully doped PPy [66]. 52
Figure 15. The overoxidation reaction of polypyrrole [118]. 52
Figure 16. General forms of PPy and their applications [74]. 53
Figure 17. (A) Annual number of scientific publications related to PPy based on Elsevier data analysis as of 7th September 2020, and (B–G) SEM micrographs of PPy with different morphologies, that is, nanoparticle, nanotube, nanofiber, thin film, thick film, and sponge-like structure, respectively [74]. 54
Figure 18. Comprehensive details of CPs-based sensors for different signal transduction modes [64]. 55
Figure 19. Schematic representation of the molecular imprinting process, where functional monomers form a complex around the template molecule to form the MIPs with the creation of binding sites. 57
Figure 20. Diagram of the classification of MIPs based on their role in pretreatment techniques, chromatography and sensor. Abbreviations: SPE, solid phase extraction; DSPE, dispersive SPE; MSPD, matrix solid phase dispersion; SPME, solid phase microextraction; SBSE, stir bar sorption extraction; QCM, quartz crystal microbalance [158]. 58
Figure 21. Evolution of publications regarding MIP-based electrochemical sensors and emerging contaminant detection in the last 10 years [159]. 59
Figure 22. Synthesis production of MIPs. The three steps followed dissolving or mixing of all the components, polymerization and extraction [160]. 60
Figure 23. Schematic representation of electrochemical polymerization process of MIP film on the surface of electrode. 61
Figure 24. Schematic representation of a typical three electrode system electrochemical setup. 71
Figure 25. The glassy carbon electrode. 73
Figure 26. Electrochemical apparatus, a) PGSTAT 128N Autolab Metrohm, b) Maxtek RQCM micro-balance. 74
Figure 27. Typical cyclic voltammogram of a reversible redox reaction. 75

Figure 28. Square wave voltammetry, A) One potential cycle, B) Single potential cycle in SWV, C) square wave voltammogram obtained during determination of isoproturon (c = 10^{-6} M). 77
Figure 29. Electrochemical quartz crystal microbalance (EQCM) setup, A) Schematic of a piezoelectric quartz crystal, B) Schematic electrochemical quartz crystal microbalance (EQCM) apparatus [198]. 79
Figure 30. IR spectrometer, a) schematically instrumentation of infrared spectroscopy, b) picture of IR spectrometer used in this work. 80
Figure 31. Raman spectroscopy, a) the principle of Raman, b) Raman spectrum. 81
Figure 32. Raman spectrometer. 81
Figure 33. Atomic force microscopy (AFM), a) the principle of AFM, b) the AFM tip. 82
Figure 34. BRUKER-Dimension ICON high performance AFM (atomic force microscope). 83
Figure 35. X-ray photoelectron spectroscopy (XPS), a) the principle of XPS, b) the XPS spectrometer used in this work. 83
Figure 36. Photolithography apparatus used in this work A), and the graphene/polystyrene substrate prepared with different sizes of controlled working area B). 85
Figure 37. The principle of photolithography process. 85
Figure 38. Schematic representation of the procedure used for the preparation of imprinted polypyrrole films on GC substrate MIP GC and the electroanalysis of isoproturon. 90
Figure 39. Voltammograms obtained on bare GC electrode for ISO (1, 2 or 3 mM) in H_2SO_4 (0,1M) (70/30 ethanol/water v/v), (····) Blank voltammograms. Scan rate 100 mV/s. 91
Figure 40. Cyclic voltammograms taken during electropolymerization of pyrrole (0.01 M) in absence (NIP) and in presence of ISO (1 mM) (MIP) onto GC electrode, electrolyte: 0.1M $LiClO_4$ in ethanol/water (20:80 v/v). Scan rate 10 mV/s 93
Figure 41. Cyclic voltammograms obtained during ISO extraction on the MIP-GC electrode: Electrolyte 0.1 M H_2SO_4 in ethanol/water (70:30 v/v). Scan rate 100 mV/s. 94
Figure 42. SWV determination of isoproturon (5 x 10^{-7} M) at GC-MIP polypyrrole electrodes after template extraction by CV at different potential ranges. 96
Figure 43. Influence of the scan number during electropolymerization of the MIP on GC electrode (A) on isoproturon response on MIP-GC electrode (B) on MIP film thickness estimated using Faraday's law from the voltammogram (C) on CV ferrocene response (2.5 mM) in NBu_4BF_4 (0.1 M) acetonitrile solution on bare and MIP-GC electrodes. Scan rate 100 mV/s 97
Figure 44. Electropolymerization of MIP-GC electrode for different ratios of ethanol/water with $LiClO_4$ 0.1M (A) film thickness calculated from chronoamperogram and (B) ISO peak intensity electropolymerization: CA 1.1 V during 600 s; pyrrole 0.01M in presence of ISO 1 mM. 98
Figure 45. EQCM study of the influence of amount of ethanol in its aqueous solution containing 0.01 M of pyrrole + 0.1 M of $LiClO_4$ on the mass growth of NIP films on gold quartz electrode. (A) Mass curves as a function of the electropolymerization time; (B) Variation of the NIP film thickness estimated by EQCM with the amount of ethanol, (C) Captured picture of the NIP film on gold quartz electrode. 99
Figure 46. Effect of electropolymerization time on the electrochemical response of 5×10^{-7}M of ISO at the MIP-GC electrode in ethanol/water (70:30 v/v) of H_2SO_4 0.1 M, (A) the thickness of the MIP film estimated from the chronoamperogram (B) isoproturon electrochemical response, MIP film was formed by chronoamperometry setting the potential at 1.1 V, incubation time 15 min (C) comparative study of the MIP film thickness estimated by Faraday's law calculations and by EQCM experiments in order to follow the chronoamperometry electropolymerization process (potential applied 1.1 V, time duration

885 s) of ISO (1 mM) and pyrrole (0.01 M) on gold quartz used as a working electrode, electrolyte: 0.1M $LiClO_4$ in ethanol/water (80:20 v/v). 100
Figure 47. EQCM study of the effect of electrodeposition material substrate by CA (+1.1V, electropolymerization time 600 sec) and by CV (0 to +0.9V, scan rate 10 mV/sec) onto gold quartz crystal electrode (A, B), and onto platinum quartz crystal electrode (C, D), electropolyerization: pyrrole 0.01 M in a solution of $LiClO_4$ (0,1M) (20/80 ethanol/water v/v). 101
Figure 48. AFM images of NIP films on gold quartz crystal electrode a) bare gold quartz electrode, b) NIP PPy CV (0 to +0.9V), and on platinum quartz crystal electrode c) bare platinum quartz electrode, d) NIP PPy CV (0 to +0.9V). 102
Figure 49. Isoproturon (5×10^{-7} M) response on the MIP-GC electrode for different incubation times. 103
Figure 50. The calibration curves of isoproturon detection obtained at MIP-GC electrode in Milli-Q water. Current-concentration calibration curve (A) includes linear 104
Figure 51. Effect of the interferences on the determination of ISO (5×10^{-7} M) using the MIP-GC electrode: (A) carbamazepine (B) carbendazim and (C) diuron. 105
Figure 52. Commune Saint-Rémy-Du-Val (72317) - Sarthe (72) province of Pays-de-la-Loire – Bretagne Region - France, an altitude of 117 m and a depth of investigation 23 m (coordinates X, Y: 446125, 2372347 (Lambert II Etendu) / 497082, 6807017 (Lambert 93). 106
Figure 53. Schematically representation of the procedure used for the preparation of ground natural water samples for the isoproturon (ISO) analysis by using GC-MIPPy electrodes. 107
Figure 54. The calibration curves for isoproturon determination obtained at MIP-GC electrode in real natural water samples (A) includes calibration linear equation (B) square wave voltammograms obtained during electrochemical detection of isoproturon. 107
Figure 55. Formation of MIP during the electrolysis at different applied potential values when GC electrode is immersed in ethanol/water (v/v:20/80) solution containing 0.01 M of pyrrole + 1 mM of ISO + 0.1 M of $LiClO_4$. (A) The comparison between the films thickness estimated theoretically by Faraday's law and the real thickness estimated by AFM scratching mode and (B) ISO current peak intensity for the MIP-PPy made at different electrolysis potential. 114
Figure 56. Cyclic voltammograms (0 to +0.7V; + 0.9V; +1.0V; + 1.1V; +1.3V; + 1.5V) taken during electropolymerization of pyrrole (0.01 M) in presence of ISO 1 mM onto GC electrode. The electrolyte was 0.1 M $LiClO_4$ in ethanol/water (20:80 v/v). Scan rate 10 mV/sec. 116
Figure 57. Electropolymerization of MIP-GC electrode made by CV at different potential ranges (0 to +7; +0.9; +1.0; + 1.1; +1.3 and + 1.5V) in ethanol/water (v/v:20/80) solution containing 0.01 M of pyrrole + 1 mM of ISO + 0.1 M of $LiClO_4$. (A) Film thickness calculated from cyclic voltammograms and (B) ISO current peak intensity for the MIP-PPy made by CV at different anodic potential range. 117
Figure 58. The influence of CV scans on the performance of MIP-GC electrode at potential range from 0 up to +0.9V/Ag/AgCl in ethanol/water (v/v:20/80) solution containing 0.01 M of pyrrole + 1 mM of ISO + 0.1 M of $LiClO_4$. (A) film thickness calculated from cyclic voltammogram and obtained by AFM (B) ISO current peak intensity for the MIP-PPy made with different CV scans. 117
Figure 59. AFM images of MIP-GC plates obtained by CV at potential range 0 to +0.9V/Ag/AgCl with different number of cycles in ethanol/water (v/v:20/80) solution containing 0.01 M of pyrrole + 1 mM of ISO + 0.1 M of $LiClO_4$, scan rate mV/s: (a) 1, (b) 3, (c) 5, (d) 10 cycles before isoproturon extraction; (e) 1, (f) 3, (g) 5, (h) 10 cycles after isoproturon extraction; and (j) AFM image of a bare GC plate. 118
Figure 60. EIS results obtained during the characterization of the NIP and MIP films, electro-synthesized on GC electrodes by CA (+1.1 V, t = 600s), in aqueous solution of 1mM $K_3[Fe(CN)_6]/K_4[Fe(CN)_6]$ + 0.1M

KCl. A) Nyquist plots obtained at bare GC, NIP and MIP electrodes before and after ISO extraction, B) equivalent circuits used to fit impedance data. 120
Figure 61. EIS characterization of NIP and MIP films fabricated on GC electrodes at different potential values: A) NIP by CA (duration time 600s), B) NIP by CV (5 cycles at scan rate 10 mV/s), C) MIP by CA (duration time 600s), and D) MIP by CV (5 cycles at scan rate 10 mV/s). 121
Figure 62. EIS characterization of the GC-MIP electrodes prepared by CA at +1.1 V (duration time 600s) at different stages when tested for the SWV isoproturon detection. 122
Figure 63. A) FTIR spectra of GC-NIPs made by CV at different anodic potentials; B) exposed to the anodic potential when electrochemical procedure is used for the removal of isoproturon. 125
Figure 64. A) FTIR spectra of GC-MIPs made by CV at different anodic potentials; B) exposed to the anodic potential when electrochemical procedure is used for the removal of isoproturon. 125
Figure 65. High resolution spectra of C1s obtained with GC-NIP films made by CV at different anodic potentials before and after extraction. 126
Figure 66. High resolution spectra of O1s obtained with GC-NIP films made by CV at different anodic potentials before and after extraction. 127
Figure 67. High resolution spectra of C1s obtained with GC-MIP films made by CV at different anodic potentials before and after extraction. 128
Figure 68. High resolution spectra of O1s obtained with GC-MIP films made by CV at different anodic potentials before and after extraction. 129
Figure 69. A) The honeycomb structure of graphene, B) Molecular arrangement of carbon in graphene and various bonding and forces involved during its self-assembly into graphite [258]. 133
Figure 70. A) Single layer graphene was first observed by Geim and Novoselov at Manchester University, B) “Scotch tape” method to isolate graphene layers from graphite by continuous peeling with an adhesive tape [233]. 134
Figure 71. Different techniques used for graphene synthesis [276]. 136
Figure 72. Electrochemical cell used for the exfoliation of graphite rod into graphene oxide/graphene flakes, A) two-electrode cell used for graphite rod exfoliation in water media, and B) three-electrode cell used for graphite rod exfoliation in organic media. 137
Figure 73. Graphite rod electrode before and after electrochemical exfoliation process. 138
Figure 74. A) Schematic representation of the mechanism of exfoliation [273], B) exfoliated graphitic sheets into graphene oxide, C) graphene oxide flakes after vacuum filtration step, D) graphene oxide in powder. 139
Figure 75. Heat treatment of graphene oxide with hydrazine hydrate. 140
Figure 76. A) Oxidation of graphite to graphene oxide and reduction to reduced graphene oxide, B) A proposed reaction [293]. 141
Figure 77. Electrochemical exfoliation at different times of exfoliation. 142
Figure 78. A) Graphene powder in pure ethanol before sonication, B) dispersed graphene powder in ethanol after 1h of sonication, C) vacuum filtration, and D) graphene powder embedded on the filter. 143
Figure 79. Schematic representation of the graphene transfer process on polystyrene used then for the fabrication of graphene electrodes. 144
Figure 80. Fabrication process of graphene electrodes with controlled working area, A) with our own method in the laboratory, and B) with photolithography. 145

Figure 81. C1s XPS spectra for graphite, graphene oxide exfoliated in aqueous media of 0.1M $(NH_4)_2SO_4$, reduced graphene oxide with hydrazine hydrate and commercial reduced graphene oxide – USA. Black curves express experimental data points and red ones are fitting curves for spectra. 146
Figure 82. O1s XPS spectra for graphite, graphene oxide exfoliated in aqueous media of 0.1M $(NH_4)_2SO_4$, reduced graphene oxide with hydrazine hydrate and commercial reduced graphene oxide – USA. Black curves express experimental data points and red ones are fitting curves for spectra. 147
Figure 83. C1s XPS spectra for graphite, for graphene exfoliated in 0.1M TBA BF_4 dissolved in NMP (1-methyl-2-pyrrolidinone) by CA at -5.0 V and at -2.5 V, and for graphene exfoliated by CA at -2.5 V exposed with photolithography. Black curves express experimental data points and red ones are fitting curves for spectra. 148
Figure 84. O1s XPS spectra for graphite, for graphene exfoliated in 0.1M TBA BF_4 dissolved in NMP (1-methyl-2-pyrrolidinone) by CA at -5.0 V and at -2.5 V, and for graphene exfoliated by CA at -2.5 V exposed with photolithography. Black curves express experimental data points and red ones are fitting curves for spectra. 149
Figure 85. The atomic percentage of different oxygenic bounds for the case of C1s (above) and for O1s (below). 150
Figure 86. Obtained values for the ratio [C (O)]/[C] for all the cases. 151
Figure 87. Raman spectra of graphite, graphene oxide (GOx), reduced graphene oxide (rGOx), commercial reduced graphene oxide (rGOx - USA). 152
Figure 88. Raman spectra of graphite, graphene -5V, and graphene -2.5V with three characteristic bands (A), and with D- and G-bands (B). 153
Figure 89. IR spectra of graphite, graphene oxide exfoliated in aqueous media of 0.1M $(NH_4)2SO_4$, reduced graphene oxide with hydrazine hydrate and commercial reduced graphene oxide..... 154
Figure 90. IR spectra of graphene (-5.0 V), graphene (-2.5 V), and graphene (-2.5 V) exposed in photolithography, exfoliated in in 0.1M TBA BF_4 dissolved in NMP (1-methyl-2-pyrrolidinone) by CA. . 155
Figure 91. Four-point probe electrical conductivity measurements of different samples transferred on polystyrene substrate. 156
Figure 92. Electrochemical stability windows of Glassy Carbon, Graphite/PS, and Graphene (-2.5 V)/PS electrode obtained by A) linear sweep voltammetry (LSV), and B) cyclic voltammetry (CV), in a solution of $LiClO_4$ (0.1M) (20/80 ethanol:water v/v). Scan rate 100 mV/s..... 157
Figure 93. Cyclic voltammetry of GCE, graphite/PS, and graphene (-2.5V)/PS electrodes in $K_4[Fe(CN)_6]$ 2.5 mM + KCl 0.1M before the performing of electrochemical window A), and after the performing of electrochemical window B), C), and D). Scan rate 10 mV/s..... 159
Figure 94. Cyclic voltammetry on graphene (-2.5 V)/PS electrode using hexaammineruthenium (III) chloride (C=2.5 mM) (A) and potassium hexacyanoferrate (III) (C=2.5 mM) (B), dissolved in KCl 0.1M, at different scanning rate, from 1000mV/s (larger curves) low to 1mV/s (smaller curves). 161
Figure 95. Cyclic voltammetry at different scanning rate on graphene (-2.5 V)/PS electrodes fabricated with our own method in the laboratory using aqueous solution of hexaammineruthenium (III) chloride (C = 2.5 mM) + KCl 0.1M with three different working electrode surface areas A) $10mm^2$, B) $3mm^2$, and C) $1mm^2$. 161
Figure 96. Cyclic voltammetry at different scanning rate on graphene (-2.5 V)/PS electrodes fabricated with our own method in the laboratory using aqueous solution of potassium hexacyanoferrate (III) (C = 2.5 mM) + KCl 0.1M with three different working electrode surface areas A) $10mm^2$, B) $3mm^2$, and C) $1mm^2$. 162

Figure 97. Variation of ΔE versus the scanning rate for both electrochemical probes A) hexaammineruthenium (III) chloride, B) potassium hexacyanoferrate (III) obtained on graphene (-2.5 V)/PS electrodes fabricated with our own method at different values of working surface area..... 163
Figure 98. Evaluation of current densities versus the square root of the scanning rate for both electrochemical probes A) hexaammineruthenium (III) chloride, B) potassium hexacyanoferrate (III) obtained on graphene (-2.5 V)/PS electrodes fabricated with our own method at different values of working surface area..... 164
Figure 99. Cyclic voltammetry at different scanning rate on graphene (-2.5 V)/PS electrodes fabricated with photolithography using hexaammineruthenium (III) chloride (C = 2.5mM) in KCl 0.1M with different working electrode surface areas A) 10mm^2, B) 5mm^2, C) 1mm^2, D) 500µm^2, E) 200µm^2, and F) 100µm^2. 165
Figure 100. The superposition of the experimental cyclic voltammograms with the simulated ones obtained during the Digisim® simulation for two electrochemical probes with using graphene (-2.5 V)/PS electrode fabricated with our own method A), B), and with graphene (-2.5 V)/PS photolithography electrode C), D). Scan rate for the curves in this figure was 50 mV/s. 168
Figure 101. Voltammograms obtained on graphene (-2.5 V)/PS electrodes fabricated with our own method at working surface area A) 10 mm^2 and B) 1 mm^2 for ISO (1, 2 or 3 mM) in H_2SO_4 (0,1M) (70/30 ethanol/water v/v). Scan rate 100 mV/s. 172
Figure 102. Voltammograms obtained on graphene (-2.5 V)/PS electrodes fabricated with photolithography at working surface area 10 mm^2 for ISO (1, 2 or 3 mM) in H_2SO_4 (0,1M) (70/30 ethanol/water v/v). Scan rate 100 mV/s. 173
Figure 103. Schematic representation of the procedure used for the preparation of imprinted polypyrrole films onto Graphene (-2.5 V)/PS electrodes, including two main steps: 1) electropolymerization of MIPs by CV and/or CA, and 2) the CV extraction of isoproturon molecules. .. 174
Figure 104. Isoproturon extraction from Graphene-MIP electrodes fabricated with our own method with different working surface area A) 10 mm^2, B) 1 mm^2, by cyclic voltammetry in an ethanol/water (70:30 v/v) solution of 0.1M H_2SO_4. Scan rate 100 mV/s..... 175
Figure 105. Isoproturon extraction from Graphene-MIP photolithography electrode with working surfacee area 10 mm^2 by cyclic voltammetry in an ethanol/water (70:30 v/v) solution of 0.1M H_2SO_4. Scan rate 100 mV/s. 176
Figure 106. Incubation (rebinding) step 176
Figure 107. The calibration plots of isoproturon detection obtained at Graphene-MIP electrodes in milli-Q water samples, the electrode substrate was graphene (-2.5 V)/PS obtained by our own method at different working surface area A) 10 mm^2 and B) 1 mm^2, and on graphene (-2.5 V)/PS photolithography electrodes with working surface area 10 mm^2 C). The electrochemical analysis was performed by square wave voltammetry (SWV) in an ethanol/water (70:30 v/v) solution of 0.1M H_2SO_4. 177

List of Tables

Table 1. Electrochemical sensors-biosensors based on Polypyrrole-Nanocomposites (PNCs) modified electrodes. 56
Table 2. MIP sensors based on electro-synthesized MIP-based polypyrrole sensing layer. 65
Table 3. List of chemical and reagents used for experiments. 69
Table 4. AFM roughness measurements of the MIP-GC films made by CV at potential range 0 to +0.9V/Ag/AgCl, with different number of cycles in ethanol/water (v/v:20/80) solution containing 0.01 M of pyrrole + 1 mM of ISO + 0.1 M of $LiClO_4$, v = 10 mV/s, before and after isoproturon extraction. 119
Table 5. Characteristic bonds obtained during the FT-IR analysis of Pyrrole 98% and Isoproturon. 124
Table 6. Data presented for the electrochemical stability windows of different electrodes. 158
Table 7. Extracted data by plotting the slopes from the evaluation of current densities versus square root of the scanning rate for graphene (-2.5 V)/PS electrodes from the Figure. 96A and 96B. 164
Table 8. Variation of ΔE versus the scanning rate for both electrochemical probes hexaammineruthenium (III) chloride obtained on graphene (-2.5 V)/PS electrodes fabricated with photolithography method at different working surface areas. 166
Table 9. Calculated active working surface area using Randles-Sevick equation for graphene (-2.5 V)/PS electrodes fabricated with our own method for both electrochemical probes. 167
Table 10. Simulated values of the heterogeneous electron transfer rate obtained by graphene (-2.5 V)/PS electrodes fabricated with our own method for the different working surface area at the different scanning rates in two electrochemical probes using Digisim® software. 169
Table 11. Simulated values of the heterogeneous electron transfer rate obtained by graphene (-2.5 V)/PS photolithography electrodes for the different working surface area at the different scanning rates in two electrochemical probes using Digisim® software. 169
Table 12. Comparison of graphene electrodes sensitivity with that one of glassy carbon electrodes. ... 178

Summary

Herbicides are widely distributed in agricultural soils, and after their migration or flowing they contaminate inland or surface waters. In this context, the study is focused on the development of sensitive and selective electrodes allowing the detection of isoproturon, a herbicide classified as a priority micropollutant for water by the European Water Framework Directive. These electrodes consist of a thin layer of molecularly imprinted polymer (MIP) of the polypyrrole type (MIP-PPy) prepared by electropolymerization on a glassy carbon electrode (GCE) or on an electrode made of 100% graphene (GRE). These modified electrodes are intended to be the core element of low-cost electrochemical sensors allowing rapid in-situ analysis of micropollutants with the aim of intensifying water quality monitoring.

The first part of this work aims to show the potential of MIP-PPy on GCE for the sensitive and selective detection of isoproturon in aqueous media. Electropolymerization by chronoamperometry on GCE in a non-toxic water/ethanol solvent made possible obtaining of MIP-PPy. During the electropolymerization process, isoproturon molecules were successfully trapped in the polypyrrole film where they created some selective isoproturon recognition cavities after electrochemical extraction. Non-imprinted polymer (NIP) films made under identical conditions but in absence of isoproturon did not show any interaction with targeted pollutant. MIP and NIP films were characterized by cyclic voltammetry in the presence of redox probes and their thickness was estimated by EQCM (Electrochemical Quartz Crystal Microbalance) and calculated using Faraday's law. MIP films were found to selectively detect isoproturon even in the presence of interferents such as carbendazim and carbamazepine. Its limit of detection (LOD) in milli-Q water, achieved by square wave voltammetry (SWV) is 0.5 $\mu g\ L^{-1}$. Analyzes carried out in real water samples lead to an LOD of 2.2 $\mu g\ L^{-1}$.

In a second part, a detailed study of the electrochemical parameters applied during the synthesis of MIP films on GCE as well as during the extraction step showed that the anode potential and the number of cycles applied, strongly impact the conductivity of MIP-PPy film and its morphology. Electrochemical Impedance Spectroscopy (EIS), Atomic Force Microscopy (AFM), EQCM (Electrochemical Quartz Crystal Microbalance), XPS (X-ray Photoelectron Spectroscopy) and IR spectroscopy were used for this study. MIP films prepared by CV at a potential lower than +1.0 V led to the optimum detection signal of isoproturon attributed to a lower degree of over-oxidation of PPy film.

The third part deals with the development of electrodes made of pure electrochemical graphene deposited on polystyrene and then with their application to the detection of isoproturon. An original method for elaboration of 100% graphene electrodes has been

developed. This consists firstly in electrochemical exfoliation of graphene at negative potentials in a single step and then in preparing electrodes by temperature compression of graphene on a polystyrene substrate. After testing different design methods for graphene electrodes, their electrochemical properties were evaluated using redox probes. XPS, Raman, IR methods and four-point probe conductivity measurements are used to finely characterize the surface chemistry and nanostructure of GREs and correlate them with their properties. Finally, the electropolymerization of MIPs has been successfully carried out on GREs and their potential for the determination of isoproturon in water has been demonstrated.

Keywords: Electrochemical sensors, Molecularly Imprinted Polymers (MIP), Electropolymerization of Polypyrrole, Electrochemical Detection of Isoproturon, Electrochemical Graphene Electrodes

Résumé

Les herbicides sont répandus largement sur les terres agricoles, et après migration dans les sols ou ruissellement, ils viennent contaminer les eaux souterraines ou de surface. Dans ce contexte, l'étude porte sur le développement d'électrodes sensibles et sélectives permettant la détection électrochimique de l'isoproturon, un herbicide classé comme micropolluant prioritaire par la directive cadre européenne sur l'eau. Ces électrodes sont constituées d'une couche mince de polymère à empreinte moléculaire (MIP) de type polypyrrole (MIP-PPy) préparée par électrosynthèse sur électrode de carbone vitreux (GCE) ou sur électrode constituée à 100% de graphène (GRE). Ces électrodes modifiées ont pour vocation d'être l'élément de cœur de capteurs électrochimiques à faible coût permettant une analyse rapide *in-situ* de micropolluants avec pour objectif une intensification du suivi de la qualité des eaux.

La première partie de ce travail a pour objectif de montrer la potentialité de MIP-PPy sur GCE pour la détection sensible et sélective de l'isoproturon en milieu aqueux. L'électropolymérisation par chronoampérométrie sur GCE en solvant non toxique eau/éthanol a permis d'obtenir des MIP-PPy. Au cours du processus d'électropolymérisation, les molécules d'isoproturon ont été piégées avec succès dans le film de polypyrrole où elles ont créé après extraction électrochimique des cavités de reconnaissance sélective de l'isoproturon. Des films de polymère non imprimé (NIP), réalisés dans des conditions identiques mais en l'absence d'isoproturon, ne présentent aucune interaction avec le polluant cible. Les films MIP et NIP ont été caractérisés par voltampérométrie cyclique en présence de sondes redox et leur épaisseur a été estimée par EQCM (Electrochemical Quartz Crystal Microbalance) et calculée en utilisant la loi de Faraday. Les films MIP se sont avérés capables de détecter sélectivement l'isoproturon, même en présence d'interférents comme la carbendazime et la carbamazépine. Leur limite de détection (LOD) dans l'eau milli Q, obtenue par voltampérométrie à vague carrée (SWV), est de 0,5 $\mu g\ L^{-1}$. Les analyses effectuées dans des échantillons d'eau réelle conduisent à une LOD de 2,2 $\mu g\ L^{-1}$.

Dans une seconde partie, une étude fine des paramètres électrochimiques appliqués lors la synthèse des films MIP sur GCE ainsi que lors de l'étape d'extraction a mis en évidence que le potentiel anodique et le nombre de cycle appliqués impactent fortement la conductivité du film MIP-PPy et sa morphologie. La spectroscopie d'impédance électrochimique (EIS), la microscopie à force atomique (AFM), l'EQCM (Electrochemical Quartz Crystal Microbalance), l'XPS (X-ray Photoelectron Spectroscopy) et la spectrométrie IR ont été utilisées pour cette étude. Les films de MIP préparés par CV à un potentiel inférieur à +1,0 V ont conduit au signal optimum de détection de l'isoproturon attribué à un degré de sur-oxydation moindre du film PPy.

La dernière partie porte sur l'élaboration d'électrodes constituées de graphène électrochimique pur déposé sur polystyrène puis sur leur application à la détection de l'isoproturon. Une voie d'élaboration originale d'électrodes 100% graphène a été mise au point. Celle-ci consiste dans un premier temps à exfolier électrochimiquement le graphène à des potentiels négatifs en une seule étape puis à préparer des électrodes par compression en température du graphène sur substrat de styrène. Après avoir testé différentes méthodes de design des électrodes GRE, leurs propriétés électrochimiques ont été évaluées à partir de sondes redox. Des méthodes XPS, Raman, IR et des mesures de conductivité par mesure quatre points ont permis de caractériser finement la chimie de la surface et la nanostructure des GRE et de les corréler à leurs propriétés. Enfin l'électropolymérisation des MIPs a été réalisée avec succès sur les GRE et leur potentialité pour la détermination de l'isoproturon dans les eaux a été démontrée.

Mots clés: Capteurs Électrochimiques, Polymères à Empreinte Moléculaire (MIP), Électropolymérisation du Polypyrrole, Détection électrochimique de l'Isoproturon, électrodes en Graphène électrochimique.

Përmbledhje (Summary in Albanian)

Herbicidet janë të përhapura gjerësisht në tokat bujqësore dhe si rezultat i migrimit ose rrjedhjes së tyre ato ndotin ujërat nëntokësore ose sipërfaqësore. Në këtë kontekst, ky studim është fokusuar në përgatitjen e disa elektrodave të ndjeshme dhe selektive të cilat mundësojnë përcaktimin kuantitativ të izoproturonit si një herbicid i cili klasifikohet si një nga mikrondotësit e ujit në kuadër të Direktivës Europiane të Ujërave WFD (ang: Water Framework Directive). Këto elektroda në sipërfaqen e tyre përmbajnë një shtresë të hollë të një polimeri i cili përmbanë gjurmë të molekulave (MIP) të llojit polipirrol (MIP-PPy), të përgatitur nga një reaksion i elektropolimerizimit në sipërfaqen e një elektrode të karbonit qelqor (GCE) ose në një elektrodë të bërë nga grafeni i pastër 100% (GRE). Elektrodat e tilla të modifikuara kanë për qëllim të jenë elementi bazë i senzorëve elektrokimikë me kosto të ulët, duke mundësuar realizimin e shpejtë të matjeve për përcaktimin e mikrondotësve në vendin e marrjes së mostrave të tyre me qëllim të intensifikimit të monitorimit të cilësisë së ujit.

Pjesa e parë e këtij punimi synon të tregojë potencialin e këtyre senzorëve elektrokimikë në përcaktimin e ndjeshëm dhe selektiv të izoproturonit në mjedise ujore. Procesi i elektropolimerizimit i zhvilluar me anë të kronoamperometrisë në elektrodat e karbonit qelqor në prani të një përzierje jo toksike ujë/etanol bëri të mundur formimin e filmave të polipirrolit me gjurmë të molekulave të izoproturonit. Gjatë procesit të elektropolimerizimit, molekulat e izoproturonit janë futur me sukses në brendi të filmave të polipirrolit, ku pas nxjerrjes ose ekstraktimit të këtyre molekulave me anë të metodave elektrokimike, ato mundësuan krijimin e disa zgavrave selektive njohëse për të njejtat molekula në filmat e polipirrolit. Filmat e polipirrolit që nuk përmbajnë gjurmë me molekula të izoproturonit (NIP), të përgatitura në kushte të njejta elektrokimike por në mungesë të izoproturonit, nuk treguan ndonjë bashkëveprim me këtë molekulë. Filmat e tillë MIP dhe NIP janë karakterizuar me anë të voltametrisë ciklike në prani të çifteve redokse dhe trashësia e tyre është vlerësuar me anë të mikrobalancës elektrokimike të kuarcit të kristaltë EQCM (ang: Electrochemical Quartz Crystal Microbalance) si dhe është llogaritur edhe teorikisht duke aplikuar ligjin e Faradejit. Me anë të filmave MIP është mundësuar përcaktimi selektiv i izoproturonit edhe në prani të molekulave tjera interferuese, të tillë si karbendazimi dhe karbamazepina. Kufiri më i ulët i përqendrimit për përcaktimin e izoproturonit LOD (ang: Limit of Detection) në mostrat e përgatitura në ujë ultra të pastër (milli-Q), i arritur me anë të voltametrisë me valë katrore SWV (ang: Square Wave Voltammetry) është llogaritur të jetë 0,5 μg/L. Matjet e realizuara në mostrat reale të ujit çojnë në një LOD prej 2.2 μg/L.

Në pjesën e dytë të këtij punimi është kryer një studim më i hollësishëm i parametrave të ndryshëm elektrokimikë të cilët janë përdorur gjatë sintezës së filmave MIP në

elektrodat e karbonit qelqor, si dhe gjatë fazës së nxjerrjes së molekulave të izoproturonit me ç'rast është vënë në pah se potenciali i aplikuar anodik dhe numri i skanimeve ndikojnë fuqishëm në përçueshmërinë dhe morfologjinë e filmave MIP-PPy. Spektroskopia me impedancë elektrokimike EIS (ang: Electrochemical Impedance Spectroscopy), mikroskopia me forcë atomike AFM (ang: Atomic Force Microscope), metoda me mikropeshore të kuarcit (EQCM), spektroskopia e fotoelektroneve me rreze X - XPS (ang: X-ray Photoelectron Spectroscopy), si dhe spektroskopia me rreze infra te kuqe IR (ang: Infra Red spectroscopy) u përdorën për realizimin e këtij studimi. Filmat MIP të përgatitur me voltametri ciklike në një potencial më të ulët se +1.0 V çuan në marrjen e sinjalit të përcaktimit optimal të izoproturonit, sinjal ky i cili i atribuohet një shkalle më të ulët të tejoksidimit të filmave të polipirrolit.

Pjesa e tretë e këtij punimi merret kryesisht me zhvillimin e elektrodave të përbëra nga grafeni krejtësisht i pastër elektrokimik i depozituar në pllakat e polistirenit të cilat më pastaj u përdorën si senzorë për përcaktimin elektrokimik të izoproturonit. Është zhvilluar një metodë origjinale për përgatitjen e elektrodave të përbëra nga grafeni 100% i pastër. Kjo metodë bazohet fillimisht në largimin elektrokimik të shtresave të grafenit në potencialet negative në një fazë të vetme dhe shndërrimin e tyre në pluhur grafeni dhe më pas në përgatitjen e elektrodave nga presimi i grafenit pluhur në temperaturë të lartë në një pllakë polistireni. Pas testimit të metodave të ndryshme për dizajnimin e elektrodave të grafenit, vetitë e tyre elektrokimike u vlerësuan duke përdorur çifte të ndryshme redokse. Metodat spektroskopike si XPS, Raman, IR dhe matjet e përçueshmërisë me kontakt fizik në katër pika u përdorën për të karakterizuar kiminë e sipërfaqeve dhe nanostrukturën e elektrodave të grafenit dhe i ndërlidhin ato me vetitë e tyre. Në fund, elektropolimerizimi i filmave MIP është kryer me sukses në elektrodat e grafenit dhe është demonstruar potenciali i tyre për përcaktimin e izoproturonit në ujëra.

Fjalët kyçe: Senzorët elektrokimikë, Polimerë me gjurmë molekulare (MIP), Elektropolimerizimi i polipirrolit, Përcaktimi elektrokimik i izoproturonit, Elektroda të grafenit elektrokimik

General introduction

Water is the main ingredient that enables the development of life processes of the living organisms, whether plants or animals, on Earth planet. Besides that, water is the main liquid compound which is used also for the development of various human activities, such as producing energy, chemical products, foods, agricultural, mining, industry, or just for the domestic use. The importance of water is mainly based on its ability to function as a universal solvent in the environment. In parallel with population growth, the development of human activities has been intensified, thus resulting in the increase of water usage. Unfortunately, these multiple uses of water caused the decreasing of its amount and its quality has degraded due to the accumulation over time of pollutants and their derivatives in large quantities or in trace amounts (micropollutants). Micropollutants, even in presence of trace concentrations in the natural water, can cause serious problems. They are classified into two major groups: inorganic micropollutants which include the metallic trace elements that are non-biodegradable and organic micropollutants including organohalogen compounds, polycyclic aromatic hydrocarbons (PAH), phthalates, drugs and in particular pesticides which can be biodegradable.

A pesticide may be a compound ore a mixture of them that is used in agriculture as plant regulator by preventing, destroying, repelling or mitigating any pest. Pesticides are classified into different groups, such as: fungicides, insecticides, and herbicides, and most often are applied as liquids sprayed on the agricultural lands or deposited directly with phytosanitary products on seeds via a coating before planting. Among groups of pesticides, herbicides are found to be very effective for the controlling the growth process of plants and have shown a rapid handling extension. Consequently, these compounds during their use are in touch with soil and can contaminate surface or ground waters. Their degradation products and metabolites were found to be very dangerous by showing negative effects for the ecosystem. In particular, isoproturon is a phenyl-urea herbicide which is used for killing weeds in agricultural soils and it was found to be an ecosystem contaminant. Due to its hazardous and toxic effects, the European Union has classified this compound as a priority micro-pollutant inside the Water Frame work Directive (WFD) since 2013 [3] and decided to ban its use since in 2016. Furthermore, inside the WFD, for isoproturon as for other priority micropollutants, is regulated the maximum level of their concentrations allowed for inland surface waters. These thresholds are updated regularly according to the adverse effects observed and the list of priority substances is also periodically reviewed to take into account new pollutants or derivatives that appear in the environment.

In order to determine if isoproturon has reached its maximum level of concentration for inland surface waters, various sophisticated sensitive and selective techniques are used. Costly analytical techniques based on chromatography are frequently used for isoproturon detection in environmental samples and have shown low detection limits. However, these techniques, in spite of their high sensitivities, remain expensive and difficult to implement for on-site and in-situ analysis. In addition, onsite sampling and its treatment involves a longer analysis time and complex additional steps to overcome matrix effects and interferences. There is an increasing need to ensure efficient and continuous on-site and in-situ monitoring of environmental waters, and to reduce the cost of analysis, which implies developing novel sensors. Therefore, efforts are ongoing to develop rapid and inexpensive sensing devices for the detection of pesticides in general and isoproturon particularly. Among all the conventional techniques, electrochemical analysis is one of the simplest and least expensive. Voltammetric-based methods have been widely reported in literature for the determination of many pesticides and isoproturon more specifically using various carbon electrode materials such as glassy carbon, graphene, wall-jet glassy carbon electrode, carbon paste, carbon fiber, doped diamond, and multiwalled carbon nanotubes (MWCNT). However, to the best of our knowledge, no sensor has yet been validated for the measurement of micropollutants in water.

More recently, numerous studies have been focused on modified electrodes with conducting polymer films. The attachment of the organic conducting polymer film on the electrode surface makes possible the increase of sensitivity and selectivity of these modified electrodes toward a targeted analyte. In this context, one of the most effective methods to achieve this goal is to prepare molecularly imprinted polymer sensors.

A molecularly imprinted polymer (MIP) electrochemical sensor is obtained by polymerization of a monomer on working electrode surface in the presence of a template molecule. After polymerization, the template molecules, trapped in the polymeric matrix, are removed leaving behind cavities that are complementary not just in shape but also in functionalities. The cavities contain functional groups of the polymer that leads to the specific uptake of the targeted analyte. High affinity and selectivity are based on the shape of the print together with the specific interactions between the functional groups from the MIPs and the target micro-pollutant. Polypyrrole was chosen as conducting polymer for environmental applications due to its properties and its ability for in-situ electropolymerization at the electrode surface with or without presence of the template molecule. In addition, the electropolymerization of polypyrrole leads to chemically and mechanically robust films. Therefore, thanks to all these properties, MIPs have been chosen, in this thesis work, as approach for electrochemical determination of isoproturon in water samples.

Graphene is currently undergoing significant development due to its very interesting physico-chemical properties, notably its very high conductivity and chemical resistance. However, for electrochemical sensor applications, it is most often used in the presence of a binder which reduces its intrinsic properties. The choice was made here to develop 100% graphene electrodes as electrode materials in order to take full advantage of the potential of this material with the objective to elaborate a MIP-graphene sensor for isoproturon detection.

This PhD was carried out at the Interfaces, Confinement, Materials and Nanostructure (ICMN) UMR CNRS-University of Orléans laboratory in the Functional Carbons for Environment and Biomaterials applications axis in cotutelle with the University of Prishtina. This study follows on from previous works of the lab concerning the functionalization of carbon materials for the development of electrochemical sensors for the detection of metallic or organic micropollutants.

This document is structured in five chapters, the first one relates to the state of the art, the second introduces the materials and methods used for the measurements and different characterizations, and three others present the experimental data.

Chapter 3 presents the work which has been performed to achieve the development of a molecularly imprinted polymer sensor on glassy carbon electrode for the determination of isoproturon in water.

Chapter 4 is dedicated to the influence of the electrochemical parameters applied during the synthesis of MIP films on GCE as well as during the extraction step on the properties of the MIP in terms of their conductivity, morphology and sensitivity, with the objective to improve the performance of MIP sensors for the isoproturon detection.

Finally, in Chapter 5, we present the results concerning the development of a new original method to prepare 100% graphene electrodes and their use as working electrodes for the electrochemical preparation of MIP sensors dedicated to the isoproturon determination in waters.

Hyrje e përgjithshme (General introduction in Albanian)

Uji është përbërësi kryesor që mundëson zhvillimin e proceseve jetësore të organizmave të gjallë që jetojnë në planetin e Tokës, qofshin ato bimë apo kafshë. Përveç kësaj, uji është substanca kryesore e lëngët e cila përdoret gjithashtu për zhvillimin e aktiviteteve të ndryshme njerëzore, të tilla si prodhimi i energjisë, prodhimi i produkteve të ndryshme kimike, për prodhimin e ushqimit, në bujqësi, në miniera, në industri, ose edhe thjesht për përdorim shtëpiak. Rëndësia e ujit bazohet, në radhë të parë, në aftësinë e tij për të funksionuar si një tretës universal në mjedis. Paralelisht me rritjen e numrit të popullsisë, zhvillimi i aktiviteteve njerëzore është intensifikuar duke rezultuar kështu edhe në rritjen e konsumimit të ujit. Fatkeqësisht, përdorimet e shumëfishta të ujit të pijshëm po shkaktojnë zvogëlimin e sasisë së tij dhe cilësia e tij është degraduar për shkak të akumulimit të ndotësve dhe derivateve të tyre në sasi të mëdha ose në sasi të vogla (mikrondotës) me kalimin e kohës. Mikrondotësit edhe në prani të përqendrimeve të tyre në gjurmë në ujin natyror mund të shkaktojnë probleme serioze. Këta mikrondotës janë klasifikuar në dy grupe kryesore: në mikrondotës inorganikë të cilët përfshijnë elementet metalike në gjurmë e që janë përbërje jo të biodegradueshme dhe në mikropondotës organikë duke përfshirë përbërjet organohalogjene, hidrokarburet aromatike policiklike (PAH), ftalatet, ilaçet dhe në veçanti pesticidet, të cilat mund të jenë përbërje të biodegradueshme.

Pesticidet janë një përzierje e substancave të ndryshme që janë synuar të përdoren në bujqësi si rregullatorë të bimëve duke parandaluar, shkatërruar, sprapsur ose zbutur ndonjë dëmtues të tyre. Pesticidet klasifikohen në grupe të ndryshme, të tilla si: fungicide, insekticide dhe herbicide, dhe më së shpeshti ato aplikohen si lëngje duke u spërkatur në tokat bujqësore ose të depozituara direkt me produkte fitosanitare në fara përmes një shtrese para mbjelljes. Midis grupeve të ndryshme të pesticideve, herbicidet kanë treguar se janë shumë më të efektshme në kontrollimin e procesit të rritjes së bimëve dhe kanë pasur një zbatim në shkallë të gjerë. Si pasojë, këta përbërës gjatë përdorimit të tyre janë në kontakt të vazhdueshëm me tokën dhe mund të ndotin ujërat sipërfaqësorë ose ata nëntokësorë. Produktet e tyre të degradimit dhe metabolitët e tyre u gjetën të jenë shumë të rrezikshëm duke treguar efekte negative për ekosistemin në tërësi. Në veçanti, izoproturoni është një herbicid i llojit fenil-ure i cili përdoret për zhdukjen e barërave të panevojshme në tokat bujqësore dhe i cili është zbuluar të jetë një ndotës i ekosistemit. Për shkak të efekteve të tij të rrezikshme dhe toksike, që nga viti 2013 [3] Bashkimi Europian e ka klasifikuar këtë herbicid si një nga mikrondotësit e rëndësisë primare në kuadër të Direktivës Europiane të Ujërave WFD (ang: Water Framework Directive) dhe në vitin 2016 vendosi të ndalojë përdorimin e tij. Për më tepër, brenda WFD, për izoproturon ashtu dhe për mikrondotësit tjerë me rëndësi

primare, është rregulluar niveli maksimal i përqendrimeve të tyre të lejuara për ujërat sipërfaqësore dhe të brendshme. Këto nivele të përqendrimit azhurnohen rregullisht në përputhje me efektet e pafavorshme të vëzhguara dhe lista e substancave prioritare gjithashtu rishikohet në mënyrë të vazhdueshme duke marrë parasysh ndotësit ose derivatet e tyre të reja që shfaqen në mjedis.

Në mënyrë që të përcaktohet nëse isoproturoni ka arritur nivelin e tij maksimal të përqendrimit për ujërat sipërfaqësore dhe të brendshme, u përdorën teknika të sofistikuara me ndjeshmëri dhe selektivitet të lartë. Teknikat e kushtueshme analitike të bazuara në kromatografi përdoren shpesh për përcaktimin e nivelit të izoproturonit në mostrat mjedisore të ujit duke treguar limite të ulëta të përqendrimit. Sidoqoftë, këto teknika, megjithë ndjeshmërisë së tyre të lartë ende mbeten si të shtrenjta dhe vështirë të zbatueshme për realizimin e analizave në vendin e marrjes së msotrave ujore. Përveç kësaj, marrja e mostrave ujore si dhe trajtimi i tyre përfshinë një kohë më të gjatë të analizës dhe hapa të ndërlikuar shtesë për të kapërcyer efektet e matricës dhe të interferentëve tjerë. Ekziston një kërkesë në rritje për të siguruar monitorim sa më efikas dhe të vazhdueshëm të ujërave mjedisore me qëllim zvogëlimin e kosotos së analizës që nënkupton zhvillimin e senzorëve të rinjë. Përpjekjet janë të vazhdueshme për zhvillimin e pajisjeve të shpejta dhe më pak të kushtueshme për përcaktimin e nivelit të pesticideve në përgjithësi dhe posaçërisht të izoproturonit. Ndër të gjitha teknikat konvencionale, metodat elektrokimike të analizës janë një nga më të thjeshtat dhe më pak të kushtueshme. Metodat e bazuara në voltametrinë ciklike janë raportuar gjerësisht në literaturë për përcaktimin e shumë pesticideve dhe izoproturonit në mënyrë më specifike, duke përdorur kështu materiale të ndryshme të elektrodave të karbonit si: karboni qelqor, grafeni, elektroda e karbonit qelqor me wall-jet, elektrodat me pastë e karbonit, ato me fibra karboni, me diamant të dopuar dhe ato me nanotubat e karbonit (MWCNT). Sidoqoftë, për sa i përket njohurive tona, asnjë senzor nuk është vërtetuar ende për matjen e mikrondotësve në ujë.

Kohët e fundit, studime të shumta janë fokusuar kryesisht në elektroda të modifikuara me filma të polimerëve përçues. Bashkëveprimi i filmit të një polimeri përçues organik me sipërfaqen e elektrodës mundëson rritjen e ndjeshmërisë dhe selektivitetit të elektrodës së modifikuar drejt një analiti të synuar. Në këtë kontekst, një nga metodat më efektive për të arritur këtë qëllim është përgatitja e senzorëve të bazuar në polimerët me gjurmë molekulare.

Një senzor elektrokimik i ndërtuar me një polimer me gjurmë molekulare (ang: MIP-Molecularly Imprinted Polymer) mund të merret nga polimerizimi i një monomeri në sipërfaqen e elektrodës të punës në prani të një molekule të analitit si model. Pas procesit të polimerizimit, molekulat ndotëse të bllokuara në brendi të shtresës së polimerit, nxirren duke lënë pas disa zgavra të cilat janë komplementare jo vetëm në

formë, por edhe në funksione të molekulës së nxjerrë. Zgavrat e tilla përmbajnë grupe funksionale të polimerit që mundësojnë kapjen në mënyrë selektive të molekulës gjatë analizës. Afiniteti dhe selektiviteti i tyre i lartë bazohen në formën e shtypjes së bashku me ndërveprimet specifike midis grupeve funksionale nga filmat MIP dhe nga molekula e mikrondotësit. Polipirroli u zgjodh si polimer përçues për shkak të vetive të tij të mira për aplikime të ndryshme mjedisore dhe aftësisë së tij për tu elektropolimerizuar në kushte in-situ në sipërfaqen e elektrodës me ose pa praninë e molekulës mikrondotëse. Përveç kësaj, elektropolimerizimi i polipirrolit çon në krijimin e filmave të fortë në aspektin kimik dhe në atë mekanik. Prandaj, falë të gjitha këtyre vetive, metodat e bazuara në MIP janë zgjedhur si strategji në këtë punim për përcaktimin elektrokimik të izoproturonit në mostrat e ujit.

Grafeni aktualisht po i nënshtrohet një zhvillimi të rëndësishëm për shkak të vetive shumë interesante të tij fiziko-kimike, veçanërisht përçueshmërisë dhe rezistencës kimike shumë të lartë të tij. Sidoqoftë, për aplikimet e tij si senzor elektrokimik, ai përdoret shpesh në prani të një lidhësi që zvogëlon vetitë e tij të brendshme. Përpjekja këtu është bërë për të zhvilluar elektroda të grafenit me pastërti të lartë 100% në mënyrë që të përfitojmë plotësisht nga potenciali i këtij materiali me qëllimin për të përpunuar një senzor MIP-grafen i cili mund të përdoret pastaj për përcaktimin e izoproturonit.

Ky projekt i doktoraturës është realizuar në laboratorin e dedikuar për studime ndërfaqësore, të izolimit, dhe të nanostrukturës së materialeve (frëngjisht: ICMN Interfaces, Confinement, Matériaux et Nanostructures - UMR CNRS-Centre National de la Recherche Scientifique) në kuadër të Universitetit të Orléans-it në degën e përdorimit të karbonit funksional për mjedisin dhe biomaterialet në bashkëpunim me Universitetin e Prishtinës. Ky studim është vazhdimësi e hulumtimeve të mëparshme të bëra në këtë laborator në lidhje me funksionalizimin e materialeve të karbonit për zhvillimin e senzorëve elektrokimikë për përcaktimin e mikrondotësve me përbërje metalike ose organike.

Ky dokument është i strukturuar në pesë kapituj, duke filluar nga i pari i cili ka të bëjë me përshkrimin e kontekstit të punës, duke u pasuar nga kapitulli i dytë i cili prezanton materialet dhe metodat e përdorura për matjet dhe karakterizimet e ndryshme, dhe tre kapitujt tjerë që paraqesin të dhënat e gjetura eksperimentale.

Kapitulli i tretë paraqet punën e cila është kryer për të arritur zhvillimin e një senzori të bazuar në polimerët me gjurmë molekulare në elektrodën e karbonit qelqor me qëllim të përcaktimit të izoproturonit në ujë.

Kapitulli i katërt i kushtohet ndikimit të parametrave të ndryshëm elektrokimikë të aplikuar gjatë sintezës së filmave MIP në elektrodat e karbonit qelqor, si dhe gjatë hapit të nxjerrjes së molekulave mokrondotëse në vetitë e filmave MIP për sa i përket

përçueshmërisë, morfologjisë dhe ndjeshmërisë së tyre, me qëllim përmirësimin e performancës së këtyre senzorëve MIP në përcaktimin e izoproturonit.

Së fundmi, në kapitullin pestë, ne kemi paraqitur rezultatet e arritura në lidhje me zhvillimin e një metode të re dhe origjinale për të përgatitur elektroda grafeni me pastërti 100% dhe për t'i përdorur pastaj ato si elektroda të punës për përgatitjen elektrokimike të senzorëve MIP të cilët u janë kushtuar përcaktimit të izoproturonit në ujëra.

- Page left intentionally blank -

CHAPTER I

"Literature review"

1. CHAPTER I: LITERATURE REVIEW

This chapter introduces the general concepts of electrochemical sensing necessary to develop electrochemical sensors, and the bibliography concerning the conductive polymer materials, their physico-chemical properties and highlighting their application for the fabrication of MIP-based sensors. This chapter is divided into five main parts, 1) the first part includes the environmental context of the work, 2) the second part concerns chemical and electrochemical sensors, 3) the third part presents the conducting polymers, their electrical conductivity and their applications, including also the study over polypyrrole as conducting polymer used in this work, 4) the fourth part deals with MIP-based sensors, and 5) the last part is dedicated to electrochemical MIP-based sensors for environmental analysis, and their analytical performances.

1.1. Pesticides and their effect on the environment

1.1.1. Water quality

Water is essential for life. According to the World Health Organization (WHO) improving access to safe drinking-water can result in benefits to health, and every attempt should be to have drinking water as safe as possible [1]. In order to define safe drinking-water, in 1977 an International Conference for World Water was held in Mer del Plata in Argentina [1]. The World Health Organization (WHO) has published three editions of *Guidelines for drinking water quality*, which continuously were up to dated, by providing the explanation of all the rules, methods and measures to be taken for a better quality and hygiene in drinking-water [1]. In these editions of *Guidelines for drinking water quality* published by WHO, it was mentioned the term of "water quality", which refers to the description of the conditions of the water, including its chemical, physical and biological characteristics, by respecting the standards that were set for each of the possible contaminants [2]. In addition, in 2000 European Union has established the Water Framework Directive (WFD), on the basis of which the chemicals and compounds are classified into different priorities for the use in agriculture, industry and environment, and according to the established rules some of the compounds are banned for use [3].

So, water quality means the relation between health of ecosystems, safety human contact, and drinking water. On the other side, due to the increase of industry and technology, natural water is used widely for fabricating, processing, washing, diluting, cooling, or transporting a product. Water is also used by smelting facilities, petroleum refineries and industries, for producing energy, chemical products, food, and paper products. Major source of industrial water are fossil-fuel power stations, particularly coal-fired plants, where many of these plants discharge wastewater into environment. In other words, the three main components of life on earth (air, water and ground) are continuing to be polluted through over the years by human due to the wastewaters coming from industry, pharmacy, agriculture, etc.

Water quality has been affected by dangerous and toxic substances, such as heavy metals (lead Pb, cadmium Cd, mercury Hg, arsenic As), by pharmaceutical products and by pesticides, causing many harmful effects in the environment for living organisms and for human as well [1].

1.1.2. The use of pesticides in agriculture

Pesticides are a mixture of substances (chemical compounds) that have been intended to use as plant regulators by preventing, destroying, repelling or mitigating any pest. These compounds are used in agriculture as nitrogen stabilizers. As known, pesticides are used in large scale in agriculture as a group including herbicides, fungicides, insecticides, bactericides, and others. During the 20th century these compounds were considered like miracle. In the beginning pesticides were used as inorganic compounds as fungicides and insecticides, containing chemical elements such as antimony, boron, copper, fluorine, manganese, mercury, selenium, sulfur, thallium, and zinc, as their active ingredients excepted for killing insects [4]. These compounds were persistent in the soil, where in some cases they caused the damage of corps due to their presence [4]. However, these inorganic pesticides were not found to be very effective as insecticides and fungicides. Later in the 1940s, people began to use organic pesticides known as herbicides.

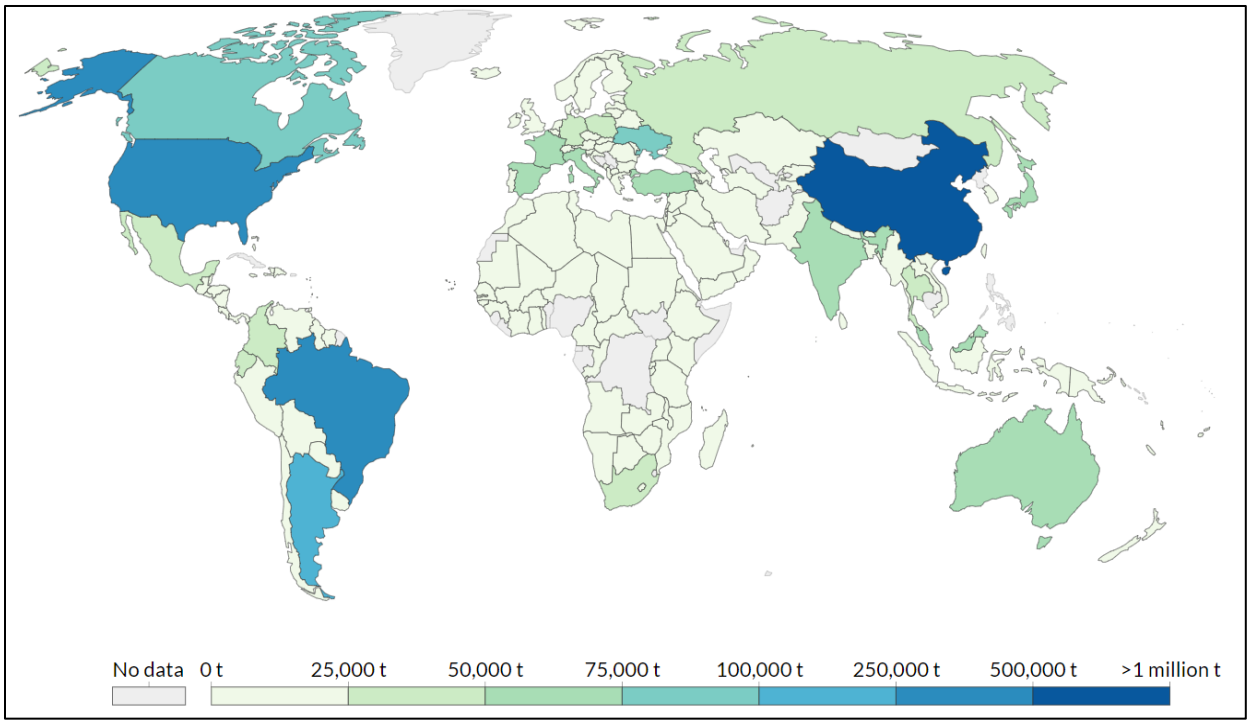

Figure 1. Global use of pesticides in 2017 [5].

Herbicides were found to be very effective for the controlling of the growing process of plants and have had a very rapid adoption. Only in India, the agricultural consumption of organic pesticides was rapidly increased from 4.000 MT in 1954-1955 to 70.000 MT in

1985-1986, and it reached about 1.500.000 MT by the year 2000 [4]. Nowadays, in India the consumption of pesticides is 0.327 kg per hectare, compared with France 3.63 kg, and with Japan 11.76 kg per hectare [5]. Figure 1 gives a general idea of the distribution of pesticide use in the world in 2017. It clearly shows a very high consumption in China as well as in the USA, Brazil and Argentina [5].

Agricultural pesticides most often are applied as liquids sprayed on the soil, and sometimes are either injected into the soil or applied as granules or as seed treatment. The quantity of used pesticide, depends on crop stage, formulation, intended target, application technique, and weather conditions and it is distributed between soil, plant foliage or crop residues, and a part losses due to drift [6]. Consequently, these compounds can get in touch with soil and surface waters on the environment. In Figure 2, is presented schematically the pesticides cycle in the environment, where as seen the pesticides can get in contact with drinking water due to their presence in the agricultural soils [7].

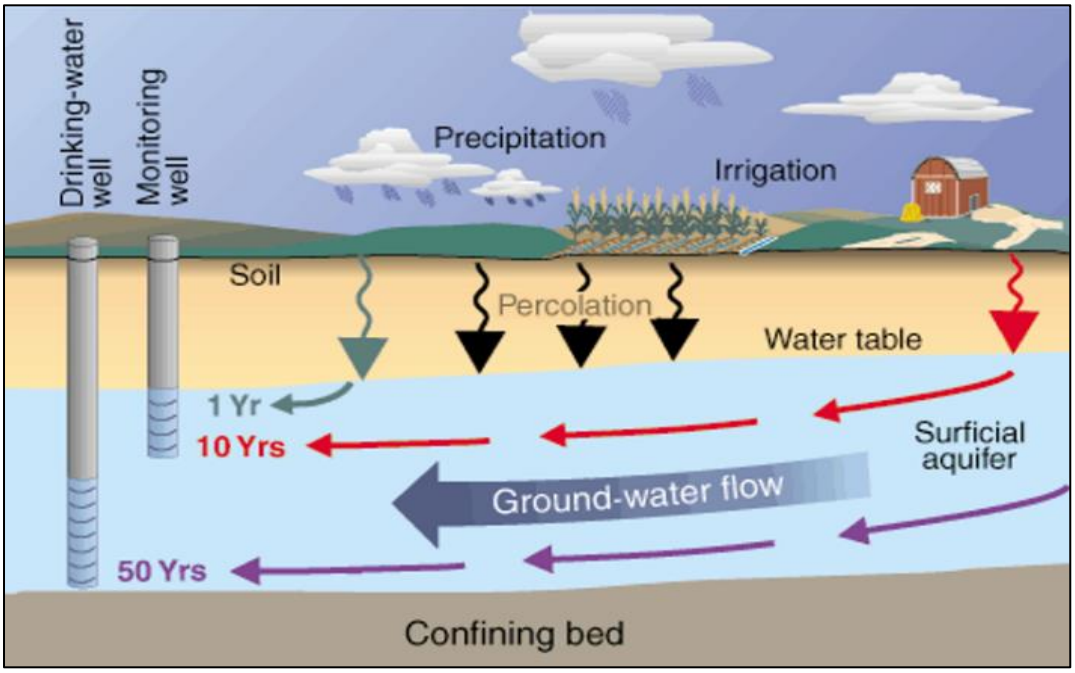

Figure 2. The pesticides cycle in the environment [7].

However, in the beginning when pesticides started to be used, their effect in the environment was not fully known. It was not well studied their mechanism and their degradation process. In the 1960s was discovered that due to the release of pesticides into the environment, they may have a negative impact on the ecosystem and human health, by indicating that their degradation products and their metabolites are really toxic and dangerous for the living organisms.

1.1.3. Isoproturon among other herbicides

There are approximately 150 herbicides active ingredients, which are formulated into hundreds of commercial products. Most are organic compounds and each herbicide has a chemical name that describes its structure and a common name, which is often a simplified version of the chemical name [8].

Isoproturon ISO (3-(4-isopropylphenyl)-1,1-dimethylurea or 3-*p*-cumenyl-1,1-dimethyl-urea) (Figure 3), is a colourless, odourless solid with a limited solubility in water (about 70 mg/L at 20 °C) [9], is soluble in most organic solvents, and it is stable to light, acids, and alkalis. Isoproturon is a herbicide belonging to the phenyl urea and amides group families, that is widely used to kill weeds in soils [10]. Recent studies indicated that isoproturon has become an ecosystem contaminant due to its intensive use [11]. In 2016, according to the rules established by WFD, the EU decided to ban its use [12]. Its hydrolysis is very slow and has a half-life of about 30 days in water while in soil its half-life is about 40 days, it can undergo some photochemical degradation to different metabolites.

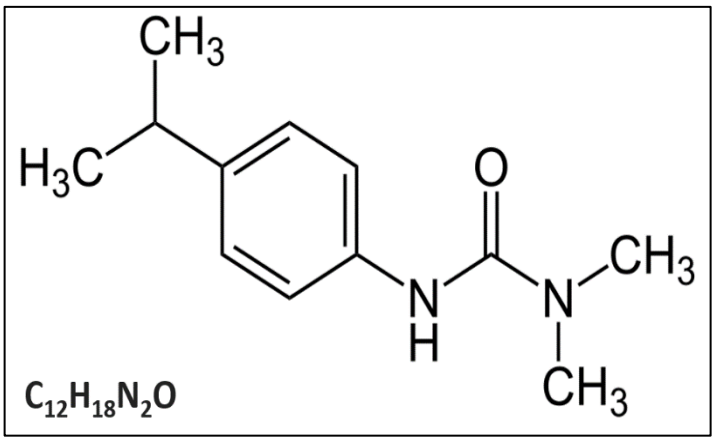

Figure 3. Isoproturon structure.

Isoproturon was found worldwide in soil, groundwater, surface water, or even in drinking water, exceeding the threshold values (e.g., the European Union threshold is 0.1 μg L^{-1} for inland surface water) [12]. Raw waters may become contaminated with isoproturon from production plant discharges and diffuse agricultural sources [12]. According to the World Health Organization (WHO), isoproturon has demonstrated toxicity to the liver system and appears to be a tumor promoter [13]. Considering its hazardous effects, the European Union (EU) has classified it as a priority micro-pollutant and has regulated its maximum level at 0.3 μg L^{-1} for inland surface waters [3].

Among other herbicides, isoproturon is one of the mostly used in agriculture. Some of others most commonly found herbicides are diuron, linuron, melamine, alachlor, atrazine, endothall, glyphosate and dacthal. These compounds were found to be toxic, and due to this the World Health Organization (WHO) and Water Framework Directive (WFD) have classified some of them as possible carcinogenic compounds [13].

1.1.3.1. Methods used for the determination of herbicides

Sensitive and specific methods are needed for the determination of phenyl urea herbicides in waters. Phenyl urea residues in food and water have been analyzed both by gas chromatography and by high-performance liquid chromatography (HPLC). GC methods usually do not allow analysis of intact phenyl urea herbicides due to their thermal instability – the HN-CO bond breaks, giving the corresponding aniline in the heated inlet [14]. HPLC separation with UV detection methods have been used for determination of phenyl urea herbicides in wastewater. Particle beam HPLC-MS has also been used for the determination of isoproturon and other pesticides, such as diuron, linuron, monuron, and siduron reaching relatively high detection limits between 2-30 μg/L [14]. Ruberu et al. 2000 developed a multiresidue HPLC method for determination of phenyl urea herbicides in water at sub part per billion (ppb) concentrations [14]. Dispersive liquid-liquid microextraction for the determination of 11 herbicides of urea derivatives family in natural waters, including isoproturon, by HPLC method was developed and detection limits vary from 0.4 – 0.04 μg/L [15].

However, these techniques, in spite of their high sensitivities, remain expensive and difficult to implement for on-site and *in-situ* analysis. In addition, onsite sampling and its treatment involves a longer analysis time and complex additional steps to overcome matrix effects and interferences [3], [12], [14]. There is an increasing need to ensure efficient and continuous on-site and *in-situ* monitoring of environmental waters, and to reduce the cost of analysis, which implies developing novel sensors. Efforts are thus ongoing to develop rapid and inexpensive sensing devices for detection of pesticides in general and particularly isoproturon.

Among all the conventional techniques, electrochemical analysis is one of the simplest and less expensive. Attempts to couple the classical methods with electrochemical ones have shown the improvement of the detection limits for herbicides from the concentration ranges of μg/L to ng/L [16]. Voltammetry based methods have been widely reported for the determination of many pesticides and isoproturon more specifically, by using various carbon electrode materials, such as: glassy carbon [17], [18], graphene [19], wall-jet glassy carbon electrode [20], carbon paste [21], carbon fiber [22], doped diamond [23], and multiwalled carbon nanotubes (MWCNT) [24].

More recently, numerous studies have focused on modified electrodes [25] and various assemblies have been investigated for applications in herbicide electrochemical sensors such as clay-modified GC electrodes [26], [27], or enzyme-modified [24], [28]–[30] and conducting polymer modified electrodes. The attachment of the organic film on the

electrode surface makes it possible to increase the sensitivity and the selectivity of these modified electrodes toward a targeted analyte. Electrochemical sensors for the detection of some of the most dangerous pesticides-herbicides, such as melamine [31], [32], atrazine [33], [34], alachlor [35], linuron [36], paraquat [37]–[45], diuron [46], and isoproturon [19], [26], [27], [47] have been made.

Among different strategies used for the modification of electrodes and for the preparation sensitive layers, electropolymerization of conducting polymer thin films on the surface of electrodes has been chosen to be as one of the best strategies. Until nowadays, still one of the most ingenious methods to achieve this goal is to prepare electrochemical sensors based on molecularly imprinted conducting polymers [48]–[50] that may be used for determination of isoproturon and other herbicides.

1.2. Definition of the chemical and electrochemical sensors

In general, a typical chemical sensor is a measurement device that can convert a chemical or physical information of a specific analyte into a measurable signal in the case of qualitative analysis, and that signal can be converted in concentration of the analyte with regard to quantitative analysis. A chemical sensor must contain the two necessary units a) a receptor and b) a transducer. The role of the receptor which is a selective unit of the chemical sensor, is to read the information and transform it into the form of energy that can be translated to a measurable signal by a transducer [51].

Given the huge number ($>10^6$) of known molecular substances, molecular sensing typically relies on recognition of molecular structure or associated reactivity. This recognition aspect is called selectivity. Sensitivity and limit of detection relate to the quantity or concentration of the chemical pollutant to be analyzed (the analyte). Chemical sensors are commonly required to detect 10^{-9} mol/L concentrations or less. Now a lot of standards for micropollutants is lower than 10^{-9} mol/L, a value very difficult to measure in real on-site analysis. Thus, the challenge of attaining the needed both sensitivity and selectivity in chemical sensing is a lock for the development of environmental sensors.

Depending on the nature of physical or chemical information, the receptor unit can be based on various principles:

- Physical – where are measured the physical properties of the analyte, such as absorbance, conductivity, temperature, mass change, etc [51].

- Chemical – where a chemical reaction is developed in order to produce the analytical signal, such as an electroreduction or electrooxidation of the analyte [51].
- Biochemical – where a biological response is converted into a quantifiable and processable signal, such as nuclei acids, cells, antibodies or enzymes as bioreceptors can be connected to Fireld Effect Transistor (FET) devices, nanowires, nanoparticles or electrodes helping to rise the signal and picked up by the transducer element [52].

In Figure 4, is presented the classification of different types of the chemical sensors, based on the nature of the transduction principle.

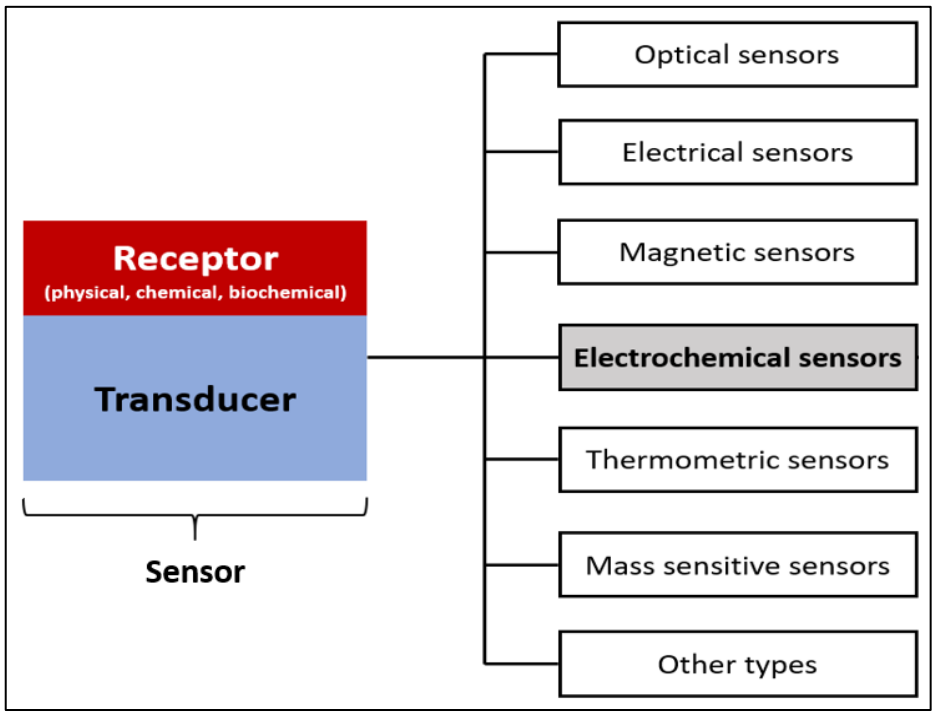

Figure 4. Classification of sensors in different types.

Electrochemical sensors, in particular, are a class of chemical sensors in which an electrode is used as a transducer element in the presence of an analyte. Electrochemical sensors are devices which can transform the electrochemical information into a measurable signal. In these sensors, electrochemical reactions occur on the electrode surface which is in contact with an electrolyte. An electrochemical sensor is presented schematically in Figure 5, the interactions between analyte and receptor take place at the surface of the working electrode, which plays the role of a receptor and a transducer

in the same time. Electrode is connected to a recording electronic equipment, usually to a potentiostat/galvanostat and where its signal is read out.

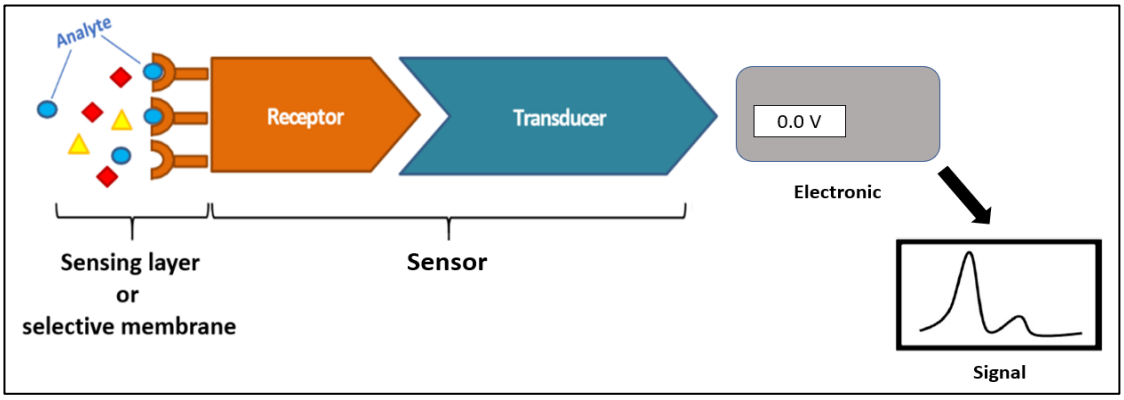

Figure 5. Schematically representation of a typical electrochemical sensor.

Electrochemical sensors are classified into three different types based on their working principle and electrochemical transduction mode: potentiometric, conductometric and amperometric/voltammetric.

Potentiometric sensors – are sensing devices that can measure the difference of the potential between a sample solution (containing dissolved ions) and a reference solution separated with a membrane which contains some ionophores that are selective to the targeted ions. This difference in the potential is related to the activity of the ions which are passed through the ionophores of the selective membrane. The measurement of this difference in the potential is usually done under zero current conditions or at a given value of the current intensity and can be calculated by using the Nernst equation:

$$E = E0 + \frac{R\,T}{z\,F}\ln\frac{a\,(ox)}{a\,(red)} \quad \ldots\ldots\ldots (1.1)$$

-where:
E: measured potential,
E°: standard potential,
R: gas constant,
T: absolute temperature,
F: Faraday constant,
n: number of the electrons involved in the redox process,
a(ox) and *a(red):* are the activities of the oxidized and the reduced species.

There exist different basic types of potentiometric sensors: ion-selective electrodes (ISEs), coated wire electrodes (CWEs), field effect transistors (IS-FETs) and chemical field effect transistors (CHEM-FETs) [53]. Two last categories of these sensors have

generated great interest due to their small size and facile miniaturization, fast response and good adherence to substrate surface. They have however two major drawbacks: the first one is that they show a thermal instability so their response signal is strictly related on temperature; and the second one is the membrane potential which is affected by the adsorption of solution components [54]. Furthermore, potentiometric sensors showed poor reproducibility and weak stability in the arrays, and they can detect only free ions and require frequent calibration [54].

Conductometric sensors – they are two-electrode devices designed to measure the conductivity of the thin electrolyte layer adjacent to the electrode surface [55]. These sensors are usually used for detection of gaseous samples, and sometimes for the liquid samples as well. The modification process during the fabrication of conductometric sensors includes organic materials such as conductive polymers or inorganic materials such as metal oxides [56]. In conductometry, the electrical conductivity of a sample containing dissolved ions, is used to measure the concentration of the ions. However, conductivity measurements are difficult, due to the variable ionic background of the samples and the relatively small conductivity changes that are observed in high ionic strength solutions. Moreover, these devices cannot be implemented to determine the concentration of the targeted molecule ions, but are used for the classical analysis of water and give information about the overall concentration in ions.

Amperometric/voltammetric sensors – these sensing devices can be used to measure the current (A) which is produced as result of an electron transfer reaction while the applied potential in the working electrode is controlled with a potentiostat/galvanostat [57]. So, the signal transduction process is accomplished by monitoring this current as a function of time. The electrochemical reaction occurs at the working electrode due to the electron transfer between the analyte (ion or molecule ions) and the receptor (electrode surface).

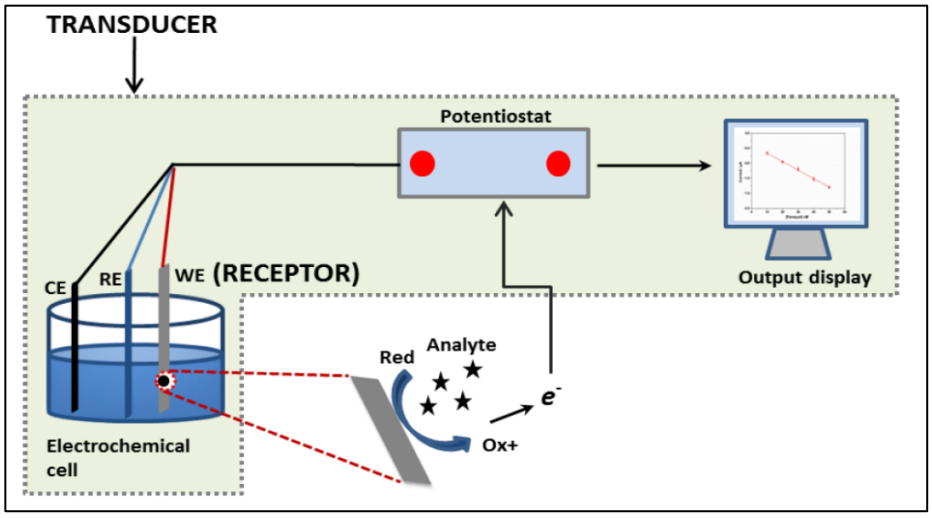

Figure 6. Schematic representation of a typical amperometric/voltammetric sensing system [58].

In the case of amperometric/voltammetric sensing system, the potential can be kept constant (potentiostatic) where only the changes in current with time I=f(t) are measured, or it can be scanned in a certain potential range (potentiodynamic) where is measured the current change with potential I=f(V). The basic instrumentation for amperometric/voltammetric sensing system is presented schematically in Figure 6, includes a potentiostat and three electrodes (working, reference and counter) dipped in a suitable electrolyte to form an electrochemical cell.

Electron transfer reactions are the most important processes at electrochemical interfaces [58]. They are determined by the interplay between the interaction of the reactant with the solvent and the electronic levels of the electrode surface [59]. Based on this, the performance of an amperometric sensor is strongly influenced by the working electrode material. In the very beginning, mercury electrode was used as a very attractive material for electrodes, because it has an extended cathodic potential range window, high reproducibility and a renewable surface [60]. However, the limited anodic potential of mercury electrodes and especially their toxicity are the principal disadvantages that to limit their use [60]. These electrodes are replaced, later on, with solid electrodes (e.g. Carbon, Pt, Au, Ag, Ni, Fe) which have been extensively used as electrode materials because of their higher potential windows, low back ground currents, chemical inertness, and suitability for various sensing and detection applications [61]. The miniaturization of the working electrodes has gained much attention where microelectrodes (ME) and ultra microelectrodes (UME) have started to be widely used [62]. Furthermore, were developed the chemically modified electrodes (CME) that result from the immobilization of an organic layer onto the electrode surface through chemical reaction, chemisorption, composite formation or polymer coating [48]. These systems possess many applications, including for instance: the development of electrocatalytic systems with high chemical selectivity and electroactivity, the coating of semiconducting electrodes with anticorrosive properties, electrochromic displays, microelectrochemical devices and electrochemical sensors. One of the common approaches for CME is to use a polymer-based interface. Most polymers are applied to electrode surfaces by a combination of adsorptive attraction and low solubility in the electrolyte solution, using pre-formed polymers or electrochemical polymerization [48]. Also, different types of inorganic films, such as metal oxide or metal ferrocyanide can also be formed onto electrode surface [56].

In this thesis work, two kinds of working electrodes have been used, the classical glassy carbon electrode (GCE) presented in the Chapter 3 and 4, and the graphene electrode presented in the Chapter 5 of the manuscript. The amperometric sensors have series of advantages, such as a low limit of detection (10^{-9}–10^{-13} g/L), high selectivity of micropollutants in several kind of samples, in food stuff or in biological liquids, small volume of the cell (0.1–5 μl), the simplicity of design, and low cost, making these devices widely used [63].

1.3. Conducting polymers (CPs)

1.3.1. Generality about CPs

1.3.1.1. Introduction to conducting polymers

Conducting polymers (CPs) represent a group of polymers that inside their structure contain conjugated systems where the motion of delocalized electrons occurs. The electronic conjugation between each repeat unit in CPs creates semiconducting molecular wire architectures that makes possible to impart CPs with interesting optical and electronic properties [64]. Figure 7 presents the conjugated structure of few conjugated polymers [65]. This structure made CPs to be very useful materials by providing the advantages of chemical diversity, low density, flexibility, corrosion resistance, easy-to-control shape and morphology, and tunable conductivity over their existing inorganic counterparts [66].

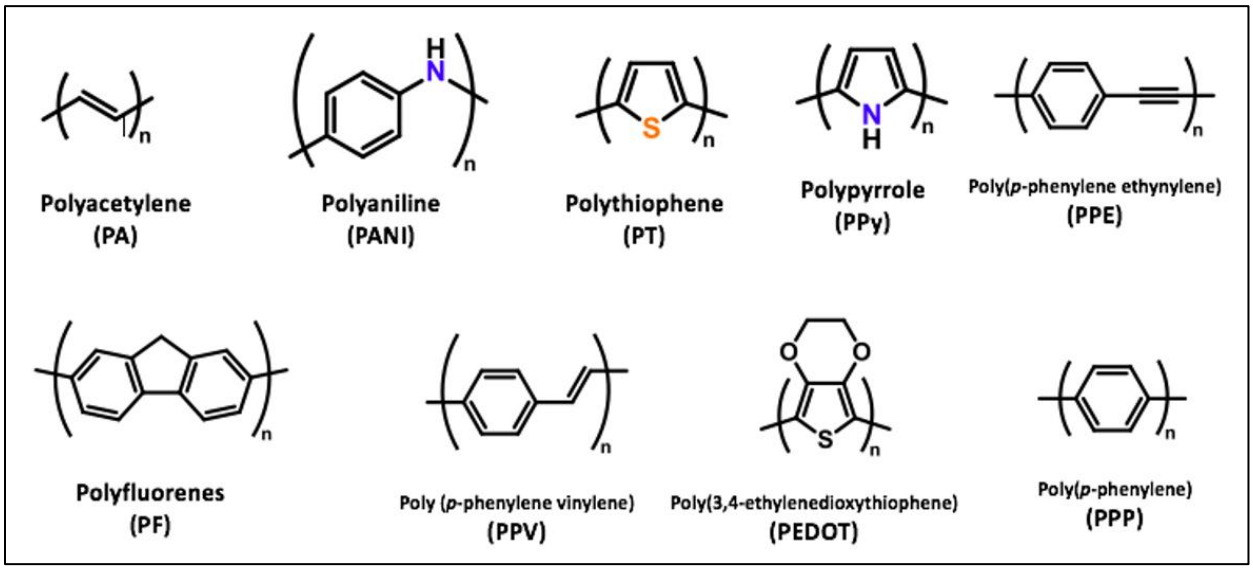

Figure 7. Different π-conjugated structures of CPs [65].

In the case of insulating saturated polymers, for example the polyethylene (-CH_2-CH_2-)n, each carbon atom has sp^3 hybridized and forms σ bonds with neighboring atoms, where there are no free charges capable for moving along the chain of the polymer. Conjugated polymers are derived from the regular repetition of monomers containing π electrons. The chemical structure of CPs is different from that of other polymers, where each carbon atom of the chain is bonded with three other atoms, and always there is one free electron that remains per each carbon atom. These electrons form π bonds which

are placed in ***pz*** orbitals. In conjugated polymers, the two types of bonds co-exist: single bonds or type σ, ensuring the cohesion of the carbon skeleton in the same way as in saturated polymers and double bonds or type π, responsible for the rigidity of polymers and limiting their solubility. So, a polymer can be conductive due to the presence of π conjugated bonds in its structure. There are different types of conducting polymers that have been extensively investigated for practical applications; and the most prominent types of CPs are polyacetylene (PA), polyphenylene (PP), polypyrrole (PPy), polythiophene (PT), polyaniline (PANI), poly (phenylene-vinylene) (PPV), and their derivatives [64].

The modern development of conducting polymers has begun in 1977, when for the first time was discovered that doping polyacetylene (PA) with iodine endowed the polymer with metal-like properties, producing copper-colored films with an increase of conductivity of 10 orders of magnitude [67]. This invention can be described as a revival of conducting polymers since 1862, when Henry Letheby prepared polyaniline by anodic aniline oxidation, and concluded it was conductive and had electrical properties [68]. PA was not stable and it was easily destroyed by oxidative degradation [67], and due to this numerous other conductive organic polymers have begun being synthesized. The abovementioned organic conducting polymers with heterocyclic structures have received great attention because of their potential applications in electronic displays.

1.3.1.2. Preparation of CPs

The most common method used for synthesizing CPs is the chemical (or electrochemical) oxidation of a conjugated monomer (oxidative polymerization). During the chemical oxidation the monomers are oxidized to radical cations (CR) in the presence, for example of Fe (III) salts, and after their interaction via a mechanism CR-CR they lead to the production of a CPs, most often in the doped state (generally in the form of a powder insoluble and infusible) [69]. Using this method, the conductivity of these CPs hardly exceeds a few tens of S/cm. Other very conductive thin films can be prepared by oxidative chemical polymerization using tosylate ferric pre-deposited on a substrate, with a controlled supply of the vapor phase monomer. Conductivities widely greater than 1000 S/cm could thus be achieved in the case of polypyrrole (PPy) and polythiophene (PTh), including in particular poly (3,4-ethylenedioxythiophene) (PEDOT) [69].

Oxidative polymerization can also be carried out electrochemically using a three-electrode system, where it can be possible to deposit conducting polymer thin films with controlled thickness on any conductive substrate, knowing that the thickness of

the deposited film is generally proportional to the quantity of electricity used during the polymerization (Figure 8).

Three main modes of electropolymerization can be implemented: i) The potentiodynamic mode [70] - developed by cyclic voltammetry during the scanning the potential of the electrode on which the polymer is deposited within a potential domain where the monomer is oxidized and gradually transformed into a polymer. The growing polymer film continuously changes from its neutral state to its doped (or conducting) state as the potential is swept back and forth. This process is accompanied by the continuous absorption and desorption of the electrolyte and the solvent to stabilize the growing film.

ii) The potentiostatic mode [71] – made by imposing a constant potential slightly higher than the oxidation potential of the monomer to drive its polymerization. In this case, the variation of the current is followed as a function of time. Polypyrrole films polymerized using potentiostatic electropolymerization (and also by galvanostatic electropolymerization) are of dendritic type and have low adhesion strength on the substrate. In contrast, when the polypyrrole is polymerized potentiodynamically, the resulting film is shiny black, adheres strongly on the substrate, and has a smooth and homogenous surface morphology. This has been explained as due to the formation of a large number of equivalent nucleation sites during the growth process. On the other hand, poly(3-methylthiophene) films showed better electrical properties (conductivity, charge mobility, number of free carriers, and band gap) when polymerized potentiostatically than when polymerized potentiodynamically.

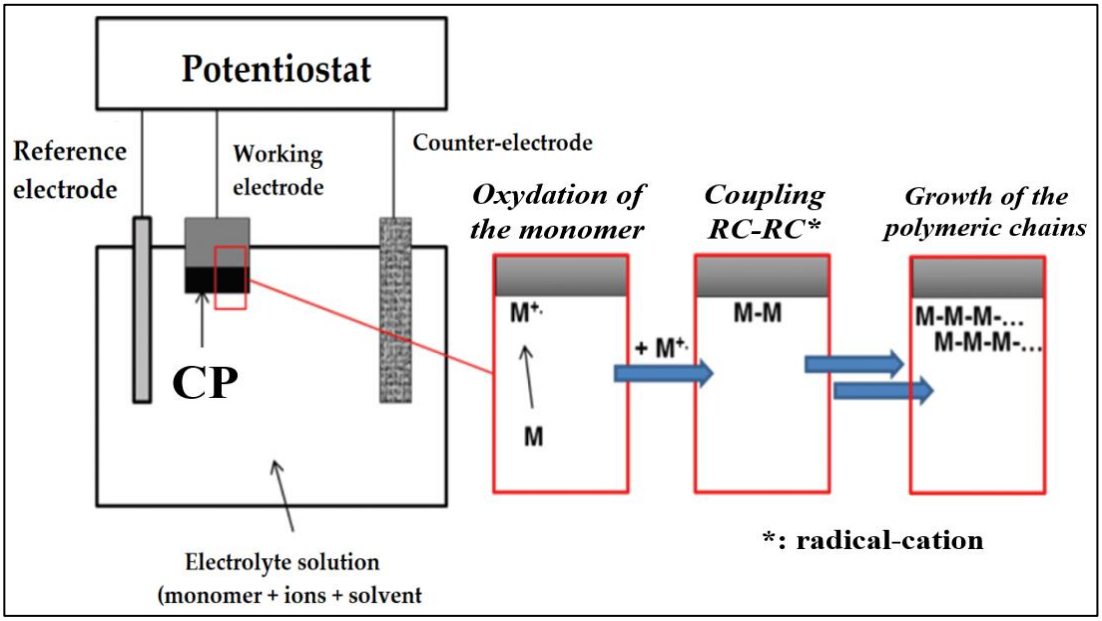

Figure 8. Electropolymerization of a conjugated monomer [69].

iii) The intentiostatic mode (or galvanostatic) [71] - is developed by imposing a constant anode current to oxidize and polymerize the monomer. Here is followed the variation of the potential of the electrode on which the polymer is deposited with time of electropolymerization. At the beginning of the electropolymerization, the potential rises for a short period and then decreases after a while. It has been explained that the sudden increase in potential is brought about by the formation of the redox-active charged oligomers in front of the electrode. The subsequent decrease in the potential is brought about by the catalytic effect of the charged oligomers to oxidize the monomers.

Each of these methods presents advantages and disadvantages, in particular for the control of the morphology and roughness of the deposited polymeric film [69]. The intentiostatic mode can be particularly advantageous to limit the formation of structural defects. In fact, by imposing a very low current and operating the polymerization at temperature below 0°C, the reaction kinetics are reduced at a level low enough to improve regularity of the sequences of the monomer units to each other. Due to the good structural regularity obtained, the electronic conductivity of the polymer formed is higher. It can be interesting to replace a conjugated monomer with one of its oligomers (dimer or trimer) which are more easily oxidizable may have some advantages. Indeed, the chemical or electrochemical polymerization will require the use of conditions for softer oxidation, by limiting the risk of overoxidation of the polymer. In order to illustrate this point, we can quote the example of thiophene which oxidizes at a high potential (+1.6 V vs. SCE), while its dimer and trimer will oxidize at a lower potential of around +0.3 and +0.5 V [69].

Finally, many chemical or electrochemical polymerizations use a reducing coupling mechanism. The principle of this synthesis is to activate chemically (or electrochemically) the C-X bond (where X is often halogen) of a conjugated monomer of type X- (π) -X to lead directly to the polymer - $(\pi)_n$ - in the neutral state [72]. This method can eliminate faults structural defects since the linkages occur exclusively at the level of C-X bonds, the only reactive sites growing monomer or chains. It has been shown also that various polythiophenes substituted by an aliphatic chain (C_nH_{2n+1} with n variant from 2 to 12) in position 3, allowed to increase the conductivity up to a factor of 100 when switching between sequences irregular head-to-head or tail-to-tail sequences regular head to tail.

1.3.1.3. Properties and applications of the conducting polymers

Conducting polymers have unique electrical and physico-chemical properties. Due to the low hydrogen content and aromatic structure, they show excellent chemical,

thermal, and oxidative stability and are practically insoluble in all common solvents [73]. They are also potentially electrical conducting materials, particularly when doped [66]. CPs provide the advantages of chemical diversity, low density, flexibility, good mechanical and optical properties, corrosion resistance, easy to control shape and morphology, and tunable conductivity [66], [74]. CPs also possess light weight enabling them to be used as replacement for metals, particularly in weight-sensitive applications [74]. Due to their good properties, CPs have attracted attention to be used as electroconductive materials due to their inexpensive and their easy way preparation nature. From the many applications of conducting polymers have, here we highlight some of the most important ones, such as thin film transistors [75], polymer light emitting diodes (LEDs) [76], corrosion resistance [77], electromagnetic shielding [78], electrochemical sensing technology [48], supercapacitors [79], and in biosensors [64], batteries, conductive textiles and fabrics, mechanical actuators, anti-static coatings and drug delivery systems [80].

Recently a good combination between conducting polymers and carbon-based materials, such as activated carbons (ACs) [81], carbon nanotubes (CNTs) [82], and graphene sheets (GS) [83], are widely used electrodes, due to the desirable physical and chemical properties that these coupled materials have shown. These properties include low cost, variety of form (powders, fibers, aerogels, composites, sheets, monoliths, tubes, etc.), ease of processability, relatively inert electrochemistry, controllable porosity and electrocatalytic active sites for a variety of redox reactions. CPs can be employed for the fabrication of sensors in two ways: (i) as transduction or sensing materials and (ii) as an immobilization matrix [64]. The basic strategy towards the design of conducting polymer based chemical sensors for molecules, ions and biomolecules (in the gaseous or solution) is to generate a measurable signal. This is achieved by connecting a molecular recognition site that uses a conducting polymer as a receptor with a signal receiving/transducing unit in such a way that a binding event between the conducting polymer and target analyte changes the properties of the conducting polymer. The redox or electronic state of the conducting polymer is modulated by interactions with the analyte and the signal generated can be quantified as the sensor response [48]. In general, the use of conducting polymers as the molecular recognition receptor allows various types of signals to be assessed. So, conducting polymer-based sensors can be formulated in different transduction modes that can be divided into a few main classes depending on the operating principle, including amperometric, potentiometric, conductometric, calorimetric, fluorometric, magnetic and gravimetric, etc [84]. Since the introduction of these materials, there has been an interest in their commercialization. Many companies in the world started to produce various electronic devices, from diodes and transistors to solar cells. So, for a very short time conducting polymers have managed to occupy a very important place in modern technology [85].

1.3.2. Conductivity of CPs

1.3.2.1. Conduction modes of CPs

The electrical conductivity of a material is mainly determined by its electronic structure. From an electronic point of view, materials are classified into three categories: insulators, semiconductors and conductors. The energy band theory is a useful way to visualize the differences among these three different kinds of materials. The band gap is the energy difference between the valence and conduction bands of a material. When the valence band overlaps the conduction band, the valence electrons are free to move and propagate in the conduction band. This classification is based on the width of the gap between the valence (VB) and conduction (CB) bands and the position of the Fermi level which can be defined as the highest electron occupied energy level of a material, whilst the material temperature level is at 0 K [86] (Figure 9). Indeed, the dynamics of electrons in materials lead to define a structure of energy levels grouped into energy bands. This structure results from the interaction of the wave function of electrons with the potential of the nucleus [87].

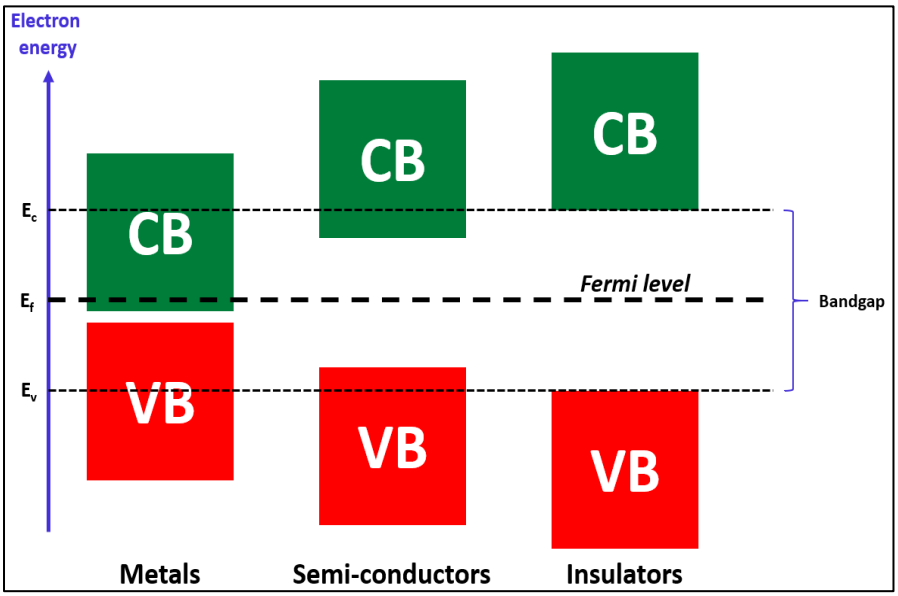

Figure 9. Band structures for the three different categories of materials.

The valence band corresponds to a band filled with electrons (saturated), and the electrons which fill this band participate in the bonds between the atoms or are bound to atomic nuclei. The upper energy band is called the conduction band, it has at least partially unoccupied energy levels which enable electronic conduction. Between these two bands there is not any other energy level therefore that difference is called bandgap or forbidden band. Its value defines material electrical properties. Metals show a very

low bandgap value and the Fermi level is at the region of conduction band, that enable the permanent presence of free electrons responsible for increased current conduction. On the other hand, in an insulator, the bandgap value is high (of the order of 10 eV), therefore if one electron wants to go at higher level, conduction band, it requires at least that quantity of energy to overcome the energy barrier. Semiconductors constitute an intermediate state that has a low bandgap value (of the order of 1 to 2 eV) and the electrons need only a small portion of energy to make the transition into conduction band (see Figure 9) [69].

In the case of CPs, conjugation leads to the fusion of the energy levels, resulting in a band structure similar to that of inorganic semiconductors. This band structure explains the singular behavior of CPs, which are semi-conductors in the neutral state and become electron conductors in the presence of an oxidant; they are positively doped (p). Different environment conditions will lead to different energy states, partially localized and comparable to a conduction band [69].

1.3.2.2. Doping of CPs

To make a conjugated polymer conductive, it is necessary to perform doping. This doping is generally carried out by oxidation reaction (p type) or reduction (n type) [69]. Doping makes it possible to accentuate very strongly the delocalization of the electronic charges, thus the new electronic formed structure allows the displacement by jumping of the charges along the carbon chain and the polymer becomes a conductor.

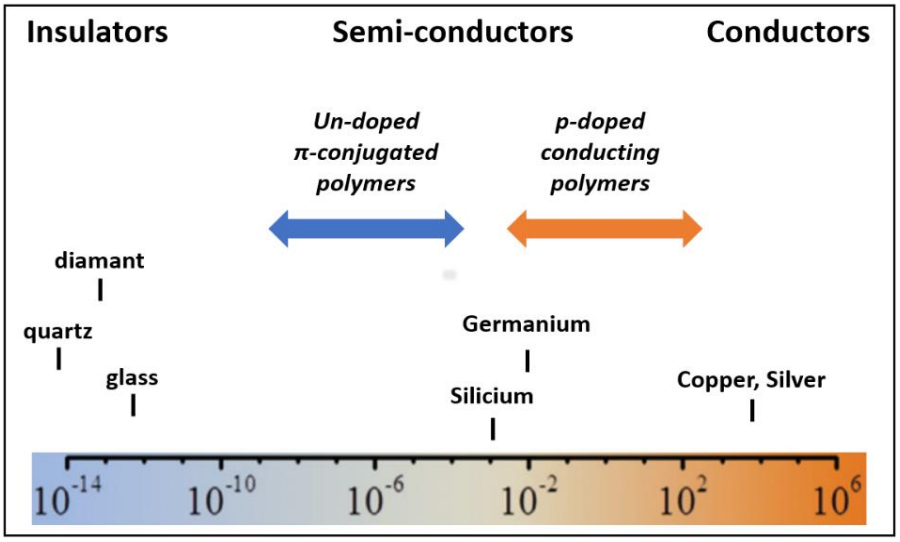

Figure 10. Conductivity (in S/cm) of CPs in their neutral states or doped compared to those of some insulating materials, semiconductors or conductors [69].

The conductivity of doped CPs depends on the length of conjugation, the type of doping and the doping rate. The conductivity of doped and undoped CPs can therefore be comparable to that of other materials (Figure 10).

Among all the CPs, the maximum conductivity reported to date is of the order of 10^7 S/m which is comparable to that of copper (5.7×10^7 S/m). This record was reached with Polyacetylene (PA) by N. Theophilou et al. in 1987 [88]. Despite its high conductivity, PA is not a good candidate to compete with metals, because it is a very unstable material when it is in contact with air. Dopants, oxidants or chemical reducers, can be small ions, for example I^{3-}, or Na^+, or also more large polymeric species, such as "poly electrolytes" which contain sulfonate groups.

Doping of CPs can be achieved in different ways, such as chemical doping, photo doping, non-redox doping, charge-injection doping and electrochemical doping [66]. Each of these methods shows its advantages and disadvantages. Electrochemically doping can be achieved when an amount of current is passed through the material and doping level can be controlled easily by using an electrochemical cell which controls the amount of current passed, and also doping/de-doping is highly reversible so clean polymer can be retrieved, and it can be achieved with many dopant species. Its disadvantage is that during the electrochemical doping process unexpected structural distortion may cause electrical conductivity decay of the material [66].

1.3.3. Polypyrrole (PPy) as a conducting polymer (CPPy)

1.3.3.1. Presentation of PPy

Among numerous conducting polymers, polypyrrole (PPy) is by far the most extensively studied [89], which is considered as the first synthesized conducting polymer [90]. PPy is a heterocyclic and positively charged conducting polymer that contains nitrogen in its oxidized form, and it loses its conductivity and charge when overoxidation occurred. Besides, PPy is electroactive in organic electrolyte and aqueous solutions and it is known for its nontoxic and biocompatibility [74].

Polypyrrole is one of the most extensively used conducting polymer in design of analytical, bioanalytical and electrochemical sensors as well as for other purposes [48]. Versatility of this polymer is determined by its unique properties, such as redox activity [91], ion-exchange and ion discrimination capacities [92] [93], electrochromic effect depending on electrochemical polymerization conditions and charge/discharge

processes [94], strong absorptive properties toward gases [95], proteins [96], DNA [97], catalytic activity [98], corrosion protection properties [99], etc. Most of these properties are depending on the synthesis procedure as well as on the dopant nature [48].

Moreover, PPy has attracted more attention due to its ease of polymerization, high conductivity and relative chemical stability and also it has an important option of wide range of modulation of its electrical properties. Early research for the different chemical methods used for the synthesis of polypyrrole can be found at [100]–[103].

1.3.3.2. Electrochemical polymerization of polypyrrole versus chemical polymerization

Two major ways are applied for polypyrrole synthesis which are based on induction of polymerization by different factors: (i) chemical initiations by oxidative agents [104] (Figure 11-A), (ii) electrochemical activation by anodic current [105] (Figure 11-B).

(i) Chemical or even biochemical methods enable an easy preparation of PPy particles of different and/or controlled size ranging from several nanometers up to several micrometers containing various inclusions. Moreover, by chemical methods it is possible to uniformly perform overoxidation of polypyrrole and to increase its stability. The polypyrrole is mainly produced in the bulk solution and just some amount of synthesized polypyrrole covers the surface of induced materials, meaning that chemical induced method is not very efficient when deposition of PPy over some surfaces is required. Moreover, polypyrrole prepared by chemical polymerization is almost insoluble in usual solvents because of strong inter-chain interactions [74]. However, the major disadvantage for the use of this method of deposition for designing of polypyrrole chains is a poor adherence of this deposit to the surface of induced materials, contrary to the film obtained by electrochemical polymerization.

(ii) Disadvantages of chemical activation could be avoided if electrochemical polymerization is applied. It allows deposition of PPy over electrodes connected to the electrochemical cell. That is the reason why electrochemical polymerization has found an application as a general deposition when thin PPy layers are requested. By electrochemical polymerization of PPy, thickness and morphology of deposited film could be controlled by application of well-defined potential and known current passing through the electrochemical cell [106]. This method of deposition can be performed in various aqueous and nonaqueous solvents (eg. ethanol, water, acetonitrile, etc). It is very important that PPy synthesis might be performed from water solution at neutral

pH, since it opens the ways for entrapment and/or doping of polypyrrole by various organic molecules.

Moreover, during electrochemical polymerization using larger potential excursion range, the overoxidation of PPy films happens. This behavior of PPy enables the molecules and/or dopants to be entrapped and/or extracted from the polymeric films, and in such cases so called molecularly imprinted polymers may be designed [74]. Furthermore, electrochemically synthesized polypyrrole has some attractive properties, such as good conductivity and very high adherence of these films leading sufficient stability for sensors application. So, there is no doubt that this polymerization method is extremely useful for deposition of PPy thin films on conductive surfaces.

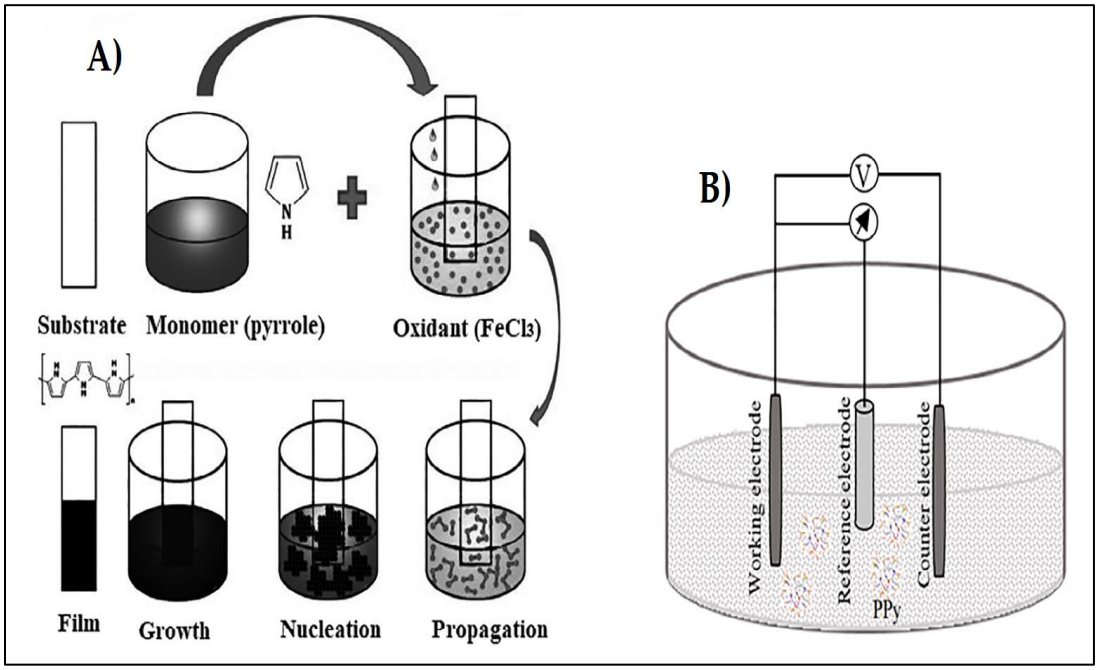

Figure 11. A) Chemical polymerization of polypyrrole, B) Electrochemical polymerization of polypyrrole [74].

1.3.3.3. Mechanism of pyrrole electropolymerization

In an electrochemical polymerization, the monomer, dissolved in an appropriate solvent containing the desired anionic doping salt, is oxidized at the surface of an electrode by application of an anodic potential. The choice of the solvent and electrolyte is of particular importance in electrochemistry since both of them should be stable at the oxidation potential of the monomer and provide an ionically conductive medium. Since

pyrrole has a relatively low oxidation potential, electropolymerization can be carried out in aqueous solutions which is not possible for thiophene or benzene, see Sadki *et al.* 2000 [107].

The electrochemical polymerization methods of pyrrole proceed in three recurrent steps following the mechanism (Figure 12) proposed initially by Diaz et al. [108] which is the most commonly cited in the literature:

a) The first step involves the oxidation of monomer and the formation of a radical cation $R^{+\bullet}$ by oxidation of the pyrrole monomer at the surface of the electrode. Radical cations $R^{+\bullet}$ can be found in several resonance forms [107], and they can undergo different reactions depending on their reactivity. When $R^{+\bullet}$ is relatively stable, it can easily diffuse into the bulk solution and is susceptible to react with other species to form soluble products with low molecular weights, but when $R^{+\bullet}$ is very unstable, it can immediately react at the vicinity of the electrode surface with the solvent or the anion forming soluble products of low molecular weight, and $R^{+\bullet}$ of moderate time living are prone to undergo dimerization reactions.

b) the second step is kinetically decisive, consists in anoxidative coupling to form a dimer (CR-CR). This step is obtained when two radical cations $R^{+\bullet}$ having a greater unpaired electron density in the α-positions dimerize between themselves forming the dimer.

c) the third step represents the loss of two protons that leads to give back the aromaticity to the dimer. Then the dimer oxidizes and creates its radical cation that further undergoes the reaction with a cation radical. Thus, the chain polymer formation happens due to the propagation of reaction sequences where electrochemical and chemical processes take place until the oligomer chains become insoluble and are deposited on the surface of the electrode.

The oxidation potential of the monomer is higher than that of pyrrole oligomers because the unpaired electron of the radical cation that follows the oxidation is more easily delocalized between two or more pyrrole rings [107]. The polymerization of the pyrrole leads to an acidification of the electrolytic medium in the vicinity of the electrode. PPy is always obtained in oxidized form, i.e. in the p doped state, as its oxidation potential is lower than that of pyrrole. The dopant, which ensures electrical neutrality, is an anion that comes from the electrolyte if the PPy is obtained by electropolymerization or from the chemical oxidant in the case of chemical polymerization.

Electropolymerization pyrrole is influenced by several experimental parameters such pH or electrolyte [107]. It has been shown that polypyrrole can be easy polymerized

onto inoxidable metal electrodes, such as platinum or gold, and on carbon electrodes by using electrochemical methods under controlled conditions [107]. The electrodeposited polypyrrole films showed high mechanical stability and strong adhesion to the metal electrode surface, making polypyrrole a good candidate which can be used as an organic conductive electrode material [109].

Diaz mechanism for PPy electrochemical synthesis is considered to be the best one due to several reasons such as the elimination of the two protons from the α-position that induces the drop in pH value of the solution during polymerization [107], and the number of electrons that are needed for the oxidation of pyrrole molecule. This number normally is 2 but in practice it is generally higher due to the polymer oxidation. This number has been determined experimentally for pyrrole and varies from 2.25 to 2.33 [107]. Furthermore, the measurement of changes in the optical absorption during the electropolymerization of pyrrole have shown a linear growth of the film with the time and not with it square root value indicating that the slowest step is the radical cation coupling and not the monomer diffusion towards the electrode [110].

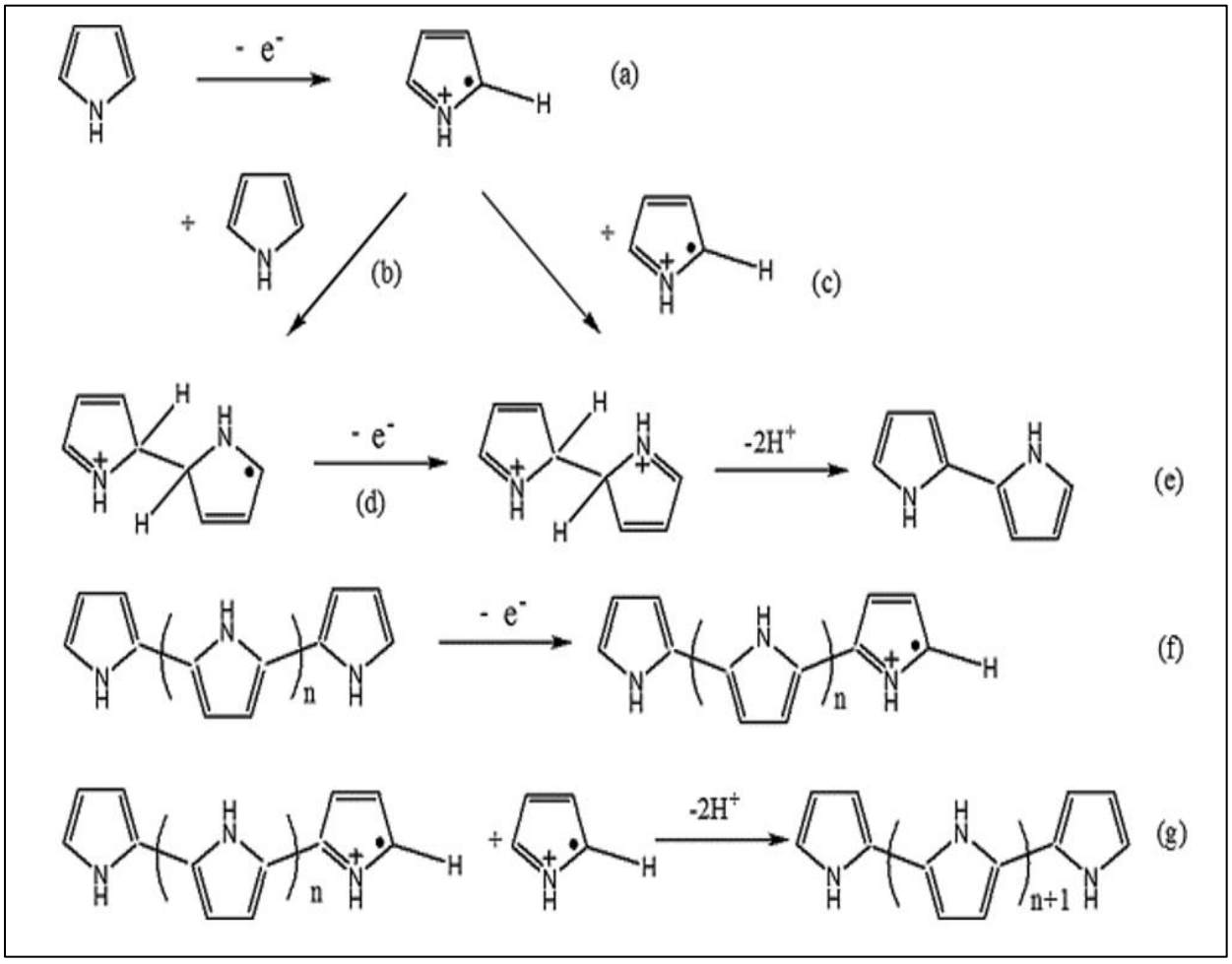

Figure 12. Electropolymerization of pyrrole by Diaz, a radical coupling mechanism [107].

1.3.3.4. Electrical conductivity of PPy

The structure of polypyrrole contains the π-conjugated bonds which are extended to polymeric chains, and thanks to them the electrons flows through the material. However, undoped polypyrrole acts as an insulator, and it must be doped in order to become a conductive material [111]. In p doped conducting polymers when electrons are removed from the oligomer chain are created polarons that induce intrinsic electrical conductivity, and the anion dopant ions are incorporated into the film to create a charge balance. Polarons as charge carriers are transferred in fully conjugated polymers [112]. As result, the polypyrrole cannot stay always in the same structure as presented in Figure 13. Electronic properties of polypyrrole structure that change with doping process were the first investigated among of CPs [110]. Figure 14-a presents the neutral form of polypyrrole, where the gap energy distance between the valence band and conduction band is high, 3.16 eV. The removal of π electrons from the valence bands of neutral PPy occurs under the oxidation conditions that generates some radical cations or polarons in the PPy chains due to a local transformation of benzoid structure to that of quinoid [113], [114]. Formation of charge carriers induces two new electronic energy levels (Figure 14-b) that are symmetrically positioned within the bandgap. If further oxidation of the polypyrrole continues with the removal of second electron, bipolarons are generated, that leads to two other electronic levels of low energy absorptions due to the transitions from the top of the valence band (Figure 14-c). Further oxidation of polypyrrole makes possible the bipolaronic energy state overlaps and forms bipolaronic bands close together (Figure 14-d). These processes provide a better and higher conductivity properties of polypyrrole as conducting polymeric material.

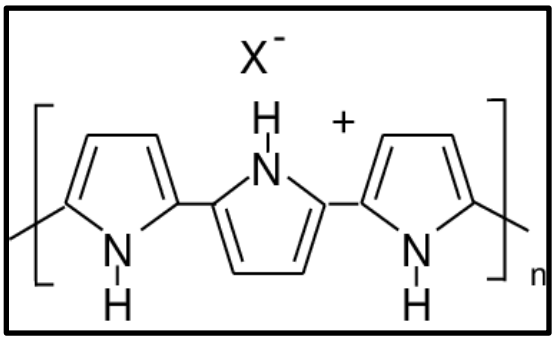

Figure 13. Polypyrrole structure with π conjugated double bonds.

Overoxidation is an electrochemical oxidative degradation process of a conducting polymer under an anodic applied potential [115]. Polypyrrole is overoxidized upon a high level of oxidation reaction which may be chemically, physically or electrochemically initiated. Electrochemically initiated PPy overoxidation leads to the reversible and/or irreversible processes. When the PPy film are obtained by electropolymerization of aqueous solution of pyrrole containing 1M KNO_3 on Pt electrode at any potentials more positive than +0.4V vs SCE reference electrode, the irreversible oxidation of polypyrrole occurs [116]. The overoxidation of the polymer

causes loss of electron mobility, as oxidation at more positive potentials can interrupt conjugation by forming of hydroxyl (-OH) and carbonyl (-CO) groups, and eventually loss of the material due to the formation of (CO_2). It is well known also that in the presence of solvents where the hydroxide ions (OH^-) may be dissolved, such as in the alkaline aqueous solutions, polypyrrole can become easily overoxidized due to nucleophilic attack of hydroxide ions to the polymer producing 3-hydroxy-pyrrole, and that loss of electroactive capacity due to breakdown of electronic conjugation ensues as further oxidation to pyrrolinone occurs [117].

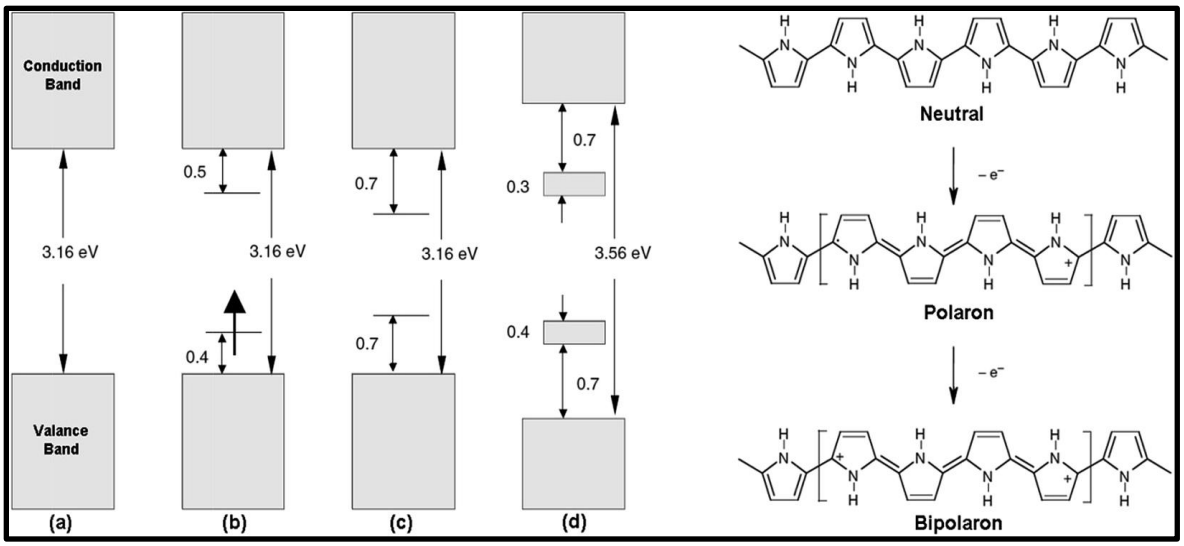

Figure 14. Electronic energy diagrams and structures for (a) neutral PPy, (b) polaron, (c) bipolaron, and (d) fully doped PPy [66].

In Figure 15, is presented the overoxidation reaction of polypyrrole [118] leading to the modification and degradation of almost all of the beneficial features of polypyrrole, such conductivity, charge storage ability, electrochromism electroactivity, conjugation, mechanical properties and adhesion to the substrate [115]. However, for the use of PPy in sensor technology, the process of overoxidation is most frequently applied, which can exhibits an improved selectivity attributed to the removal of positive charges from PPy films due to introduction of oxygen functionality, such as carbonyl groups [48].

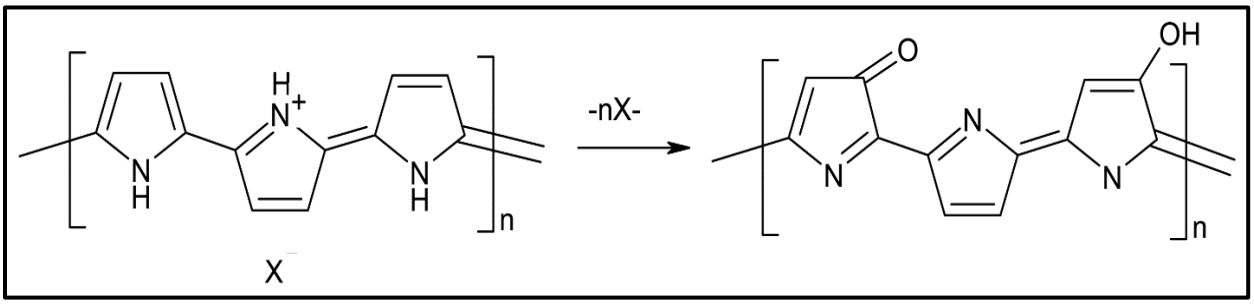

Figure 15. The overoxidation reaction of polypyrrole [118].

1.3.3.5. Properties and applications of PPy

PPy properties such as high electronic conductivity, very good thermal and chemical stability in air and aqueous media are widely used for many purposes. Figure 16 presents some of the general forms of PPy and their applications. PPy is electroactive in organic electrolyte and aqueous solutions [119], and also it is known for its nontoxicity properties [120].

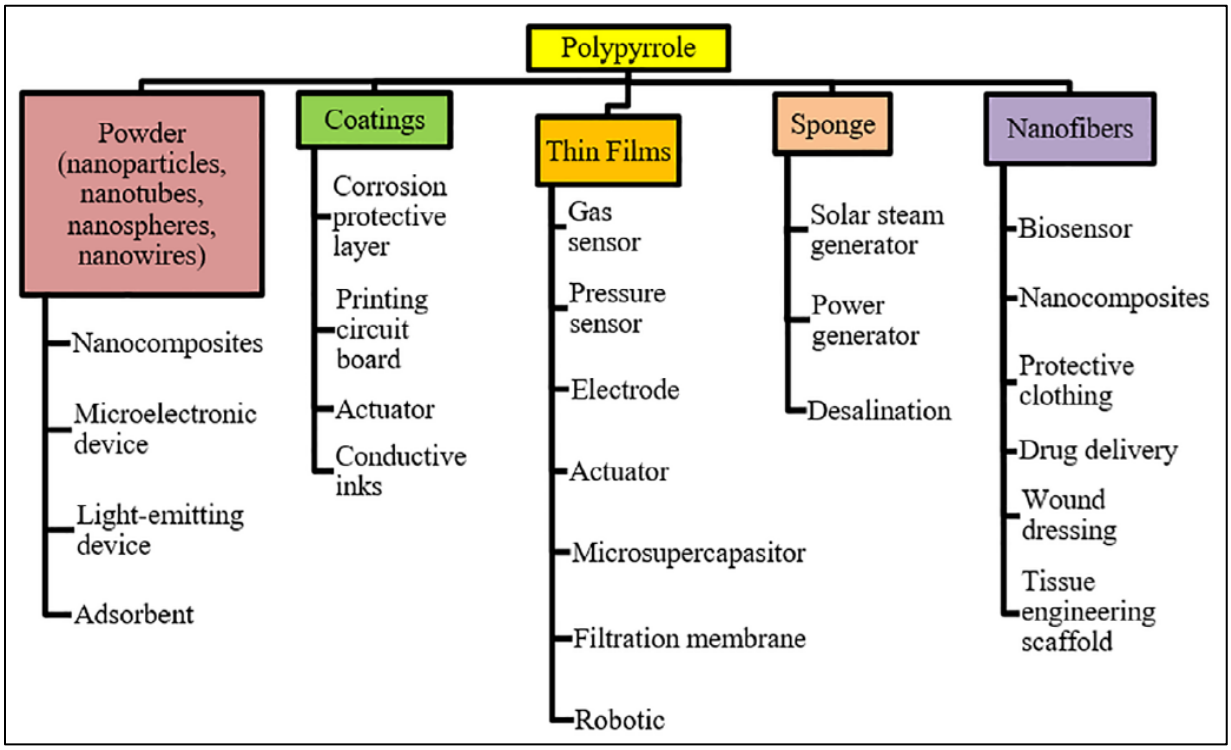

Figure 16. General forms of PPy and their applications [74].

Owing to the good properties of PPy, such as mechanical stability, compact materials, environmental stability and good electrical conductivity [64], many reports and articles about this material have been published during the last decade [74] (Figure 17A). PPy was considered as one of the best candidates for modern materials and for commercial and industrial applications. Mechanical and chemical stability of polypyrrole can be improved due to ability of polypyrrole chains to be embedded in a polymeric matrix forming composite materials [121]. The mechanical stability of the polymeric matrix influences the chain relaxation and thus the stability of the electrical conductivity of the polypyrrole composites. Despite the tremendous number of published papers on polypyrrole and its composites, relatively few papers concentrate systematically on the stability of the electrical conductivity of polypyrrole and its composites under different conditions. In fact, the stability of the electrical conductivity is very important for the industrial application of PPy and its composites. Among these good properties of

polypyrrole, it has also some advantages related to its fabrication methods, where is important to point that polypyrrole can be fabricated easily through either by an oxidatively chemical or electrochemical polymerization [112].

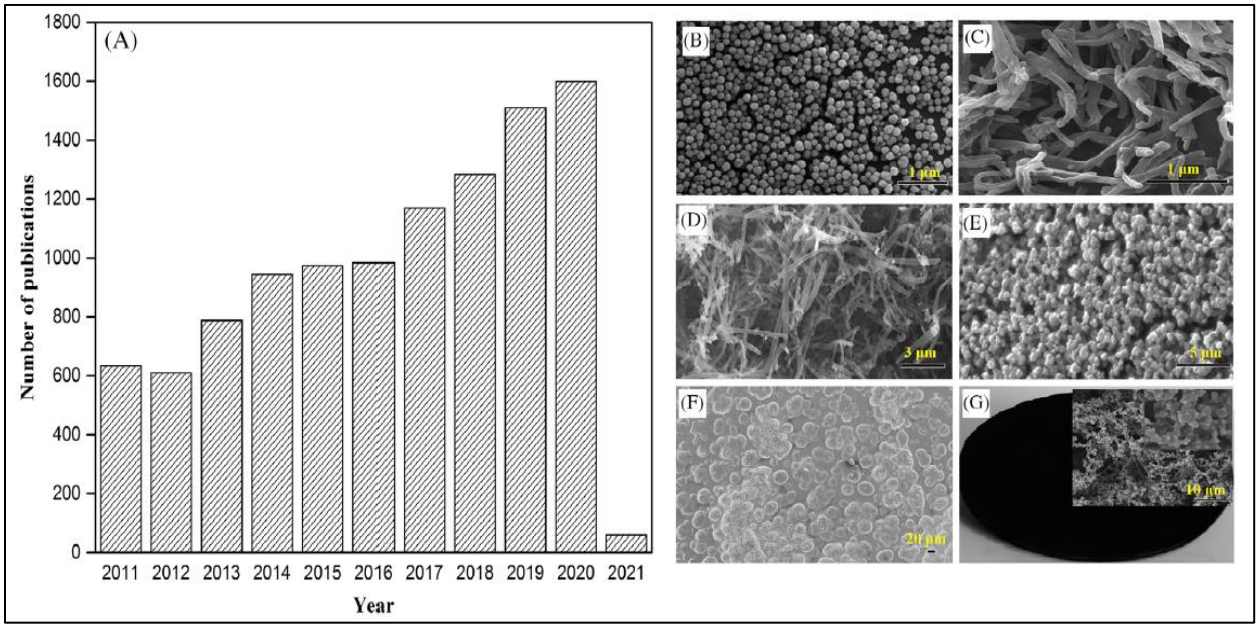

Figure 17. (A) Annual number of scientific publications related to PPy based on Elsevier data analysis as of 7th September 2020, and (B–G) SEM micrographs of PPy with different morphologies, that is, nanoparticle, nanotube, nanofiber, thin film, thick film, and sponge-like structure, respectively [74].

Figure 17-B-G represents the scanning electron microscope (SEM) micrographs of PPy at different form with different morphologies obtained from different conditions, such as nanoparticle (17-B) [122], nanotube (17-C) [123], nanofiber (17-D) [124], thin film (17E) [125], thick film (17-F) [126], and spong-like structure (17-G) [127].

PPy has shown lot of applications in different fields, such as solid electrolytic capacitators [128] [104], nano wires [129], microactuators [130], antielectrostatic coatings and corrosion protectors [131], biosensors [48] [64] [132] [133], gas sensors [134] [135], electronic devices and functional membranes [64], etc. Nowadays polypyrrole becomes one of the major tools for nanotechnological applications. In our interest are the applications of PPy for sensing electrodes.

1.3.3.6. PPy for sensor applications

Recently, numerous studies have been focused in the modification of the materials for generation of selectively electrochemical sensors and for that issue, electropolymerization of

CPs, especially of PPy, is one of the easiest way to develop modification of the electrodes with thin polymeric films [4], for sensing applications [31], [33], [83], [136]–[147], due to the good mechanical and environmental stability, and a simply and low cost experimental apparatus preparation [110], [70].

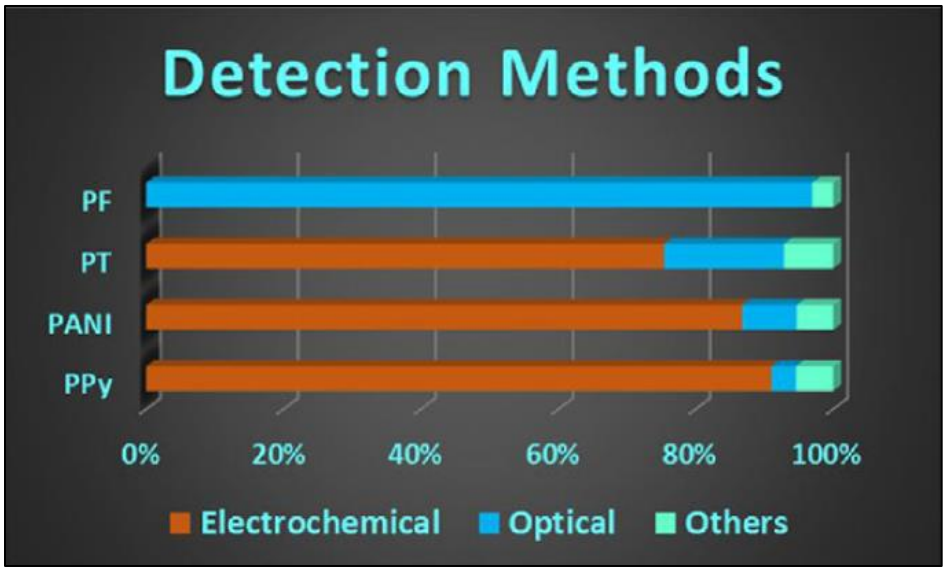

Figure 18. Comprehensive details of CPs-based sensors for different signal transduction modes [64].

The histogram presented in Figure 18 shows the dispersion of applications of different CPs for MIP sensing devices [64]. Polyfluorenes (PF) applications are mainly dominated for optical MIP sensors. Polythiophenes (PT), polyaniline (PANI), and PPy applications were dominated for electrochemical MIP sensing devices, where PPy stands as the most widely used conducting polymer. However, the use of different types of CPs provided nowadays to have in disposition many kinds of electrochemical MIPs sensors that could be used to the detection of different types of targeted molecules and reach very low limits of detection, and which may be good candidates for sensing devices challenging more sophisticated and expensive techniques used so far for the detection of targeted molecules.

In Table 1 are presented some data found in literature for the applications of the PPy nanocomposites in analytical chemistry for the fabrication of electrochemical sensors of different materials used for detection of various environmental pollutant molecules.

In these examples, PPy is used as the conductive matrix of the composite electrodes. However, in a large number of publications concerning sensor applications, PPy is often used as MIP to selectively capture the analyte. The application of polypyrrole and other

conducting polymers for MIP sensor fabrication will be discussed in the following sections.

Table 1. Electrochemical sensors-biosensors based on Polypyrrole-Nanocomposites (PNCs) modified electrodes.

Sensor material	Analyte	Detection limit	Sample	Reference
PA-PPy-GO-GCE	Cd (II), Pb (II)	213 μgL^{-1} 0.41 μgL^{-1}	Tap water	[148]
PPy-CNSs-SPE	Hg (II) Pb (II)	0.0214 nM 0.0041 nM	Real water	[149]
GR-PPy-CS-GCE	Nitrite	0.1 μM	River and lake water	[150]
PPy-PGE	Zn^{2+}	8 x 10^{-6}M	Water	[151]
PPy-SDS-SPE	Fe^{2+}	8.8 x 10^{-7}M	River water	[152]
PA-PPy-GCE	Cu^{2+}	3.33 μgL^{-1}	Real water	[129]
PPy-g-NGE-GCE	Paraquat	41 - 58 nM	Ground and lake water	[153]

Abbreviations for the Table 1: PA-phytic acid, **PPy**-polypyrrole, **GO**-graphene oxide, **GCE**-glassy carbon electrode, **CNSs**-carbonaceous nanospheres, **SPE**-screen printed electrode, **GR**-graphene, **CS**-chitosan, **PGE**-pencil graphite electrode, **SDS**-sodium dodecyl sulfate, **-g**-grafted, **NGE**-nitrogen-doped graphene electrode.

1.4. Molecularly imprinted polymers (MIPs)

1.4.1. Introduction to Molecularly Imprinted Polymers (MIPs)

The term imprinting polymer appeared for the first time in 1984 [154]. The Molecularly Imprinted Polymers (MIPs) contain some recognition sites that are complementary in shape, size and functional groups to a specific chemical targeted molecule [143]. These cavities are created by an imprinting process involving the "template" molecule inside the polymer structure. The template molecule plays the most important role during the preparation process of the MIPs acting as a coordination center in a complex formation with the "functional monomers" which act as ligands containing electronegative functional groups (e.g. hydroxyl groups) that allow for dipole-dipole interactions or hydrogen bonding with the template molecule [53], [145]. The interactions between the template molecule and the functional groups of the growing polymer are formed during the polymerization process (Figure 19). During the polymerization step, the functional monomers become locked in place, creating binding sites around each template molecule [155]. In a second step just after the polymerization, the template molecules which have been embedded should be extracted from the polymer matrix. The removal of the template molecules leads then to the formation of some cavities. These cavities have the shape and size of the template molecule and are able to create reversible selective interactions with it. The process of extraction can be achieved by using a suitable physical, chemical or electrochemical method [64].

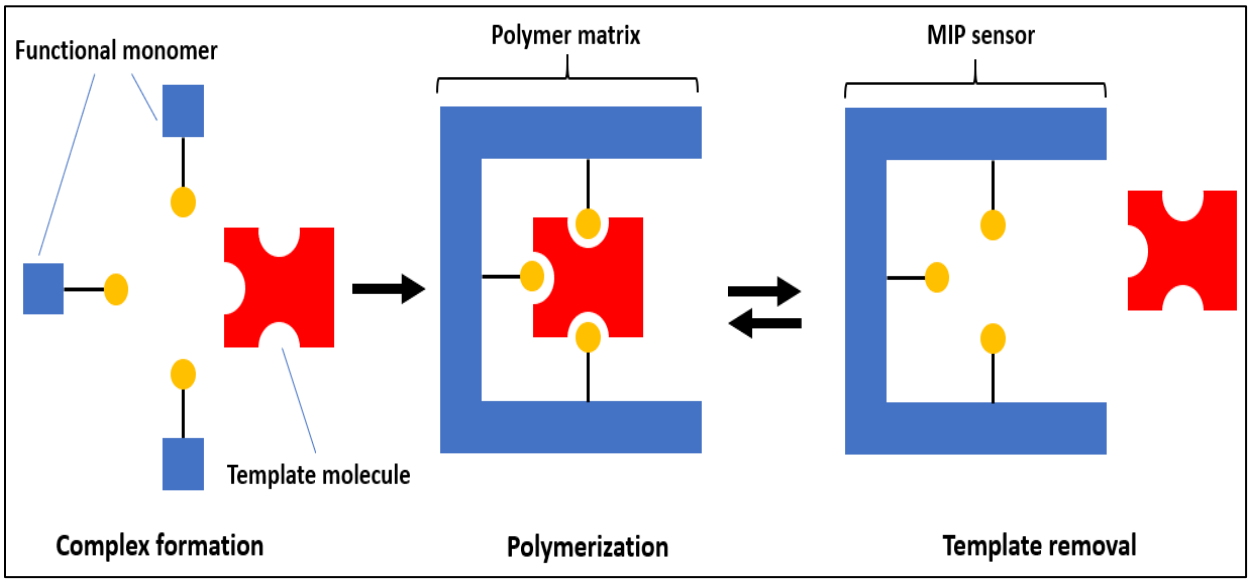

Figure 19. Schematic representation of the molecular imprinting process, where functional monomers form a complex around the template molecule to form the MIPs with the creation of binding sites.

1.4.2. General concepts of MIPs

Molecular recognition is a very common process in nature, that is triggered mainly by many non-covalent interactions such as ionic interactions, hydrogen bonding, van der Waals forces, and hydrophobic effects [64]. This phenomenon is expressed by the formation of an energetically favorable complex between the template molecule and the polymer on the basis of electrostatic and stereochemical complementarity. The principle of MIPs is based on "lock and key" concept, an analogy for molecular recognition in catalyzed enzyme reactions [64]. So, in the case of molecularly imprinted polymers the "lock" is the polymer film matrix, whereas the targeted molecule is the "key".

There is a quite high number of published papers mostly about MIPs but also NIPs (Non-Imprinted Polymers) in order to compare the difference that imparts in MIP films the presence of the cavities. NIPs are fabricated always in the same procedure as MIPs, but in absence of the template molecule, therefore at the end of the NIPs fabrication process, the polymer matrix and theoretically NIPs cannot recognize the targeted molecules due to the lack of its imprints. The extraction mechanism is a main problem mentioned in the literature concerning MIPs performance because the presence of un extracted templates molecules within the polymer matrix caused confusion during the recognition step [53]. The extraction process depends on the nature of the targeted molecule and the nature of the polymer matrix.

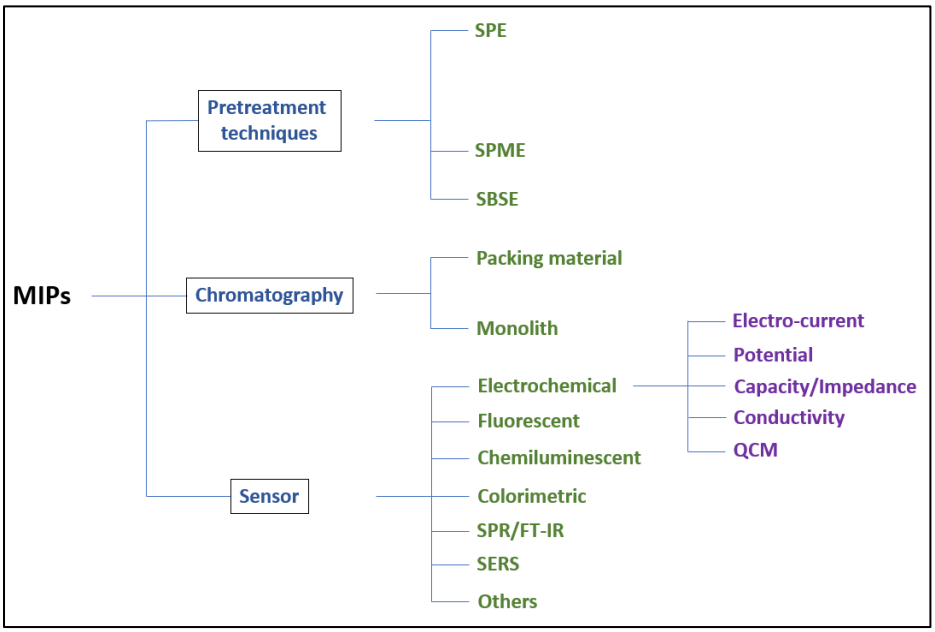

Figure 20. Diagram of the classification of MIPs based on their role in pretreatment techniques, chromatography and sensor. Abbreviations: SPE, solid phase extraction; DSPE, dispersive SPE; MSPD, matrix solid phase dispersion; SPME, solid phase microextraction; SBSE, stir bar sorption extraction; QCM, quartz crystal microbalance [158].

MIP applications are mainly oriented towards analysis: pre-treatment techniques, chromatography and sensors. First practical use of MIPs at commercial level was introduced for molecular separation applications. Later, in the 21st century the use of MIP to environmental molecular sensing has considerably raised and was attested by a tenfold increase of published papers [53]. Nevertheless, the number of applications for sensing issues remain still lower that for separation [156]. In Figure 20, is presented schematically the diagram of MIPs classification according to their applications. They can be used as devices for pretreatment techniques, chromatography methods and sensors. Samples of pretreatment techniques, especially those for trace/ultratrace level analytes, need to be preconcentrated or converted into optimal forms prior to their experimental analysis, therefore the choice of the adequate sample pretreatment technique plays an important role in qualitative and quantitative determination [157].

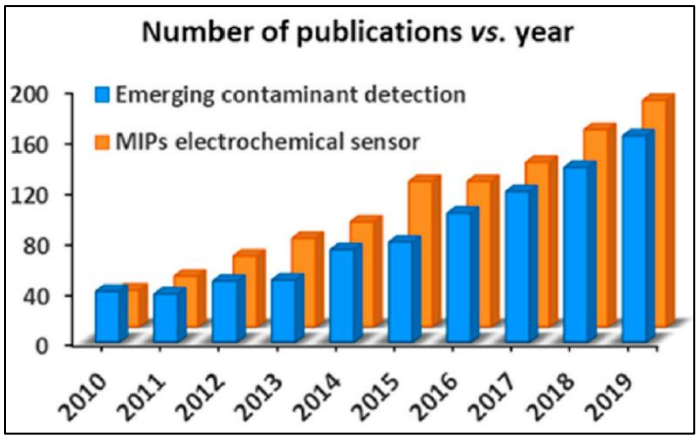

Figure 21. Evolution of publications regarding MIP-based electrochemical sensors and emerging contaminant detection in the last 10 years [159].

MIPs in principle show their very high affinity towards target template molecules and therefore are prone to act as selective sorbent materials in the pretreatment techniques, such as solid phase extraction (SPE), solid phase microextraction (SPME) and stir bar sorption extraction (SBSE) which are frequently used for extraction of wide variety of compounds [157]. The existence of very specific interactions between the target analyte and the polymer matrix enables the use of MIPs as stationary phases in chromatography techniques, such as HPLC, capillary electrochromatography (CEC), capillary LC (CLC), and thin layer chromatography (TLC). Only in the last decade, the development of MIP-based electrochemical sensors has exploded as well as the concern about emerging contaminants (see Figure 21), and combining MIPs and electrochemical sensing strategies has shown great potential to benefit environmental pollution control [158]. In this manuscript throughout different chapters, we will describe the MIPs used as sensor devices, and more attention is paid to their application as electrochemical sensors.

1.4.3. The preparation methods of MIPs

Several techniques have been examined in literature for the preparation of MIP powders or films. There are several MIPs fabrication methods as follows: (a) electrochemical or chemical MIPs synthesis from monomers in the presence of the template [159], (b) phase inversion that enables polymer precipitation by addition of non-solvent or by solvent evaporation from a solution of polymer plus template [156], and (c) soft lithography or surface stamping for large molecule sensing [160], which are less often used. The choice of the polymerization method is a very important step, that makes possible a better understanding of the form, size and structure of the generated MIP films.

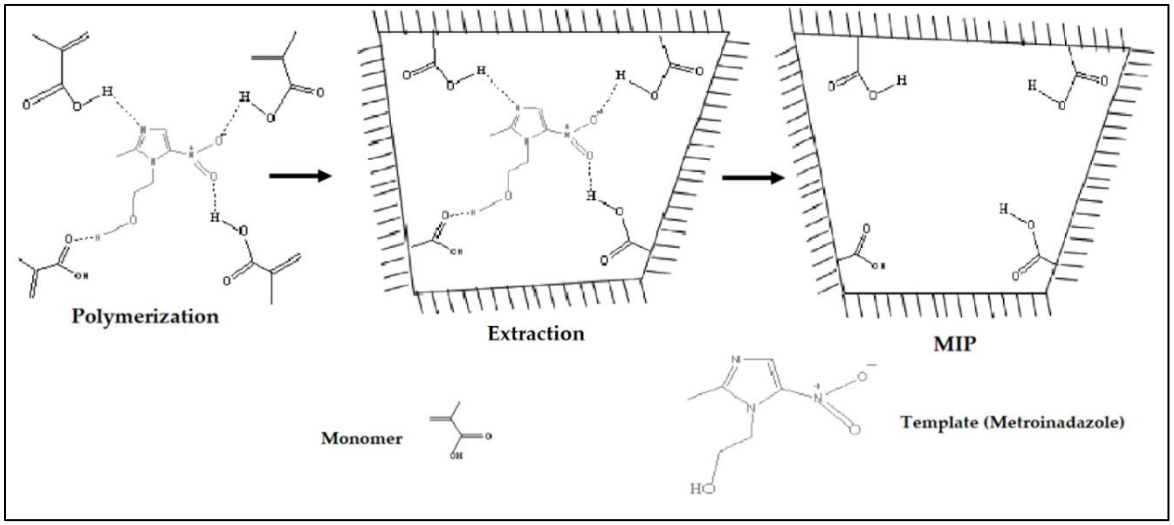

Figure 22. Synthesis production of MIPs. The three steps followed dissolving or mixing of all the components, polymerization and extraction [160].

The most spread method for MIP preparation is synthesis which enables the specific interaction of a monomer with the target molecule in solution and the creation of a network of covalently or noncovalently interacting species [156]. The suitable monomer makes possible, for example, the creation of hydrogen bonding functionality that assures a covalent bond between the polymer and the template. Some common functional monomers used are acrylamide [161], methyl methacrylate (MMA) [162], methacrylic acid (MAA) [163], aniline [164], and pyrrole [165]. Initiation of chemical polymerization of functional monomers in the presence of a cross-linking agent and a polymerization initiator as chemical species is made by heating or by radiation. This assemblage facilitate the start of polymerization reaction for MIP synthesis [159]. In Figure 22, is presented a typically example, where for the preparation of a MIP targeted

to metroindazole, 1- (2-hydroxyethyl) – 2 – methyl – 5 – nitroimidazole, used to target protozoan infections. Prior to synthesis process, all the needed components, including the template, the functional monomer MAA, the EGDMA cross-linker, and the AIBN initiator, are dissolved in the DMF porogen solvent heated for 24 hours. A cross-linker is used to form a cross-linked rigid polymer even after the removal of templates, whereas porogenic solvents generally act as dispersion media and pore forming agents in the polymerization process [157]. After grinding and sieving, Soxhlet extraction is used to remove the template, leaving behind binding cavities. However, the polymerization method is not suitable due to long time procedures and the use of various toxic chemicals. MIPs can be synthesized by different polymerization methods, such as bulk polymerization [166], precipitation polymerization [167], suspension polymerization [168], [169], emulsion polymerization [167], and electropolymerization [53], [64].

Electropolymerization method is the most widely used for the preparation of MIPs applied to electrochemical sensors [53], [64], because they have superior properties on adherence to the transducer surface, as well as simplicity and speed of preparation. Electropolymerization is also more friendly environmental way than the chemical one. Moreover, it provides easy control of the film thickness and morphology, high reproducibility, and enables polymer synthesis in aqueous solution. The procedure is quite simple and is achieved in an electrochemical cell containing the solution of monomer, template and supporting electrolyte. The monomer is oxidized on the surface of an electrode used as working electrode by applying an anodic potential or current [165], see Figure 23.

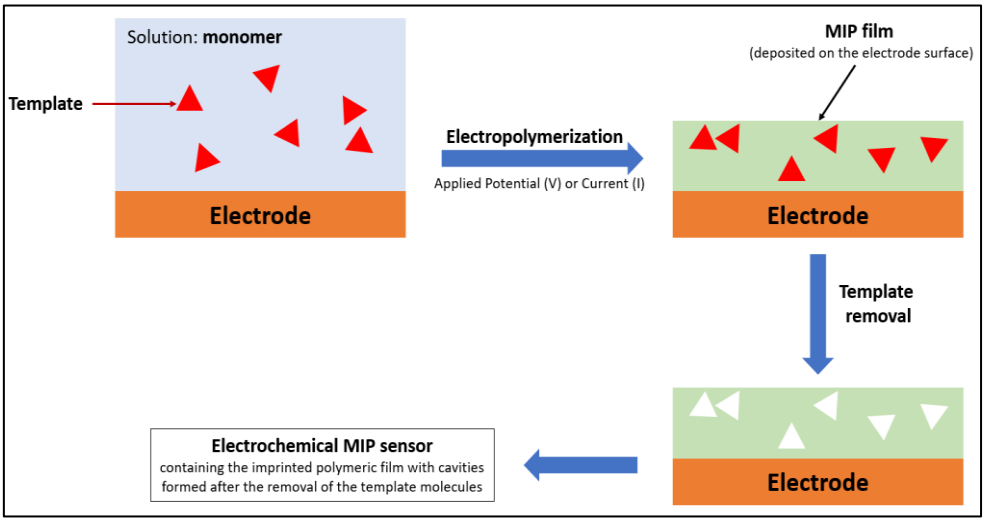

Figure 23. Schematic representation of electrochemical polymerization process of MIP film on the surface of electrode.

After a certain polymerization time, the electrode is coated with the resulting conductive polymeric film which is attached to the surface of the electrode and plays the role of imprinted material [53], [64]. Metals (Cu, Fe, Au, Pt), carbon materials (GC, CNTs, Graphene) or composite conductive materials are usually used as working electrodes. Polyaniline is used for the preparation MIPs [170], but the most studied polymer is clearly polypyrrole.

The twin objectives for a sensor are high specificity and high sensitivity and may be achieved by combining the concept of molecularly imprinted polymers with the use of conducting polymers [33]. To do that it is important to describe how molecular imprinted conducting polymers (MICPs) can act as transducers for the selective recognition and real-time determination of targeted molecules. Electrochemical synthesis of MICPs sensors, is affected by different factors, such as the morphology, doping levels and porosity of the resulting polymeric materials. These parameters may influence directly to the selectivity of the target and sensitivity of the sensing process [64]. The increased polymer conductivity originate from charge carriers generated by oxidation (p-doping) or by reduction (n-doping) [33]. When p-doping occurs for the conducting polymers, such as PPy, polarons and bipolarons positive charges carried by the polymer backbones are counterbalanced by negative charges carried by dopant anions [33], [64]. Therefore, the properties of a PPy film, are dependent on the dopant and the electropolymerization conditions [66]. The size and characteristics of the dopant ions influence the sensor properties, and the polymer network spacing as generated by the presence into the polymer matrix of dopant ions controls the porosity of CPs [33]. The matrix structure of an electropolymerized PPy film facilitates the doping with specific ions by entrapping the dopants in the film during its deposition onto an electrode surface.

Overoxidation of PPy film make it more porous and therefore increase the detection performance for small target molecules due to the increase of surface area. The presence of oxygen rich groups like carbonyl and carboxyl in the polymer film, induced by overoxidation, increase the hydrophilic properties of the sensor and the permeability [64]. In addition, target molecules susceptible to create hydrogen bonds may form easily MIPs with pyrrole because its nitrogen atom is donor and acceptor of hydrogen atom and facilitate the interaction between atoms of binding sites of the target unit and atoms of recognition sites of the MIP [171]. Further, when template contains unsaturated carbon bonds, π-π interactions between the MIP and the template increase the selectivity of the sensor due to the stabilization of dispersive interactions between them [171].

1.5. Electrochemical MIP-sensors for environmental analysis

There are different types of electrochemical MIP-based sensors which are based on various electrochemical transduction mode techniques. These transduction techniques represent the most basic measurement methods for sensor implementation with MIP recognition polymers. They are based on e.g. field-effect transistors, chemiresistors or amperometric, voltametric, impedimetric, capacitive and conductometric readout principles [172]. Electrochemical MIP-based sensors are extremely powerful and have shown to capable of analyzing samples in all phases, though gaseous and liquid samples are preferable [173]. Except conducting polymers [48], carbon nano-tubes and metallic nanoparticles have been accepted as methods for incorporating of MIP sensors for environmental analysis [173].

Most conductometric-impedimetric methods for MIP sensing applications found in the literature involve gas-phase sample analysis [156], [173]. These methods include capacitive sensors, chemoresistors, field-effect transistors and electrochemical impedance spectroscopy. However, to date only a limit number of MIP-based conductometric sensors have been developed [174], [175]. Furthermore, quartz crystal microbalance (QCM) MIP sensors are useful for both gas- and liquid-phase samples [156], which utilizes a metallic surface coated with the MIP and offer real time measurements. Despite this, these methods can be time-consuming and need specialized instruments, which hinder their onsite application [176]. The QCM methods are often coupled with voltametric/amperometric in the design of the MIP-based electrochemical sensors. On the other side, electrochemical MIP sensors based on voltametric/amperometric methods where common measured properties are the current as the potential is varied (voltammetry) or the current at a fixed voltage (amperometry), have continued to be the most popular largely due to their simplicity and ease of production and the low cost of the devices and instrumentation [172].

In this point of view, in the next subsection will be presented the bibliographic study over the electrochemical voltametric/amperometric as main MIP-based sensors dedicated to the environmental analysis.

1.5.1. The main electrochemical MIP-based sensors

Voltammetric and amperometric sensors based on MIPs nowadays are widely used as sensing devices [64], [173]. These sensing techniques are primarily applied to liquid samples and involve a three electrodes system, where the MIP layer is applied to the

working electrode that is assembled with counter and reference electrodes in a cell [156]. When current is measured based at constant potential, the method of analysis is called amperometric I = f(t) (chronoamperometry), whereas current measurements during varying potentials are known as potentiometric methods I = f(V) (cyclic voltammetry). Thus, the peak current which is obtained during electrochemical analysis of the template molecule using the MIP-based electrochemical sensor by scanning the potential, is proportional to the concentration of the target molecule [156]. The basic concepts for these two electrochemical methods remain the same.

Voltammetric approaches are highly interesting for environmental sensing due to their versatility and low noise [173]. The voltage is swept within a defined range and the resulting current is monitored in time in response to increasing concentrations of the analyte of interest. Other advantages of voltammetric sensing are the compatibility with aqueous samples and the fact that the electrodes do not have to be noble metals with many applications relying on e.g. carbon-based electrodes [177]. Electrochemical interferences can be suppressed by the use of pulsed methods such as differential pulse voltammetry (DPV) or square wave voltammetry (SWV), while also increasing the sensitivity towards the desired analyte. These types of electrochemical sensors can detect various types of pollutants in the environment including pharmaceuticals, heavy metals, and pesticides [158]. Amperometric detection methods are a subset of voltammetric approaches that operate at a fixed or optimal potential [173]. The analyte becomes trapped by a MIP and is reduced or oxidized at the operating potential, generating a current that is dependent to the concentration of the analyte [173].

As known over the past 50 years, global sales of pesticides have increased because their importance in agricultural production. They inhibit and prevent the growth of harmful animals, insects, invasive plants, weeds and fungi. As described in the part 1.1. of this Chapter, among all available pesticides, herbicides, insecticides, and fungicides are the most used types, which appeared to be harmful for the environment and living organisms as well. Although electrochemical detection of pharmaceuticals in water samples using MIPs is still an unexplored area, and mostly many publications have been reported about their use for trace analysis of pesticides [158].

Conducting polymers have been mainly used as sensing layers for the preparation of electrochemical MIP-based sensors for the determination of pesticides and other types of contaminants in the environmental water samples, and among all, polypyrrole is most widely used for this application.

1.5.2. Volt-amperometric MIP-based sensors with PPy

Polypyrrole is by far the most widely used for electrochemical MIP-based sensors. The electropolymerization process of pyrrole monomer has been studied since decades [107], [108], [178], showing that it can be generated onto different electrode materials (carbon or metal electrodes) [70], [108], due to their easy *in-situ* electropolymerization at the electrode surface with or without the presence of the template molecule [179]. The formation of polypyrrole film is fast and it is well known to be a partially crosslinked polymer so that there is no need to add a cross-linker agent [179]. The properties of PPy described in the paragraph 1.3.3.5. have made the polypyrrole as the most used conducting polymeric material for the electrochemical fabrication of MIP-based sensors.

Recently, numerous works have been reported for the use of MIP-PPy based sensors to the detection of various micropollutant that were found in waters, such as pharmaceutical pollutants [136] and pesticide molecules [143]. In Table 2 are presented some of the developed electrochemical sensors based on molecularly imprinted polypyrrole used for the determination of various targeted analytes.

Table 2. MIP sensors based on electro-synthesized MIP-based polypyrrole sensing layer.

MIP sensing layer	Template/Analyte	Electrochemical detection method	LOD (mol · L^{-1})	Ref.
PPy	Dimethoate	SWV	(0,075 – 2) x 10^{-9}	[180]
PPy	Bovine	Pulse amperometry	-	[181]
PPy	Melamine	SWV	1,1 x 10^{-7}	[31]
PPy	Trimethoprim	SWV	1,3 x 10^{-7}	[83]
PPy	Paracetamol	DPV	7,9 x 10^{-7}	[136]
PPy	Dopamine	SWV	5,7 x 10^{-12}	[137]
PPy	Norfloxacin	SWV	4,6 x 10^{-8}	[144]
PPy	Ascorbic acid (Vitamin C)	DPV	7,4 x 10^{-5}	[145]
PPy	Phenothiazine	DPV	3 x 10^{-7}	[182]
PPy	2-isopropoxyphenol	DPV	0,09 x 10^{-6}	[139]
PPy	Sulfadimethoxine	Amperometric	7 x 10^{-5}	[140]
PPy	Glyphosate	DPV	1,6 x 10^{-9}	[141]
PPy	2,4-dichlorophenoxy acetic acid	CV	8,3 x 10^{-7}	[142]
PPy	Sulfamethoxazole	SWV	24.1 x 10^{-9}	[183]

The sensors shown in Table 2 use the same operation strategy, which includes three main steps described in the paragraph 1.4.3. The development of a MIP-based polypyrrole sensor for electrochemical determination of herbicide (isoproturon) is presented in the Chapter III of this work, whereas the analytical performances of volt-amperometric MIP-based sensors are shown in Appendix 1.

- Page left intentionally blank -

CHAPTER II

"Experimental section"

2. CHAPTER II: EXPERIMENTAL SECTION

In this chapter is presented an overview of different chemicals and procedures that have been used to carry out experiments in the present work. Experimental section involves different parts, where initially is presented a list with all the chemicals and reagents used, following with electrodes and the electrochemical cell, and are described briefly all the analytical techniques, and all the spectroscopy techniques used in this study.

2.1. Chemicals

Table 3. List of chemical and reagents used for experiments.

Chemicals and reagents				
Name	**Formula**	**MW ($g.mol^{-1}$)**	**Purity %**	**Purchase from**
Monomer				
Pyrrole	C_4H_5N	67,09	>98	Sigma-Aldrich
Electrolytes				
Lithium perchlorate	$LiClO_4$	106.39	>99	ACROS ORGANICS
Potassium chloride	KCl	74.55	99.9	Sigma-Aldrich
Sulfuric acid	H_2SO_4	98.08	93 - 98	Sigma-Aldrich
Ammonium sulfate	$(NH_4)_2SO_4$	132.14	/	/
Tetrabutylammonium	NBu_4BF_4	329.27	>99	Sigma-Aldrich
Solvents				

Ethanol	C_2H_5OH	46.07	>99	Carlo Erba
Acetonitrile	C_2H_3N	41.05	99.9	Sigma-Aldrich
NMP (1-methyl-2-pyrrolidinone)	C_5H_9NO	99.13	99.5	Sigma-Aldrich
Herbicides, pesticides and interferents				
Isoproturon (ISO)	$C_{12}H_{18}N_2O$	206.3	>99	Sigma-Aldrich
Diuron (DIU)	$C_9H_{10}Cl_2N_2O$	233.1	>99	Sigma-Aldrich
Carbendazim (Cbd)	$C_9H_9N_3O_2$	191.187	>99	Sigma-Aldrich
Carbamazepine (Cbmz)	$C_{15}H_{12}N_2O$	236.269	>99	Sigma-Aldrich
Redox probes				
Potassium hexacyanoferrate	$[K_3Fe(CN)_6]$	329.24	>99	Sigma-Aldrich
Ferrocene	$C_{10}H_{10}Fe$	186.03	98	Sigma-Aldrich
Hexaammineruthenium (III) chloride	$[Ru(NH_3)_6]Cl_3$	309.61	98	Sigma-Aldrich
Other chemicals				
Toluene	C_7H_8	92.14	99.8	Sigma-Aldrich
Acetone	C_3H_6O	58.08	>98	Sigma-Aldrich
Hydrazine hydrate	N_2H_4 x H_2O	50.05	/	/

2.2. Electrodes and electrochemical apparatus

In this work, a three electrodes electrochemical cell has been used for the electrochemical measurements, such as for electropolymerization of the MIPs, electrochemical detection of micropollutants and for the characterization of the electrodes. A three electrodes electrochemical cell include a reference, a counter and a working electrode. In Figure 24, is presented schematically the apparatus setup used for electrochemical experiments.

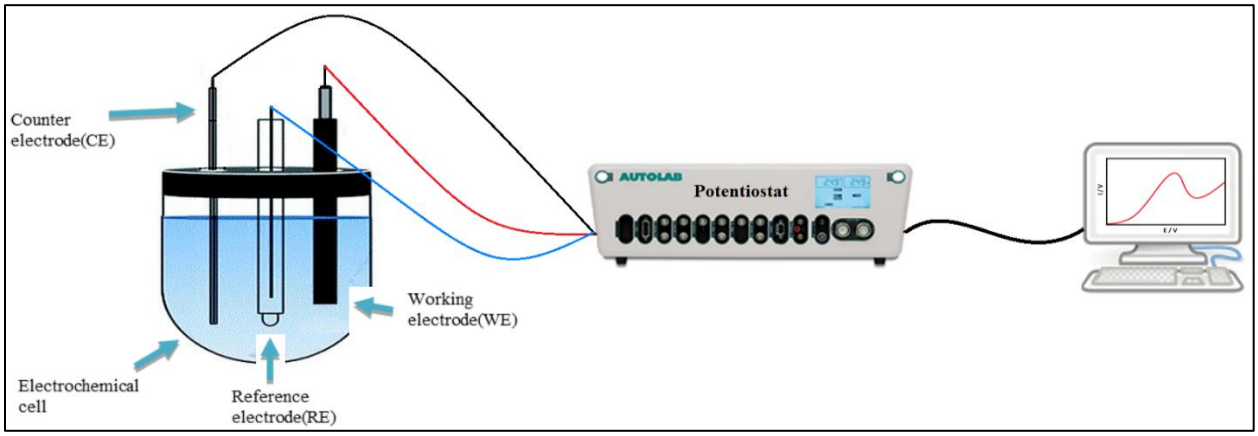

Figure 24. Schematic representation of a typical three electrode system electrochemical setup.

2.2.1. Reference electrode

Reference electrode (RE) in an electrochemical setup holds a well-known potential. It is used as a point of reference for potential control and measurements. Current which flows through reference electrode is kept close to zero (ideally zero) which is achieved by closing the current circuit by counter electrode and by high input impedance on the electrometer [184]. A reference electrode has some characteristics e.g. (i) its potential should be governed by Nernst equation (should be chemically and electrochemically reversible) (ii) potential should remain constant when a small current is passed and back to original value after small current flow (iii) thermal coefficient of potential should be small.

Most commonly used reference electrodes and their chemical equation with standard potential (E°) are as follows:

a) Normal hydrogen electrode (NHE)

$$2H^+ + 2e^- \leftrightarrow H_2 \quad (E° = 0.000V) \qquad (2.1)$$

b) Saturated Calomel Electrode (SCE)

$$\mathbf{Hg_2Cl_2 + 2e^- \leftrightarrow 2Hg + 2Cl^- \quad (E° = 0.268V \text{ vs. } NHE)} \qquad (2.2)$$

c) Silver/Silver chloride electrode (Ag/AgCl)

$$\mathbf{AgCl + e^- \leftrightarrow Ag + Cl^- \quad (E° = 0.222V \text{ vs. } NHE)} \qquad (2.3)$$

In this study reference electrode, Ag/AgCl saturated with 3M KCl (purchased from Metrohm, Switzerland) has been used for aqueous and organic solutions.

2.2.2. Counter electrode

Counter electrode (CE) or auxiliary electrode is used to close the current circuit in an electrochemical cell and it does not participate in electrochemical reaction. Usually, counter electrode is made up of different stainless materials, such as: Pt, graphite, glassy carbon, stainless steel, etc. During an electrochemical reaction when the current flows between working and counter electrode, total surface area of counter electrode should be approximately ten times higher than working electrode so that it does not limit the kinetics of reaction under investigation. As counter electrode, for most of the electrochemical experiments, a curved platinum wire was chosen to be used, whereas for EQCM measurements as counter electrode was used a carbon screen printed plate. In the case of electrochemical exfoliation of graphite rod electrodes, as a counter electrode we have used a platinum mesh cylinder electrode.

2.2.3. Working electrode

Several working electrodes (WE) were used for different experiments in this work. During electrochemical experiments the main reaction takes place on the surface of the working electrode (WE). In the beginning of this PhD work, as main working electrode used for the optimization of the electrochemical experiment (MIP and NIP growing, characterization, detection) was chosen a glassy carbon electrode (GCE) disc (area of 0.07 cm^2) (Figure 25).

Glassy carbon is known also as vitreous carbon, is a non-graphitized carbon which combines glassy and ceramic properties. Glassy carbon material has some excellent properties, such as high temperature resistance, extreme resistance to chemical attack, impermeability to gases and liquids, and good conductivity. Its electrical resistivity was measured to be around 45 – 50 x 10^{-4} Ωcm [185]. Due to these advantages, these materials are widely used as an electrode material in electrochemistry.

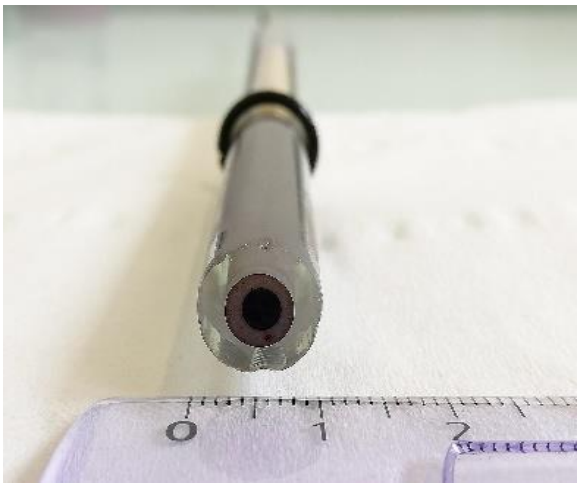

Figure 25. The glassy carbon electrode.

Gold and platinum quartz working electrodes used for EQCM measurements have some good properties as well and are suitable disc electrodes for polymeric film electropolymerization and characterization. The electrochemical experiments have been tested on graphene electrode. The graphene electrode development is described in the last chapter.

2.2.4. Electrochemical apparatus

Electrochemical measurements were carried out using a potentiostat/galvanostat PGSTAT 204 and PGSTAT 128N Autolab Metrohm interfaced with a PC using Nova 2.2 software. The potentiostat/galvanostat is connected with three electrodes in a one-compartment cell (Figure 26-a). The EQCM measurements were performed by a Maxtek RQCM micro-balance (Figure 26-b).

In the case of graphite exfoliation, the potentiostat/galvanostat was coupled with a voltage booster.

Figure 26. Electrochemical apparatus, a) PGSTAT 128N Autolab Metrohm, b) Maxtek RQCM micro-balance.

2.3. Electrochemical techniques for analysis

2.3.1. Cyclic voltammetry (CV)

Usually every electrochemistry study of any compound starts with cyclic voltammetry [186]. Nowadays, cyclic voltammetry (CV) is one of the basic techniques performed in electrochemical studies providing qualitative and quantitative informations for the electrochemical reactions that are studied.

A cyclic voltammetry measurement involves applying a potential to the working electrode, where it scans the potential of an electrode, which is immersed in an unstirred solution, and measuring the resulting current. Mainly, the current (A) flowing through the working electrode is recorded as a function of applied potential (V), resulting plot which is constructed (current vs potential) is called cyclic voltammogram. When we analyze a cyclic voltammogram of a reversible redox probe (Figure 27), we see that it has two mains potential peaks (Epc, Epa) in cathodic (suffix c) and in anodic (suffix a) sides, which always present two peaks current values (*i*pc, *i*pa).
If we consider X and Y as solution dissolved species, for a reversible reaction we have:

$$X \pm e^- \leftrightarrow Y \qquad (2.4)$$

For better understanding, as example is shown the redox couple of potassium hexacyanoferrate [$K_3Fe(CN)_6$], so this compound in solution is dissolved in hexacyanoferrate ions as $Fe(CN)_6^{3-/4-}$, due to the potential application reducing and oxidizing on the working electrode surface as follow:

reduction reaction: $\mathbf{Fe(CN)_6^{3-} + e^- \rightarrow Fe(CN)_6^{4-}}$ (2.5)

oxidation reaction: $\mathbf{Fe(CN)_6^{4-} \rightarrow Fe(CN)_6^{3-} + e^-}$ (2.6)

whereas in the case of hexaammineruthenium III chloride redox probe dissolved in the solution, the ions will be undergoing with the following reactions:

reduction reaction: $\mathbf{Ru(NH_3)_6^{3+} + e^- \rightarrow Ru(NH_3)_6^{2+}}$ (2.7)

oxidation reaction: $\mathbf{Ru(NH_3)_6^{2+} \rightarrow Ru(NH_3)_6^{3+} + e^-}$ (2.8)

Except reversible reactions there exist also quasi reversible and irreversible reactions, which can be studied by using cyclic voltammetry. In this work cyclic voltammetry was used to study the electrochemical behavior of different chemicals for initial electrochemical characterization, for electropolymerization of pyrrole into NIPs and MIPs, at different stages of electrodes modification to analyze and optimize different electroanalytical parameters and for electroanalytical detection of micropollutants.

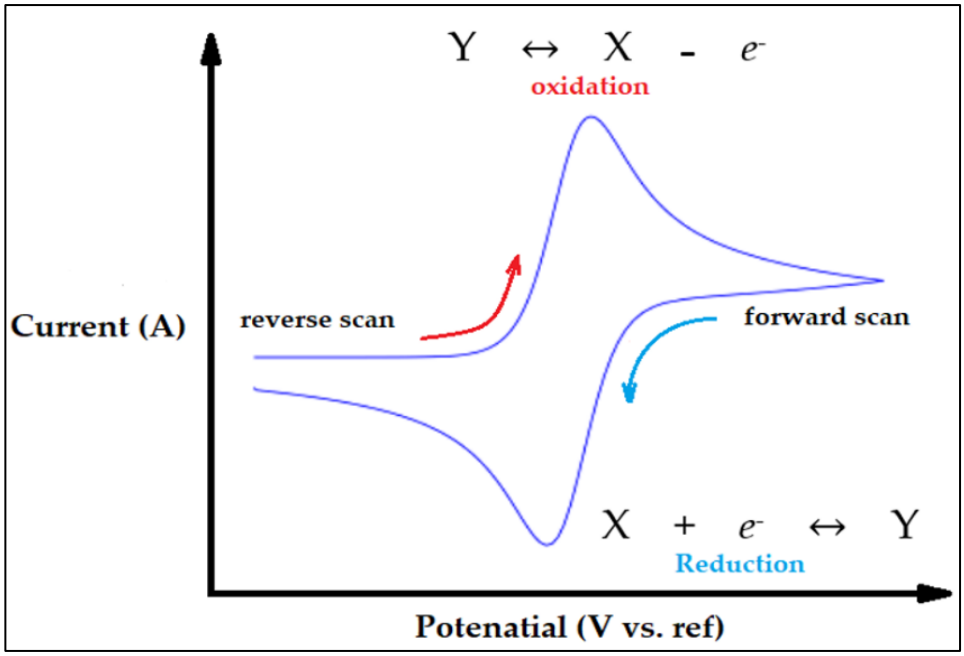

Figure 27. Typical cyclic voltammogram of a reversible redox reaction.

2.3.2. Chronoamperometry (CA)

While during the cyclic voltammetry (CV) measurements the potential on the working electrode varies I = f(V), in the case of chronoamperometry (CA) measurements the potential applied on the working electrode is fixed and unchanged. CA is an electrochemical technique in which the potential of the working electrode is stepped and the resulting current from faradaic processes occurring at the electrode (caused by the potential step) is monitored as a function of time I=f(t).

In this work chronoamperometry has been used for electropolymerization of pyrrole on the working electrode for NIP and MIP films electrochemical fabrication, for their characterization and for optimization of various important parameters in order to improve the performance of the PPy-MIP electrochemical sensors. During the optimization of electroanalytical parameters, results obtained with chronoamperometry have been compared with results obtained with cyclic voltammetry in order to find put which of the methods is the most suitable MIP sensing applications.

The method of chronoamerometry has been used also for the exfoliation of graphite rod electrodes electrochemically into graphene flakes in TBA-BF_4 in 1-methyl-2-pyrrolidinone media.

2.3.3. Square wave voltammetry (SWV)

Square wave voltammetry (SWV) is one of the most powerful electrochemical technique mostly used for quantitative applications and mechanistic study of electrode processes. In a square wave voltammetry experiment, the current at a (usually stationary) working electrode is measured while the potential between the working electrode and a reference electrode is swept linearly in time. The potential waveform can be viewed as a superposition of a regular square wave onto an underlying staircase, by considering SWV a modification of staircase voltammetry. SWV suppressed background making it much more effectively than cyclic voltammetry for quantitative analysis and for electrochemical sensors application [187]. So, a typical modulation in SWV consists of a staircase potential ramp modified with square shaped potential pulses (Figure 28-A). At each step of staircase ramp, two equals in height and opposite in direction potential pulse are imposed to give rise to a single potential cycle in SWV (Figure 28-B). This potential cycle in SWV is repeated at each step of the staircase ramp during the voltammetric experiment [188]. A typically square wave voltammogram is presented in

Figure 28-C. In this work, square wave voltammetry measurements were performed for the electrochemical determination of micropollutants. Optimized square wave voltammetry conditions used were; duration 5 s, E_{step} 3 mV, Amplitude 50 mV, and Frequency 25 Hz.

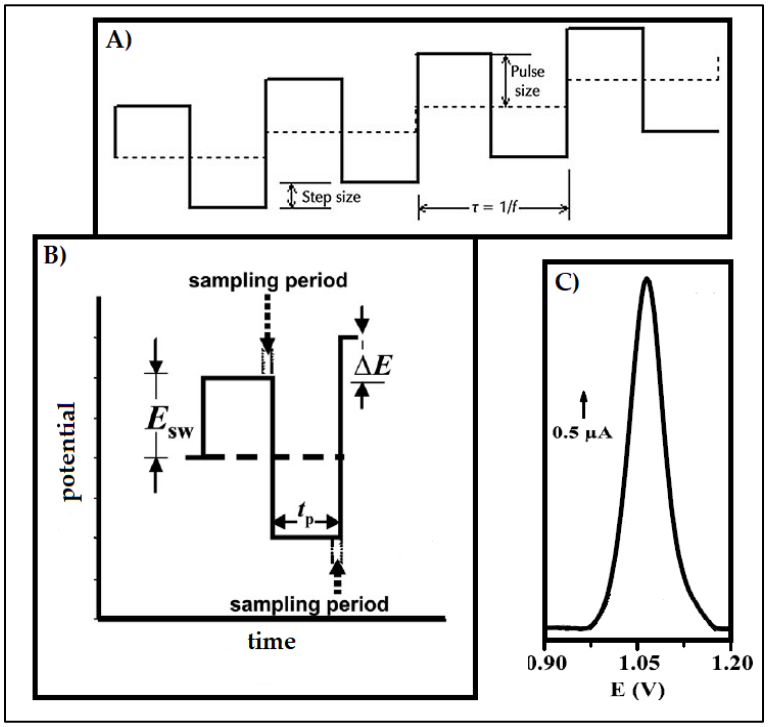

Figure 28. Square wave voltammetry, A) One potential cycle, B) Single potential cycle in SWV, C) square wave voltammogram obtained during determination of isoproturon (c = 10^{-6} M).

2.3.4. Electrochemical impedance spectroscopy (EIS)

Early EIS has been applied to the determination of the double-layer capacitance and in ac polarography, but nowadays it is used to characterize electrode processes and complex interfaces [189]. However, EIS is very surface sensitive, which makes many changes visible that other techniques don't see, for example changes in polymer layers due to swelling, surface changes due to protein adsorption or penetration of corrosion protection layers [189]. It was termed as impedance spectroscopy due to its ability to be applied at different frequencies.

Advantages of EIS include sensitivity, large amount of data, fine-tuning mechanisms and determination of kinetics of processes, resistance, capacitance and real surface areas in situ.

In general, the applications of EIS include:

a) Interfacial processes: Redox reactions at electrodes, adsorption, electrosorption and kinetics of homogenous reactions in solution combined with redox processes.
b) Geometric effects: linear, spherical, cylindrical mass transfer, limited volume electrodes, porous electrodes and determination of solution resistance.
c) Applications in power sources systems: (Batteries, fuel cells, membranes) corrosion studies, electrocatalytic reactions, self-assembly monolayers and sensors.

Electrochemical impedance spectroscopy (EIS) has been used also for the characterization of thin polymeric materials synthesized through electrochemical methods. Mainly the method was focused in the explanation of the molecularly imprinted polymers used as membranes and as sensors, for a better understanding of the porosity of these materials. Some recently reported papers about MIP sensing have shown EIS as a technique used for the characterization of imprinting phenomenon, before and after the template molecule removal [106]–[109].

In this work the measurements were carried out on both bare and NIP-MIP electrodes and compared. The experiments were performed by using a PGSTAT 100 apparatus and controlled by NOVA 2.1.4 software. Conditions for impedance measurements were; Potential applied +0.250 V, wait time 180 s, Highest frequency 100 kHz and lowest was 0.01 Hz, Amplitude 0.01 VRMS, and current ranges highest 100 mA and lowest 100nA. Fitting and simulation were carried out using analysis tool in the software of Z-View.

2.3.5. Electrochemical Quartz Crystal Microbalance (EQCM)

Electrochemical quartz crystal microbalance (EQCM) has been used mainly for the investigation and characterization of mechanisms of polymeric film formation onto quartz working electrodes. It has been presented as an extremely sensitive method [176], capable to measure the changes in mass in nanogram ranges. The QCMs are piezoelectric devices fabricated of a thin plate of quartz, usually with gold thin sheet deposited onto each side of the plate which plays the role of the working electrode [193], (see Figure 29-A). The quartz working electrode must be placed in a quartz holder and then connected with the electrochemical cell with both counter and reference electrodes, and also with a frequency analyzer (see Figure 29-B). Before starting the

electropolymerization process of polymeric film on the working electrode surface, the quartz electrode is oscillating with a certain frequency (5 MHz). During the polymeric film formation, the frequency value changes (Δf) due to the variation of the mass on the quartz. It is possible to measure the change of the film mass (Δm) [194], calculated automatically with the following equation:

$$\Delta f = -2.26 \cdot 10^6 f_0^2 \Delta m / S \qquad (2.9)$$

where Δf is the observed frequency change, MHz; f_0 is the oscillation frequency of the dry crystal, MHz; Δm is the mass change in grams (g); and S is the working surface area of the QCM working electrode, cm^2 [194]. EQCM has such advantages as low cost, simplicity, and capable to reach very low detection limits [195]. These advantages made the method to be used for study and characterization of various electroanalytical purposes [114]–[116], as well as for the study of imprinting effects for MIP sensing applications [160], [195], [199], [200].

In this work, the EQCM measurements were performed by using a Maxtek RQCM micro-balance on Maxtek 5 MHz Au-Cr crystals and on Maxtek 5 MHz Pt-Cr crystals, controlled with a Maxtek software and with NOVA 2.1 in the same time, in order to analyze the mechanism of electropolymerization of pyrrole with different electroanalytical methods and for the real thickness calculation of the NIP and MIP films from the mass values obtained during their EQCM characterization.

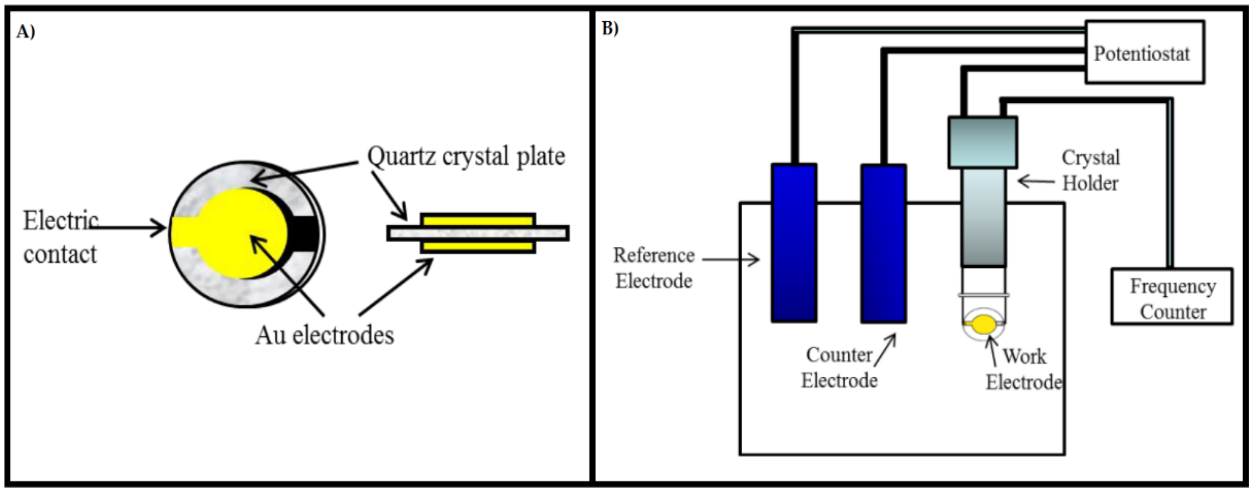

Figure 29. Electrochemical quartz crystal microbalance (EQCM) setup, A) Schematic of a piezoelectric quartz crystal, B) Schematic electrochemical quartz crystal microbalance (EQCM) apparatus [198].

2.4. Techniques used for the characterization of chemical, structural and morphology of the electrode materials

2.4.1. Infrared spectroscopy (IR)

The principle of infrared (IR) spectroscopy is based on the absorption of light by most molecules in the infrared region of the electromagnetic spectrum and converting this absorption into molecular vibration. This absorption corresponds specifically to the bonds present in the molecule. The infrared spectrum is considered as a chemical identity card of the molecule (Figure 30-A).

Here we used a Nicolet iS50 FTIR Spectrometer from Thermo Fisher Scientific with the ATR mode (diamond monocrystal) (Figure 30-B) to analyze the surface of the graphene electrode and the chemical function present in the MIP and the NIP.

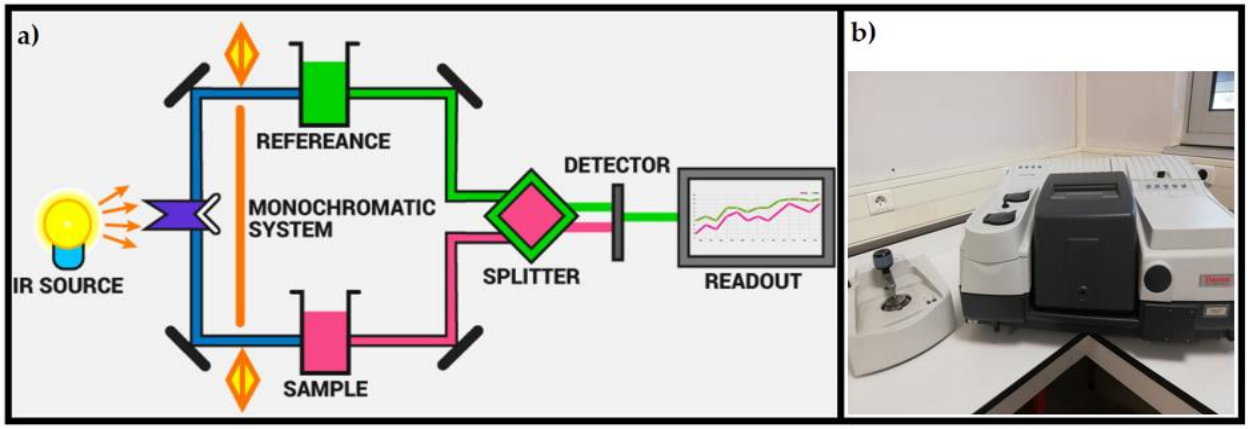

Figure 30. IR spectrometer, a) schematically instrumentation of infrared spectroscopy, b) picture of IR spectrometer used in this work.

2.4.2. Raman spectroscopy

Raman spectrometry is a vibrational spectroscopy typically used to determine vibrational modes of molecules, although rotational and other low-frequency modes of systems may also be observed. The principle is based on an inelastic light scattering by a material, which is correlated by a variation of the frequency of the scattered light (Figure 31-a). Indeed, most of the scattered light has the same frequency as the incident

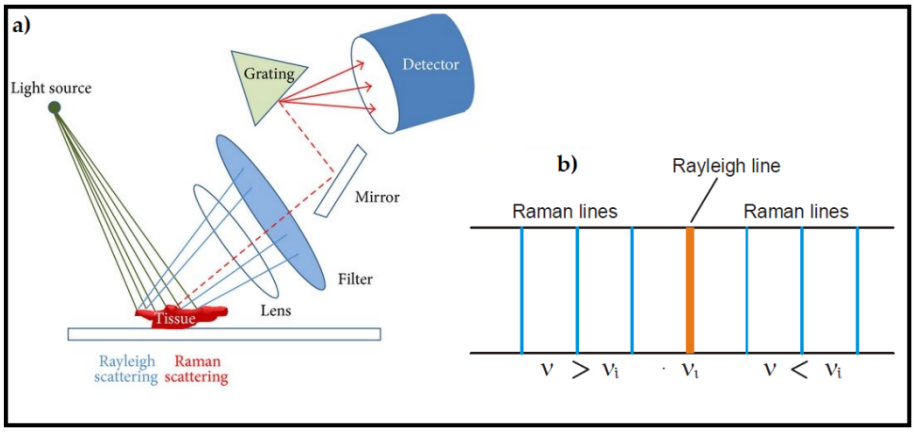

Figure 31. Raman spectroscopy, a) the principle of Raman, b) Raman spectrum.

light. This type of scattering which occurs without a change in the incident frequency is termed *Rayleigh scattering*. Raman discovered that a very small fraction of the scattered light has frequencies higher or lower than the incident frequency. The scattering which occurs with a change in the frequency which is called Stokes and anti-Stokes diffusion. The phenomenon is called *Raman effect*. In a Raman spectrum, the sharp line in the middle corresponds to Rayleigh scattered light is cut by a Notch Filter. Raman scattered light records a series of lines on either side of the Rayleigh line. These are called Raman lines and constitute Raman spectrum (see Figure 31-b).

Raman spectroscopy is widely used in chemistry to identify molecules and study chemical bonding and intramolecular bonds. In nanotechnology, a Raman microscope can be used to analyze nanowires to better understand their structures, and the radial breathing mode of carbon nanotubes is commonly used to evaluate their diameter. Recently workers have been focused in using Raman spectroscopy for analyzing and characterization of graphene materials [201].

Figure 32. Raman spectrometer.

In this work Raman spectroscopy (Figure 32) has been used for the characterization of graphene oxide and reduced graphene oxide at different stages during the electrode's fabrication process. Raman spectra were performed in ambient condition using a Renishaw INVIA Reflex spectrometer equipped with a solid-state laser source (514 nm wavelength, i.e., 1.94 eV), focused through a Leica microscope.

2.4.3. Atomic force microscopy (AFM)

Atomic force microscopy (AFM) can generate topological images with nano scale resolution with minimum sample preparation by scanning very small surfaces. The AFM principle is based on a cantilever/tip assembly that interacts with the sample as a probe. The up/down and side to side movements of the AFM tip during scanning of surface of the material sample is monitored through a laser beam reflected and detected by a positive sensitive photo detector (PSPD) (Figure 33-a). The deflection sensitivity of these detectors has to be calibrated in terms of how many nanometers of motion correspond to a unit of voltage measured on the detector. As result is obtained a three-dimensional topography image of the sample where can be analyzed its morphology. The AFM tip is very sharp with a radius 5 - 10 nm and it can be with a triangular shape (Figure 33-b). In Figure 34, is presented a BRUKER-Dimension ICON high performance

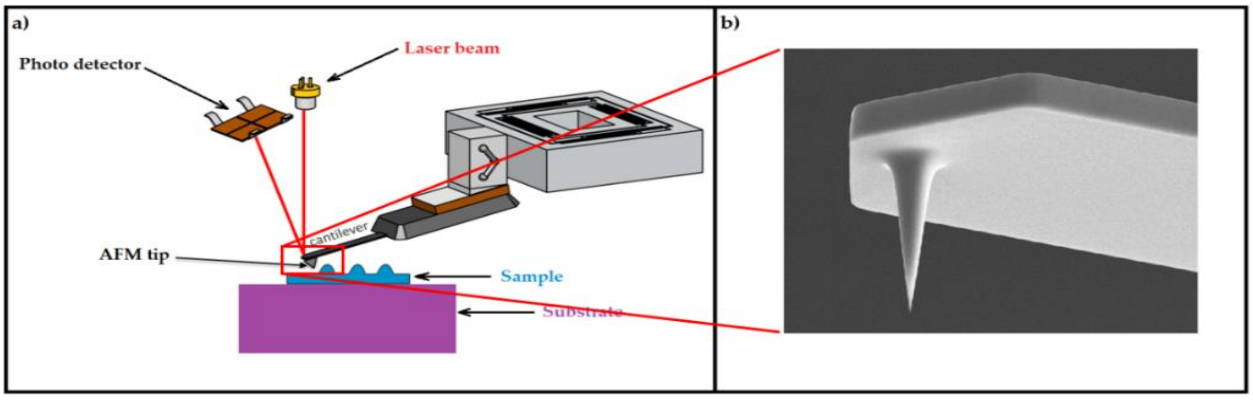

Figure 33. Atomic force microscopy (AFM), a) the principle of AFM, b) the AFM tip.

AFM microscope used in this work. Here AFM was used to analyze the topography and morphology by tapping mode of NIP and MIP films generated on glassy carbon, gold and platinum electrode substrates and compared their roughness values before and after template molecule removal process. Moreover, the method has been employed for the real NIP and MIP films thickness measurement by using AFM scratching mode. The images data have been treated with a PC using Gwyddion 2.53 software.

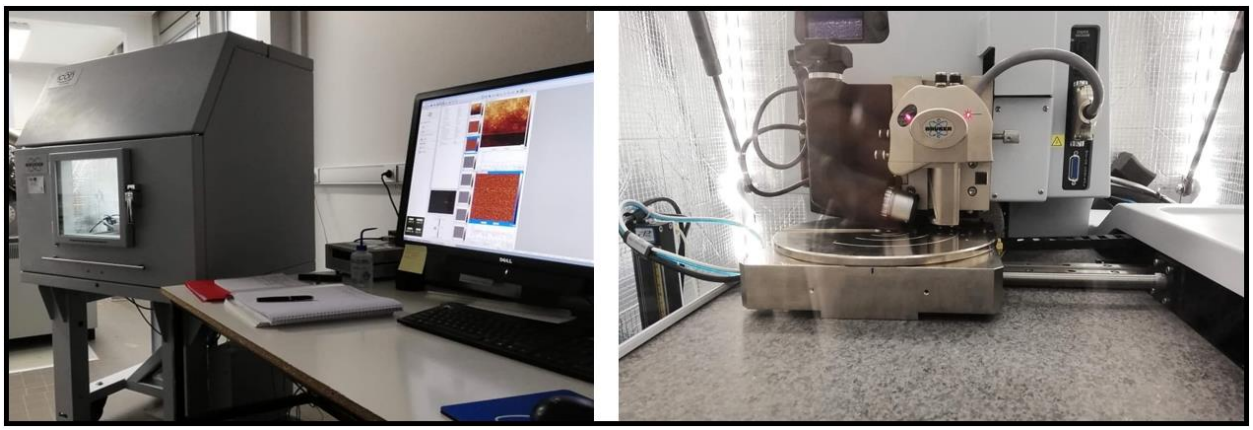

Figure 34. BRUKER-Dimension ICON high performance AFM (atomic force microscope).

2.4.4. X-ray photoelectron spectroscopy (XPS)

X-ray photoelectron spectroscopy (XPS) is a surface-sensitive qualitative and quantitative spectroscopic technique used for measuring the elemental composition of the material's surface and the electronic state of the elements. The principle (Figure 35-a) is based on the irradiation of the material surface with a beam of X-rays while simultaneously measuring the kinetic energy and the number of electrons that escape from this probed region. XPS needs a high vacuum space (P ~ 10^{-8} millibar) or ultra-vacuum space (P<10^{-9} millibar) in the chamber where the sample is analyzed. XPS was mainly used for the characterization of carbonaceous materials, such as graphene materials, as well as for the analysis of polymeric thin film materials such as polypyrrole [202]–[205].

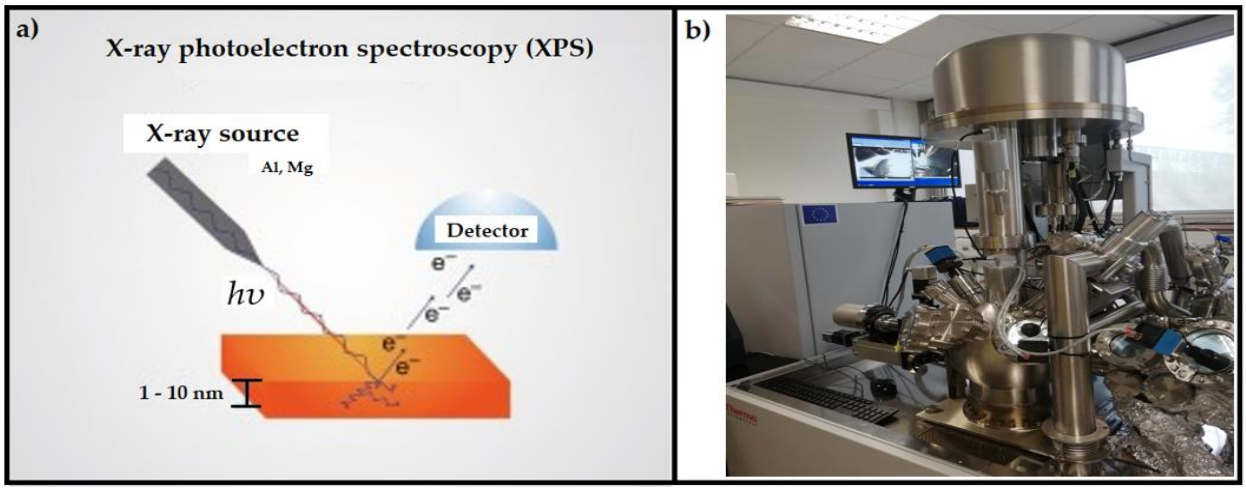

Figure 35. X-ray photoelectron spectroscopy (XPS), a) the principle of XPS, b) the XPS spectrometer used in this work.

In Figure 35-b is presented the XPS spectrometer used in this work for the characterization of NIP and MIP films, as well as for the graphite, graphene oxide, reduced graphene oxide and graphene materials. X-Ray Photoelectron (XPS) Analysis have been carried out using a Thermofischer Escalab Xi system operating, under 10^{-10} milli bars, in the constant pass energy mode at 200 eV, with a spot size of 600 microns. The spectrometer is equipped with a non-monochromatic dual anode X-Ray source providing Al K\alpha or Ag L\alpha photons of energy of 1486.6 eV or 3000 eV. A background, based on the Shirley iterative method, has been used to subtract the inelastic background to all the XPS spectra.

2.4.5. Photolithography

Photolithography, also called as optical lithography or UV lithography, is a method which has been used for the microfabrication to pattern parts on a thin film or the bulk of a substrate (also called a wafer). The main principle of this method is based on the transfer of the UV light on a geometric pattern from a photomask (optical mask) to a photosensitive (light-sensitive) chemical photoresist on the substrate (Figure 37). The method has high precision and provides developing covered material flat surfaces containing well shaped and controlled surfaces. We used this method onto our graphene – polystyrene flat samples, in order to fabricate electrodes with precise and controlled working area.

Exposure under with UV light during the manufacturing process must be performed under vacuum conditions using reflective mirrors and masks since all materials strongly absorb ultraviolet light (Figure 36-A). By using a special photomask for photolithography, we have been able to fabricate graphene electrodes with different sizes of working area, such as $10mm^2$, $5mm^2$, $1mm^2$, $500\mu m^2$, $200\mu m^2$, $100\mu m^2$, and $10\mu m^2$ (Figure 36-B), which squares are the regions where the electrochemical contact with the electrolyte solutions in an electrochemical cell occurs.

The experimental conditions for performing photolithography on graphene samples have been set to 2500 rpm (rotations per minute), time was set to be 3 up to 30 seconds, with a heating energy 150 kJ/cm^2, and the type of insulating layer used was S-1813.

The photolithography in this work was performed with a «cube» : KLOE UV-KUB 2 and in an alignment (aligneur) : Süss MicroTec MA/BA6 Gen. 4.

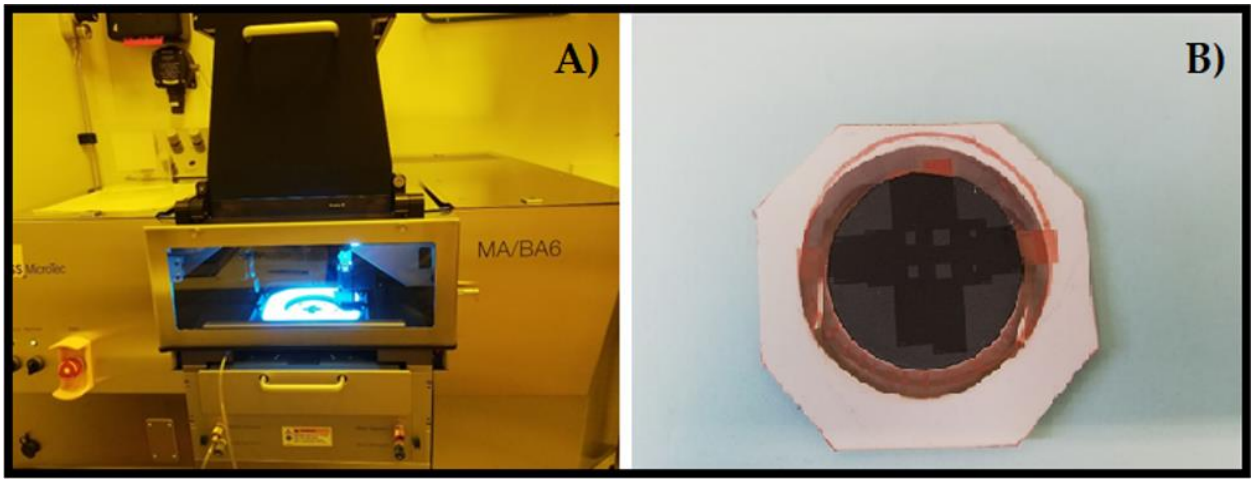

Figure 36. Photolithography apparatus used in this work A), and the graphene/polystyrene substrate prepared with different sizes of controlled working area B).

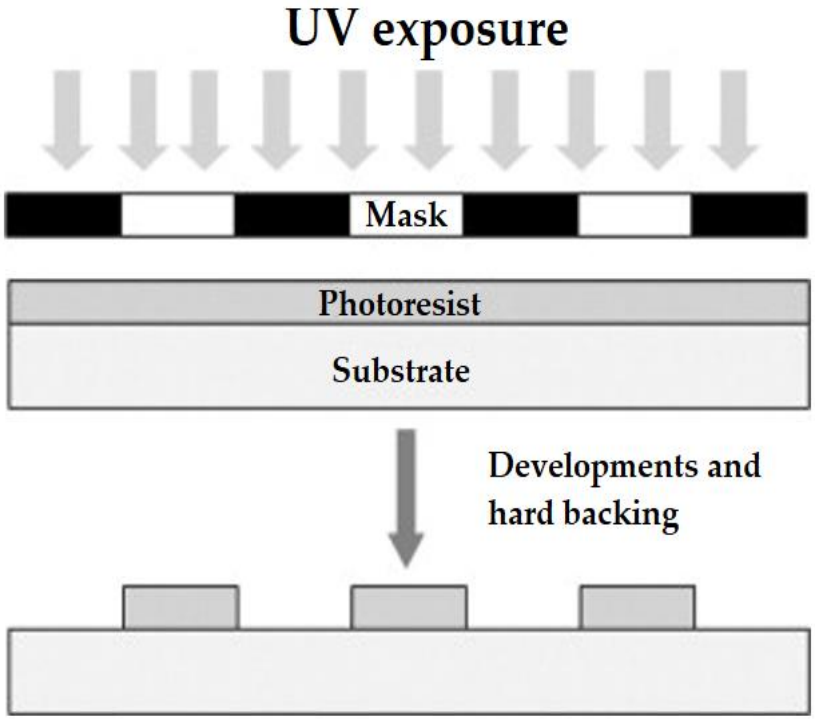

Figure 37. The principle of photolithography process.

- Page left intentionally blank -

CHAPTER III

"Development of a Molecularly imprinted polymer modified glassy carbon electrode for the electrochemical analysis of isoproturon in water"

3. CHAPTER III: Development of a molecularly imprinted polymer modified glassy carbon electrode for the electrochemical analysis of isoproturon in water

3.1. Introduction

Researches are ongoing to develop rapid and inexpensive sensing devices for the detection of pesticides in general and particularly isoproturon. Voltammetric-based methods have been widely reported for the determination of many pesticides and isoproturon more specifically using various carbon electrode materials such as glassy carbon [18], [20], graphene [19], wall-jet glassy carbon electrode [20], carbon paste [21], carbon fiber [22], doped diamond [23], and multiwalled carbon nanotubes (MWCNT) [24]. More recently, numerous studies have focused on modified electrodes [25] and various assemblies have been investigated for applications in isoproturon electrochemical sensors such as clay modified GC electrodes [26], [27], or enzyme-modified [24], [28]–[30] and conducting polymer modified electrodes [206]. The attachment of the organic film on the electrode surface makes it possible to increase the sensitivity and the selectivity of these modified electrodes toward a targeted analyte. As we mentioned in the first chapter, one of the most ingenious methods to achieve this goal is to prepare molecularly imprinted polymers. Various types of electro-synthesized polymers based on molecular imprinting have been reported including polyphenol, polymethacrylic-acid [46], polyaniline [164], [207], [208] and polypyrrole [83], [137], [138], [209]. Recently the use of some Metal Organic Frameworks (MOFs) based on the electropolymerization of monomer-functionalized gold nano-particles was reported [179]. Although many MIPs have been proposed for the development of electrochemical sensors for organic molecules, no publication mentions the development of MIP electropolymerization for the electrochemical detection of isoproturon. Among the abovementioned polymers, we choose to develop polypyrrole MIP film on glassy carbon electrode, because the electroplymerization of PPy is fast and it is well known to be a partially crosslinked polymer so that there is no need to add a cross-linker agent [179]. Extraction and rebinding of the template can be conducted electrochemically since polypyrrole is a conducting polymer, to some extent [179]. In addition, the electropolymerization of polypyrrole leads to chemically and mechanically robust films [137], [210].

Li et al. [47] developed a new molecularly imprinted polyaminophenol electrochemical luminescence sensor (MIP-ECL sensor) for isoproturon determination based on the

competition reaction between isoproturon and glucose oxidase [211]. However, even though the method has provided very low detection limits of 3.8 x 10^{-12} M (0.8 ng/L), the use of additional reagents, the equipment required and the complex preparation of the samples remain incompatible with *in-situ* measurements. Singh et al. (2013) developed an *ex-situ* polymethacrylic imprinted polymer solid phase extraction for isoproturon detection [212] and reached a detection limit of 9.7 x 10^{-7} M (0.2 mg/L) which is unfortunately too high in light of current standards [13]. In addition, an *ex-situ* MIP synthesis involves additional steps, which complicates the implementation of the sensor.

In this context, the aim of this chapter was to develop an electrochemically polypyrrole MIP based electrode for the sensitive and selective detection of isoproturon. It has been studied the influence of the experimental parameters on the characteristics of the polymer matrix and its ability to recognize and to concentrate isoproturon. In order to maximize isoproturon signal detection we adjusted several parameters during the MIP electrosynthesis. The analytical performances of the modified electrodes were then assessed.

3.2. The working procedure of the MIP-GC electrodes

The whole procedure of using the MIP-GC sensors can be divided in two main stages:

- the synthesis of MIP-GC electrodes
- the electroanalytical procedure

The synthesis stage of MIP-GC includes the fabrication process of the MIP-GC electrodes and prepare them for the electrochemical analysis of isoproturon. In this stage are involved two steps:

i) electropolymerization step which represents the electrochemical polymerization of MIPs and NIPs on the glassy carbon electrode surface achieved either by using cyclic voltammetry (CV) or by using chronoamperometry (CA), and

ii) the extraction of the template molecule step which can be achieved electrochemically by cyclic voltammetry (CV) in order to remove the stripped isoproturon molecules from the polymeric matrix and create the cavities.

The electroanalytical procedure includes the process of using the MIP-GC electrodes for the analysis of isoproturon in water. This procedure involves two steps:

j) the incubation or rebinding step which provide the filling of the cavities with the isoproturon molecules coming from the analyte samples and,

jj) electrochemical detection of isoproturon achieved by square wave voltammetry (SWV).

In Figure 38, is presented schematically all of these abovementioned steps used for the preparation of MIP-GC electrodes.

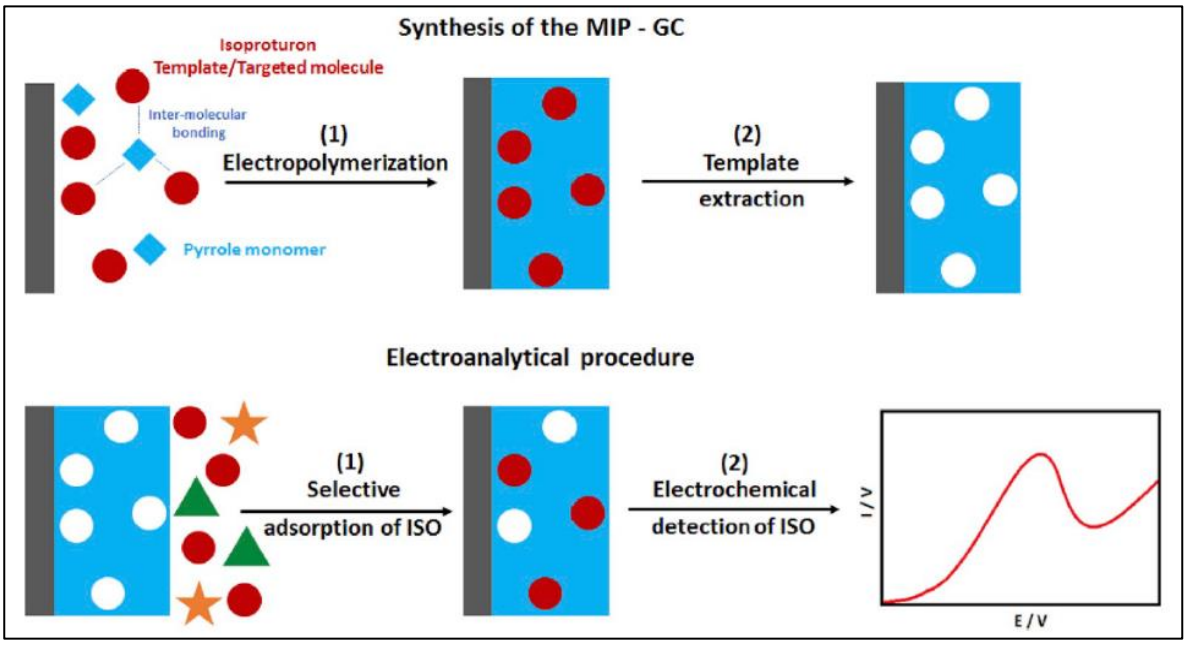

Figure 38. Schematic representation of the procedure used for the preparation of imprinted polypyrrole films on GC substrate MIP GC and the electroanalysis of isoproturon.

However, the study of the experimental parameters of this whole procedure and all the above-mentioned steps are described and discussed in details in this chapter.

3.3. Experimental conditions

The experimental conditions for this study have been chosen from the PPy-MIP literature [33], [48], [137], [141], [156], [158] and from preliminary experiences.

3.3.1. Electrochemical behavior of isoproturon

Pesticides due to their organic structure, have a limited solubility in water: 70.2 mg/L for isoproturon at 25 °C. In order to work only in environmentally friendly solvents, we decided to use only water and ethanol as solvents in the different steps of the working procedure. The electrochemical behavior of isoproturon is studied by cyclic voltammetry in a 0.1M $LiClO_4$ ethanol/water solution prepared with different concentrations of isoproturon (Figure 39). The oxidation peak potential appeared at +1.1 V vs Ag/AgCl that is about 200 mV higher than the optimum conditions for the electrochemical deposition of polypyrrole film.

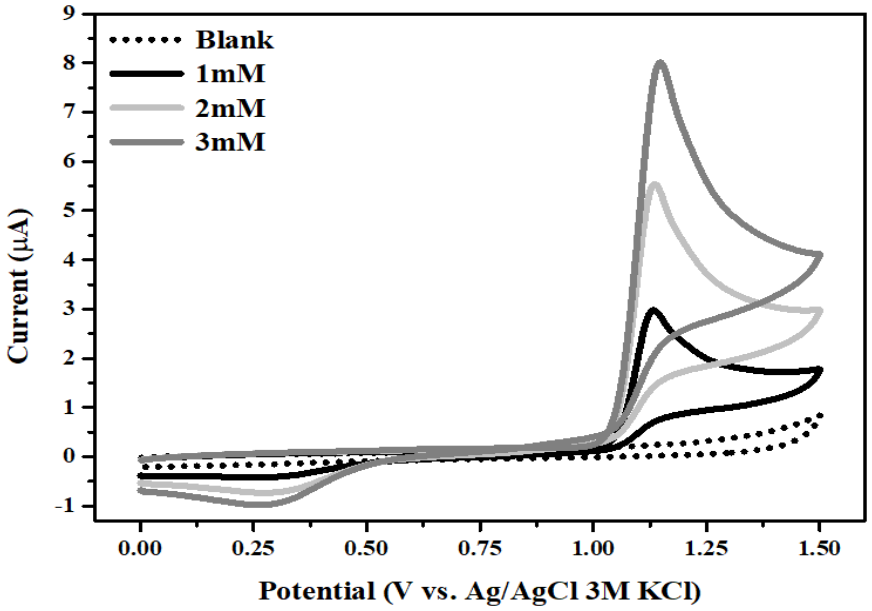

Figure 39. Voltammograms obtained on bare GC electrode for ISO (1, 2 or 3 mM) in H_2SO_4 (0,1M) (70/30 ethanol/water v/v), (····) Blank voltammograms. Scan rate 100 mV/s.

To the best of our knowledge, only several articles have been published for the electrochemical study of pesticides, especially for the electrochemical behavior of isoproturon [17], [26]. Manisankar *et al.* 2002, have reported the electrochemical behavior of isoproturon molecule at different electrochemical conditions claiming that the electrochemical oxidation of isoproturon depended on the conditions of the reaction [17]. They have studied different parameters and found that the most favorable

medium for electrochemical oxidation of isoproturon was at lower pH values (pH ~1.0) in aqueous acidic solutions. Moreover, they claimed that the electrochemical oxidation of isoproturon is an irreversible, diffusion controlled, and two-electron transfer reaction [17]. Further they mentioned that during electrochemical oxidation of isoproturon, it is oxidized into *4 – isopropylaniline*, and as a result of this intermediate undergoes a quasi-reversible redox reaction [17]. Based on these facts sulfuric acid is chosen to be used as the medium for the electrochemical study of isoproturon (pH ~1.0).

3.3.2. Synthesis of NIP-GC and MIP-GC electrodes

The electro-synthesis of molecularly imprinted polymer (MIP) films and that of non-imprinted polymer (NIP) films was performed on glassy carbon electrodes, respectively named MIP-GC and NIP-GC, in an ethanol and water (20/80) solution containing 10 mM of pyrrole and 0.1 M of $LiClO_4$ as electrolyte. For the preparation of MIP-GC, the template molecule, 1 mM of isoproturon, was added. The ratio between the concentration of monomer and the concentration of isoproturon as template molecule in the electrolyte solution prepared for the electropolymerization was chosen to be (monomer conc. 10/1 isoproturon conc.) in accordance of the condition usually used in the PPy-MIP electropolymerization [213]. Electropolymerization was accomplished either by applying cyclic voltammetry (CV), 5 scans in the potential range from 0 to 1.4 V vs Ag/AgCl at a scan rate: v = 10 mV s^{-1}, or by chronoamperometry (CA), with a potential set at 1.1 V vs Ag/AgCl for a duration of 600 s. The MIP-GC electrodes, once prepared, were rinsed with milli-Q water and immersed in an ethanol/water (70:30 v/v) solution of 0.1M sulfuric acid. They were biased to a potential excursion between −0.4 V and 1.5 V vs Ag/AgCl for several scans until complete extraction of the embedded isoproturon molecules. After extraction the MIP-GC electrode was used for isoproturon detection.

3.3.3. Detection of isoproturon by MIP-GC electrodes

The MIP free of isoproturon and NIP coated electrodes were immersed in an aqueous solution containing isoproturon as template molecule at low concentrations, under stirring, during an optimized time. Both electrodes were then rinsed with Milli-Q water in order to remove the isoproturon just deposited on the MIP-GC and NIP-GC surface. The electrochemical detection of isoproturon was achieved by square wave voltammetry (SWV), in an ethanol/water (70:30 v/v) solution containing 0.1 M of sulfuric acid.

3.4. Elaboration of the MIP-GC electrode

3.4.1. Electropolymerization of pyrrole

The electropolymerization of pyrrole in the presence of isoproturon leads to the inclusion of the template molecule in the polymer matrix during polymer growth. Isoproturon extraction by CV creates cavities within the MIP, which are complementary in shape and functionalities to the template molecule. These prints should therefore allow selective rebinding by isoproturon, as the artificial receptors are shaped by the template [214], and finally the use of SWV will enable to confirm the presence and to determine isoproturon concentration.

The electrochemical polymerization of pyrrole on the GC electrode surface was performed by cyclic voltammetry (CV) or by chronoamperometry (CA) with and without the presence of the template molecule (isoproturon) in the dissolved monomer solution. In Figure 40 are presented the cyclic voltammograms obtained during electropolymerization of NIPs and MIPs. For both cases, we can observe the anodic current that increase after +0.75 V vs Ag/AgCl due to the oxidation of the pyrrole on GC electrode with the current peak at +0.95 and +1.15 V vs Ag/AgCl respectively in the solutions without and with 1 mM of the ISO template. The potential shift is probably due to the presence of isoproturon in the solution which itself is oxidized at a potential around +1.0 V. In a second scan, voltammograms of MIP and NIP electropolymerization show that the pyrrole oxidation peak decreases drastically due to the change in the

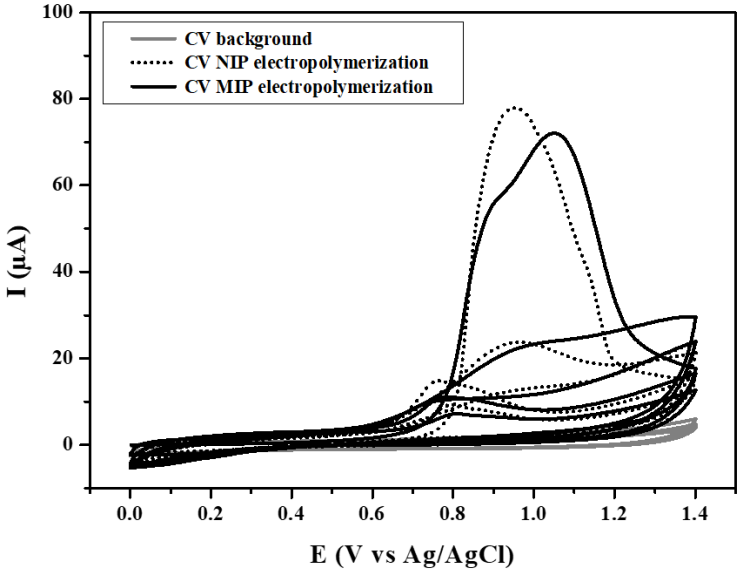

Figure 40. Cyclic voltammograms taken during electropolymerization of pyrrole (0.01 M) in absence (NIP) and in presence of ISO (1 mM) (MIP) onto GC electrode, electrolyte: 0.1M $LiClO_4$ in ethanol/water (20:80 v/v). Scan rate 10 mV/s.

nature of the electrode surface after the deposition of a polypyrrole layer that is less conductive than the carbon itself [215]. In the case of chronoamperometry (CA) electropolymerization, the process was carried out in the same electrolyte conditions, but the applied potential value has been fixed where indeed it is impossible to see any difference between the NIP and MIP films electrochemical polymerization.

3.4.2. Extraction of the template molecule

The extraction of the template molecules from polymer matrix in the case of electrochemically fabrication of MIP dedicated to the different micropollutants detection, is reached often using organic reagents or buffer solution as eluent [33], [137], [139], [140], [145]. In these cases, even though low limits of detection were reached, it is not sure that the removal of the template molecules has been achieved in its entirety. On the other side, there are reported various articles where the extraction of the template molecules has been reached electrochemically by using cyclic voltammetry or other methods [31], [83], [136], [141], [142], [144], [182], providing an easy and a shorter procedure with avoiding the use of dangerous organic solvents as eluents. However, there is a lack of explanation for the process of the template molecules extraction.
In this work, the template isoproturon molecule extraction was obtained by cyclic voltammetry (CV). During the process of template extraction was observed an oxidation peak, at around +1 V vs Ag/AgCl, corresponding to the isoproturon trapped within the polymeric matrix. Several scans were made until the oxidation peak was no

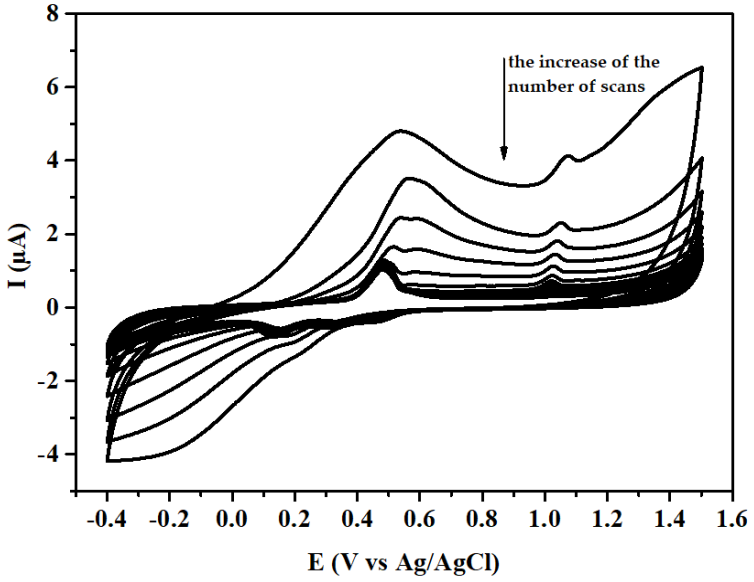

Figure 41. Cyclic voltammograms obtained during ISO extraction on the MIP-GC electrode: Electrolyte 0.1 M H_2SO_4 in ethanol/water (70:30 v/v). Scan rate 100 mV/s.

longer observed due to the release of the isoproturon, which was disappeared with the increase of the number of cyclic voltammetry scans (Figure 41). The well-known reversible oxidation-reduction behavior of polypyrrole [216] is also clearly observed at +0.4 V vs Ag/AgCl for the polypyrrole oxidation process and −0.25 V vs Ag/AgCl for the reduction process in our MIP-GC electrode. On the voltammogram of the NIP electrode (not shown), no peak at +1.0 V was observed while the polypyrrole signal was present in the same region as for the MIP. This method of template extraction has various advantages if compared with chemically methods, it is easy to achieve and avoids the use of a variety of dangerous organic solvents as eluent reagents. Moreover, the voltammograms obtained validated the removal of the template, and like this the binding sites inside the polymeric film were created. At this stage, the modified GC/MIPPy/ISO sensors have been prepared and stored in air at room temperature and were ready to use for the further electrochemical analysis of isoproturon.

3.5. Optimization of the MIP-GC elaboration procedure

In this section, the detection signal of isoproturon served as a tool for the electrochemical synthesis optimization of the MIP-GC electrode. The ISO detection was performed as follows: after the electrochemical release of ISO, MIP-GC electrodes were immersed in a 5×10^{-7} M isoproturon water solution during 15 min and the analyses were performed by SWV in an ethanol/water solution (70:30 v/v) of 0.1M sulfuric acid. The sensing properties of MIP-GC electrodes obtained by CV and by CA were compared after optimizing the impact of the scan number for CV and the electrolysis time for CA and establishing the influence of the ratio of ethanol in the electrolyte solution.

3.5.1. Influence of potential range in the CV extraction process of isoproturon

Different potential ranges are used for the CV extraction of isoproturon from the MIP polypyrrole films, in order to figure out if there is any influence in the isoproturon current signal. Figure 42 shows the results obtained during isoproturon electrochemical detection by SWV at the GC-MIPPy electrodes after the CV extraction of template molecule at different potentials, ranging from +0.9 V up to +1.9 V. As seen in the figure, at lower potentials than +1.1 V the extraction of isoproturon was not reached totally, due to its oxidation potential (see Figure 39 and section 3.3.1.), whereas at higher potential values +1.3 V up to +1.9 V the oxidation signal of isoproturon was observed to be in line, even though there is overoxidation region of polypyrrole. However, the

overoxidation of the polypyrrole did not affect in the determination signal of isoproturon.

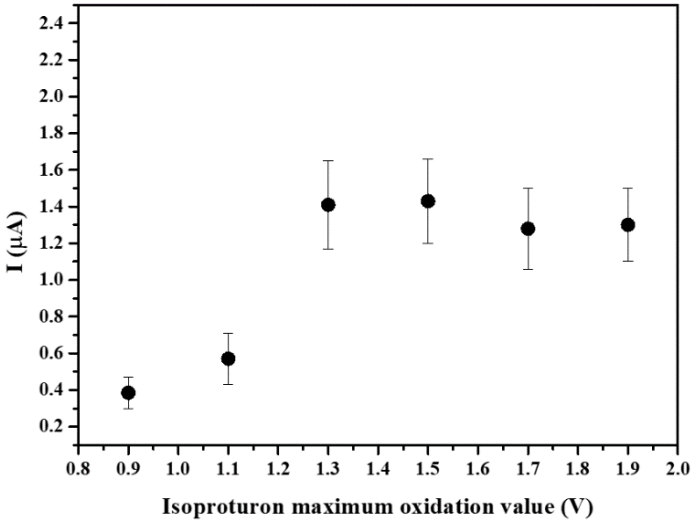

Figure 42. SWV determination of isoproturon (5 x 10^{-7} M) at GC-MIP polypyrrole electrodes after template extraction by CV at different potential ranges.

3.5.2. Preparation of isoproturon MIP-GC electrodes by cyclic voltammetry (CV): influence of the scan number

In order to determine the effect of the number of cycles during electropolymerization on the response of isoproturon detection by MIP-GC, the film was prepared with 1, 3 and 5 cycles, (see Figure 43-A). It clearly shows that the response of isoproturon is improved with the number of scans due to the increase in the thickness of the polymeric matrix and consequently the number of cavities. In order to verify this assumption, the theoretical thickness of the layer was estimated from the electrical charge (Figure 43-B). To correlate polypyrrole thickness x (cm) and electrical charge, Faraday's law was used assuming 100% current efficiency for polypyrrole:

$$x = qM / \rho AzF \quad \ldots\ldots\ldots\ldots\ldots\ldots\ldots\ldots(3.1)$$

where q (C) is the electrical charge associated with polypyrrole formation, M (g/mol) is the molar mass of the monomer, F is Faraday's constant (C mol^{-1}), A (cm^2) is the area of the working surface, ρ (g cm^{-3}) is the polymer density and z (mol) is the number of electrons involved in the electropolymerization process of pyrrole which in this case is 2.25 [9],[174]. The nominal density for polypyrrole films (ρ) was taken as 1.5 g cm^{-3} [216]. By taking into consideration all the above-mentioned parameters, the required

charge density to grow a film with an average thickness of 290 nm is 10.4 mC/cm^2 [76]. We can see, in Fig. 46B, that the estimated thickness increases with the number of cycles to reach 290 nm after 5 scans in the case of MIP-GC. To confirm this result, the behavior of a ferrocene 2.5 mM redox probe in acetonitrile solution containing 0.1M NBu_4BF_4 on MIP layers obtained at 1, 3 and 5 cycles was studied (Figure 43-C).

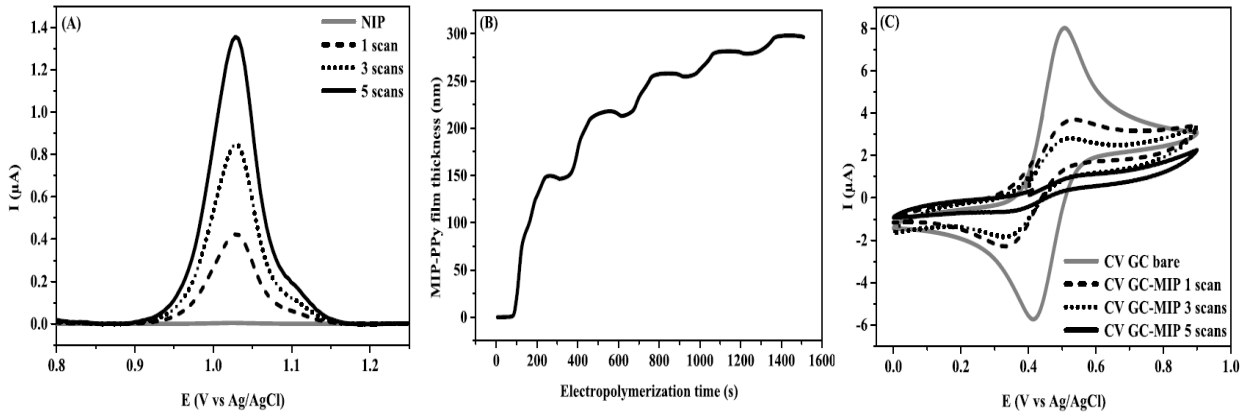

Figure 43. Influence of the scan number during electropolymerization of the MIP on GC electrode (A) on isoproturon response on MIP-GC electrode (B) on MIP film thickness estimated using Faraday's law from the voltammogram (C) on CV ferrocene response (2.5 mM) in NBu_4BF_4 (0.1 M) acetonitrile solution on bare and MIP-GC electrodes. Scan rate 100 mV/s.

It shows that the blocking effect for the ferrocene signal increases with the number of cycles due to the growth of the insulating polymer layer because of the overoxidation conditions [212]. Finally, in order to determine the electropolymerization efficiency, one experimental thickness of the MIP layer deposited by EQCM assuming a density of MIP 1.5 g/cm [215], [216] and the corresponding charge was measured. The electropolymerization yield was calculated from the ratio between the experimental and the theoretical thicknesses and was found to be close to 63%.

3.5.3. Preparation of isoproturon MIP-GC electrodes by chronoamperometry (CA)

3.5.3.1. Effect of solvent – the role of ethanol/water ratio

During the electropolymerization of a MIP film, knowing that the solubility of isoproturon is limited in water (70.2 mg/L at 25 °C) we added ethanol in water at different quantities. Figure 44-A shows the film thickness calculated from chronoamperometry curves for a constant electropolymerization time using Faraday's law for different ratios of ethanol. It is shown that the thickness of the MIP film produced is directly dependent on the amount of ethanol, hence when the amount of

ethanol is greater than 40% the film thickness is less than 50 nm. Below 40% of ethanol, the film thickness increases linearly until it is six-fold the initial thickness. The same MIP-GC electrodes were used for ISO detection. Figure 44-B shows the ISO peak current as a function of the ethanol ratio. The best results were achieved with MIP-GC electrodes prepared in water/ethanol solutions containing lower amounts of ethanol. MIP films produced with a maximum between 15 and 20% of ethanol showed the best performance for ISO detection. This value was therefore chosen for further study.

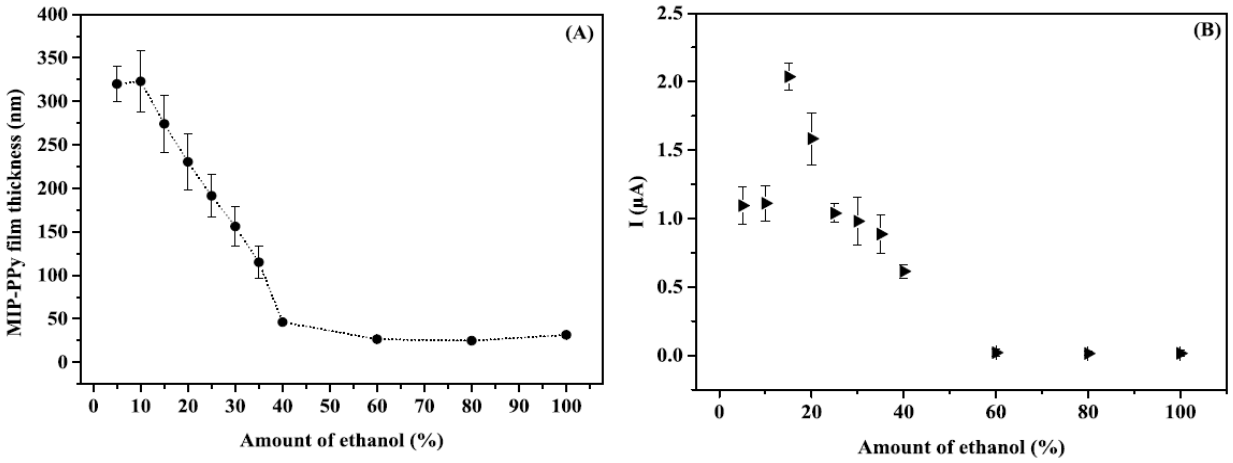

Figure 44. Electropolymerization of MIP-GC electrode for different ratios of ethanol/water with $LiClO_4$ 0.1M (A) film thickness calculated from chronoamperogram and (B) ISO peak intensity electropolymerization: CA 1.1 V during 600 s; pyrrole 0.01M in presence of ISO 1 mM.

The influence of the ethanol is therefore very important for the thickness of the MIP. In order to compare whether the influence of the solvent is also impacting on the electropolymerization of PPy in the absence of the template. Electrochemical quartz crystal microbalance (EQCM) has been used for the further investigation of solvent ratio to the quality of NIP-PPy films. Electropolymerization of NIPs was performed on gold quartz electrodes at different ratios ethanol/water solutions of pyrrole 10 mM with $LiClO_4$ 0.1 M. The mass growth of the NIP films with electropolymerization time is shown in Figure 45-A. Figure 45-B shows the variation of thickness of the NIP films calculated directly from the mass obtained (equation: thickness = mass of the film / density of the films) with amount of ethanol present in the electrolyte. One can observe that the films fabricated in the solutions with the amount of ethanol >50% are too thin and leveled off, while those obtained in the presence of 20% ethanol showed to be thicker and more visible on the gold electrodes surface (Figure 45-C, inset in the Figure 45-B). This result is similar with NIP film thickness in relation with ethanol percentage in the solution obtained on GC electrode.

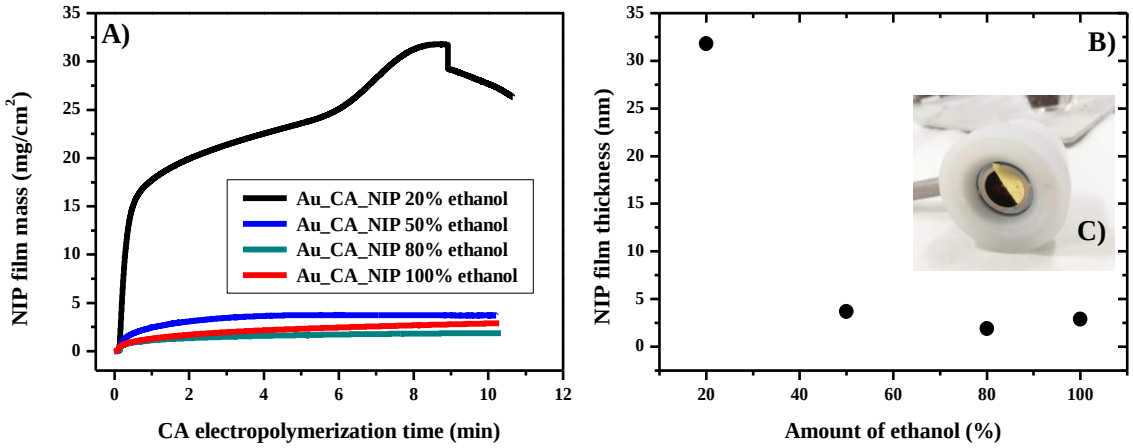

Figure 45. EQCM study of the influence of amount of ethanol in its aqueous solution containing 0.01 M of pyrrole + 0.1 M of $LiClO_4$ on the mass growth of NIP films on gold quartz electrode. (A) Mass curves as a function of the electropolymerization time; (B) Variation of the NIP film thickness estimated by EQCM with the amount of ethanol, (C) Captured image of the NIP film on gold quartz electrode.

3.5.3.2. Influence of electropolymerization time

The influence of the electropolymerization time was studied for the MIP films prepared by CA at 1.1 V vs Ag/AgCl at different times that were used later for ISO detection. The theoretical thickness of the growing layer was estimated from the chronoamperograms in Figure 46-A and a rapid increase in this thickness up to 100 s was observed. Thereafter, its further growth is slowed down, reaching an almost linear increase after 200 s. This is most probably because of the decrease in the electronic transfer due to the thickness of the layer and to the partially insulating character of the MIP. The electrochemical detection ability of isoproturon on MIP-GC electrodes prepared by CA at different electropolymerization times is presented in Figure 46-B. These results are in agreement with those presented in Figure 44-A. During the first 100 s, the ISO detection signal was very significant, corresponding to the film thickness growth. From 100 s to 600 s, the signal of the target analyte increased more slowly. We can assume that the blocking effect of the charge transfer limits the oxidation of isoproturon during detection. Moreover, the thicker the film is, the more difficult it is for isoproturon molecules to access the cavities and to reach the conducting surface. The sharp signal decrease after 600 s is probably due to the film breaking during its growth. This assumption was validated with measures made by EQCM (Figure 46-C). The sharp mass decline also started after 600 s. It should be noted that the sharp decrease both in

the ISO peak detection and in the MIP layer mass was observed for the thickest MIP films but not always at the same time. This fact is due most probably to mechanical constraints in the thick films.

As for CV MIP preparation, the electropolymerization yield obtained from CA with EQCM measurement was calculated and the corresponding charge was found to be close to 66%. This value is of the same order as that obtained with CV electropolymerization. For both methods, the charge loss is consistent with the high potentials applied during the MIP-GC preparation.

These results show that the optimal electropolymerization time for the isoproturon response is 600 s. In addition, the sensitivity and the reproducibility of the MIP-GC (results not shown) are better for films prepared by chronoamperometry, which is consistent with the literature [83].

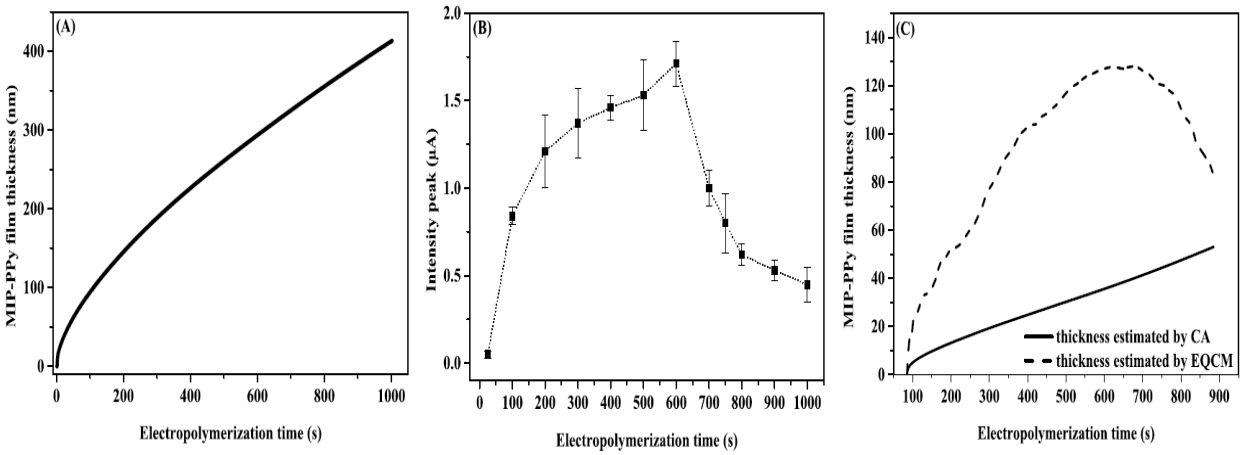

Figure 46. Effect of electropolymerization time on the electrochemical response of 5×10^{-7}M of ISO at the MIP-GC electrode in ethanol/water (70:30 v/v) of H_2SO_4 0.1 M, (A) the thickness of the MIP film estimated from the chronoamperogram (B) isoproturon electrochemical response, MIP film was formed by chronoamperometry setting the potential at 1.1 V, incubation time 15 min (C) comparative study of the MIP film thickness estimated by Faraday's law calculations and by EQCM experiments in order to follow the chronoamperometry electropolymerization process (potential applied 1.1 V, time duration 885 s) of ISO (1 mM) and pyrrole (0.01 M) on gold quartz used as a working electrode, electrolyte: 0.1M $LiClO_4$ in ethanol/water (80:20 v/v).

3.5.4. The influence of the electrodeposition substrate material: EQCM study of NIPs obtained by CA and CV onto gold and platinum electrodes

Since electrodeposition of conducting polymers is only possible on metallic or semiconducting substrates, it is often necessary to explore the nature of the substrate and to determine its contribution on the polymer film growing mechanism and its morphology. EQCM was used to investigate the impact of CA and CV to the growing process of the NIPs onto different quartz substrate electrodes, on gold (Au-quartz) and on platinum (Pt-quartz). In Figure 47-A is presented the process of the NIP electropolymerization by CA (potential applied +1.1 V, electropolymerization time 600 sec), as seen the mass of the NIP films increased rapidly in the first two minutes, the mass of the film after one minute of electropolymerization was nearly 18 μg/cm^2, and for higher time the mass leveled off gradually. Figure 47-C shows the electropolymerization process obtained by CA on Pt quartz electrode. One can observe that the rate of the NIP film formation is not the same in the start of the electrolysis compared to the gold quartz electrode, the film growth about two times slowly.

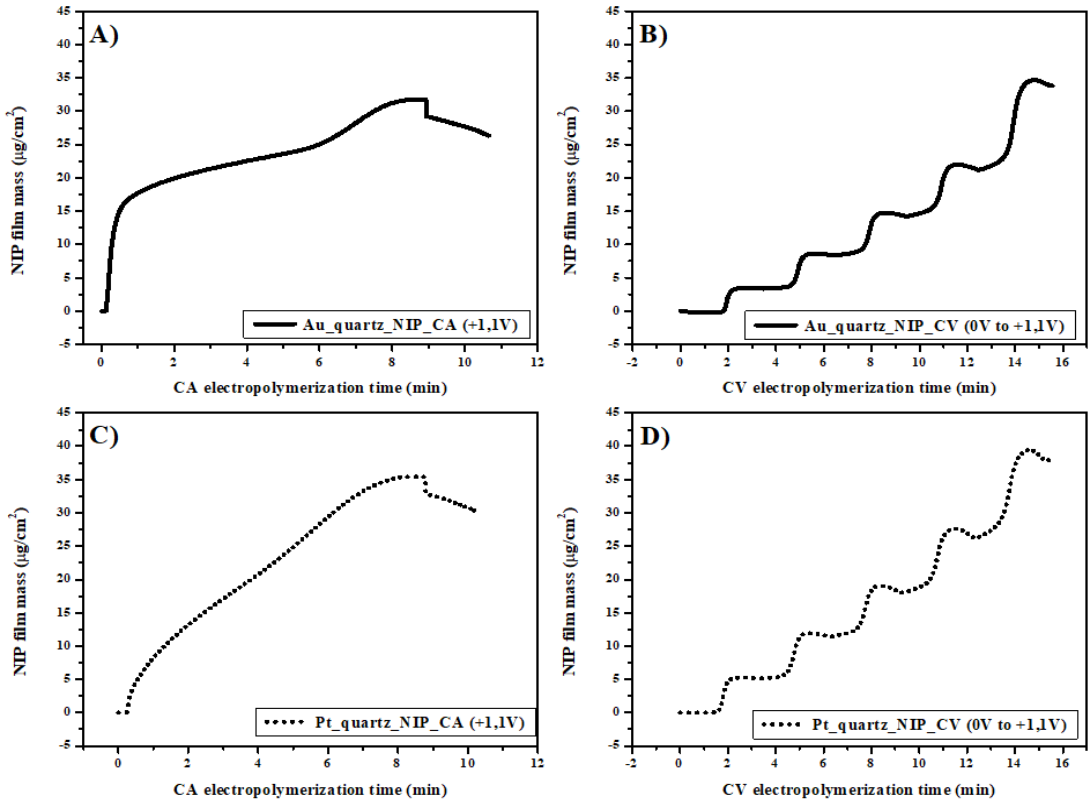

Figure 47. EQCM study of the effect of electrodeposition material substrate by CA (+1.1V, electropolymerization time 600 sec) and by CV (0 to +0.9V, scan rate 10 mV/sec) onto gold quartz crystal electrode (A, B), and onto platinum quartz crystal electrode (C, D), electropolymerization: pyrrole 0.01 M in a solution of $LiClO_4$ (0,1M) (20/80 ethanol/water v/v).

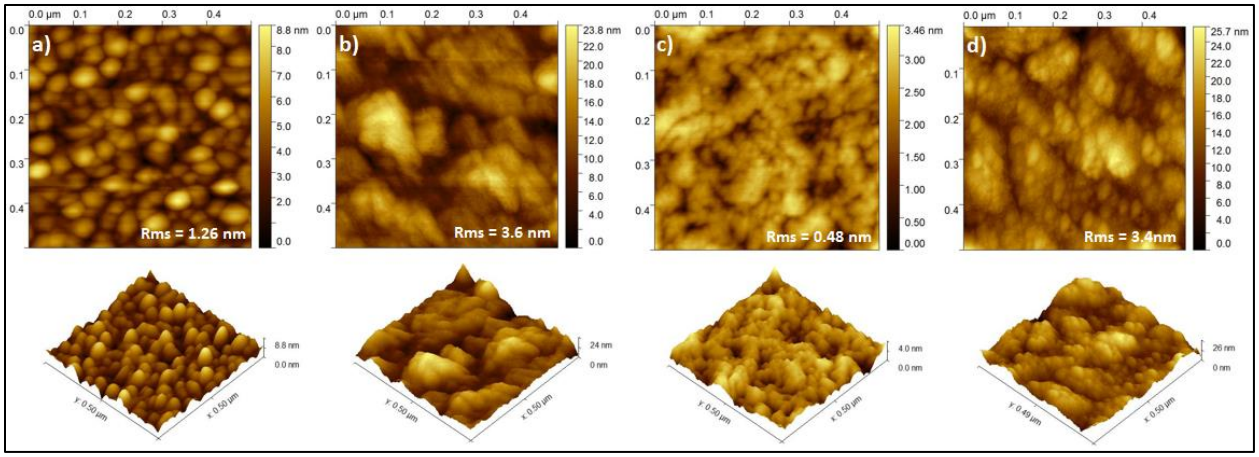

Figure 48. AFM images of NIP films on gold quartz crystal electrode a) bare gold quartz electrode, b) NIP PPy CV (0 to +0.9V), and on platinum quartz crystal electrode c) bare platinum quartz electrode, d) NIP PPy CV (0 to +0.9V).

In both cases is observed a decrease of the NIP film mass due to its degradation after about 10 min of electropolymerization. In the other side when the electropolymerization of NIPs is obtained by CV at potential range between 0 V up to +0.9 V vs ref. (Figures 47-B and 47-D) the mass growth of the NIP films was shown to be similar in both cases, and increases with number of cycles.

For the further characterization of the films fabricated onto these electrodes by CV, they were observed under AFM in order to see their morphology (see Figures 48-b and 48-d), the NIP film deposited on Au-quartz electrode showed a surface with higher roughness values (Figure 48-b) compared with the NIP film deposited on Pt-quartz electrode (Figure 48-d).

3.6. Electrochemical detection of isoproturon by the GC-MIP electrode: Optimization of incubation (rebinding) time

The incubation time is an important parameter in the analytical procedure since it will impact the overall time of the analysis. The influence of the incubation time in the range of 0–40 min on the isoproturon signal responses was evaluated in aqueous media containing 5×10^{-7} M of isoproturon. As illustrated in Figure 49, the isoproturon oxidation peak intensity increases proportionally with the incubation time in the first 15 min due to its rebinding to the created cavities. Beyond 15 min, the rebinding kinetic slows down, suggesting the beginning of saturation of the cavities or a more difficult access of isoproturon.

An incubation time of 15 min was therefore chosen to obtain the best analytical performances for this study. This parameter impacts the quantification: in the linearity domain, the longer the time, the more the lower limit of quantification (LOQ) diminishes. Moreover, a lower incubation time leads to less accurate values because monitoring the immersion time is less easy and the signal is lower.

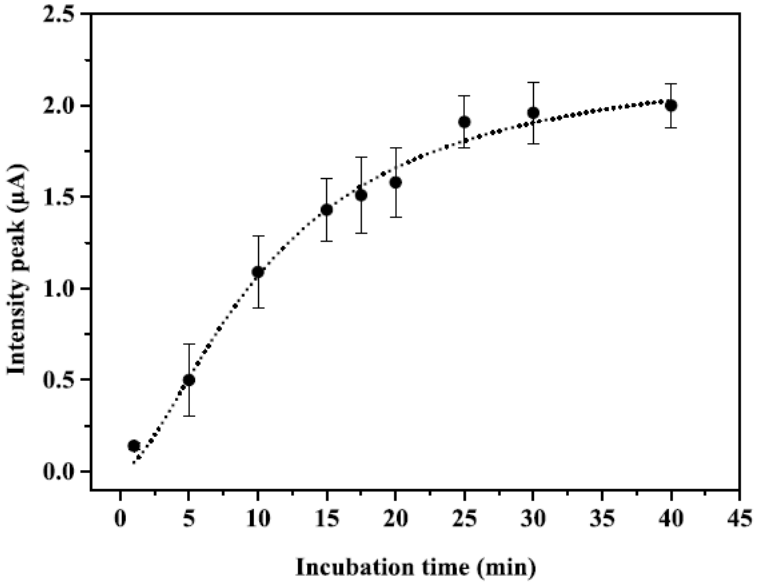

Figure 49. Isoproturon (5×10^{-7} M) response on the MIP-GC electrode for different incubation times.

3.7. Electroanalytical performances of the GC-MIP electrodes

3.7.1. Calibration curve and determination of LOD/LOQ

In this subsection, the optimal conditions to achieve the best sensitivity for isoproturon detection were selected: the MIP-GC film obtained by CA at +1.1 V vs Ag/AgCl during 600 s was used and isoproturon detection by SWV was carried out in an ethanol/water solution (70:30 v/v) of 0.1M sulfuric acid free of isoproturon after 15 min immersion of the film in a milli Q water solution containing isoproturon at concentrations in the range of 2.5×10^{-9} M – 5×10^{-6} M. The calibration curve is presented in Figure 50-A. The square wave voltammograms clearly showed a current peak increasing with concentration during ISO detection in Figure 50-B. The sensitivity was obtained from the slope of the calibration curve; its value was 4.8701 A/M. The calibration plot was found to be linear between 0 and 10^{-7} M and obeyed the following relation:

$$\boldsymbol{I\ (\mu A) = 4.8701\ [Isoproturon] - 0.0043}\ (R^2 = 0.9959)\ \ldots\ldots\ldots(3.2)$$

The isoproturon limits of detection (LOD) and quantification (LOQ) that were calculated statistically [218] were 2.76×10^{-9} M (0.5 μg L^{-1}) and 9.2×10^{-9} M (1.9 μg L^{-1}) respectively. Repeatability was evaluated after seven analysis replicates of isoproturon 5×10^{-7} M solution with a single electrode. Well-shaped voltammograms were obtained for all experiments: the calculated relative standard deviation (RSD) was 7.6%. Reproducibility of the procedure was evaluated by performing a series of analyses with five different electrodes. The RSD obtained was 12%. These results indicate that isoproturon MIP-GC electrodes are reliable tools for isoproturon detection and quantification. Each MIP-GC electrode can be used for 25 cycles of analyses with a change of the isoproturon peak intensity less than 20%. Then a decrease of the signal is observed during the 20 next analyses with an extinction of the signal comprising between 50 and 90% depending on the electrode.

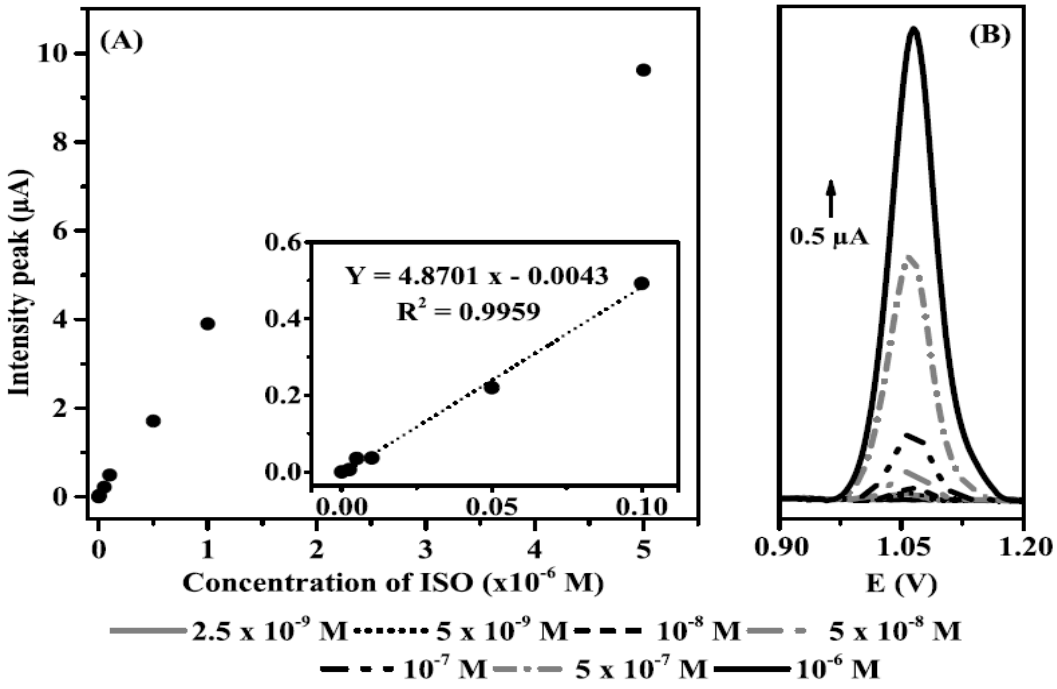

Figure 50. The calibration curves of isoproturon detection obtained at MIP-GC electrode in Milli-Q water. Current-concentration calibration curve (A) includes linear

3.7.2. Interference study

The selectivity of the prepared MIP-GC electrodes toward isoproturon was tested for three interfering molecules (see Figure 51): carbendazim, diuron and carbamazepine, at two concentrations, 5×10^{-6} M, 5×10^{-7} M and 10^{-7} M, for each molecule, in the presence of isoproturon at 5×10^{-7} M. These molecules are widely found in environmental waters and have a structure and oxidation potentials quite close to those of isoproturon. Thus, these molecules may interfere with the determination of isoproturon. The results, presented in Figures 51-A and 51-B show that according to the RSD found (see previous sub-section), neither carbendazim nor carbamazepine seem to affect the MIP-GC sensitivity toward isoproturon, whereas the presence of diuron (Figure 51-C) at the same concentration or at a concentration 10 times higher as isoproturon lowers its signal by 50% and 80% respectively. However, in natural environments, diuron is found at concentrations up to 17 times lower than that of isoproturon [219]. Thus, we can reasonably assume that diuron does not exhibit major interferences with isoproturon.

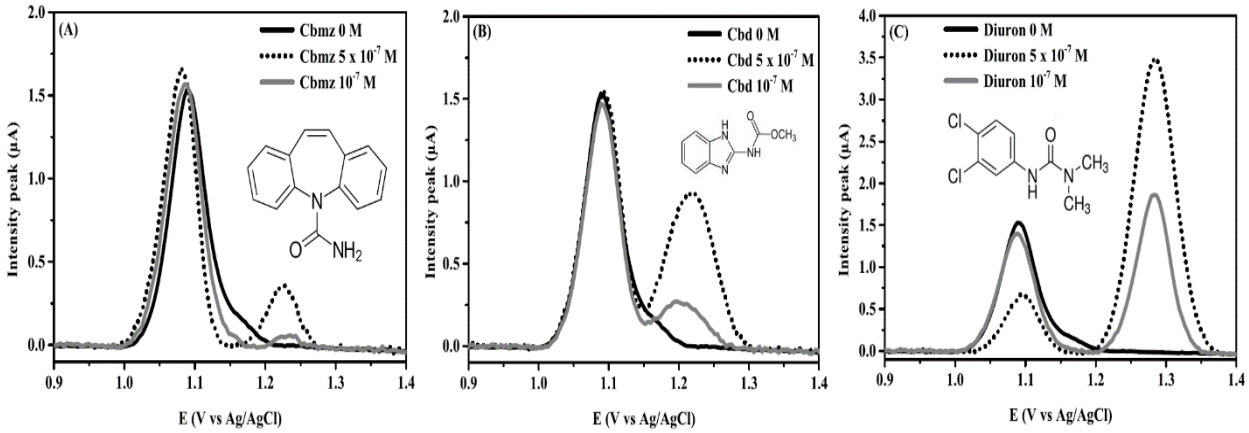

Figure 51. Effect of the interferences on the determination of ISO (5×10^{-7} M) using the MIP-GC electrode: (A) carbamazepine (B) carbendazim and (C) diuron.

3.7.3. Application of the electrochemical sensors in real water samples

The electrochemical methods developed were applied to the detection of isoproturon in a real water sample. A groundwater sample located in France, Region Centre, was chosen in accordance with the funding project (CAPEL MIP) (see Figure 52). The site is located in the commune of Saint-Remy-Du-Val (Sarthe, province of Loire-Bretagne region). The monthly monitoring performed in this aquifer revealed that the groundwater is contaminated by several pesticides and notably triazines and chloroacetanilides and their metabolites, but does not contain isoproturon (< 0.005 μg L^{-1}).

The samples were prepared with this natural groundwater as seen in Figure 53, adding a known quantity of isoproturon to obtain concentrations from 1×10^{-8} M to 5×10^{-7} M.

The calibration plot obtained with these samples was found to be linear between 0 M and 5×10^{-7} M (see Figures 54-A, 54-B) and obeyed the following relation:

$$\boldsymbol{I\ (\mu A) = 4.1853\ [Isoproturon] + 0.0056}\ (R^2 = 0.999)\ \text{…….(3.3)}$$

Figure 52. Commune Saint-Rémy-Du-Val (72317) - Sarthe (72) province of Pays-de-la-Loire – Bretagne Region - France, an altitude of 117 m and a depth of investigation 23 m (coordinates X, Y: 446125, 2372347 (Lambert II Etendu) / 497082, 6807017 (Lambert 93).

The LOD and LOQ were 1.1 × 10^{-8} M (2.2 μg L^{-1}) and 3.7 × 10^{-8} M (7.6 μg L^{-1}), respectively. The sensitivity obtained from the slope of the calibration curve was 4.1853 A/M. The oxidation current of the preconcentrated isoproturon in the MIP film is easily visible in the solutions that contain concentrations higher than 1×10^{-8} M of isoproturon.

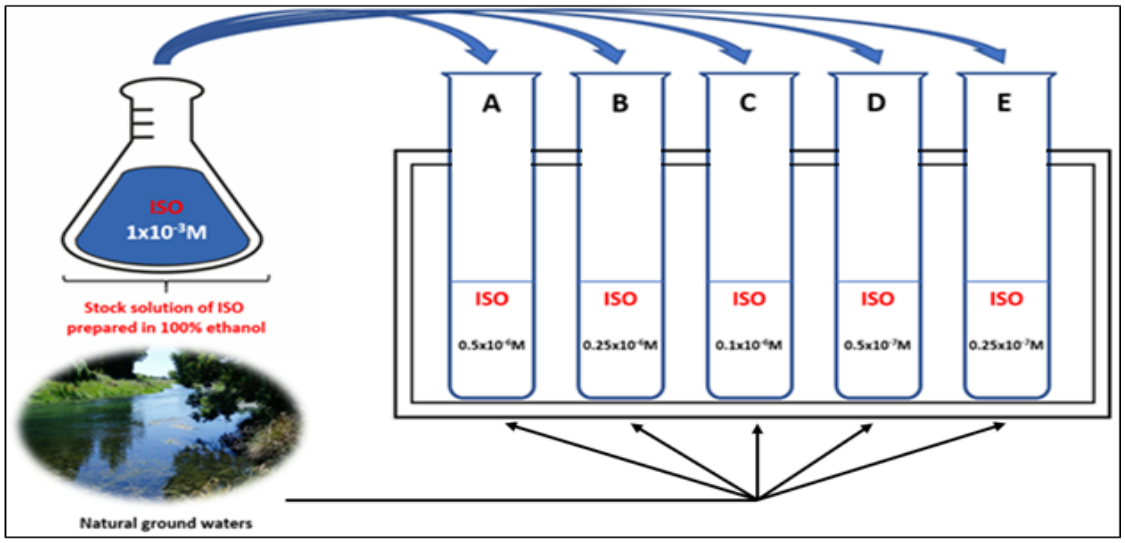

Figure 53. Schematically representation of the procedure used for the preparation of ground natural water samples for the isoproturon (ISO) analysis by using GC-MIPPy electrodes.

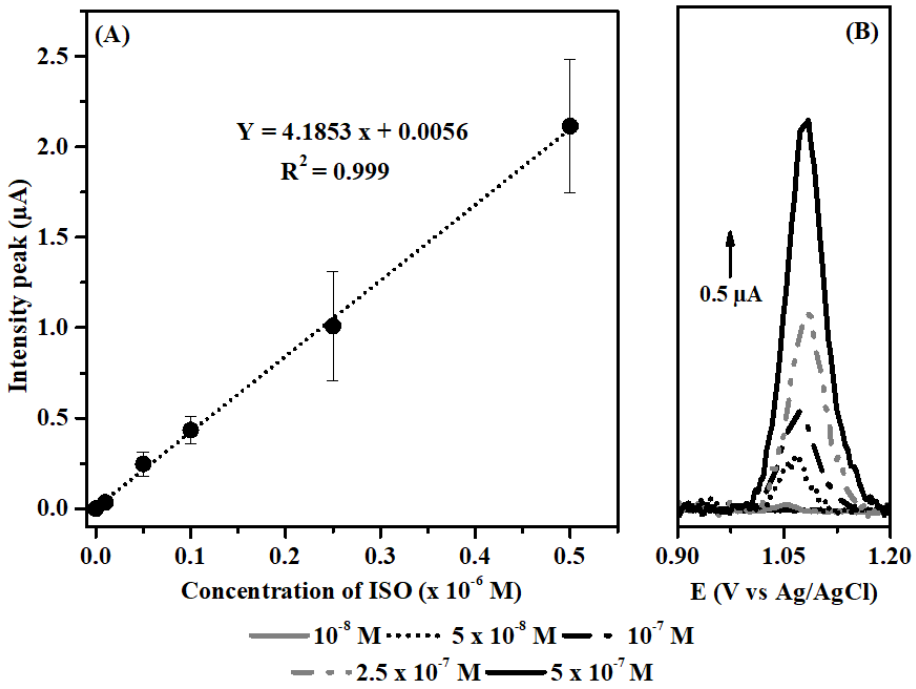

Figure 54. The calibration curves for isoproturon determination obtained at MIP-GC electrode in real natural water samples (A) includes calibration linear equation (B) square wave voltammograms obtained during electrochemical detection of isoproturon.

3.8. Conclusion and perspectives

In this part of our work, a novel electrochemical sensor for the sensitive and selective SWV determination of isoproturon, a priority micro-pollutant, was developed. It is shown that ultra-sensitive MIP films for its detection can be prepared in a simple way by CV or CA onto GC electrodes. Firstly, it was studied the electrochemical behavior of isoproturon as the targeted pollutant molecule. Furthermore, the key parameters of MIP electro-synthesis such as electrodeposition time, scan number, solvent ratio and incubation time were optimized. The extraction step of the template molecule was conducted electrochemically in aqueous solution, thus avoiding the use of toxic organic solvents. The MIP-GC sensor was able to detect isoproturon in nano-molar concentration with good reproducibility and repeatability. The functionalized electrode surfaces showed good robustness during the use for about one week of experimental analyses.

The performances in terms of LOD, LOQ and selectivity are satisfactory for the contaminated natural waters of the Loire-Bretagne region, where isoproturon concentrations up to 5.8 nM (1.2 $\mu g\ L^{-1}$) have been measured in 67% of the stations [219]. For other sites, this LOQ is not low enough as worldwide occurrence in the environment showed for effluent a maximum concentration of 1.3 nM (0.27 $\mu g\ L^{-1}$) with a 51% frequency of detection in the effluent of conventional wastewater treatment plants in Europe [78], and for surface water of inland seas a maximum concentration of 0.3 nM (0.06 $\mu g\ L^{-1}$) with a 100% frequency of detection in estuaries on the Baltic coast [219]. But in spite of these good performances, they are still higher than the maximum allowed levels set by the WFD.

Thus, at this stage the investigations must be focused into the nanostructuration of the polypyrrole path in order to enhance the sensitivity of these sensors and to increase the number of accessible cavities. For achieving this, we look forward to use more sophisticated methods in order to study the correlation of the MIP properties in terms of conductivity and sensitivity to the isoproturon detection, where this part will be discussed in the Chapter IV.

- Page left intentionally blank -

CHAPTER IV

"Optimization parameters of Molecularly Imprinted Polymer films for Isoproturon detection: impact of anodic potential on the overoxidation of polypyrrole"

4. CHAPTER IV: Optimization parameters of Molecularly Imprinted Polymer films for Isoproturon detection: impact of anodic potential on the overoxidation of polypyrrole

4.1. Introduction

In the previous chapter, the developed electrodes were able to detect isoproturon present at nanomolar concentrations in water. The results obtained show the interest of this approach in the development of isoproturon's electrochemical sensors. The influence of experimental parameters such as solvent and choice of electrochemical method on the detection signal of isoproturon was studied. The optimized experimental conditions consist quite classically to used anodic potential leading to an overoxidation of the PPy film both for the formation of the MIP and during the template extraction step. There are relatively few studies in the literature dealing with the consequences of this overoxidation on the properties of the MIP, particularly in terms of conductivity and porosity, the two key properties for the MIP electrochemical sensors.

PPy is a well-known partially cross linked polymer frequently used for the development of MIP electrochemical sensors without any further need for another cross linker due to the use of an overoxidation potential [157], . Moreover, the electrochemical properties of PPy are strongly dependent on their redox state. When PPy film is biased under more positive potential, its overoxidation occurs, leading to the partial degradation of polymeric backbone and introduction of carboxylic, carbonylic and hydroxylic groups that determines semi-permeability as well as ability to recognize imprinted molecules [220]. The best results are achieved when during electrochemical deposition, overoxidized PPy is imprinted by small molecular weight molecules [220]. The electropolymerization parameters such as nature of the solvent, size and nature of the dopant counter-anions, electropolymerization method, electrode substrate, and other parameters can have a strong influence on all the properties of the PPy films including conductivity, mechanical properties, structure and morphology [202]. Most optimized parameters during the electropolymerization found in the literature are: electrodeposition method [221], electropolymerization time [165], [221], [222] and nature of solvent [223]. Yang et al. 2015 developed a molecularly imprinting polypyrrole sensor (MIP-PPy) on carbon aerogel electrodes for electrochemical determination of dopamine [224]. By optimizing the film thickness using cyclic voltammetry they reached to increase the current response for dopamine detection. A thinner MIP-PPy layer contains less recognition sites for dopamine while a very thick

layer has less accessible imprinted sites because the templated molecules situated at the inner area of the MIP-PPy film cannot be completely removed from the polymer matrix resulting in a decrease in the number of recognition site [224].
As it concerns polymer film conductivity and porosity, electrochemical impedance spectroscopy (EIS) was used quite often as a sophisticated method. EIS measurements enabled characterization of the different parameters in the polymeric MIP films generated on the electrode surfaces such as resistivity, porosity and ability for catching targeted molecules by mainly focusing in the study of the behavior of the MIP films before and after the release of the template molecule [32], [35], [191], [192], [225], [226].
Herein we present the impact of several experimental parameters that imparts the performance of electrochemically synthesized MIP-PPy sensor for ISO. Some of them such oxidation potential used for MIP-PPy preparation, time electrolysis and extraction potential for ISO removal have a direct impact in terms of sensor conductivity and sensitivity to the targeted molecule detection.

4.2. Experimental conditions

4.2.1. Preparation of MIP and non-imprinted polymer (NIP) electrodes

Electrochemical MIP and NIP film synthesis are performed onto glassy carbon electrodes, in an ethanol and water (20/80) solution containing 10 mM of pyrrole and 0.1 M of $LiClO_4$ as supporting electrolyte and the template molecule, 1 mM of isoproturon, for the preparation of MIP-GC. Pyrrole electropolymerization is made either by applying cyclic voltammetry (CV), 1-10 cycles, at different anodic potential ranges vs Ag/AgCl with scan rate, v = 10 mV s^{-1} or by chronoamperometry (CA), for time duration 600 s. MIP-GC electrodes, once prepared are rinsed with milli-Q water and after immersion in an ethanol/water (70:30 v/v) solution of 0.1 M sulfuric acid are biased under potential excursion between -0.4 V and 1.2; 1.3; or 1.5 V for several scans until the complete extraction of the embedded ISO molecules. This electrode is ready for the ISO detection. The working electrode was a glassy carbon (GC) disc (area of 0.07 cm^2), replaced with the glassy carbon plates, Au quartz and Pt quartz crystal electrodes for used for the characterization of polymeric MIP films.

4.2.2. Characterization of the MIP polypyrrole film

In order to investigate the influence of electrochemical parameters at each step of MIP-PPy and NIP-PPy fabrication process, we have used glassy carbon plates, gold quartz crystal and platinum quartz crystal electrodes. These modified electrode surfaces are used for the film's morphology and thickness characterization by AFM, while EQCM permitted the monitoring of the film mass growth. XPS and IR measurements were performed to study the impact of anodic potential of the MIP-PPy and NIP-PPy quality when prepared by CA and CV at different potentials, and after the template extraction. The electrochemical behavior of ISO was studied onto bare GC electrode. EIS characterization of MIPs and NIPs is made at the same electrodes as for the ISO detection. EIS was scanned at the formal potential of 0.25 V in the frequency range from 100 kHz to 100 mHz, using an AC voltage of 10 mV amplitude and 10 points per decade.

For AFM characterization, the MIP and NIP polypyrrole thin films electropolymerized on glassy carbon plates have been washed in toluene (>99% extra pure), in acetone (~99%), and in ethanol (~99%) for about 15 minutes in each solvent, and analyzed with a BRUKER-Dimension ICON high performance microscope. XPS characterization measurements were performed with a Thermo Fisher Scientific's Escalab 250Xi X-ray photoelectron spectrometer. FT-IR spectra were recorded with a Thermo Fisher Scientific IR spectrometer. The impedance data were represented in the complex impedance with Nyquist plots, and the Z-View software was used to fit and analyze the impedance spectra using an appropriate equivalent electrical circuit. The EQCM measurements were performed by a Maxtek RQCM micro-balance on Maxtek 5 MHz Au-Cr crystals and on Maxtek 5 MHz Pt-Cr crystals.

4.3. The influence of the electrodeposition method

4.3.1. Electrochemical synthesis of MIP and NIP polypyrrole films by CA

Polymerization of pyrrole that enables the formation of MIP and NIP-PPy films onto GC electrodes is made by chronoamperometry at different oxidation potential during 600 s [109]. As seen in Figure 55-A, the increase in the anodic electrolysis potential value affects the film thicknesses measured by AFM scratching mode (see Appendix 2). This thickness is compared with that calculated theoretically by Faraday's law [109], [146], [165], [178] and one can see at all electrolysis potential values, the thickness of the MIP-PPy films generated by CA is very close to that calculated by Faraday's law. The performance of GC-MIP electrodes was tested for the ISO electrochemical determination at low concentrations solution (concentration 5.10^{-7} M) (Figure 55-B). It is shown that the peak current detection of ISO increased for the MIP-PPy made at the electrolysis potential 0,9 V and 1,1 V while for them prepared at higher values, it decreases. The catching abilities of the MIP-PPy films for a certain molecule, as for ISO are not only dependent on the conductivity of the polypyrrole films, but also on the film thickness [145], [224], as consequence the value of the detection signal also varies. These results highlight the good efficiency of the faradic process during electropolymerization.

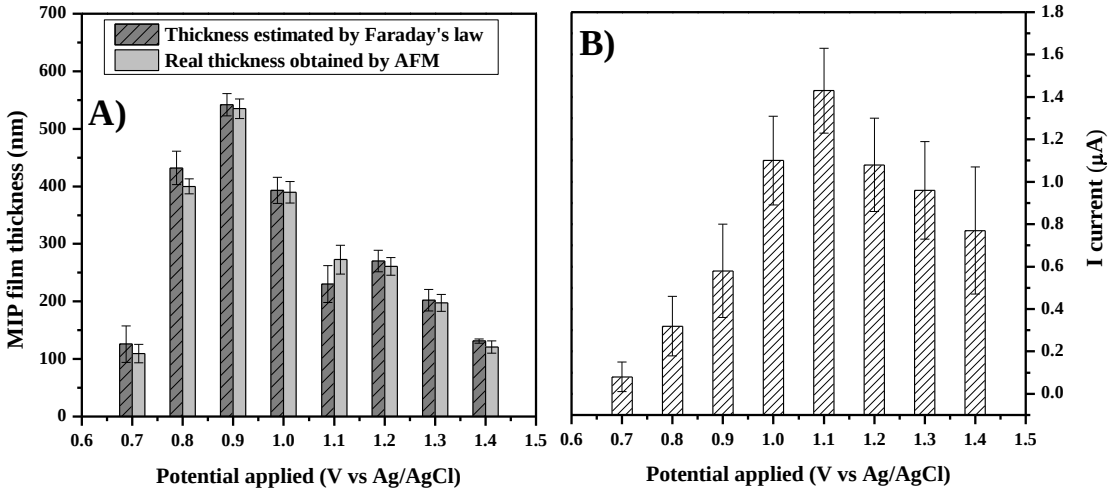

Figure 55. Formation of MIP during the electrolysis at different applied potential values when GC electrode is immersed in ethanol/water (v/v:20/80) solution containing 0.01 M of pyrrole + 1 mM of ISO + 0.1 M of $LiClO_4$. (A) The comparison between the films thickness estimated theoretically by Faraday's law and the real thickness estimated by AFM scratching mode and (B) ISO current peak intensity for the MIP-PPy made at different electrolysis potential.

These results put also in evidence that catching abilities of the MIP-PPy films for a target molecule, here for ISO are not only dependent on the film thickness [26], [36], but also to other film properties particularly on the conductivity of the polypyrrole films. And consequently, there is a shift between the maximum of the variation of the thickness and that of the peak intensity of the ISO detection (Figure 56-B).

4.3.2. Electrochemical synthesis of MIP and NIP polypyrrole films by CV

4.3.2.1. Influence of the potential range

The electropolymerization of MIP-PPy films is also made by cyclic voltammetry at different ranges of the potential to find out the impact of this parameter on the sensor performance. In Figure 56, are presented the voltammograms obtained during electropolymerization of MIP-PPy. As seen from the Figure 56-A, during the first anodic scan, the current begins to rise at potential around +0.6 V vs Ag/AgCl as result of the formation of radical cations of monomers. In this case, during the following scans the current increased and there is a fivefold difference between the first and the fifth scan. Figures 56-B and 56-C, show voltammograms obtained at with higher anodic potential which gave higher currents during consecutive scans with a current peak at 0.9 V/Ag/AgCl due to the electrochemical polymerization of pyrrole. Figure 56-D shows a slightly decrease of current during consecutive scans when the anodic potential limit went until 1.1 V/Ag/AgCl probably due to a partial polymer film over oxidation. This effect is much more pronounced when the imposed anodic potential was higher, 1.3 and 1.5 V/Ag/AgCl, see Figures 56-E and 56-F. In both figures, during the first scan were observed the oxidation peaks of isoproturon and polypyrrole molecule species, which disappeared after the second scan.

Higher overoxidation degree of MIP-PPy film induced by electrode potential rise may impart its conductivity which has a direct but limited effect on the film thickness calculated from current charge as is shown in Figure 57-A. Comparison of the figure 56-B and 56-F highlights that the film keeps a conductivity in the first case after five cycles and loss its conductivity in the second case for a same value of total charge after five cycles.

The electrochemical response of the modified GC electrodes with MIP films at different potential range in the ISO detection is done in Figure 57-B. The maximum current peak is obtained for the MIP-PPy prepared when potential excursion went until 0.9 V/Ag/AgCl while for its higher values, it is clearly shown a decrease in the peak of

current. The impact of MIP-PPy overoxidation is higher on the intensity of the ISO detection peak than on the thickness of the polymer film. This could be attributed to a combination of both the loss of thickness and therefore the number of cavities present in the film, but also the loss of conductivity within the more overoxidized films.

The current intensity shrinks to nothing during the potential scan between 0 V up to +0.7 V/Ag/AgCl so we do not see the detection peak of ISO. This happens because during the electropolymerization process the oxidation potential of ISO is not reached, as result it has not made its cavities within PPy film (see Figure 39 in Chapter III).

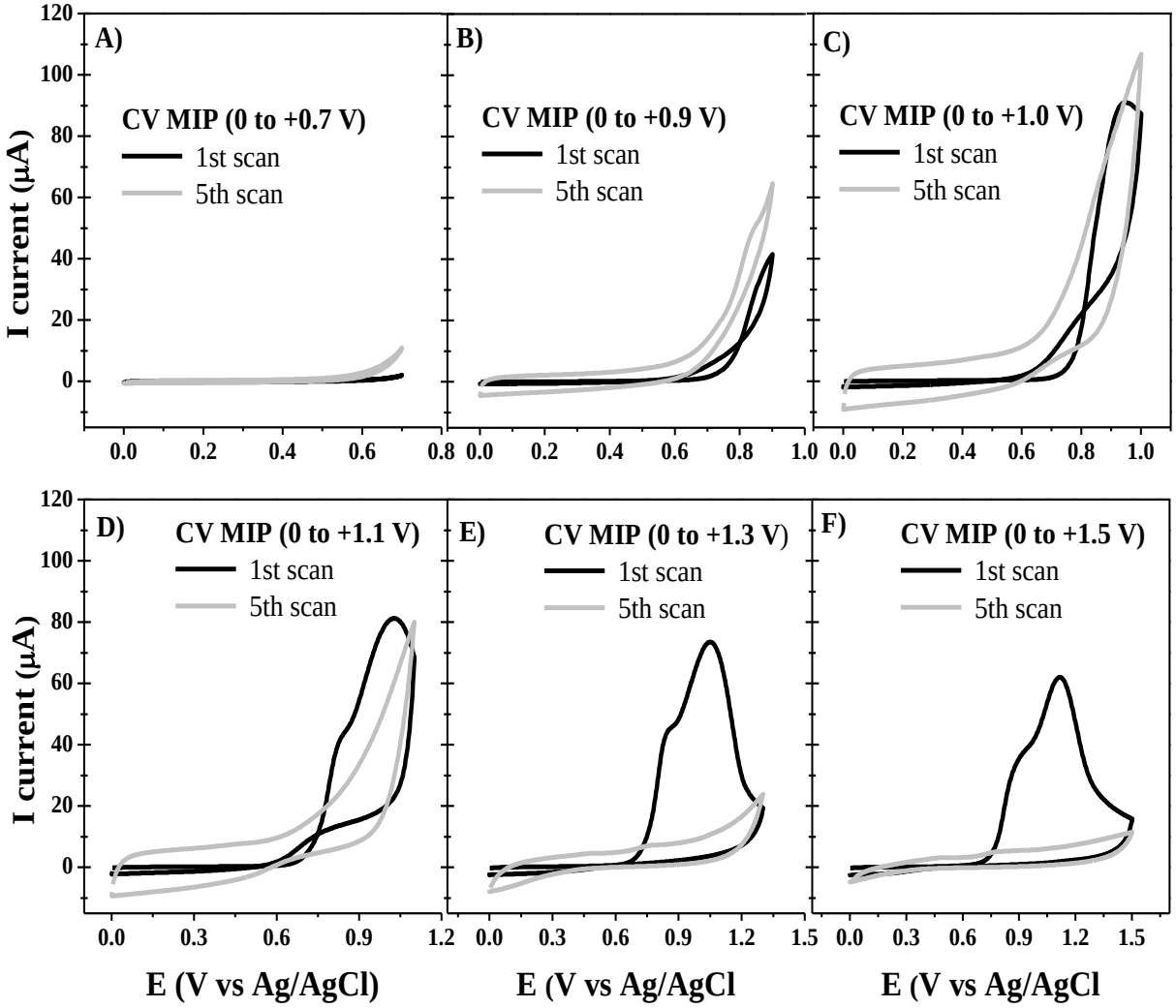

Figure 56. Cyclic voltammograms (0 to +0.7V; + 0.9V; +1.0V; + 1.1V; +1.3V; + 1.5V) taken during electropolymerization of pyrrole (0.01 M) in presence of ISO 1 mM onto GC electrode. The electrolyte was 0.1 M $LiClO_4$ in ethanol/water (20:80 v/v). Scan rate 10 mV/sec.

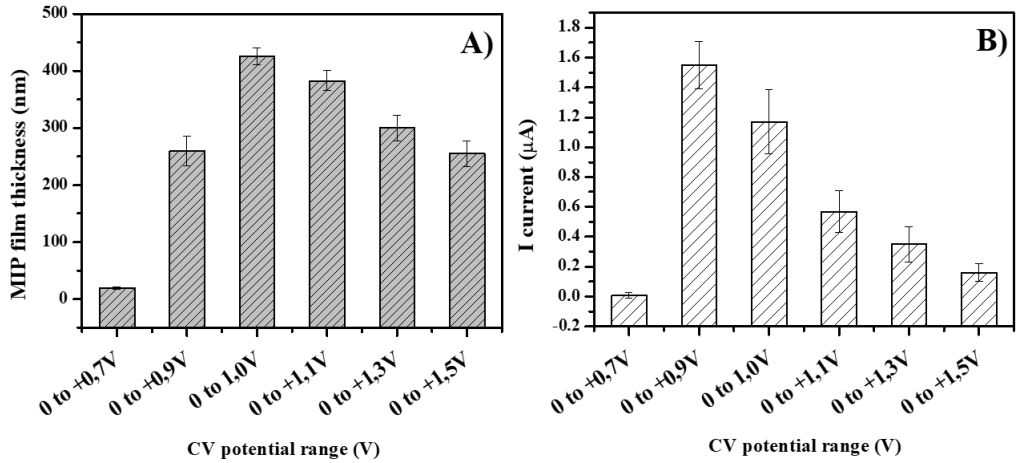

Figure 57. Electropolymerization of MIP-GC electrode made by CV at different potential ranges (0 to +7; +0.9; +1.0; + 1.1; +1.3 and + 1.5V) in ethanol/water (v/v:20/80) solution containing 0.01 M of pyrrole + 1 mM of ISO + 0.1 M of $LiClO_4$. (A) Film thickness calculated from cyclic voltammograms and (B) ISO current peak intensity for the MIP-PPy made by CV at different anodic potential range.

4.3.2.2. The influence of number of cycles

Once we have found the optimal potential region for the MIP-PPy electrochemical synthesis on GC electrode, we have continued to study the impact of CV cycles in its quality and properties. MIP-PPy film thicknesses measured by AFM and calculated by Faraday's law obtained with different number of cycles at potential range from 0 up to

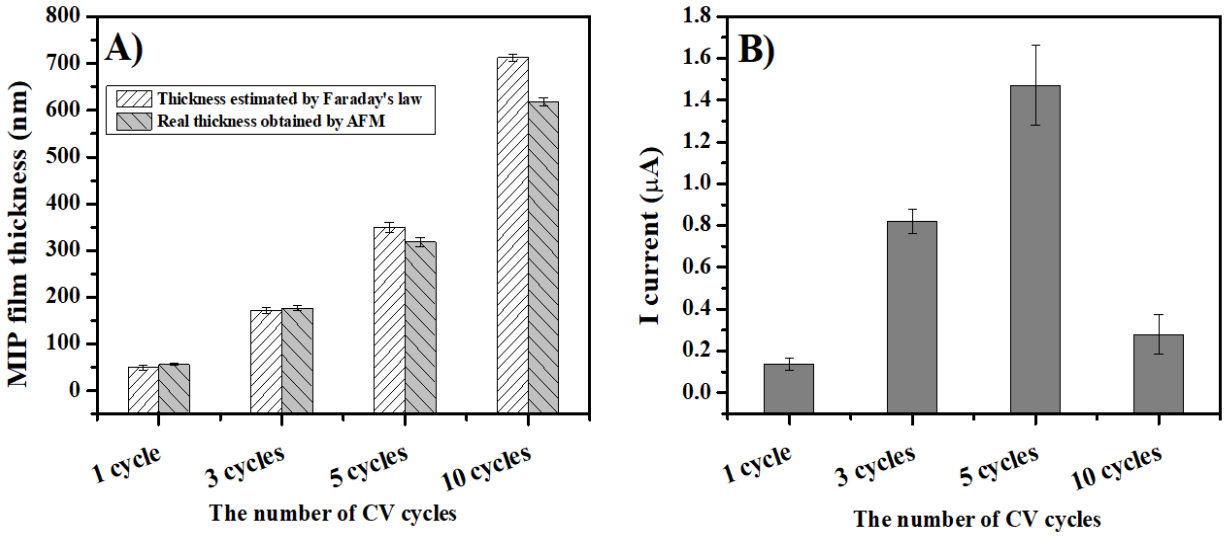

Figure 58. The influence of CV scans on the performance of MIP-GC electrode at potential range from 0 up to +0.9V/Ag/AgCl in ethanol/water (v/v:20/80) solution containing 0.01 M of pyrrole + 1 mM of ISO + 0.1 M of $LiClO_4$. (A) film thickness calculated from cyclic voltammogram and obtained by AFM (B) ISO current peak intensity for the MIP-PPy made with different CV scans.

0.9 V/ Ag/AgCl are shown in Figure 58-A. One can see that the thickness of the fabricated MIP films was not the same. Raising the number of voltammetric cycles has contributed to the growth of the MIP-PPy as the number of induced charges have increased. Film thickness measured by AFM is coherent with its theoretical calculated value for a small number of scans while it is slightly lower for higher number of scans. Sensing properties of these polymers were tested for the electrochemical determination of ISO (concentration 5.10^{-7} M, incubation time 15 min) (see Figure 58-B). One can observe an increase of ISO current peak detection of MIP-PPy layer obtained with five cycles, whereas for films made at higher scans the current was significantly lower. The drastic decrease of the detection current for the MIP-PPy-GC prepared with 10 cycles can be explained by a too important thickness of the film which leads to important mechanical stresses in the film and possible internal micro-breakage leading to a loss of conductivity of the film, and the difficulty for the ISO molecules to penetrate in all the film thickness.

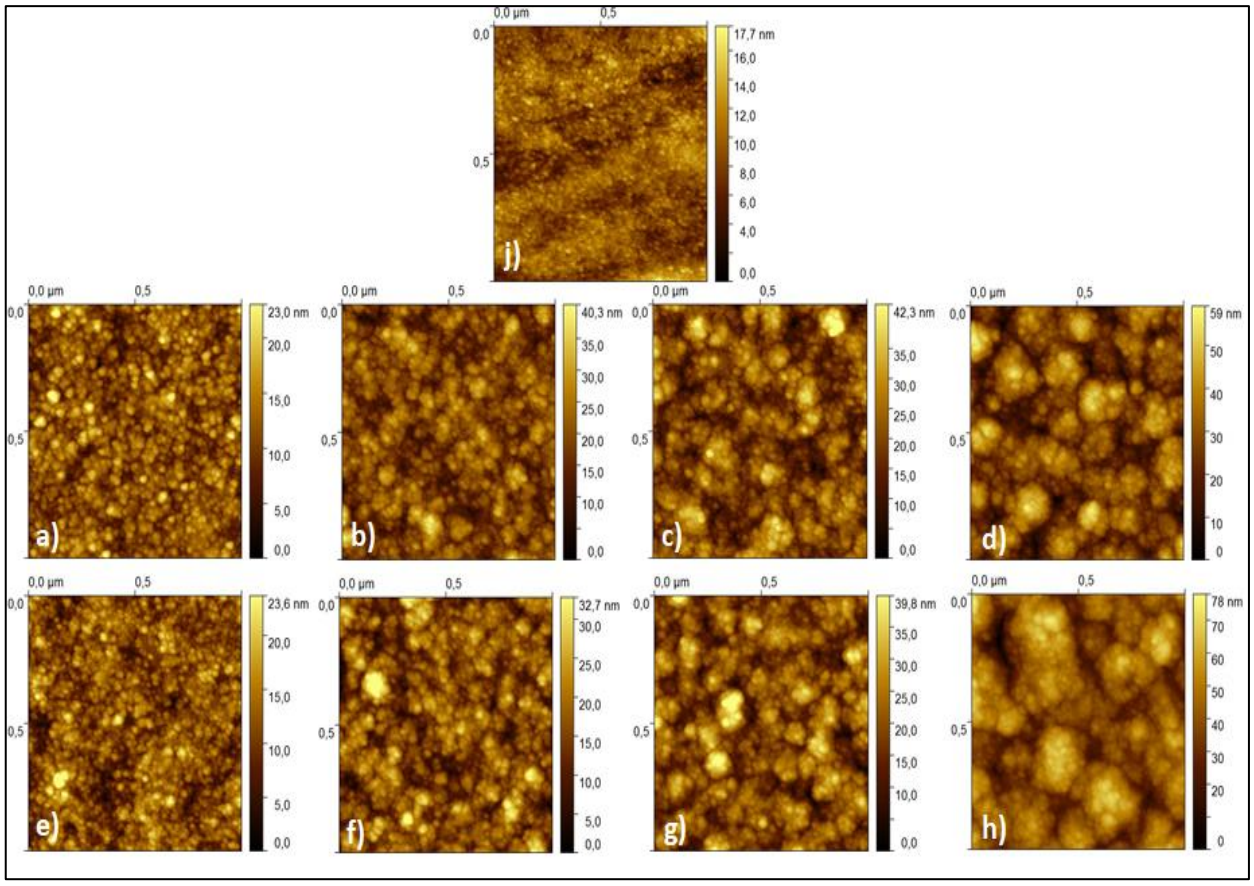

Figure 59. AFM images of MIP-GC plates obtained by CV at potential range 0 to +0.9V/Ag/AgCl with different number of cycles in ethanol/water (v/v:20/80) solution containing 0.01 M of pyrrole + 1 mM of ISO + 0.1 M of $LiClO_4$, scan rate mV/s: (a) 1, (b) 3, (c) 5, (d) 10 cycles before isoproturon extraction; (e) 1, (f) 3, (g) 5, (h) 10 cycles after isoproturon extraction; and (j) AFM image of a bare GC plate.

In Figure 59 are presented the AFM images of the MIP-PPy films fabricated on glassy carbon electrodes by CV at potential range from 0 up to +0.9V vs ref. Ag/AgCl at different number of cycles. AFM images were taken on the same films prior and after isoproturon extraction process. A clear difference in the film morphology was obtained for samples prepared with different number of cycles. As the scan number rises the MIP-PPy roughness increases (see Table 4). Film roughness (RMS: root mean square) after isoproturon extraction is slightly higher. This may happen due to the creation of the cavities when the isoproturon molecules were removed from the polypyrrole films, leaving the cavities on the surface that could increase the roughness of the films. The same behavior has been obtained also in the case of GC-MIP-PPy fabricated by CA at different potentials, where the film roughness is increased after the isoproturon removal, for GC-MIP-PPy made by CA at +0.8 V have shown an increase of their roughness after the isoproturon extraction from 3.66 nm up to 4.08 nm, while the film roughness of the MIP-PPy prepared by CA at +1.1 V was increased from 5.4 nm up to 5.2 nm, and by CA at +1.4 V was increased from 2.13 nm up to 3.13 nm.

Table 4. AFM roughness measurements of the MIP-GC films made by CV at potential range 0 to +0.9V/Ag/AgCl, with different number of cycles in ethanol/water (v/v:20/80) solution containing 0.01 M of pyrrole + 1 mM of ISO + 0.1 M of $LiClO_4$, v = 10 mV/s, before and after isoproturon extraction.

		Magnification (1 x 1 μm)	
Sample	**Real thickness (nm)**	**Before extraction (RMS)**	**After extraction (RMS)**
CV MIP (1 cycle)	56,5	3,1	3,4
CV MIP (3 cycles)	176,7	5,2	5,2
CV MIP (5 cycles)	318,5	6,6	6,4
CV MIP (10 cycles)	618	9,5	11,3

4.3.3. Influence of the overoxidation potential applied on the properties of MIP-PPy film

4.3.3.1. The effect of the overoxidation potential on the conductivity of the film: characterization by EIS

Electrochemical impedance spectroscopy (EIS) is a suitable technique that has been used for the characterization of thin polymeric materials synthesized by electrochemical methods [32], [35], [191], [192], [226]. Mainly the method was focused in the explanation of the porosity of the molecularly imprinted polymers used as membranes and as sensors, by measuring the EIS parameters before and after the template molecule removal [32], [192], [226].

The removal of isoproturon molecules from the MIP-PPy fabricated by CA on GC electrodes, was achieved by scanning the potential between -0.4 V and +1.5 V vs Ag/AgCl (50 scans at the scan rate v = 0.1 V/s) until the complete extraction of the embedded isoproturon molecules has been reached. This step is necessary in order to create the cavities on polymeric matrix of the MIP film which are complementary shaped to the ISO molecules and can selectively detect them when sensor operates. =

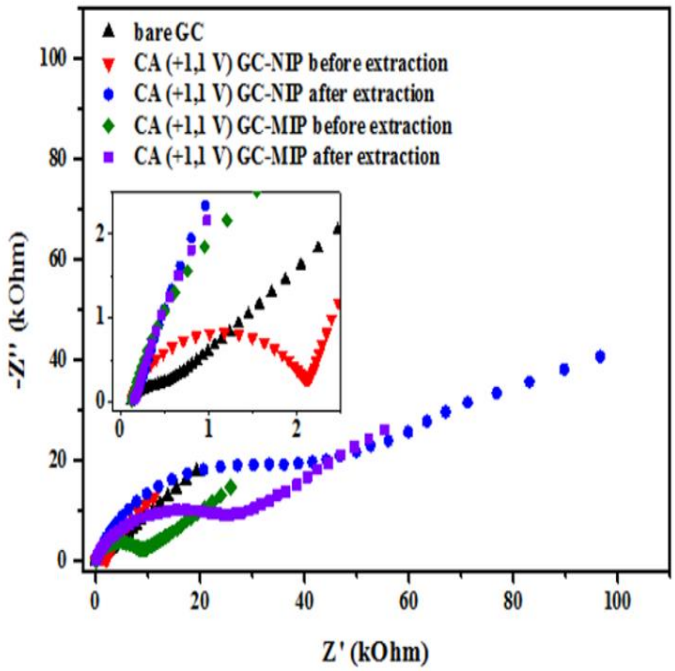

Figure 60. EIS results obtained during the characterization of the NIP and MIP films, electro-synthesized on GC electrodes by CA (+1.1 V, t = 600s), in aqueous solution of 1mM $K_3[Fe(CN)_6]/K_4[Fe(CN)_6]$ + 0.1M KCl. Nyquist plots obtained at bare GC, NIP and MIP electrodes before and after ISO extraction

We have repeated the same procedure for the NIP film in order to put in evidence the role of the excursion potential in the film conductivity although there is not isoproturon template within the film. EIS spectra were recorded immediately after the MIP and NIP formation during the electrolysis time 600 s at the potential 1.1 V /Ag/AgCl and after 50 scans by CV in order to remove ISO completely. In Figure 60, are presented the Nyquist plots for NIPs and MIPs before and after ISO extraction. The charge transfer resistance for NIP film measured immediately after its electrochemical synthesis was 1.7 kΩ while that for the MIP film was about 10 kΩ. This difference of charge transfer resistance between NIP and MIP films may be induced by the presence of isoproturon molecules within the film matrix that influence the intrinsic film conductivity.

We observed even much higher charge transfer resistances for both films when they were biased at the potential range between -0.4 V to 1.5 V in order to remove the isoproturon molecules. Patois et al. have electrochemically synthesized PPy films with much lower conductivity on Fluorine doped Tin Oxide electrode when deposition potential was 1.3 and 1.7 V/SCE [109]. Based also on their results one can conclude that extraction procedure for isoproturon apparently damaged MIP and NIP films and this

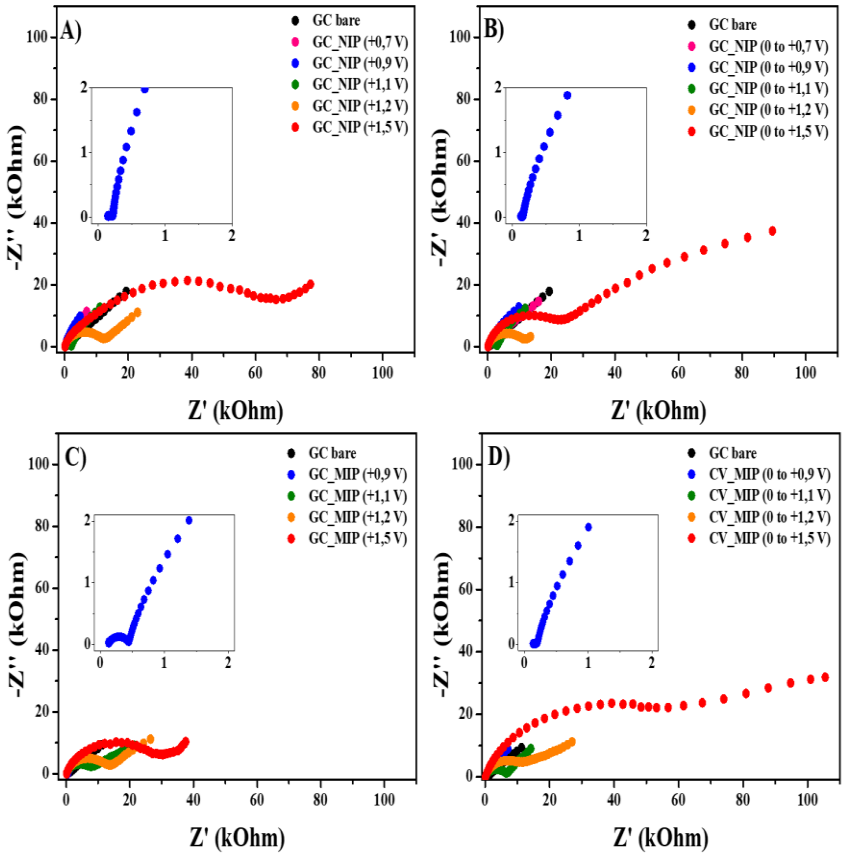

Figure 61. EIS characterization of NIP and MIP films fabricated on GC electrodes at different potential values: A) NIP by CA (duration time 600s), B) NIP by CV (5 cycles at scan rate 10 mV/s), C) MIP by CA (duration time 600s), and D) MIP by CV (5 cycles at scan rate 10 mV/s).

effect is much more pronounced with the NIP film because its charge transfer resistance rises 30 times, from 1.7 kΩ to about 50 kΩ, while that of the MIP film increases 3 times, from 10 kΩ to about 30 kΩ.

The decrease of conductivity of MIP film after the release of ISO is however surprising because it is different comparing with the behavior of other MIPs [35], [192] for detection of alachlor and tetrabromobisphenol A templates where film conductivity increases once the imprinted target molecule is removed. Nevertheless considering the same impact of the anodic potential on our synthesized NIP and MIP-PPy films, where NIP film conductivity has a tenfold higher decrease, it is implicitly shown that MIP film obtained with ISO molecule as template has the same attitude as above-mentioned MIPs but it is difficult to put in evidence due to the over-oxidation effect induced on the MIP-GC when the electrode is biased with high anodic potential [35], [192]. The increase of the film polarization resistance due to the overoxidation of the MIP polypyrrole during the CV scanning is also showed by Marchesi *et al.* 2011 [196]. They have investigated with EIS the degradation of the polypyrrole thin films by cyclic voltammetry [196], claiming that at potentials +0.58 V polypyrrole can already be over oxidized and degraded in the same time resulting in the increase of its film resistance. According to their findings at much lower anodic potential, one can consider as normal the decrease of the MIP film conductivity with ISO because it was prepared a much more anodic potential, about 0.9 V/Ag/AgCl and the effect of template molecule release is hidden by the decrease of the film conductivity due to the polypyrrole over oxidation.

The impact of the potential at 1.5 V/Ag/AgCl in the film degradation is seen in the Figure 61-A where the charge transfer resistance is about 70 kΩ for the NIP film. The same tendency is observed for NIP films obtained by CV at different excursion

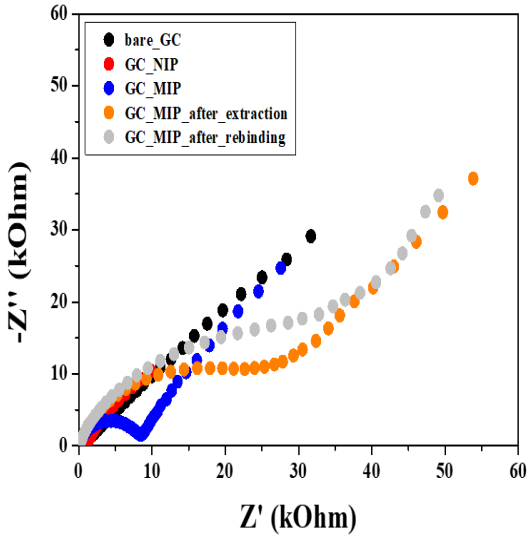

Figure 62. EIS characterization of the GC-MIP electrodes prepared by CA at +1.1 V (duration time 600s) at different stages when tested for the SWV isoproturon detection.

potentials presented in Figure 61-B. One can see that the polarization resistance is about 3.0 kΩ for the film obtained (5 scans until 1.1 V/Ag/AgCl) while it increases about tenfold times during the potential excursion until 1.5 V. The polarization resistance for the films obtained at the potential lower than 1.1 V is very small. EIS results obtained with MIP-PPy films prepared by CA and CV are shown in the Figure 61-C and 61-D. They are similar with those of NIPs a decrease of film conductivity when anodic potential is increased and they also confirm why the potential of 0.9 V is much more favorable for the preparation of MIP.

Moreover, in Figure 62 are presented the EIS spectra obtained for GC-MIP-PPy electrodes when tested for the isoproturon determination, where is seen that the resistivity of the MIP films was increased about 20 kΩ, after the first extraction of the ISO molecules, and further increased around 40 kΩ after the use of the sensor for ISO detection, rebinding step. This last result is important because it confirms that MIP film shown in Figure 61-A, before extraction, has higher charge transfer resistance due to the presence of ISO molecules than NIP synthesized at the same electrolysis potential.

In conclusion the EIS measurements indicate that the film conductivity is highly affected during the removal of the template molecule.

4.3.3.2. Effect of the overoxidation on the composition of the film: FT-IR and XPS characterization

Main characteristic peaks of FTIR spectra of pyrrole and isoproturon are summarized in Table 5. Furthermore, we have performed FTIR spectra of modified GC samples with NIPs and MIPs prepared by CV at different potential range before and after isoproturon extraction Figure 63 and 64 show the spectra region between 1200 and 1800 cm^{-1}. The IR spectra of three GC-NIPs made by CV during potential excursion until 0.9; 1.1 and 1.5 V/Ag/AgCl shown in Figure 63-A. FTIR spectrum of GC-NIPs made until 0.9 V/Ag/AgCl show a small peak at 1550 cm^{-1} attributed to >C=C< vibrations while FTIR spectra of GC-NIPs made at 1.1 and 1.5 V/Ag/AgCl show the band that has a higher intensity and the apparition of another band at 1700 cm^{-1}. This band is attributed mainly to N-C=O stretching vibrations of pyrrole units for the GC-NIPs prepared when the anodic potential reached 1.1 V and 1.5 V. This result clearly indicate the impact of anodic potential during the GC-NIP electrochemical synthesis that is attributed mainly to N-C=O stretching vibrations of pyrrole units for the GC-NIPs [227]. A small shift of this peak toward higher wave number value is observed for the potential 1.5 V that is attributed to the presence of C-C=O [227]. Figure 63-B shows that GC-NIPs were biased

under anodic potential until 1.5 V/Ag/AgCl, the standard extraction procedure for the isoproturon removal in the case of GC-MIPs. There is not a notable difference for the GC-NIPs made at 1.1 V and 1.5 V while one can see the apparition of a signal at the region 1700 cm^{-1} for the FTIR spectrum of GC-NIP prepared at 0.9 V due to the overoxidation of the film during this procedure mimicking the extraction step.

FTIR spectra of GC-MIPs made by CV at different anodic potentials are shown in Figure 64-A and those obtained after the isoproturon extraction are shown in Figure 64-B. These spectra show the same features as the GC-NIPs that means that the polymer films are oxer oxidized when they are exposed to higher anodic potentials.

Table 5. Characteristic bonds obtained during the FT-IR analysis of Pyrrole 98% and Isoproturon.

Pyrrole, 98%	**Wavelength (cm^{-1})**		
Radical bonds	**Literature**	**FT-IR reading**	**Inferences**
C = C	1700 - 1500	1529 1569	C=C bonds in the molecule (strong)
C – H	860 - 680	735.3 839.5	Bonding of C-H in the molecule (elongation)
C – N	1200 - 1025	1048.17 1074.05 1140.15	C-N bonds in the molecule (elongation)
N – H	3500 - 3300	3403.18	N-H bonding in the molecule (deformation)
Isoproturon	**Wavelength (cm^{-1})**		
Radical bonds	**FT-IR reading**		**Inferences**
>N-H	3307.35		>N-H bonds in the molecule
=C-H	2954.33		=C-H bonds in the molecule
C-H	2863.89		C-H bonds in the molecule
>C=O	1639.6		>C=O bonds of amides with nitrogen in structure
$-NH_2$	1595.75		Scissors deformation of $-NH_2$
>C=C<	1514.6		>C=C< elongation aromatic
C-N<	1413.98		C-N< elongation amines
2H-aromatic ring	823.7		Deformation of aromatic rings containing 2H bonded to the aromatic nuclei

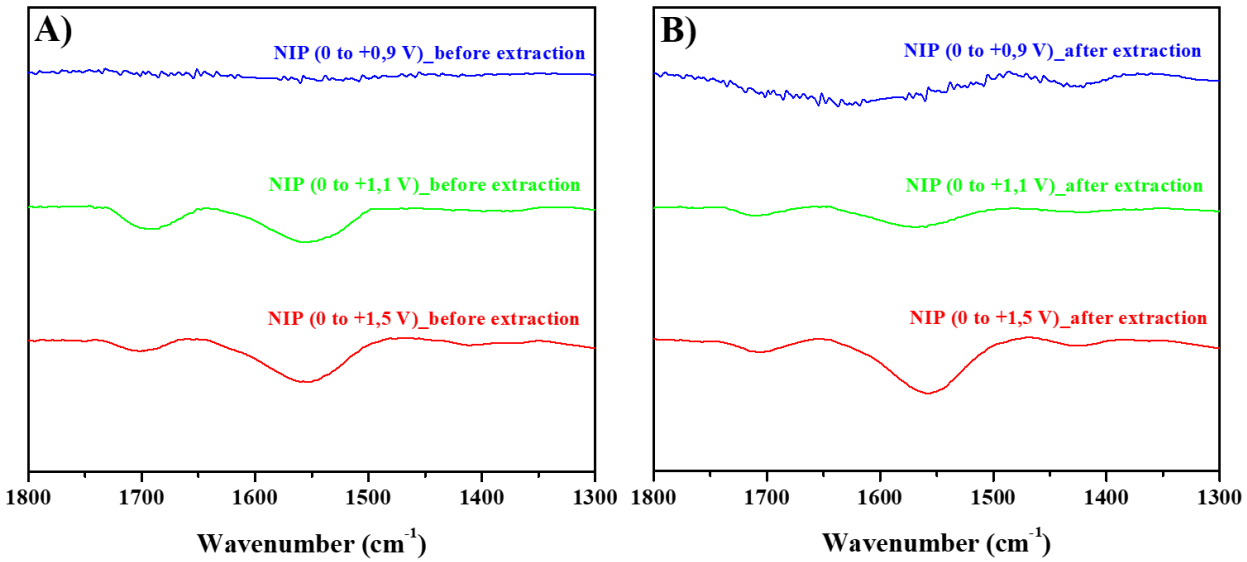

Figure 63. A) FTIR spectra of GC-NIPs made by CV at different anodic potentials; B) exposed to the anodic potential when electrochemical procedure is used for the removal of isoproturon.

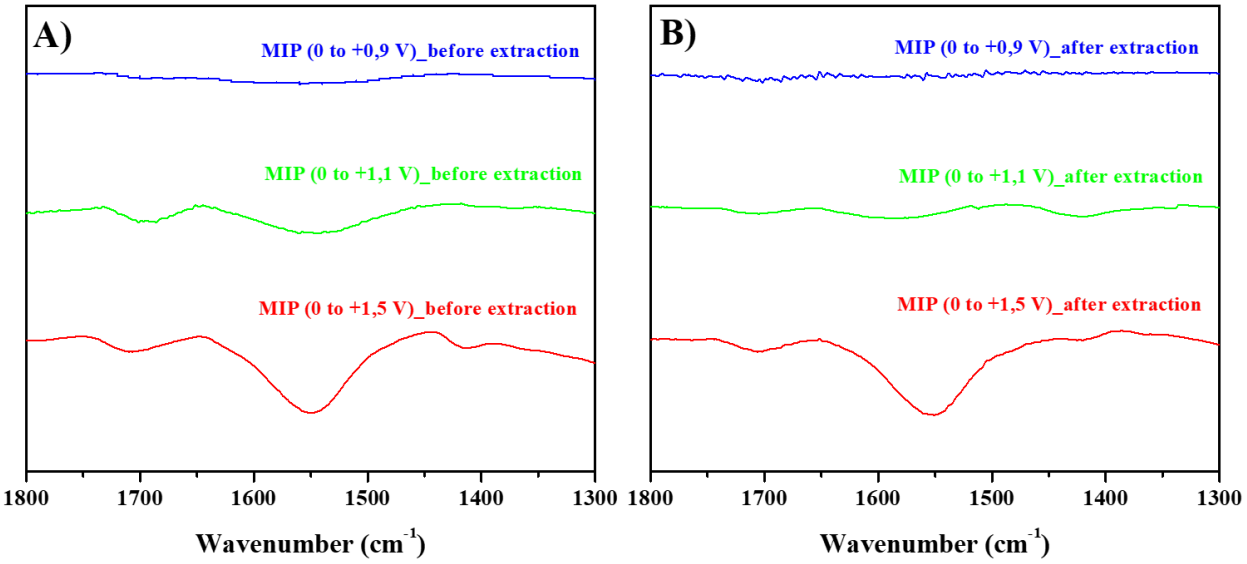

Figure 64. A) FTIR spectra of GC-MIPs made by CV at different anodic potentials; B) exposed to the anodic potential when electrochemical procedure is used for the removal of isoproturon.

GC-NIP and GC-MIP samples were also analyzed by XPS. Survey spectra (not shown) show the main peaks of C1s, O1s and N1s that attest the presence of polymer film on the carbon surface. Figure 65 and 66 shows high resolution spectra of C1s and O1s contribution in GC-NIPs made by CV at different potentials before and after isoproturon extraction. After deconvolution of C1s signal one can see the main component centered in 285 eV with a small contribution at lower energy attributed to the presence of pyrrole α and ß carbons [228].

The C1s signal also contains other contributions centered at 286 eV, 287 eV and 288.5 eV attributed C-O, C-N, C=O, C=N, N-C=O and O-C=O bonds. The contribution of the C1s peaks at higher energy is mainly observed for GC-NIP films electrochemically synthesized by CV at anodic potentials 1.1 and 1.5 V and their contribution increase after the extraction procedure. The presence of C=O contribution is observed even in the sample of GC-NIP prepared at 0.9V and exposed to the extraction procedure for isoproturon. This result confirms the overoxidation of GC-NIP as we have already by FTIR measurements.

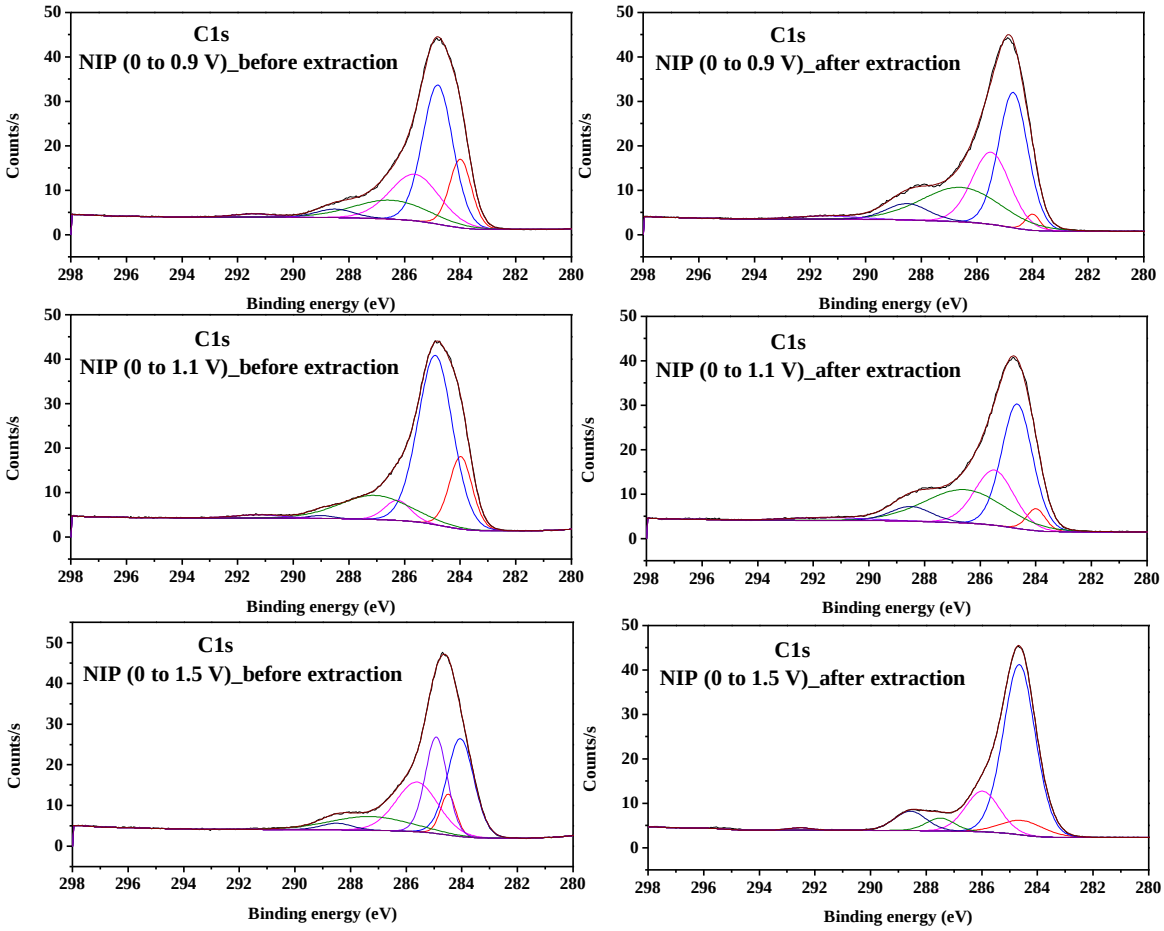

Figure 65. High resolution spectra of C1s obtained with GC-NIP films made by CV at different anodic potentials before and after extraction.

XPS high resolution O1s spectra of GC-NIPs are shown in Figure 66. One can see the shift of the O1s main peak from 532.5 eV to values lower than 532 eV due to the increase of the presence of C=O and O-C=O groups when GC-NIPs are exposed to higher anodic potentials [229]. The same tendency is observed for GC-MIPs in the Figure 68 for GC-

MIPs. Therefore, these XPS findings confirms without any doubt the impact of anodic potential in the overoxidation of PPy films.

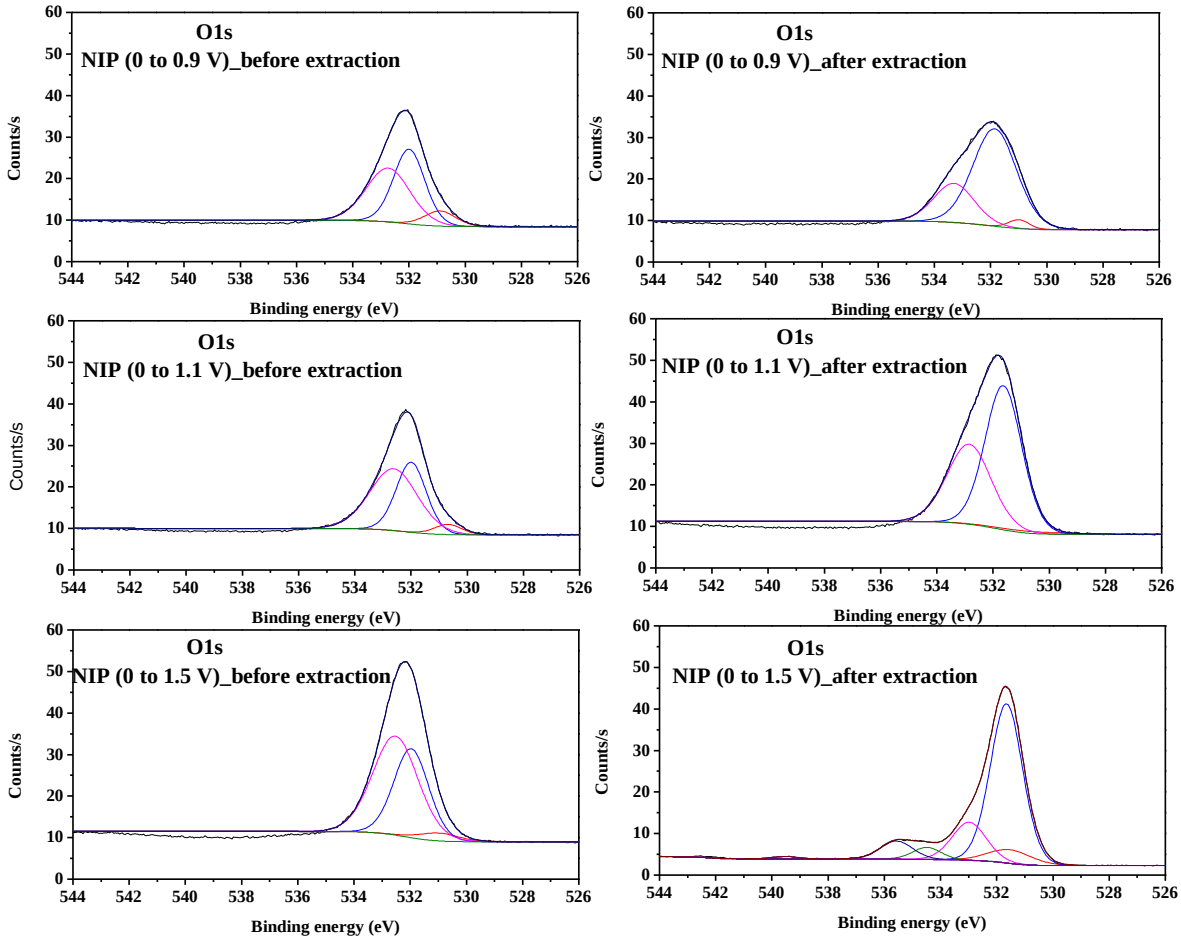

Figure 66. High resolution spectra of O1s obtained with GC-NIP films made by CV at different anodic potentials before and after extraction.

XPS high resolution spectra of C1s at GC-MIPs are shown in the Figure 67. The C1s signal show the main component at 285 eV and also contains other contributions centered at 286 eV, 287 eV and 288.5 eV attributed C-O, C-N, C=O, C=N, N-C=O and O-C=O bonds. Here also is shown the contribution of the C1s peaks at higher energy for GC-MIP films electrochemically synthesized by CV at anodic potentials 1.1 and 1.5 V and their contribution increase after the extraction procedure. The effect of the anodic potential in the overoxidation of the PPy film is present even in the sample of GC-MIP prepared at 0.9 V and exposed to the removal procedure for isoproturon.

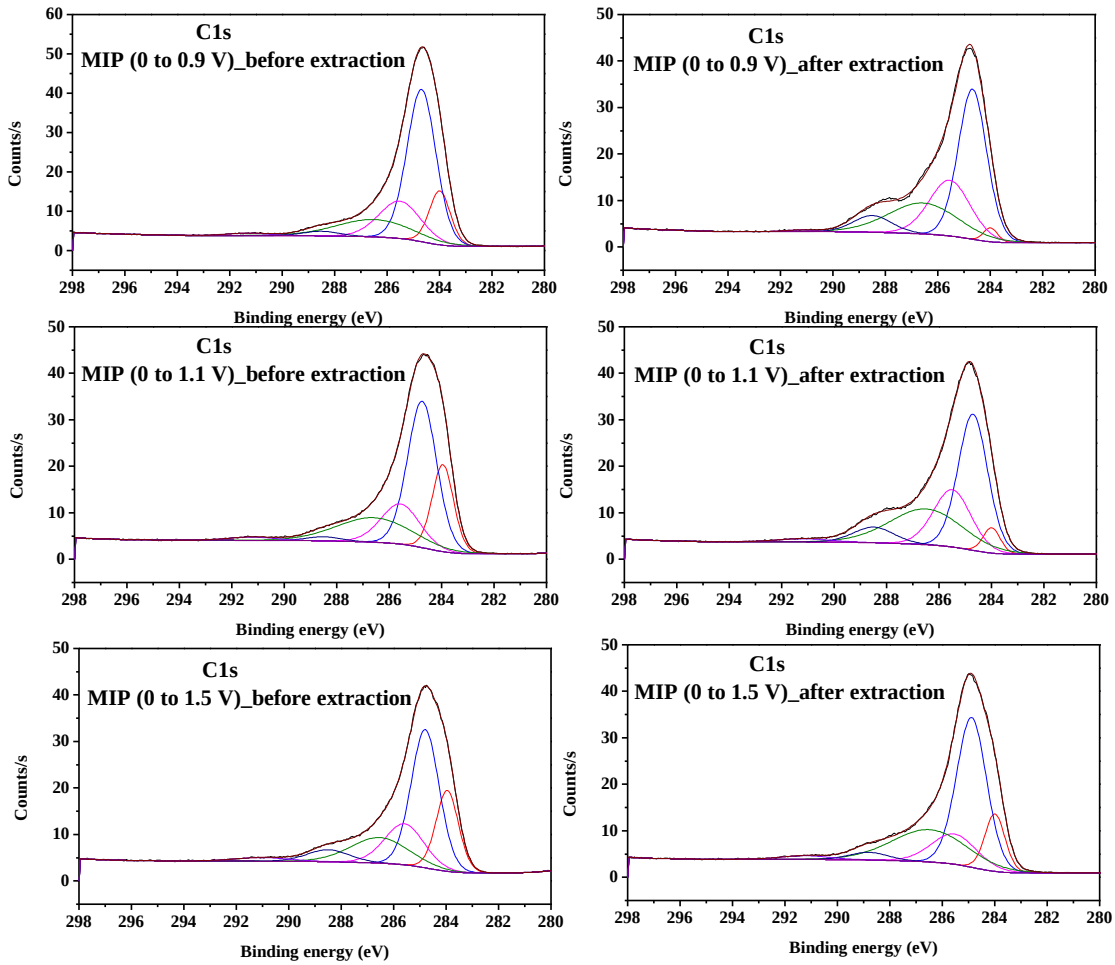

Figure 67. High resolution spectra of C1s obtained with GC-MIP films made by CV at different anodic potentials before and after extraction.

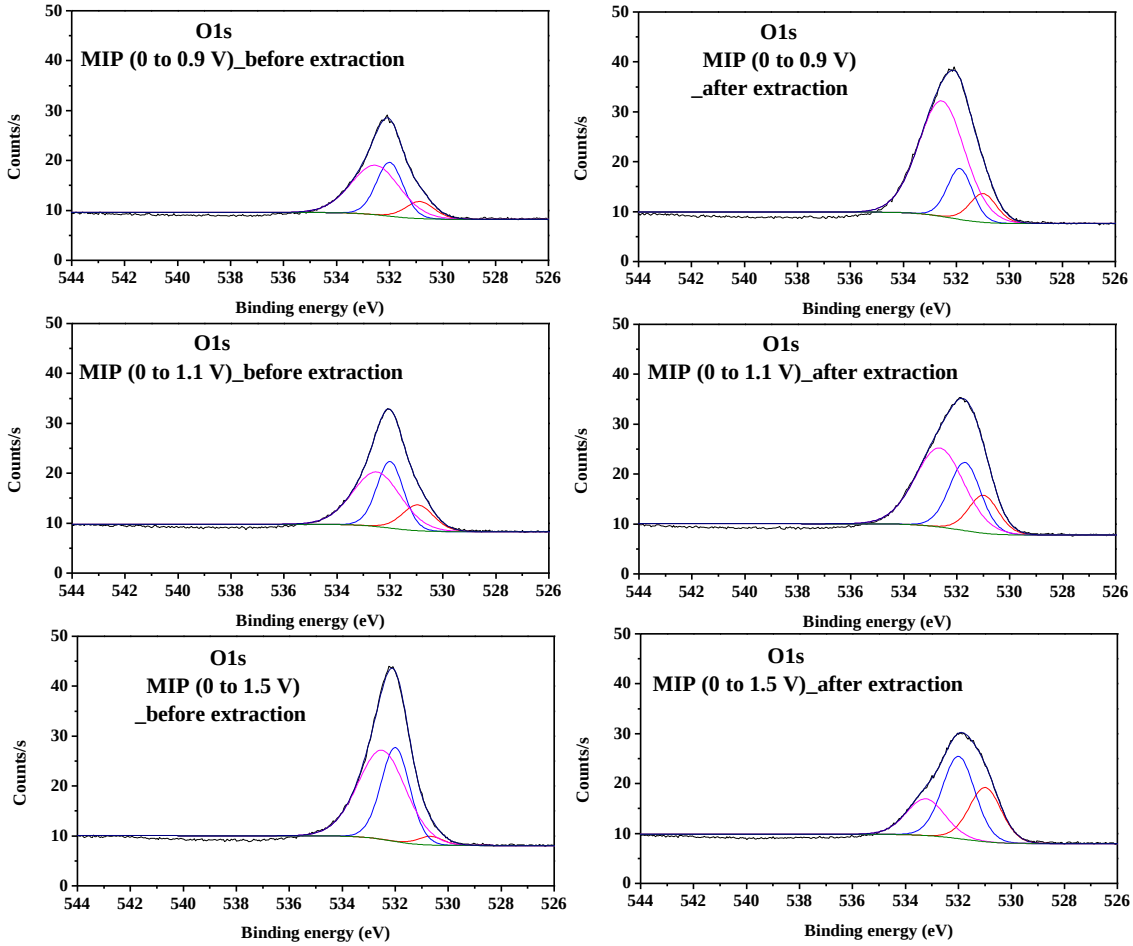

Figure 68. High resolution spectra of O1s obtained with GC-MIP films made by CV at different anodic potentials before and after extraction.

4.4. Conclusion and perspectives

In this chapter we have shown the impact of several parameters in the behavior of MIP sensor for the detection of the isoproturon. The MIP and NIP films were prepared either by chronoamperometry or cyclic voltammetry and are characterized by Electrochemical Impedance Spectroscopy (EIS), Atomic Force Microscopy (AFM) and EQCM (Electrochemical Quartz Crystal Microbalance). EIS has permitted to put in the evidence the influence of the excursion potential during the film formation or the isoproturon release in the film conductivity. The removal potential of isoproturon at 1.5 V/Ag/AgCl induces the overoxidation of the polypyrrole film and screens the increase of the film conductivity due to the removal of isoproturon. This phenomenon is confirmed by XPS and IR measurements which indicated a higher degree of presence of oxygen content for MIP and NIP-PPy films prepared or exposed to higher oxidation potential. These data permitted us to explain why the MIP polypyrrole films fabricated by cyclic voltammetry at potential range lower than +1,0 V showed a better signal for the isoproturon determination because the MIP film conductivity was preserved.

- Page left intentionally blank -

CHAPTER V

"Electropolymerization of molecularly imprinted polymer (MIP) film onto pure graphene electrodes for isoproturon detection"

5. CHAPTER V: Electropolymerization of molecularly imprinted polymer (MIP) film onto pure graphene electrodes for isoproturon detection

As graphene is known for its exceptional properties, the aim of this chapter is to evaluate its applicability related to electroanalysis. The literature is abundant in references to graphene-based electrochemical sensors for the detection of a wide range of pollutants, but most often the graphene is mixed with several carbon materials as carbon black and binders as polymers. It is therefore difficult to assess the intrinsic properties of this material for electroanalytical applications.

In this chapter we have developed 100% graphene electrodes from a graphene that is compatible with industrial development, because it is inexpensive: graphene produced by electrochemical method. In a second part we studied the possibility of using these graphene electrodes for the detection of isoproturon by methods similar to those of the previous chapters.

5.1. Introduction

Graphene is the name given to a two-dimensional sheet of sp^2 – hybridized carbon atoms [230]. It is one carbon atom thick layer, and its extended honeycomb network is the basic building block of the other carbon allotropes, such as carbon nanotubes, fullerene, and graphite [231]. Graphene can be stacked to form 3D graphite, rolled to

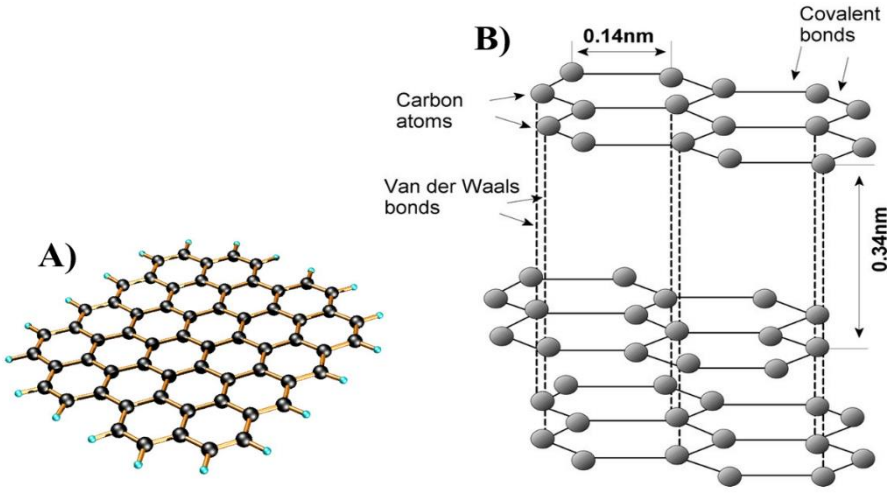

Figure 69. A) The honeycomb structure of graphene, B) Molecular arrangement of carbon in graphene and various bonding and forces involved during its self-assembly into graphite [258].

form 1D carbon nanotubes, and wrapped to form 0D fullerenes [230]. Long range π-conjugation in graphene yields extraordinary thermal, mechanical, and electrical properties (Figure 69-A). The average distance between two carbon atoms (single and double bonds) in the structure of graphene has been found to be 0.142 nm. The 2D graphene layers intercalate in either a hexagonal or rhombohedral arrangement to form a graphite crystal lattice. The distance between the two layers of graphene is found to be approximately 0.34 nm, and is subject to weak Van der Waals forces [232] (Figure 69-B). Since its first exfoliation when Geim and co-workers at Manchester University reached to isolate single-layer samples from graphite [233] (Figure 70-A), graphene has attracted huge interest in scientific and in industrial communities and many extensive research activities [211], [233]–[237] due to its physical and chemical properties. The Manchester group performed a mechanical exfoliation of the graphene layers from graphite (see Figure 68B). This way of production was the first one used at a large scale by the scientific community in order to produce graphene samples. After 2004, new ways of graphene production were developed in the laboratory. Graphene today can be produced by using different methods, such as by a top-down mechanical exfoliation [233] or by chemical exfoliation [238]–[243], a bottom-up chemical vapor deposition (CVD) method [244]. In this work we adopt a top-down method involving the electrochemical exfoliation of graphene layers from graphite electrode in a liquid media. Fabrication of graphene in liquid media involving the production of graphene oxide, either by acid exfoliation such as Hummers method or by electrochemical oxidative exfoliation of bulk graphite electrode, followed by chemical reduction of the intermediate graphene oxide products [245], provided to reach an easy way for the production of graphene. The graphene products resulted to contain oxygen functional groups which may be formed due to the oxidation between the graphene sheets which facilitate the dispersion of the graphene sheets in aqueous and organic solvents leading

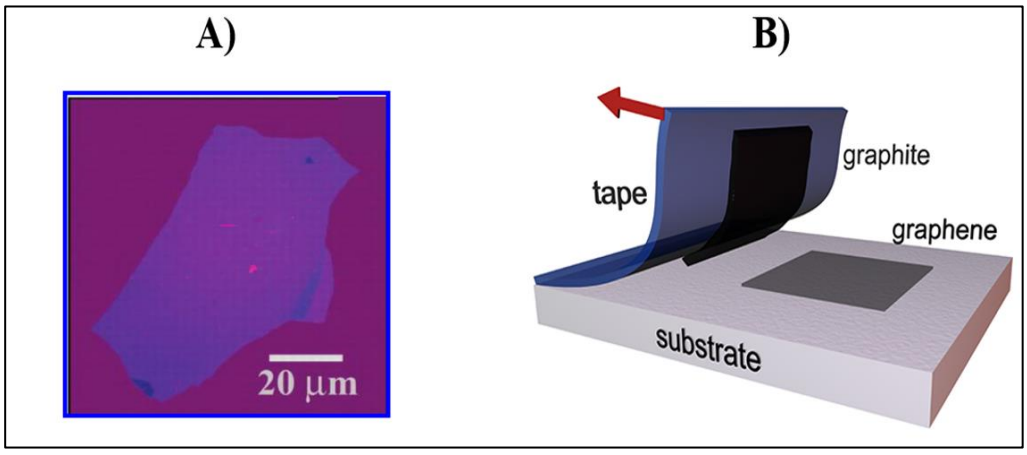

Figure 70. A) Single layer graphene was first observed by Geim and Novoselov at Manchester University, B) "Scotch tape" method to isolate graphene layers from graphite by continuous peeling with an adhesive tape [233].

to increased yields of exfoliate. But these oxygen containing functional groups decrease the electrical conductivity of graphene sheets, and cannot be removed totally from its structure through further chemical reduction processes [230], [246], [247]. The reduced graphene oxide has a high density of sp^3 defects and is always contaminated with graphene oxide and other undesired carbonaceous species [248], [249]. Finding a route which leads to the production of less oxidized graphene sheets was always a big challenge for the graphene production technology. Another way for graphene production is sonication in organic solvent [250], but its disadvantages as method include low yields and large amount of energy associated with any scale-up of the process. At this stage it was known that in organic solvents the exfoliated graphene, obtained either by chemical, physical or electrochemical methods can contain less oxygen functional groups [251].
Furthermore, it has been shown that anions and cations can intercalate effectively between the graphene sheets in bulk forms of graphite, for example anionic intercalation can lead successfully to the exfoliation of graphite anode, but due to the positive potentials required for anionic exfoliation these methods resulted generally in the formation of functionalized graphene sheets [247], [250], [252]–[258]. The challenge was to develop cationic intercalation which would avoid the formation of oxidative products and reduce the presence of oxygen containing functional groups in the structure of graphene. In the late 1970s was reported the graphitic electrode expansion work driven by the intercalation of tetraalkylammonium cations [259], [260], but no way for production of graphene was resented in that time. It was reported later that tetrabutylammonium (TBA) can be chemically intercalated into graphitic carbon structure and result in the formation of graphite intercalation complex (GIC) [258], where the intercalated TBA ions can separate the graphite layers by 0.467 nm. However, this process was not controlled electrochemically. Electrochemical intercalation is a more controlled route for the formation of intercalated species [261]–[263].

Recently, some new methods have been developed for highlighting the graphene yield and being cost-effective. These new methods are based in the modified Hummer's method [264], and widely used to produce graphene [246], [265]–[272]. However, through these methods the produced graphene should pass through different stages. Firstly, graphene oxide (GOx), a single monomolecular layer of graphite with various oxygen-containing functional groups as most common type of chemically modified graphene [247] should be reduced via thermal, chemical, electrochemical or photochemical methods. The final product is a reduced graphene oxide (rGOx) which is similar to pristine graphene. Furthermore, electrochemical exfoliation methods have been also used for the exfoliation of graphite rod electrodes into graphene flakes based on the intercalation of salt ions in-between the graphite layers during the exfoliation process [25], [247], [248], [273]–[275]. The electrochemical exfoliation in aqueous salts

leads to production of highly oxidative graphene flakes, which then can be converted into reduced graphene oxide (rGOx) by any other reduction process. Some attempts have been appeared through the years in the development of new electrochemical exfoliation methods of graphite electrodes in organic salts media, leading in the production of graphene flakes which are less oxidized and high yield [274], [275]. These methods are less cost and easy prepared, which provide producing graphene from graphite electrodes in-situ for just one or two small and fast stages.

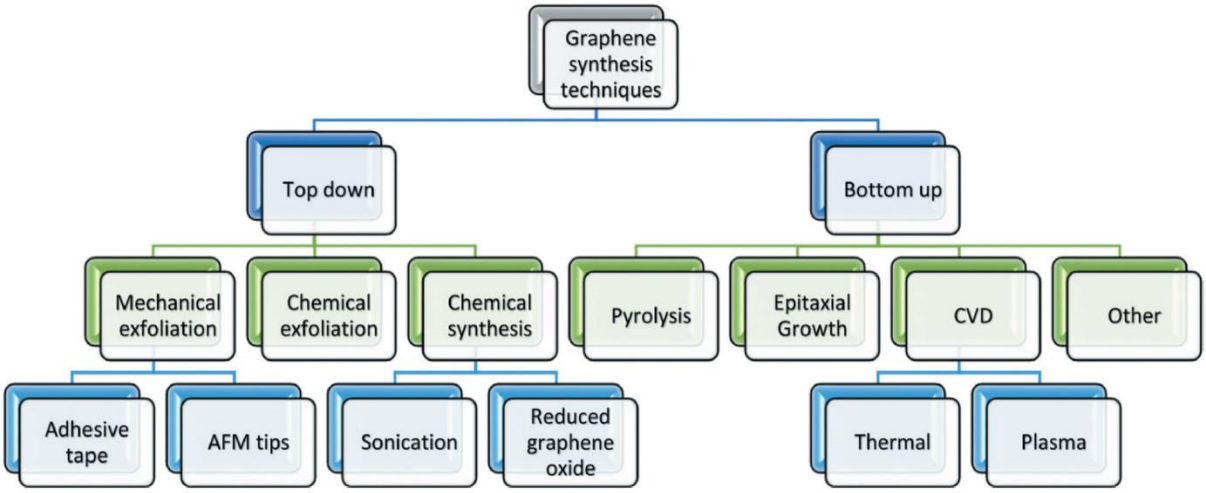

Figure 71. Different techniques used for graphene synthesis [276].

A detailed summary of the synthesis of graphene using various techniques was recently given by Bhuyan et al. 2016 [276] (Figure 71). Due to its interesting physico-chemical properties, graphene has attracted interest for lots of applications, especially for electronic devices, such as field effect transistors [233], [246], [277], [278], solar cells [279], and for chemical sensing devices [280], [281]. Moreover, the electrochemical exfoliated graphene electrodes modified with polypyrrole have been developed recently and showed good properties for supercapacitor applications [282]. On the other side another MIP-graphene-glassy carbon modified electrode has been developed for determination of trimethoprim as antibacterial drug [83].

However, to the best of our knowledge, until nowadays no direct MIP-graphene electrodes were developed for sensing applications. In this chapter we present a new original method for the preparation of high purity graphene based on the electrochemical exfoliation of graphite rod electrode in two different salt mediums, in aqueous and in organic media. A mechanical method for the transferring of graphene powder material onto polystyrene substrates has also been developed, which then were used for the preparation of graphene/PS electrodes used for the electrochemical fabrication of molecularly imprinted polypyrrole films dedicated to the isoproturon detection.

5.2. The fabrication process of graphene/polystyrene electrodes through electrochemical exfoliation of graphite rod

The electrochemical exfoliation of graphite was performed in a two-electrode cell for the case of graphite rod electrode exfoliation in aqueous liquid media, with a platinum counter electrode (Figure 72-A). A three-electrode cell has been used for the electrochemical exfoliation of graphite rod electrode in organic liquid media, where as a reference electrode was used an Ag/AgCl electrode, and as a counter electrode was used a platinum mesh cylinder electrode (Figure 72-B).

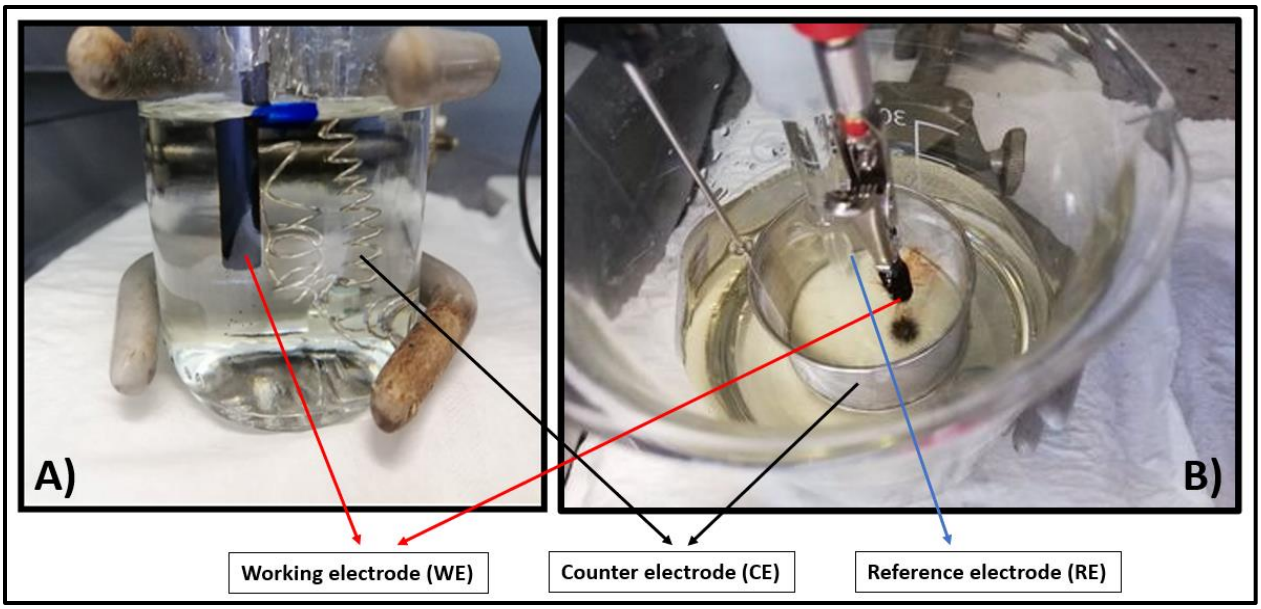

Figure 72. Electrochemical cell used for the exfoliation of graphite rod into graphene oxide/graphene flakes, A) two-electrode cell used for graphite rod exfoliation in water media, and B) three-electrode cell used for graphite rod exfoliation in organic media.

The above-described setup apparatus was connected to a potentiostat/galvanostat and controlled with a PC using NOVA software. Electrochemical exfoliation process was developed when the ions from the solution to intercalate between the graphite sp^2 layers, destroying the Van der Waals weak bonds and leading to the graphene flakes which fall at the bottom of the beaker under the gravitational force.

In Figure 73 is presented the graphite rod electrode before and after its electrochemical exfoliation process. It can be clearly seen that graphite electrode has changed color from ash to black after the process of its electrochemical exfoliation, leading to the loss of its mass which go away as graphene flakes detached from the graphite electrode.

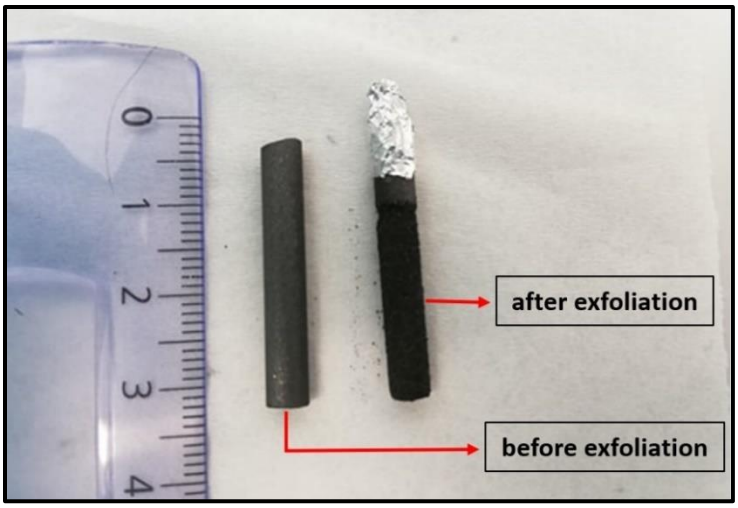

Figure 73. Graphite rod electrode before and after electrochemical exfoliation process.

5.2.1. Electrochemical exfoliation of graphite rod into graphene flakes in aqueous liquid media

In aqueous solutions, the electrochemical exfoliation process of graphite rod electrode into graphene flakes contains some steps between: the first step includes the electrochemical exfoliation of graphite rod electrode into graphene oxide (GOx) powder, whereas the second step includes the reduction of obtained graphene oxide with hydrazine hydrate into reduced graphene oxide (rGOx).

Electrochemical exfoliation of graphite has been performed in a two-electrode system using a platinum curved wire as counter electrode and graphite rod as a working electrode. Sulfate-containing salt such as $(NH_4)_2SO_4$ was chosen to be used as electrolyte solution for the exfoliation step, as the best inorganic salt with highest exfoliation efficiency, and the superior exfoliation efficiency of sulfate salts compared to other anions can be attributed to the lower reduction potential of SO_4^{2-} (+0.20 V) to generate SO_2 gas [273]. Electrolyte solution was prepared by dissolving $(NH_4)_2SO_4$ in water (concentration of 0.1 M and pH ~6.5–7.0). A direct current voltage +10 V has been applied to a graphite rod, and the current has been kept constant thanks to a voltage booster (Autolab Booster) for several hours until the exfoliation step has been finished. During the electrochemical exfoliation step the graphite sheets begin to dissociate and disperse into the electrolyte solution, due to the intercalation phenomenon of salt ions through the graphite sheets. The whole this process has been presented schematically in Figure 74-A. When applying bias voltage results in a reduction of water at the cathode, creating hydroxyl ions (OH^-) that can act as a strong nucleophile in the electrolyte. The

nucleophilic attack of graphite by OH^- ions initially occurs at the edge sites and grain boundaries. The oxidation at the edge sites and grain boundaries then leads to depolarization and expansion of the graphite layers separation, thereby facilitating the intercalation of sulfate ions (SO_4^{2-}) within the graphitic layers. During this stage, water molecules may co-intercalate with the SO_4^{2-} anions. Reduction of SO_4^{2-} anions and self-oxidation of water produce gaseous species such as SO_2, O_2, and others, as evidenced by the vigorous gas evolution during the electrochemical process [283], [284]. These gaseous species can exert large forces on the graphite layers, which are sufficient to separate weakly bonded graphite layers from one another [285].

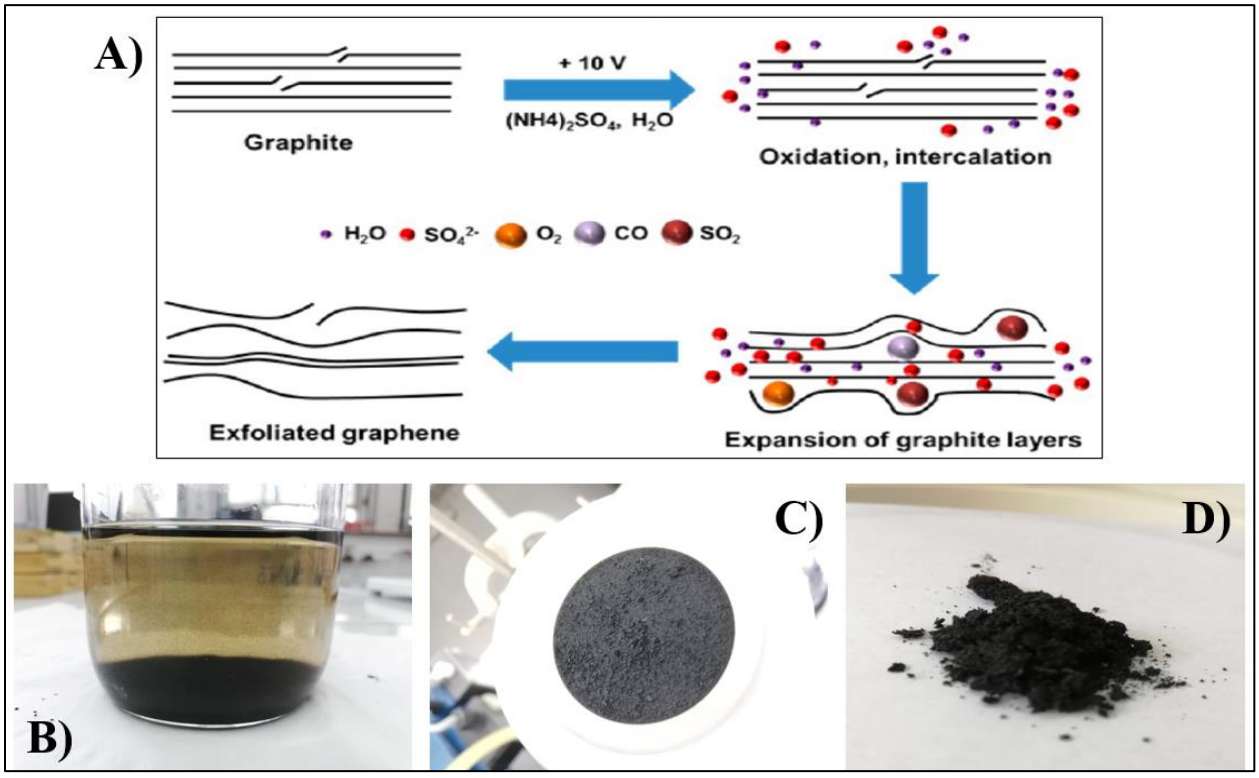

Figure 74. A) Schematic representation of the mechanism of exfoliation [273], B) exfoliated graphitic sheets into graphene oxide, C) graphene oxide flakes after vacuum filtration step, D) graphene oxide in powder.

After the exfoliation step the graphite rod electrode at the bottom of the cell is obtained the amount of graphene oxide flakes, where a small amount is dispersed in the solution (Figure 74-B). Afterward, the exfoliated product was collected by vacuum filtration (Figure 74-C) and repeatedly washed with water to remove any residual salts. At the end of the exfoliation step is obtained the graphene oxide powder (Figure 74-D). Furthermore, the next step in the graphene electrode production process is the reduction step of graphene oxide, as very important step which defines the basic properties of the reduced graphene oxide materials. Consequently, the degree of reduction of graphene oxide significantly influences the physical properties of

chemically reduced graphene oxide materials [286]. There are different methods that have been used for conversion of "graphene oxide" into "chemically reduced graphene oxide", such as by ultra-high vacuum heat [229], by chemical treatments (with hydrazine/hydrazine derivatives [238], [277], [287], [288] or high-concentration solutions of NaOH/KOH [289], by other chemical reductants, such as hydroquinone, and sodium borohydride [290], [291] which may offer the advantages of being cheap and up-scalable for fabricating graphene films. However, according to Directive 67/548/ EEC [292] hydrazine/hydrazine derivatives and NaOH/KOH are considered to be dangerous substances labelled as T-N (toxic and dangerous for the environment) and C (corrosive) respectively. Additionally, these methods have shown to be difficult to derive relatively pure reduced graphene oxide with an oxygen/carbon atomic (O/C) ratio of less than 6.25% [292].

However, in the very beginning of our work on graphene fabrication electrodes we have chosen to use hydrazine hydrate (NH_2-NH_2 x H_2O) as chemical reductant for the reduction of graphene oxide. The chemical treatment of graphene oxide with hydrazine hydrate is realized in a boiling flask in temperature (100 ˚C).

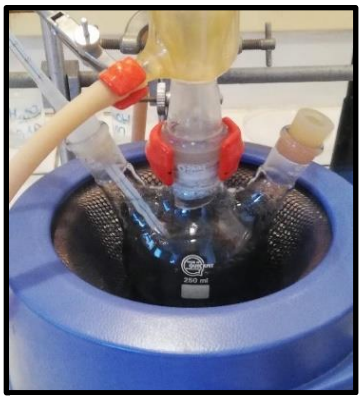

Figure 75. Heat treatment of graphene oxide with hydrazine hydrate.

In a boiling flask (250 ml) was added graphene oxide powder with pure water in concentration (3 mg/ml), and sonicated for about 1h until the whole amount of graphene oxide was dispersed in water and the mixture turns in dark brown color. Then it was added (2 ml) hydrazine hydrate and boiled at (T = 100 ˚C) for about 24h (Figure 75). After the treatment, the mixture was filtered and dried in oven at (T = 70 ˚C) for one night, in order to provoke evaporation and remove the whole amount of the solution. The reduced graphene oxide (rGOx) was then stored in a clean and dried place for the further uses and characterization. Hydrazine hydrate has been chosen as reductant because it does not react with water and was found to be the best one in producing very thin and fine graphene-like sheets [293].

During the reduction process, the brown colored dispersion of graphene oxide in water turned black and the reduced sheets aggregated and precipitated [201], [294]. Hydrazine takes part in ring-opening reaction with epoxides and forms hydrazine alcohols [293].

The reduction of graphene oxide sheets occurs only on the surface (Figure 76-A), where the carboxylic functional groups were unlikely to be reduced from the graphene oxide structure, whereas at the edge of the sheets the hydroxyl groups were still present even after the reduction process [293]. So, the possible mechanism of the reduction of graphene oxide with hydrazine has been shown in Figure 76-B.

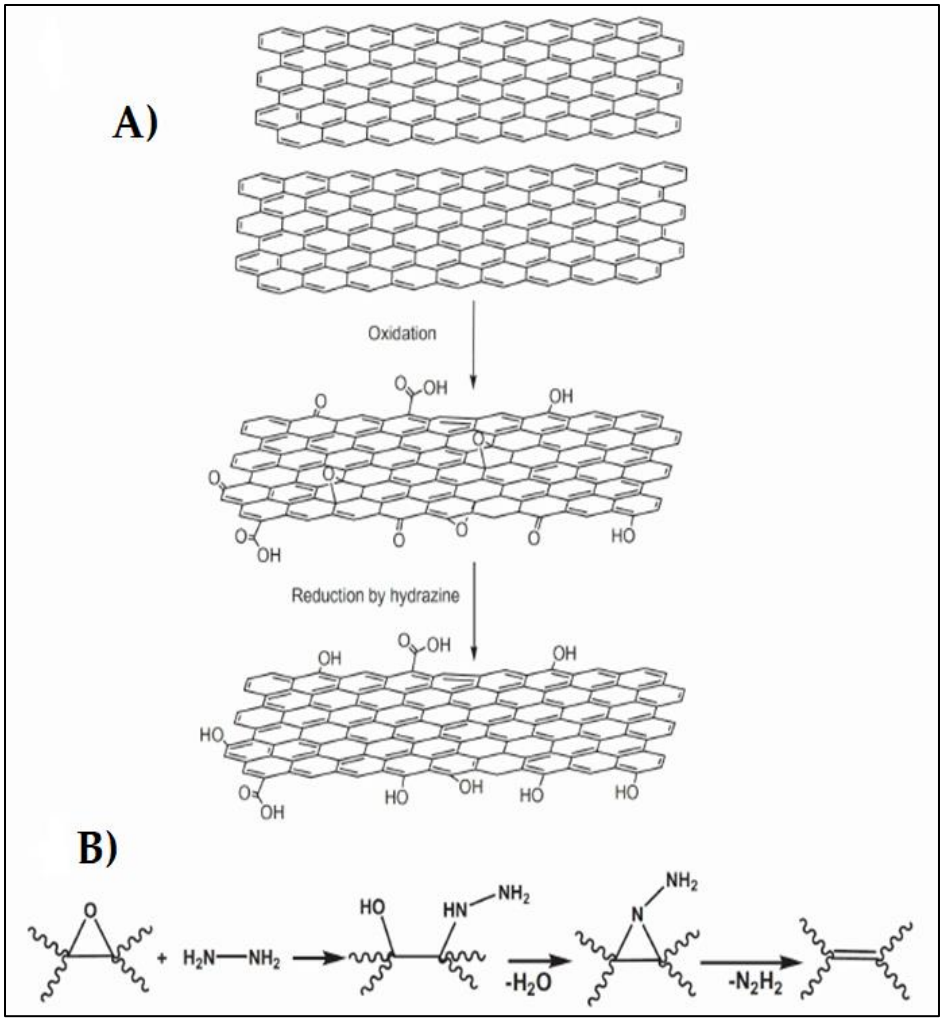

Figure 76. A) Oxidation of graphite to graphene oxide and reduction to reduced graphene oxide, B) A proposed reaction [293].

Except hydrazine hydrate, there exist other possible routes to reduce graphene oxide, such as using sodium borohydride ($NaBH_4$) in aqueous solution where sodium borohydride is more effective than hydrazine as a reductant of graphene oxide although it can be slowly hydrolyzed by water [295]. The using of $NaBH_4$ treatment leaded to the elimination of all the parent oxygen containing groups and the resultant solid became IR inactive like pure graphite. There have also been developed some other strategies for the reduction of graphene oxide, such as using hydroquinone [296], gaseous hydrogen (after thermal expansion) [297], and strongly alkaline solutions [289]. Moreover, thermal reduction was found to be another approach to reduce graphene oxide into reduced graphene oxide by using the heat treatment to remove the oxide functional groups from graphene oxide surfaces [298]. However, the attempt for the development a new single stage route to produce highly quality of reduced graphene oxide still remain a challenge.

5.2.2. Electrochemical exfoliation of graphite rod into graphene flakes in organic media

Cooper et al. 2014 have developed a single stage electrochemical exfoliation method for the production of few-layers graphene via intercalation of tetraalkylammonium cations [274], where it was stated that the electrochemical exfoliation of graphite rod electrode can be achieved easy without sonication by intercalation of TBA cations [274].

In this work, we present a single stage of electrochemical exfoliation of graphite rod electrode method for the production of graphene layers via intercalation of tetrabutylammonium tetrafluoroborate (TBA BF_4) cations. NMP (1-methyl-2-pyrrolidone) was used as organic solvent due to its wide electrochemical window and suitable organic solvent for exfoliation processes [299]–[303]. A three-electrode cell has been employed for the electrochemical exfoliation of graphite rod electrode. Chronoamperometry has been used as electrochemical method for the exfoliation of graphite rod electrode at two different fixed potentials -5 V and -2.5 V for a time 6h (21600 secs) and compared with each other. As an electrolyte is used tetrabutylammonium tetrafluoroborate (TBA BF_4) C=0.1M dissolved in NMP (1-methyl-2-pyrrolidone).

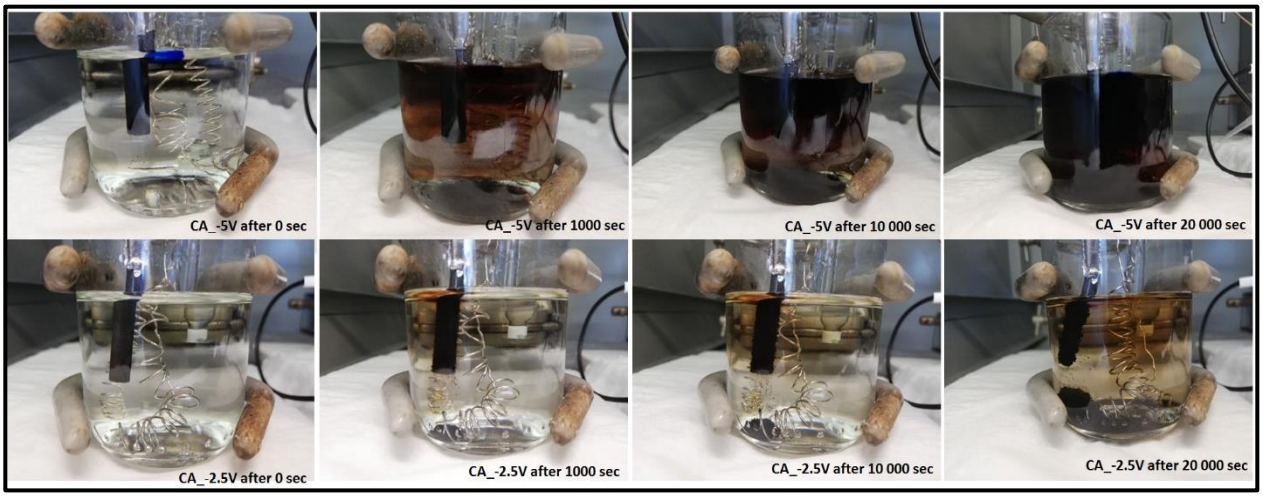

Figure 77. Electrochemical exfoliation at different times of exfoliation.

In Figure 77 is shown the electrochemical cell during the chronoamperometry exfoliation of graphite rod electrode, and the images were taken at different times of exfoliation. As seen at both of the potentials the exfoliation of graphite rod was successfully reached after only 1000 s, but at -5 V the solution turns darks earlier than in the case of exfoliation at -2.5 V.

This method used for the fabrication of graphene from the direct electrochemical exfoliation of graphite rod electrode has many advantages, such as: no need to use current booster for the application of high voltage, and no need to perform reduction of the exfoliated graphene products. Just after this step the graphene powder was then filtered and dried in oven for about 10 hours at temperature around 100˚C and then stored in a clean place for the further treatment and characterization.

5.2.3. The transfer process of graphene powder onto polystyrene plates

For the fabrication of graphene electrodes, the graphene product as powder has been transferred onto polystyrene plates through a mechanical pressing and heating process. The whole graphene transfer process onto polystyrene plates begins with the dispersion of graphene in pure ethanol (>99.99 %) in a concentration of 0.3 mg/ml under sonication for about 1 h. In Figure 78 is illustrated the dispersion of graphene powder in ethanol before (Figure 78-A) and after the sonication process (Figure 78-B).

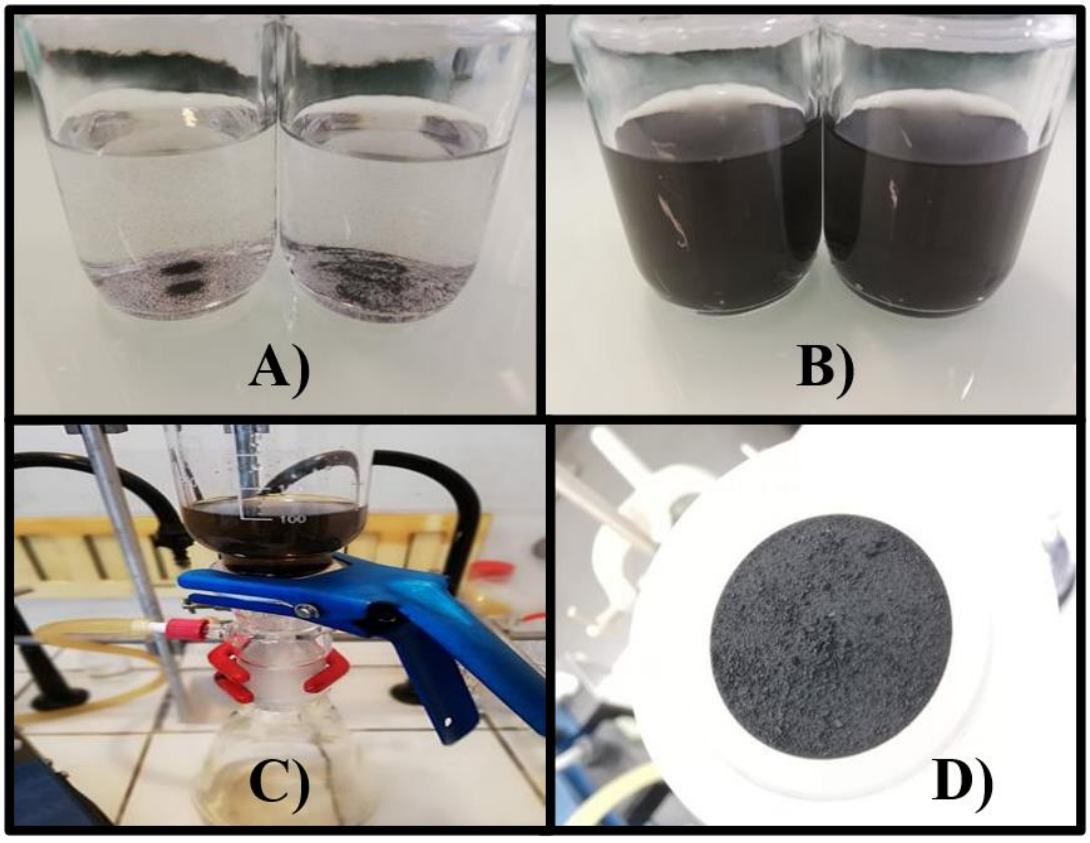

Figure 78. A) Graphene powder in pure ethanol before sonication, B) dispersed graphene powder in ethanol after 1h of sonication, C) vacuum filtration, and D) graphene powder embedded on the filter.

After the dispersion step, the mixture (graphene dispersed in ethanol) is then filtered under vacuum system with a paper filter size 0.25 μm (Figure 78-C), where the graphene powder was embedded in the filter as precipitate (Figure 78-D). The filter with graphene was inverted and placed in the center of a polystyrene plate, covered with an aluminum foil and then fixed in a pressing machine under the conditions of pressing 5 tons for 3 mins at the temperature 90 °C, see in Figure 79 the schematically representation of the graphene transfer process on polystyrene plate.

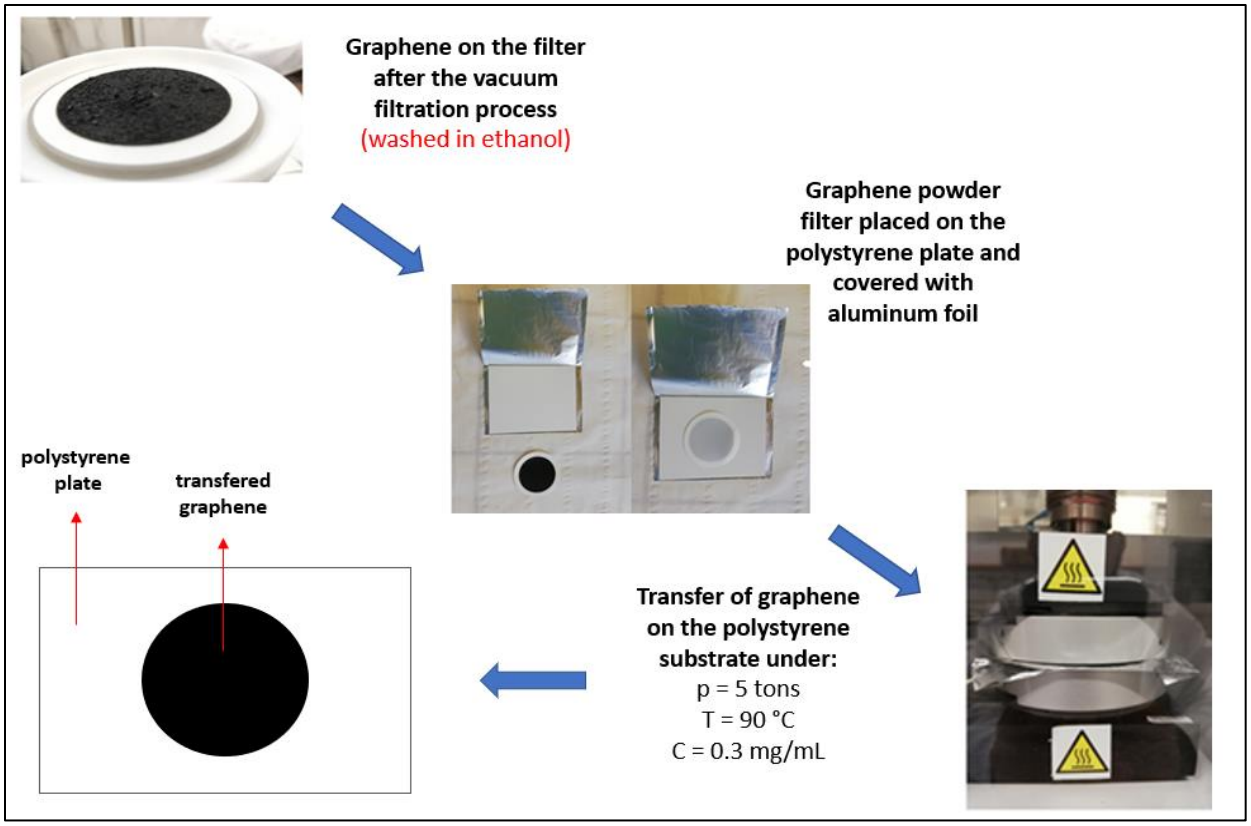

Figure 79. Schematic representation of the graphene transfer process on polystyrene used then for the fabrication of graphene electrodes.

As result of the transfer process, we reach to have the transferred graphene onto polystyrene plate which can be used then as substrate for the graphene electrode preparation. The electrodes of graphene with a controlled working surface area have been prepared through two different ways, through our own method in the laboratory (the electrodes with circle working surface area) and through photolithography (the electrodes with square working surface area). With our own method at the laboratory, we were able to prepare the graphene electrodes with controlled surface area at (10 mm^2 and 1 mm^2), whereas with photolithography by using a mask we were able to prepare

the graphene electrodes at several different surface areas (10 mm^2, 5 mm^2, 1 mm^2, 500 μm^2, 200 μm^2, 100 μm^2). In Figure 80 are presented the two mentioned ways.

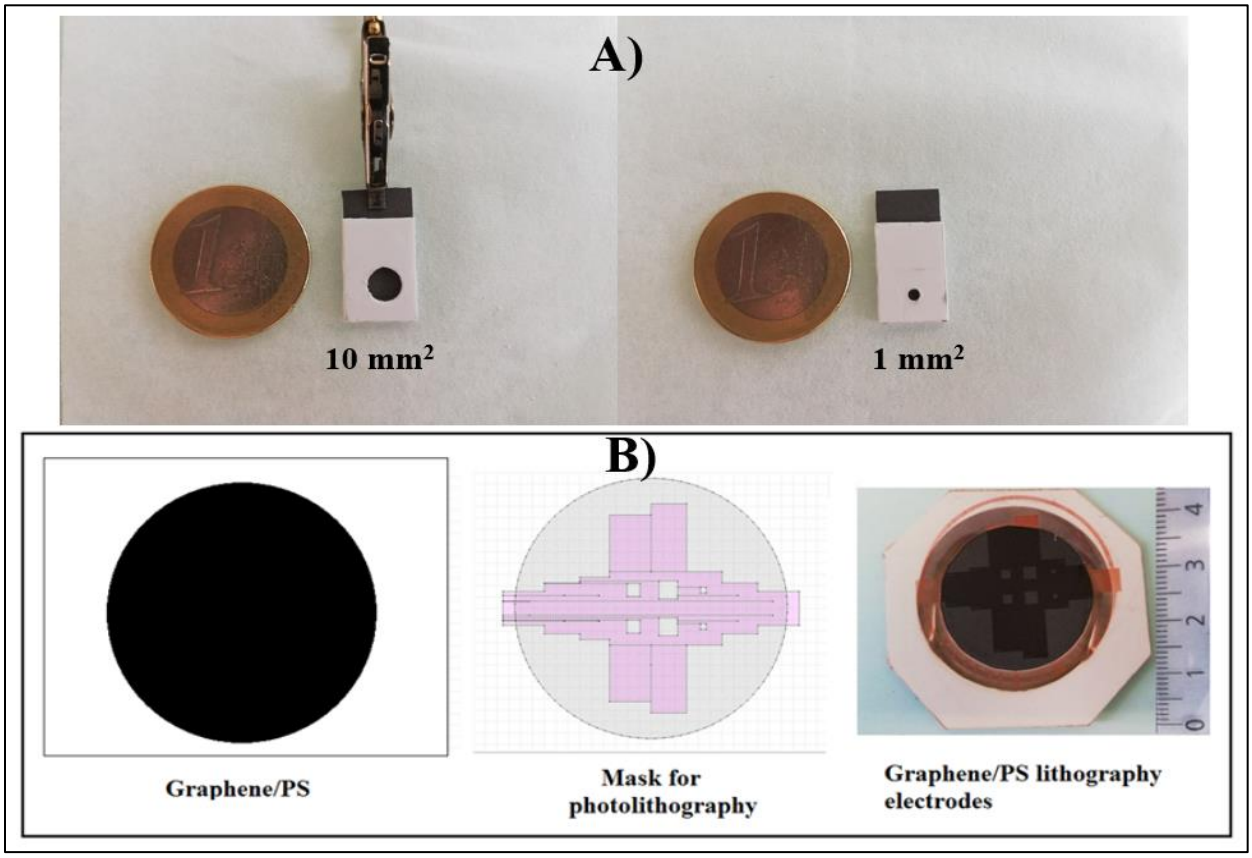

Figure 80. Fabrication process of graphene electrodes with controlled working area, A) with our own method in the laboratory, and B) with photolithography.

With the same procedure we have been able to prepare the electrodes with other kinds of powders, such as with graphene oxide (GOx) exfoliated in aqueous media, reduced graphene oxide (rGOx) with hydrazine hydrate, reduced graphene oxide (commercial one bought from USA), graphene exfoliated in organic solvent (at potentials -5 V and -2.5 V).

In the following sections of this chapter, we present different ways of characterization of these electrode materials which are divided in two parts, the part of physical characterizations and the part of electrochemical characterizations of our electrode materials, followed by the Graphene-MIP sensors preparation and use them for the isoproturon electrochemical determination.

5.3. Characterization of different forms of graphene/polystyrene electrodes by using various spectroscopy techniques

5.3.1. XPS characterization

XPS spectroscopy has been used for the chemical composition analysis of the graphene materials at each stage during the production of graphene by using two different ways, exfoliation in aqueous and in organic media, where the two methods have been compared and showing different levels of oxidation. XPS spectrum of graphite is performed and added to all the cases for comparison. Firstly, there are presented the XPS spectra of graphene materials obtained during the electrochemical exfoliation of graphite in aqueous media. The two regions C1s and O1s are presented here.

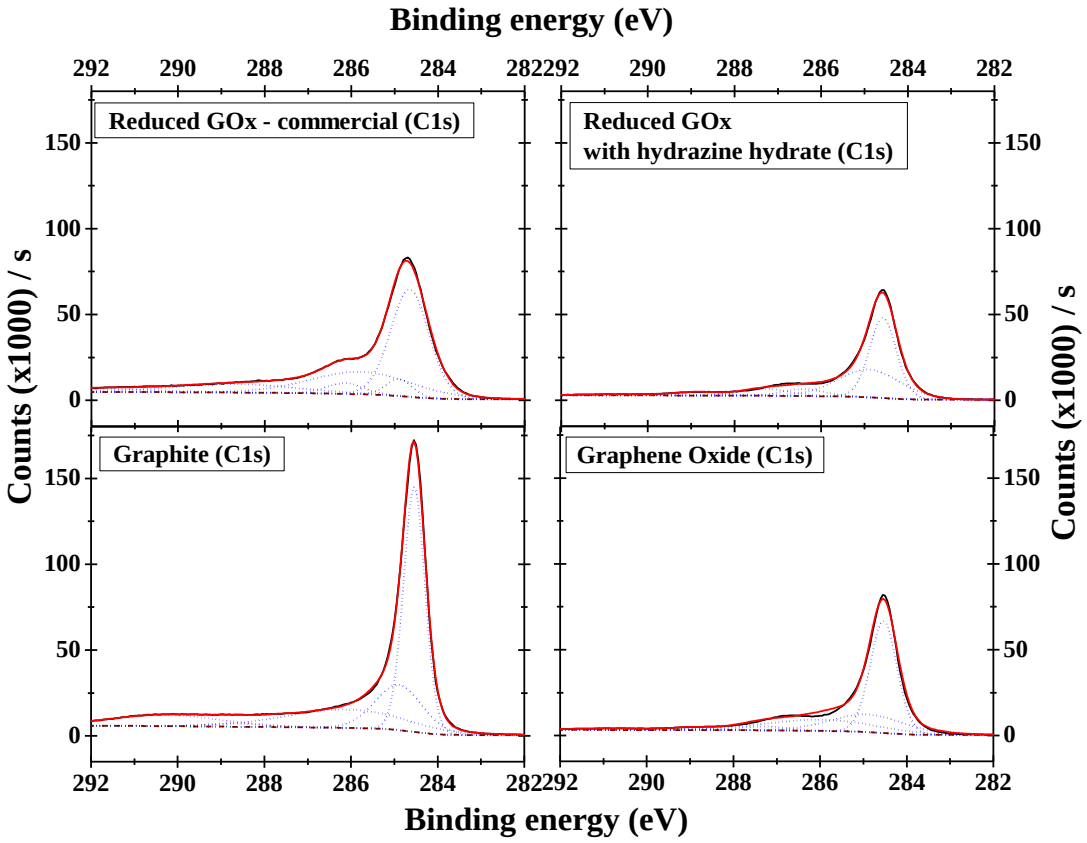

Figure 81. C1s XPS spectra for graphite, graphene oxide exfoliated in aqueous media of 0.1M $(NH_4)_2SO_4$, reduced graphene oxide with hydrazine hydrate and commercial reduced graphene oxide – USA. Black curves express experimental data points and red ones are fitting curves for spectra.

The C1s region is appeared with an asymmetric peak (Figure 81) at 284.5 eV for the case of graphite [304]. This main peak appeared for the XPS C1s spectra in all the cases, and

it is explained as many-electron interactions of the metallic conduction electrons induced by low energy electron-hole excitations resulting from absorption of X-rays [305], and originates in both sp^2 – hybridized graphite-like carbon atoms as a C-C sp^2 contribution and in carbon atoms bound to hydrogen atoms, whereas a peak at 285.1 eV is assigned to sp^3 – hybridized carbon atoms as in diamond-like carbon as a C-C sp^3 contribution [305]. The C1s spectra have been fitted using a Gaussian contribution centered [304]–[306]. Peaks with higher binding energies located at 286.6 eV for graphene oxide and for reduced graphene oxide have been observed, and at 286.3 eV for commercial reduced graphene oxide [229], as C-O-, C=O, COO- and π-π contributions.

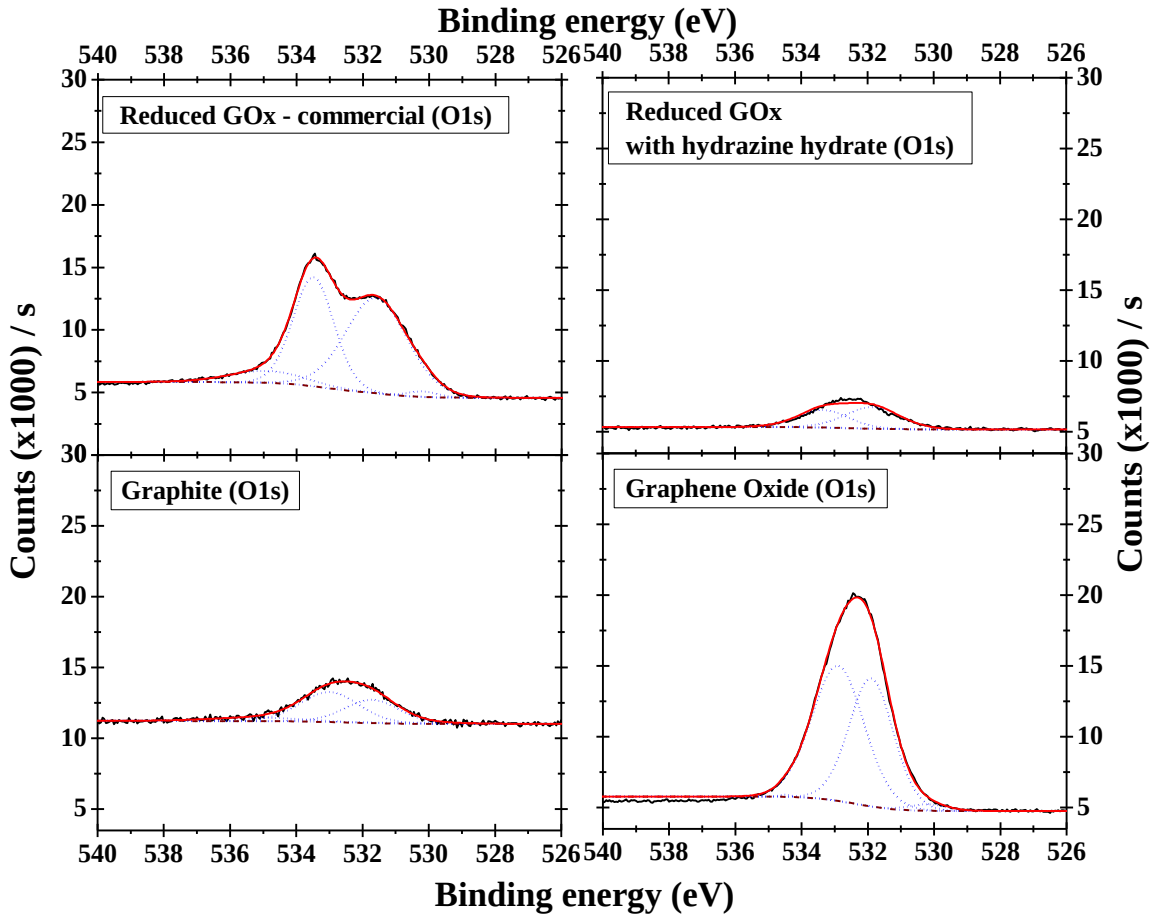

Figure 82. O1s XPS spectra for graphite, graphene oxide exfoliated in aqueous media of 0.1M $(NH_4)_2SO_4$, reduced graphene oxide with hydrazine hydrate and commercial reduced graphene oxide – USA. Black curves express experimental data points and red ones are fitting curves for spectra.

In Figure 82 is presented the O1s spectra for all the cases, where is shown that after the chemical reduction of graphene oxide with hydrazine hydrate the O1s main peak was decreased indicating an efficient chemical reduction process of the graphene oxide, lowering the degree of oxidation from 30% to 17.5%, whereas in the case of commercial

reduced graphene oxide for O1s are observed two main peaks (at 531.6 eV and at 533.5 eV) increasing the degree of oxidation at around 45% [229].

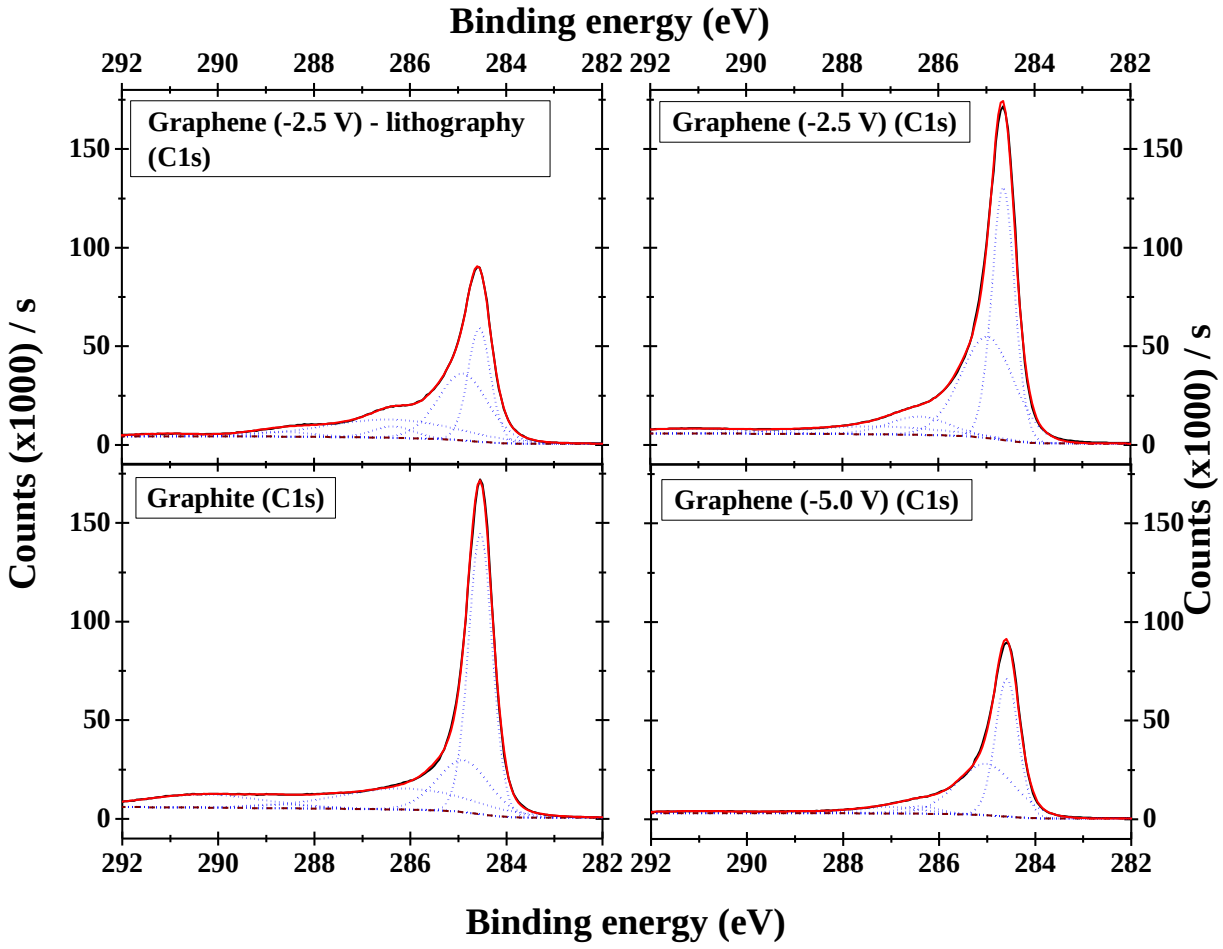

Figure 83. C1s XPS spectra for graphite, for graphene exfoliated in 0.1M TBA BF_4 dissolved in NMP (1-methyl-2-pyrrolidinone) by CA at -5.0 V and at -2.5 V, and for graphene exfoliated by CA at -2.5 V exposed with photolithography. Black curves express experimental data points and red ones are fitting curves for spectra.

In the case of graphene exfoliated in 0.1M TBA BF_4 dissolved in NMP (1-methyl-2-pyrrolidinone), the C1s XPS main spectra presented in Figure 83, showed a higher peak intensity for graphite than in the graphene exfoliated at -5.0 V, while compared to the peak intensity observed in the case graphene exfoliated by CA at -2.5 V, equal intensity values can be read. According to the XPS spectra for graphene exfoliated by CA at -2.5 V after exposing with photolithography was showed a lower peak intensity compared to that one without performing photolithography. On the other side, in Figure 84 are showed the O1s XPS spectra observed at higher binding energies, where clearly can be seen that in the case of graphene exfoliated at -2.5 V exposed with photolithography

compared to the other structures, it shows a higher peak values intensity for the presence of oxygenic groups on its structure.

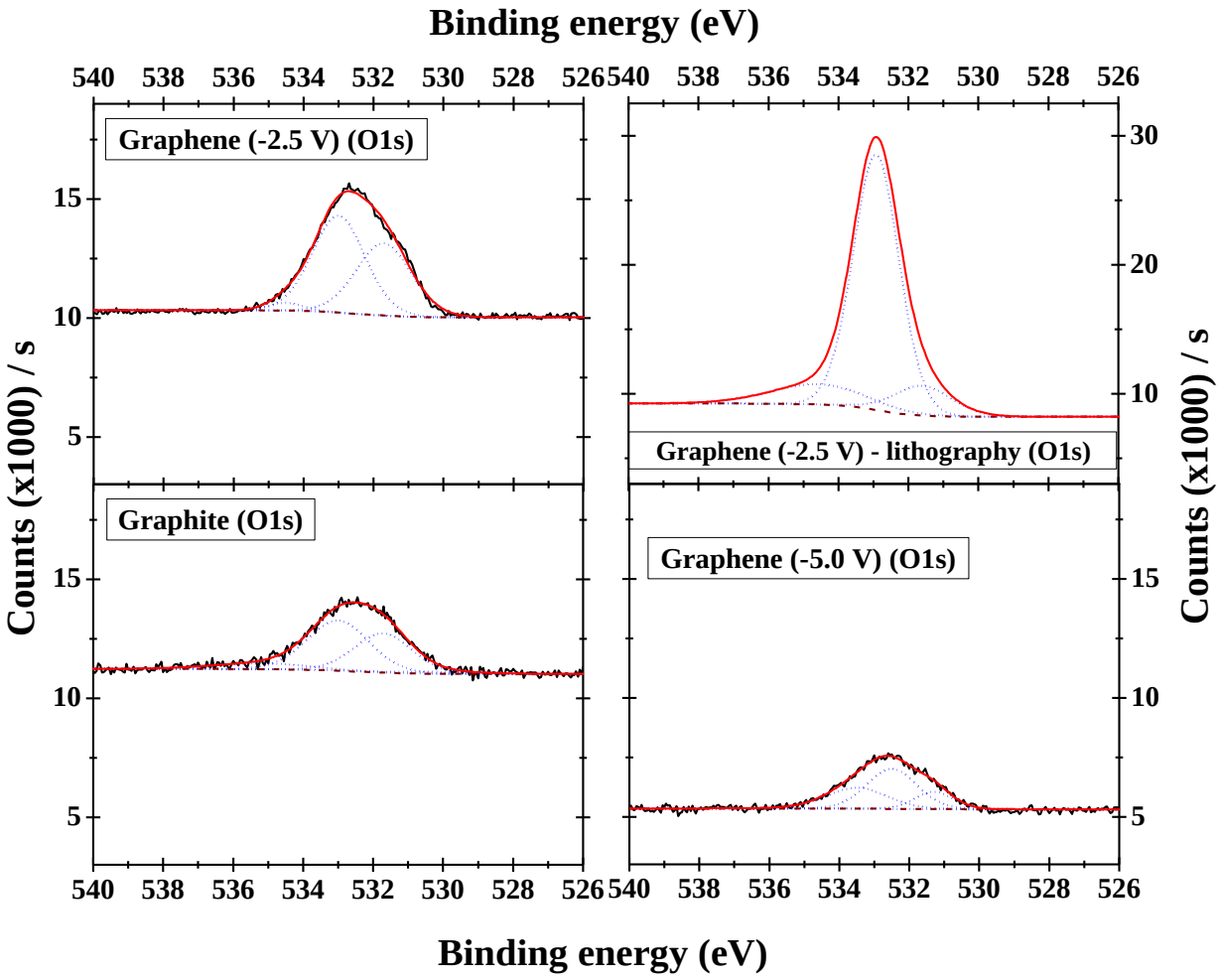

Figure 84. O1s XPS spectra for graphite, for graphene exfoliated in 0.1M TBA BF_4 dissolved in NMP (1-methyl-2-pyrrolidinone) by CA at -5.0 V and at -2.5 V, and for graphene exfoliated by CA at -2.5 V exposed with photolithography. Black curves express experimental data points and red ones are fitting curves for spectra.

The histograms presented in Figure 85 show the atomic percentage of the different bounds for all the cases indicating that graphene materials exfoliated in 0.1M TBA BF_4 dissolved in NMP (1-methyl-2-pyrrolidinone) showed to contain less oxygenic functional groups in their structure, whereas the graphene oxide exfoliated in 0.1M $(NH_4)_2SO_4$ which was further reduced with hydrazine hydrate shows to be more contaminated with oxygenic functional groups, including that one of commercial reduced graphene oxide [229].

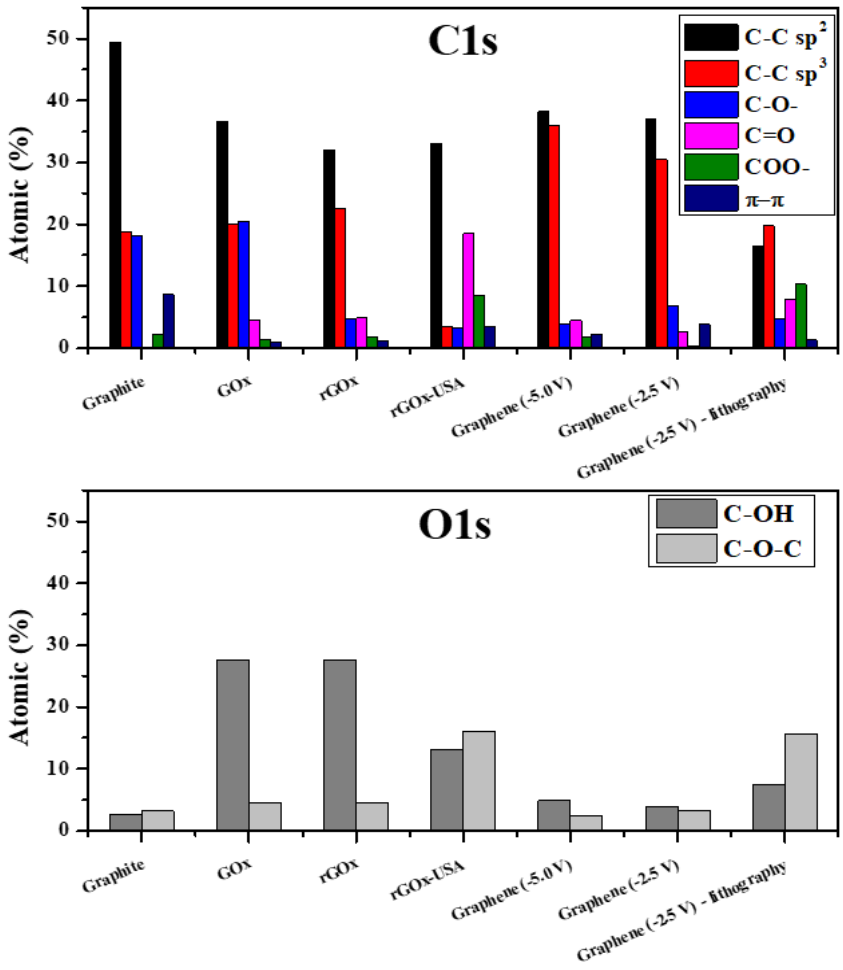

Figure 85. The atomic percentage of different oxygenic bounds for the case of C1s (above) and for O1s (below).

In the case of reduced graphene oxide with hydrazine, it has been shown a decrease of main C1s peak, where no difference was obtained in higher binding energies, whereas in the case of commercial reduced graphene oxide both peaks intensity has been increased and their positions shifted a little, due to the presence of oxygenic functional groups and high defect levels in its structure.

In Figure 86 is presented the ratio [C(O)]/[C] determined from the Gaussian fits to the peaks of the O1s XPS data calculated according to the following equation [306]:

[C (O)]/[C] = total content of C (O) (%)/total content of C1s (%) ……..(5.1)

High ratio values were obtained for graphene oxide, commercial reduced graphene oxide and for graphene exfoliated at -2.5 V exposed with photolithography. Low ratios are obtained for graphene exfoliated in 0.1M TBA BF_4 dissolved in NMP (1-methyl-2-pyrrolidinone) at potential -2.5 V. Hence, the overall analysis of XPS results demonstrates that during the electrochemical exfoliation of graphite in solution of $(NH_4)_2SO_4$ 0.1M resulted in production of highly oxidized graphene, whereas the graphene produced by electrochemical exfoliation of graphite in organic solution showed lower ratio values. Summary analysis of XPS data were presented with table in Appendix 3.

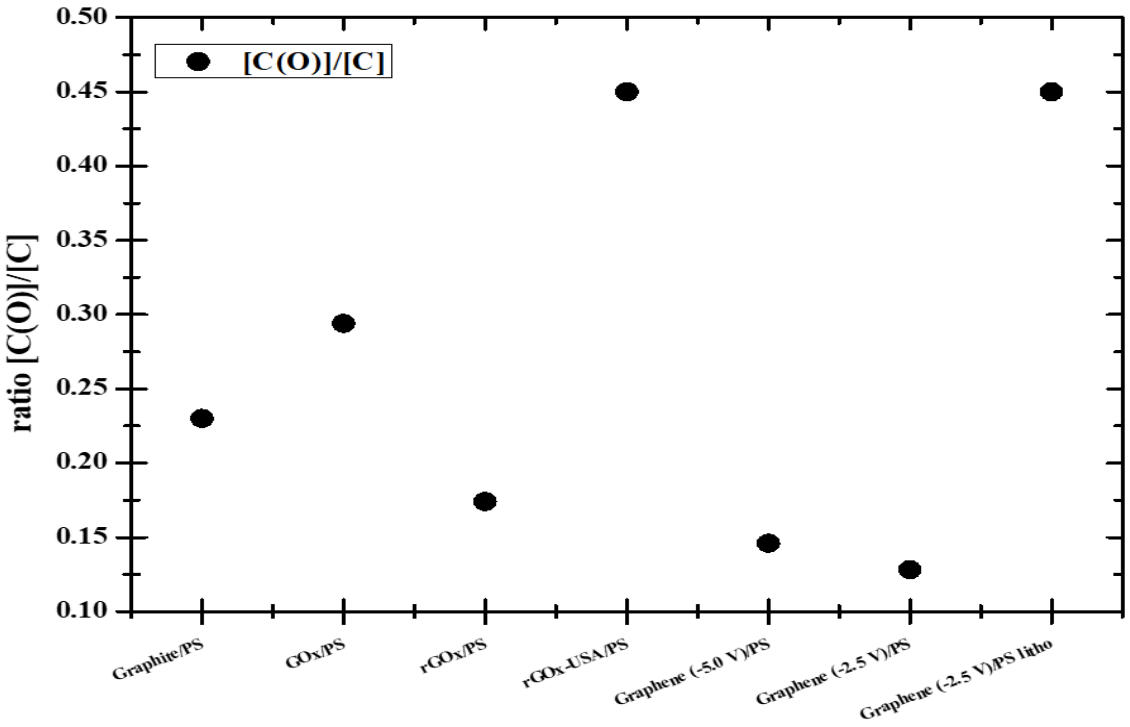

Figure 86. Obtained values for the ratio [C (O)]/[C] for all the cases.

5.3.2. Raman characterization

Raman spectroscopy as a standard non-destructive tool can be used for the analysis of structural configuration of carbon materials, such as graphite, diamond, carbon nanotubes, graphene and graphene oxide [304], [307]. Raman spectra were carried out for all the graphene samples at each step of the procedures during the electrochemical exfoliation of graphite in both aqueous and organic mediums. As a reference the Raman

spectrum of graphite has been performed and added to all the cases for comparison. In Figure 87 and in Figure 88 are presented the Raman spectra of the different graphene and graphite samples produced and used during this PhD thesis work. In all the cases three characteristic bands are observed. The **D-band** which is correlated with the presence of a given density of defects in the structure of the carbon materials was observed at around **1332cm^{-1} – 1340cm^{-1}**. The **G-band** observed at around **1580cm^{-1}** comes from the in-plane vibration of carbon atoms with sp^2 hybridization [308]. A strong band at around **2680cm^{-1}** known as **2D-band** (or G' band) which comes from two-phonon process which occurs between the K and K; point of Brillouin space, is correlated with the electronic structure of the graphene and graphite samples and is independent with the presence or not of defects in the structure [308] (Figure 87). According to the results shown in Figure 87, an increasing of the **D-band** peak intensity is observed after the electrochemical exfoliation of graphite in aqueous media, and this band decreased after the chemical reduction with hydrazine hydrate. In the case of commercial graphene, obtained by Hummer's method the structuration of the **D-band** spectral windows highlighted a high degree of defects and a low degree of organization of the crystallographic structure.

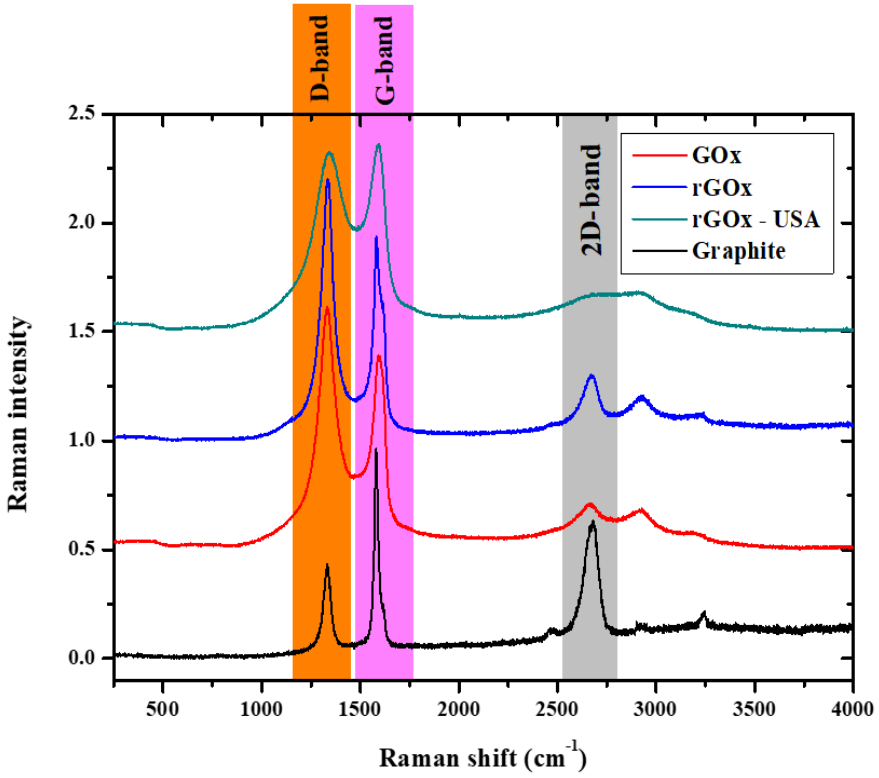

Figure 87. Raman spectra of graphite, graphene oxide (GOx), reduced graphene oxide (rGOx), commercial reduced graphene oxide (rGOx - USA).

These Raman spectra show the structure of graphene oxide exfoliated in aqueous media, reduced graphene oxide with hydrazine and commercial reduced graphene oxide contain high defects which are due to the size of the graphene flake and to the presence of oxide generated by the electrochemical exfoliation of graphite rod electrodes in aqueous media. In the case of the Raman spectra of graphene exfoliated from graphite rod electrode in 0.1M TBA BF_4 dissolved in NMP (1-methyl-2-pyrrolidinone) by CA at potentials -5.0 V and -2.5 V (Figure 88), the intensity of **D-band** peak obtained for graphene (-5.0V) is higher than that one of graphite, but not in the case of graphene (-2.5V) which shows a lower **D-band** intensity (Figure 88-B). From the analysis of these Raman results is shown that graphene exfoliated from graphite rod electrode in organic media by CA at potential -2.5 V shows a low degree of defects in its structure, even less than graphite used as base material for the graphene fabrication.

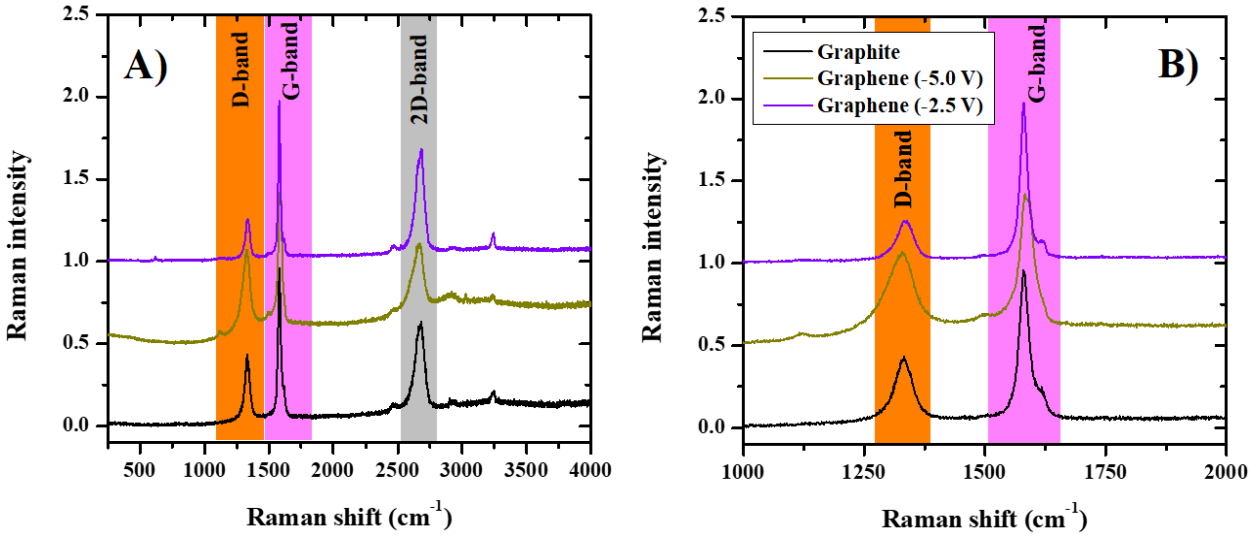

Figure 88. Raman spectra of graphite, graphene -5V, and graphene -2.5V with three characteristic bands (A), and with D- and G-bands (B).

As the starting material is the same for all graphene i.e., the graphite rod, the difference in the D-band intensities between the two ways of graphene exfoliation, is correlated with the oxidation of the graphene sheets induced by the exfoliation in water compared to the exfoliation in organic media. Finally, the Raman spectra highlighted that the graphene samples obtained by exfoliation in organic media presented a low degree of defects, and high degree of organization, according to the 2D band compared to the graphene exfoliated in water. The high degree of oxidation of the water media exfoliated graphene despite the reduction step by using hydrazine is highlighted by the high intensities of the D-band.

5.3.3. IR characterization

IR spectroscopy has been used in order to study the different types of functional groups formed in the structure of graphene powder at different steps during the electrochemical exfoliation in aqueous and organic media.

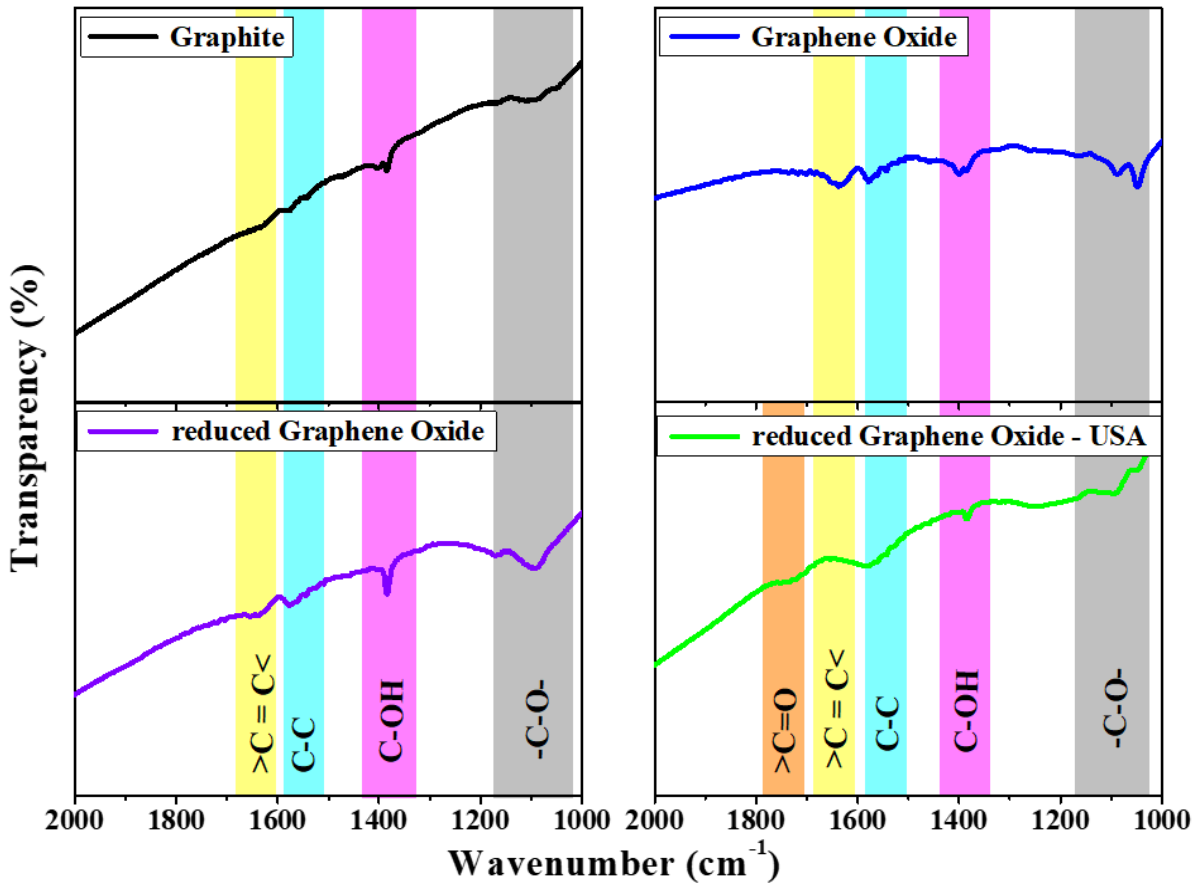

Figure 89. IR spectra of graphite, graphene oxide exfoliated in aqueous media of 0.1M $(NH_4)2SO_4$, reduced graphene oxide with hydrazine hydrate and commercial reduced graphene oxide.

The IR spectra of graphite, graphene oxide exfoliated in aqueous media of 0.1M $(NH_4)_2SO_4$, reduced graphene oxide with hydrazine hydrate, and commercial reduced graphene oxide are presented in Figure 89. A band has been observed at **1573 cm^{-1}** due to the presence of **C-C** stretching in graphite electrode, and also it was obtained in all the other samples [309]. At around **1385 cm^{-1}** was observed the **C–OH** band which is characteristic for phenols [310] was obtained in all these cases, apparently in the case of graphene oxide and reduced graphene oxide the band was more intense [304]. The **C-O-** band was observed at around **1000 - 1150 cm^{-1}**, which is characteristic for stretching of ether group [304], and was obtained for all the samples. Based on these analyzed IR results we claim that during the electrochemical exfoliation of graphite rod electrode in

aqueous media, we further increase oxidation level of the material, and that is why we see the presence of high oxygenated functional groups. Moreover, in the case of IR spectrum of the commercial reduced graphene oxide it was obtained the **C=O** band at around **1700 - 1760 cm^{-1}** which is typically for carboxylic acids or esters. Furthermore, the band obtained at **1600 – 1640 cm^{-1}** is **>C=C<** aromatic stretching band characteristic for aromatic rings and was obtained for all the samples presented in Figure 86. In the other hand, when the electrochemical exfoliation of graphite rod electrodes has been performed in 0.1M TBA BF_4 dissolved in NMP (1-methyl-2-pyrrolidinone) by CA at the potential (-5.0V) and (-2.5V) the presence of different oxygenated functional groups at the same regions was not obtained anymore. As seen from Figure 90 in the case of **Graphene (-5.0 V)** and **Graphene (-2.5 V)** samples at the region **1600 - 1640 cm^{-1}** the structure of graphene showed a much higher presence of **>C=C<** aromatic stretching band characteristic for aromatic rings. At around **1000 - 1150 cm^{-1}** the **C-O-** band was observed for the case of graphene exfoliated at -5.0 V and for the case of graphene exfoliated at -2.5 V after exposure in photolithography, but not in the case of pure graphene exfoliated at -2.5 V. Here, we express that the graphene products exfoliated in organic solvents media have shown to contain less oxygenated functional groups than the graphene one which has been exfoliated in aqueous solvents.

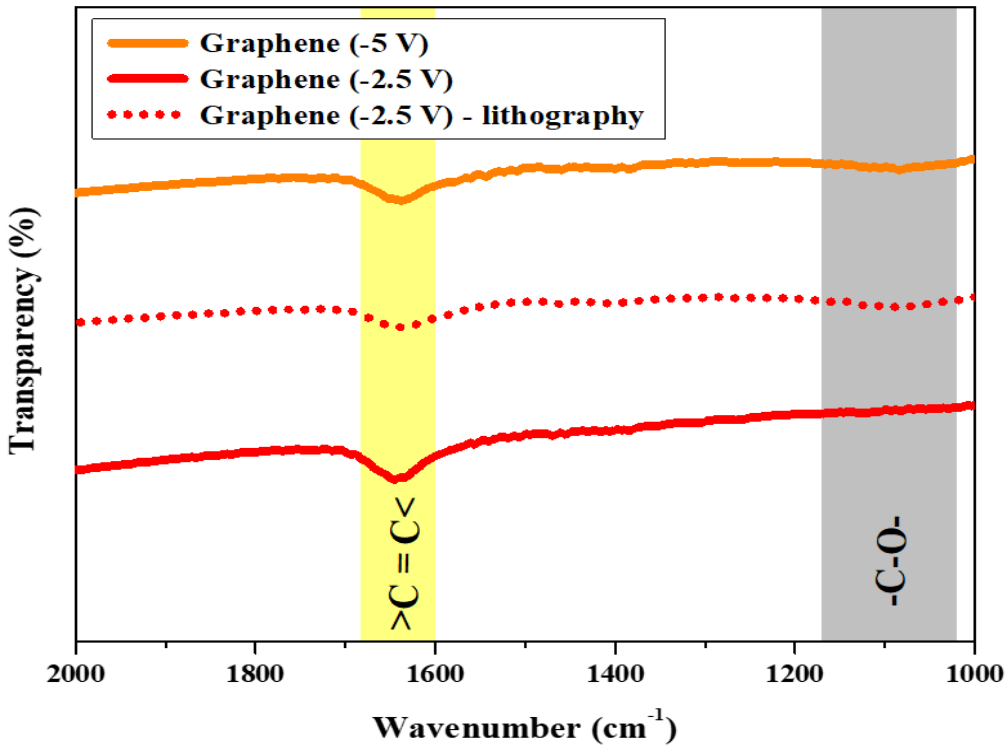

Figure 90. IR spectra of graphene (-5.0 V), graphene (-2.5 V), and graphene (-2.5 V) exposed in photolithography, exfoliated in in 0.1M TBA BF_4 dissolved in NMP (1-methyl-2-pyrrolidinone) by CA.

5.3.4. Electrical conductivity measurements

After the transfer of the powder of graphite, graphene oxide exfoliated in aqueous media, reduced graphene oxide with hydrazine hydrate, commercial reduced graphene oxide, graphene exfoliated in organic solvents by CA at potentials -5.0 V and -2.5 V and that one exfoliated at -2.5 V after exposure in photolithography onto polystyrene wafers, the samples were analyzed by measuring their resistance with a four-point probe system (Keithley 2700 Multimeter) [311]. The conductivity of the electrodes has been presented with histogram in Figure 91.

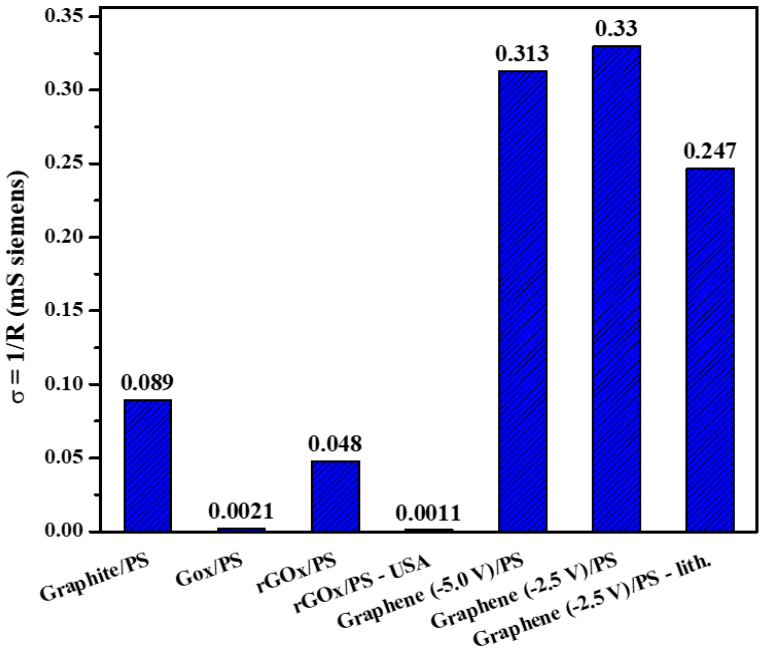

Figure 91. Four-point probe electrical conductivity measurements of different samples transferred on polystyrene substrate.

The conductivity of the graphene oxide exfoliated in aqueous media of 0.1M $(NH_4)_2SO_4$ was around 40 times lower than graphite as base material, whereas after the chemical reduction with hydrazine hydrate the conductivity was increased and is only 2 times lower than graphite material. Whereas in the case of graphene exfoliated in 0.1M TBA BF_4 dissolved in NMP (1-methyl-2-pyrrolidinone) at the potential -2.5 V has shown the highest electrical conductivity, about 4 times higher than graphite sample, and around seven times higher than the reduced graphene oxide, and showing to be the best one. Low electrical conductivity has been observed on the samples of commercial reduced graphene oxide. Graphene (-2.5 V) after exposure with photolithography showed a lower electrical conductivity that without lithography.

5.4. Electrochemical characterization of graphene/polystyrene electrodes

5.4.1. Electrochemical window

The electrochemical window (EW) of a substance is the potential range (voltage range) between which the substance is neither oxidized nor reduced. The EW is one of the most important characteristics to be identified for electrodes, solvents and electrolytes used in electrochemical applications. In this context we have tested the best graphene (-2.5 V) transferred on polystyrene plate electrodes for the electrochemical activity. Two methods have been used for the study of electrochemical window of different kinds of graphene electrodes, linear sweep voltammetry (LSV) and cyclic voltammetry (CV). The electrochemical working area for all kinds of electrodes was A = 3 mm^2. In Figure 92 have been shown the measurements obtained for the glassy carbon electrode (GCE), graphite/PS electrode and for graphene (-2.5 V)/PS electrode in a solution of lithium perchlorate $LiClO_4$ (0.1M) dissolved in an ethanol/water solvent (20/80 v/v), whereas the data extracted for all the electrodes are presented in Table 6.

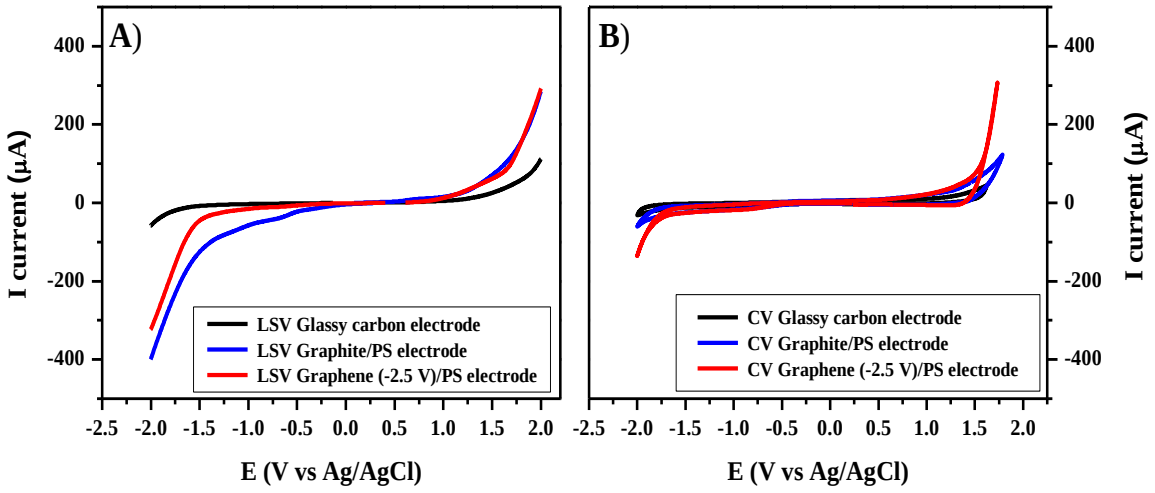

Figure 92. Electrochemical stability windows of Glassy Carbon, Graphite/PS, and Graphene (-2.5 V)/PS electrode obtained by A) linear sweep voltammetry (LSV), and B) cyclic voltammetry (CV), in a solution of $LiClO_4$ (0.1M) (20/80 ethanol:water v/v). Scan rate 100 mV/s.

According to results presented in Figure 92-A, the graphene (-2.5 V)/PS electrode exfoliated in 0.1M TBA BF4 in NMP (1-methyl-2-pyrrolidinone) prepared without photolithography shows the highest anodic stability (1.85 V) when compared to the

others and widest electrochemical window (3.8 V). Electrochemical activity is also improved compared to that one of glassy carbon electrode (see Table 6), whereas in the case of graphene (-2.5 V)/PS prepared with photolithography the electrochemical activity it was not as satisfied. The graphene oxide/PS electrode exfoliated in 0.1M $(NH_4)_2SO_4$ and graphene oxide/PS electrode reduced with hydrazine hydrate did not show any electrochemical activity. Moreover, the capacitive currents measured from the cyclic voltammograms (Figure 92-B) at +0.1V showed the same behavior of the electrodes, a very high capacitive current for the case of graphene oxide/PS and reduced graphene oxide/PS electrodes, and tightly capacitive currents for the graphene (-2.5 V)/PS electrodes.

Table 6. Data presented for the electrochemical stability windows of different electrodes.

Electrode	Cathodic limit (V)	Anodic limit (V)	Electrochemical window (V)	Capacitive current (μA)
GCE	-2	1.8	3.8	5.5
Graphite/PS	-1.75	1.4	3.15	8.5
GOx/PS	0	0	0	327
rGOx/PS	0	0	0	300
Graphene(-5V)/PS	-1.65	1.75	3.4	16
Graphene(-2.5V)/PS	-1.95	1.85	3.8	5
Graphene(-2.5V)/PS - lithography	-1.75	1.75	3.5	8.3

These data indicated that graphene which has been exfoliated electrochemically from graphite rod electrode in organic solvents showed a better electrochemical activity than that one which has been exfoliated in aqueous media.

5.4.2. Electrochemical probes characterization

5.4.2.1. Delamination study of the graphene electrodes

The delamination is a very common issue in electrodes prepared from the powder materials, such as graphite and graphene when transferred by pressing and heating onto polystyrene plates used as substrate material, and this happens due to the adhesion strength between the electrode layer and substrate. In order to check the adherence between the graphene powder and the substrate here we characterize the delamination phenomenon of electrodes by cyclic voltammetry in a redox probe of ferricyanide $K_4[Fe(CN)_6]$ (2.5 mM) dissolved in 0.1M KCl. The idea was to obtain the cyclic voltammetry in this electrolyte with GC electrode, graphite/PS electrode and

graphene (-2.5 V)/PS electrode before and after the performing electrochemical window in order to see if these electrodes are stable at higher and lower potentials, within their electrochemical windows respectively. Figure 93-A presents the voltammograms observed at the GCE, graphite/PS and graphene (-2.5 V)/PS electrodes before performing the electrochemical window, where was shown that the anodic peak which presents the oxidized state of ferricyanure ions, was observed at +0.25 V for GCE, at +0.205 V for graphite/PS and at +0.18 V for graphene (-2.5 V)/PS electrode, whereas the cathodic peak which presents the reduced state of ferricyanure ions was observed at +0.09 V for GCE, at +0.05 V for graphite/PS electrode and at +0.11 V for graphene (-2.5 V)/PS electrode.

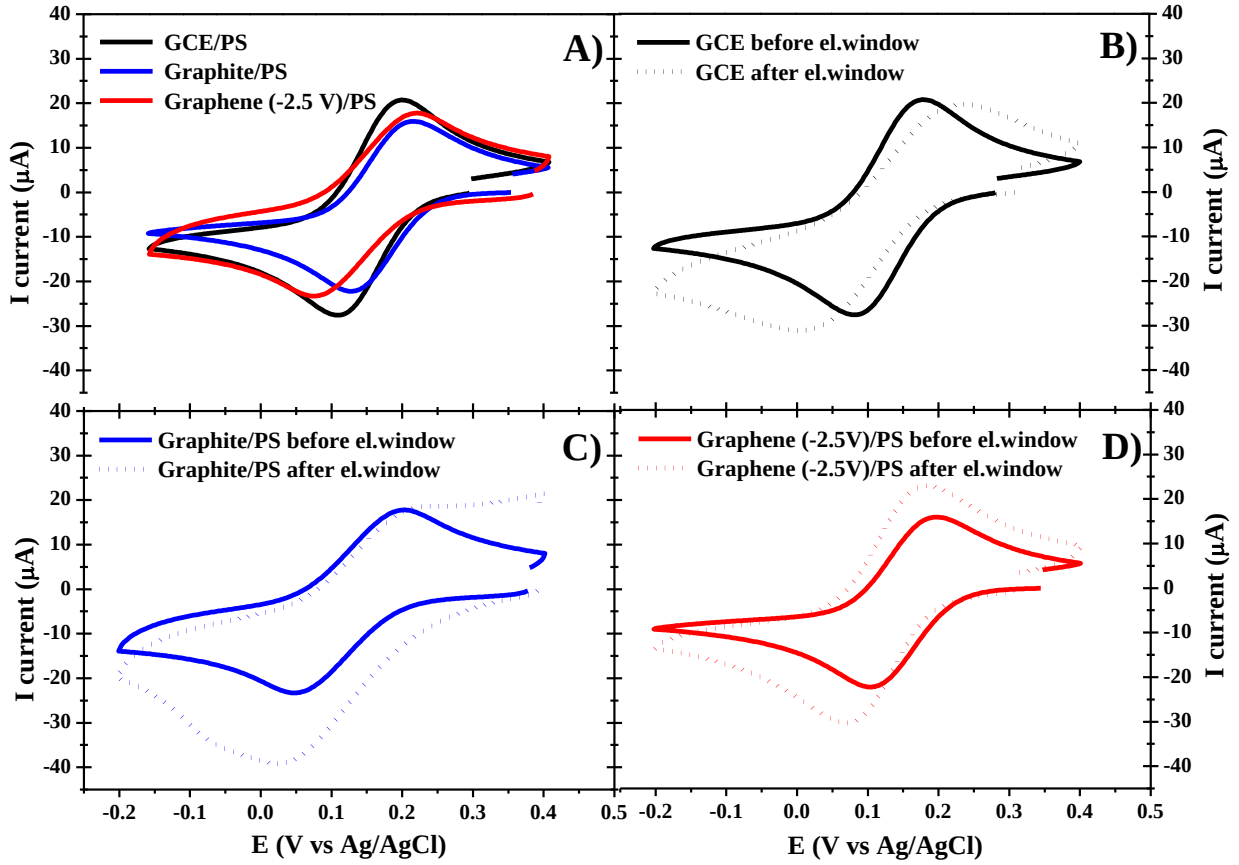

Figure 93. Cyclic voltammetry of GCE, graphite/PS, and graphene (-2.5V)/PS electrodes in $K_4[Fe(CN)_6]$ 2.5 mM + KCl 0.1M before the performing of electrochemical window A), and after the performing of electrochemical window B), C), and D). Scan rate 10 mV/s.

Just after this step the same electrodes have been used for evaluating electrochemical window (already presented in section 5.4.1.), and then electrodes have been tested once again with redox probe. The Figures 93-B, 93-C and 93-D present the superposition of the voltammograms observed before and after window. The GCE and graphene (-2.5 V)/PS electrodes did not show big difference, but in the case of graphite/PS electrode we

see widest (Ipa/Ipc) ratio after performing the electrochemical window leading in delamination of graphite powder from the polystyrene. As known the delamination process of the electrodes happens gradually [312]. In addition, was performed the CV redox probe on graphene (-2.5 V)/PS electrodes for about 50 scans, but no difference between the scans was observed, providing a strong adherence between the graphene powder and the polystyrene with no causing of the delamination.

5.4.2.2. Evolution of the electrochemical active area

Furthermore, we decided to use for the future analysis was decided to be used the graphene which has been exfoliated in 0.1M TBA BF_4 dissolved in NMP (1-methyl-2-pyrrolidinone) by CA at potential -2.5 V and transferred onto polystyrene substrate, as best material for electrode preparation. The graphene (-2.5 V)/PS electrodes have been fabricated at different working areas with two methods: with our own method at the laboratory and with the method of photolithography (see section 5.2.3. in this Chapter). The graphene (-2.5 V)/PS electrodes fabricated with our own method in the laboratory were in circle shape at surfaces of 10 mm^2, 3 mm^2 and 1 mm^2, whereas the graphene (-2.5 V)/PS electrodes fabricated with the method of photolithography were in square shape at surfaces of 10 mm^2, 10 mm^2, 500 μm^2, 200 μm^2, and 100 μm^2. For the evaluation of electrochemical active area, cyclic voltammetry responses were recorded in two different redox probes, in hexaammineruthenium (III) chloride and/or in potassium hexacyanoferrate (III) [$K_4 Fe(CN)_6$], both at concentration (2.5 mM) and dissolved in KCl 0.1M at different scanning rates (1000 mV/s, 750 mV/s, 500 mV/s, 250 mV/s, 100 mV/s, 50 mV/s, 25 mV/s, 20 mV/s, 15 mV/s, 10 mV/s, 5 mV/s, and 1 mV/s). In the case of graphene (-2.5 V)/PS electrodes fabricated by our own method in the laboratory the oxidation and reduction peaks were well defined for the both redox probes, whereas those fabricated with photolithography responded only in Ru III redox probe, and no response is shown in ferrocyanide probe. In Figure 94-A and 94-B are presented one example of cyclic voltammograms obtained at different scanning rates by using graphene (-2.5 V)/PS electrode with a geometrical working surface area (10 mm^2) in both redox probes with following redox reactions:

$$Ru(NH_3)_6^{3+} + e^- \leftrightarrow Ru(NH_3)_6^{2+} \text{.....(5.2)}$$

$$Fe(CN)_6^{3-} + e^- \leftrightarrow Fe(CN)_6^{4-} \text{.....(5.3)}$$

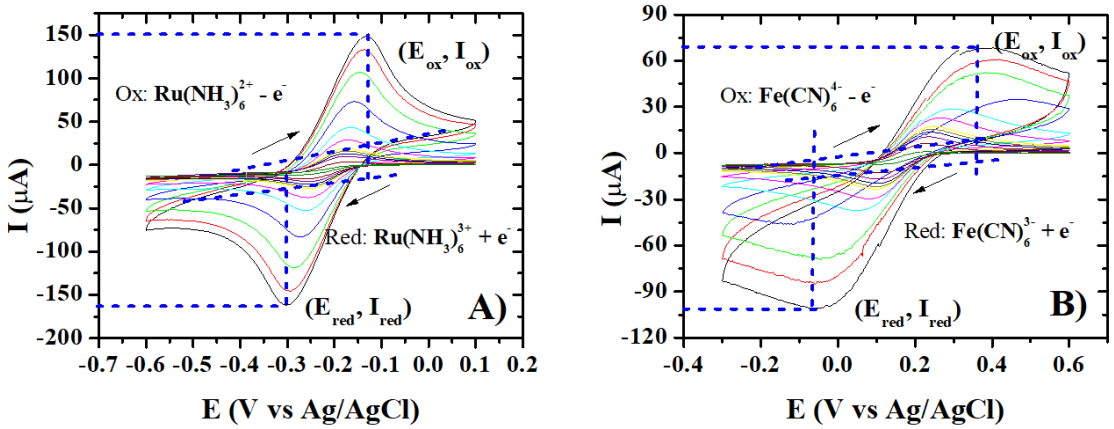

Figure 94. Cyclic voltammetry on graphene (-2.5 V)/PS electrode using hexaammineruthenium (III) chloride (C=2.5 mM) (A) and potassium hexacyanoferrate (III) (C=2.5 mM) (B), dissolved in KCl 0.1M, at different scanning rate, from 1000mV/s (larger curves) low to 1mV/s (smaller curves).

The same evolution as presented in Figure 94 was obtained for all the graphene electrodes fabricated with controlled working surface area by using the two methods, our own method in the laboratory and photolithography. Representative cyclic voltammograms of hexaammineruthenium (III) chloride redox in its aqueous solution containing also KCl (Figure 95) show the effect of changes of the scan rate obtained on graphene (-2.5 V)/PS electrodes fabricated in the laboratory at different working areas 10 mm^2, 3 mm^2, and 1 mm^2.

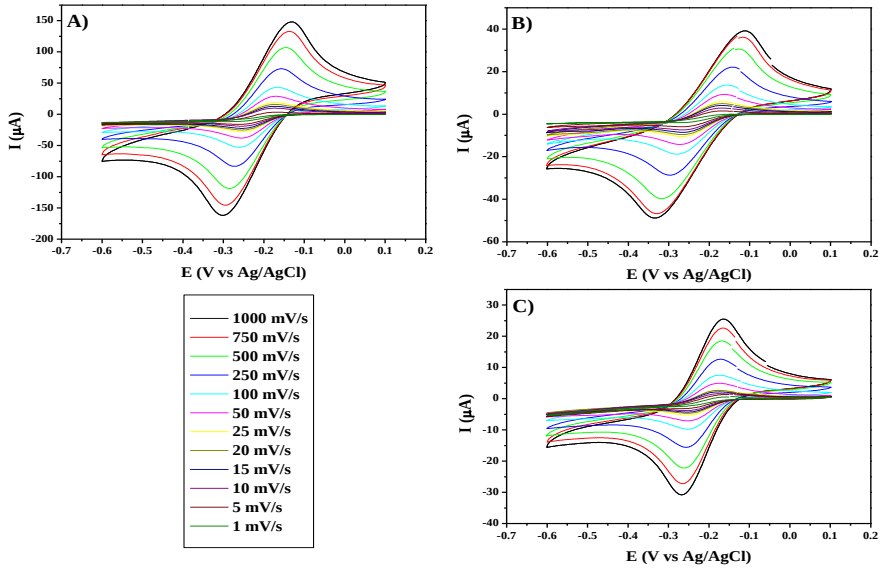

Figure 95. Cyclic voltammetry at different scanning rate on graphene (-2.5 V)/PS electrodes fabricated with our own method in the laboratory using aqueous solution of hexaammineruthenium (III) chloride (C = 2.5 mM) + KCl 0.1M with three different working electrode surface areas A) 10mm^2, B) 3mm^2, and C) 1mm^2.

The voltammograms illustrate that as the voltage becomes more positive, an anodic peak current (I_{ox}) is observed at the peak potential (E_{ox}), indicating that hexaammineruthenium ions are converted at oxidized form $Ru(NH_3)_6^{3+}$ according to reaction (5.2). During the return scans, the voltage becomes less positive and the process is inversed, consequently a reduction process of $Ru(NH_3)_6^{3+}$ ions is now occurring and a cathodic peak current (I_{red}) is observed at the cathodic peak potential (E_{red}). Hexaammineruthenium (III) chloride redox probe exhibits reversible oxidation in all the graphene electrodes at all the working areas.

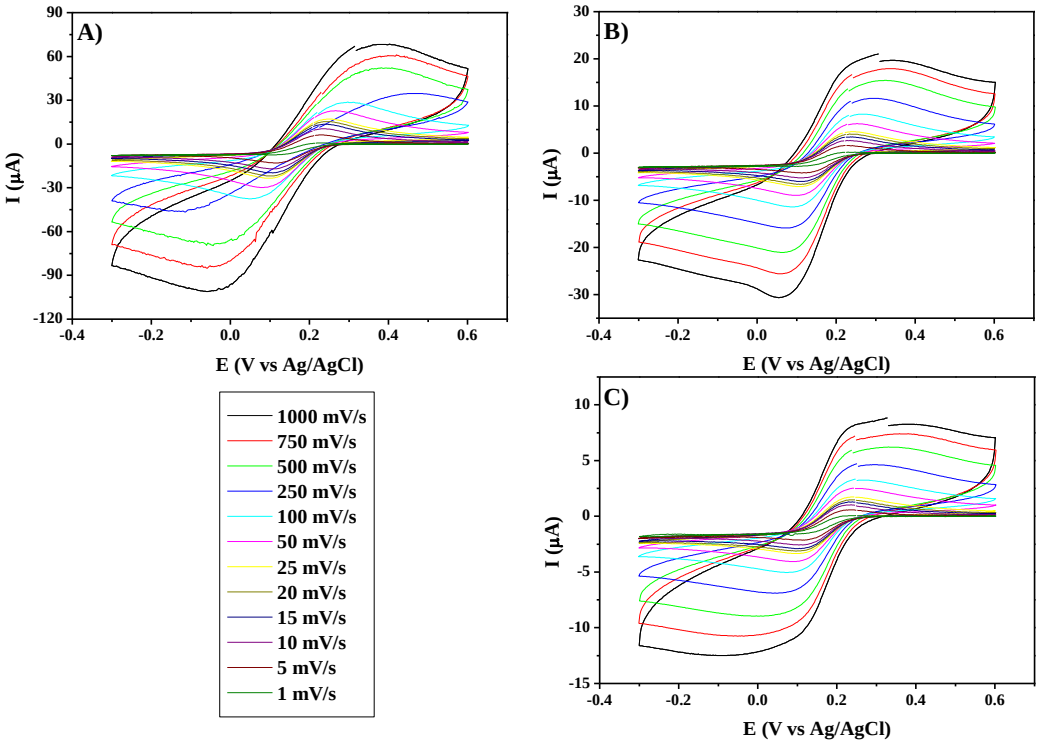

Figure 96. Cyclic voltammetry at different scanning rate on graphene (-2.5 V)/PS electrodes fabricated with our own method in the laboratory using aqueous solution of potassium hexacyanoferrate (III) (C = 2.5 mM) + KCl 0.1M with three different working electrode surface areas A) 10mm^2, B) 3mm^2, and C) 1mm^2.

In Figure 96 are presented the cyclic voltammograms of potassium hexacyanoferrate (III) redox probe in KCl with the changes of scanning rate obtained on graphene (-2.5 V)/PS electrodes fabricated in the laboratory at different working areas 10 mm^2, 3 mm^2, and 1 mm^2. Also, here when the voltage becomes more positive an anodic peak current (I_{ox}) was observed at potential (E_{ox}) indicating that the hexacyanoferrate ions are converted in oxidized form $Fe(CN)_6^{3-}$, whereas in return scan at less positive potentials the reduction occurs according to the equation (5.3). The anodic and cathodic peak

potential separation ($\Delta Ep = E_{ox} - E_{red}$), and the intensities I_{ox} and I_{red} are followed versus the scanning rate. These evolutions are summarized in Figure 97-A for the case of hexaammineruthenium (III) chloride probe, and in Figure 97-B for the case of potassium hexacyanoferrate (III) probe.

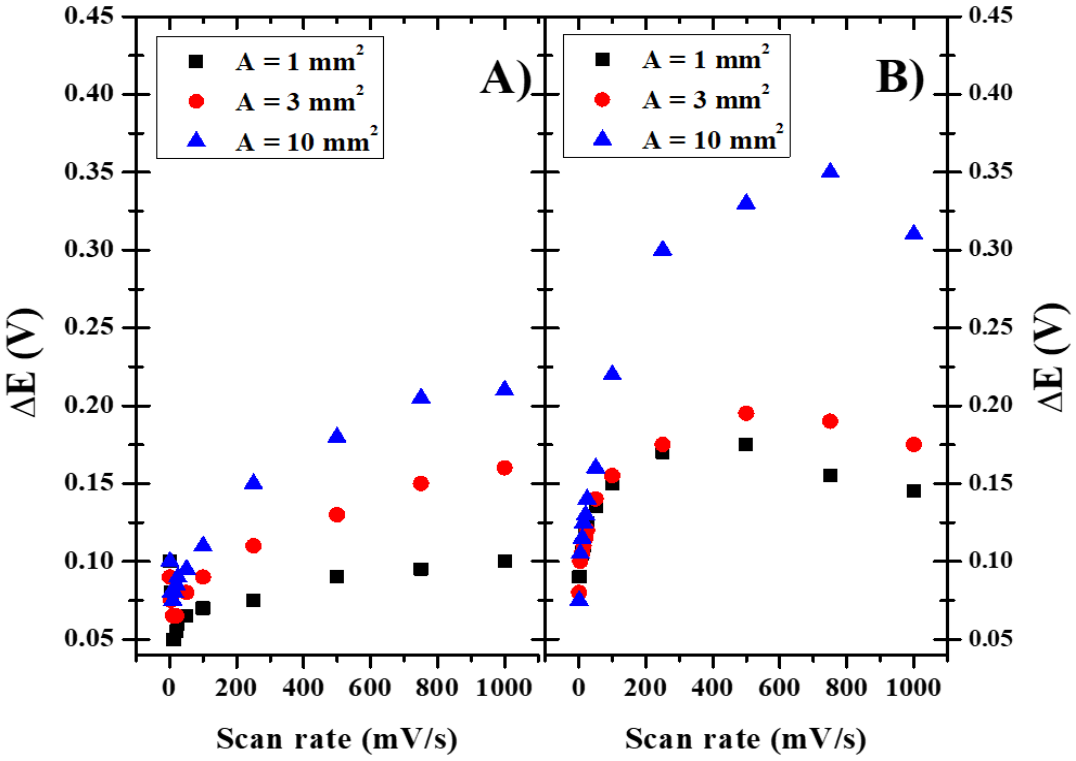

Figure 97. Variation of ΔE versus the scanning rate for both electrochemical probes A) hexaammineruthenium (III) chloride, B) potassium hexacyanoferrate (III) obtained on graphene (-2.5 V)/PS electrodes fabricated with our own method at different values of working surface area.

In hexaammineruthenium (III) chloride probe, the separation potential values (ΔE) can be considered as constant according to the error bars. At low scanning rates the ΔE was found to be between 50±3.6 mV and 100±5.2 mV, indicating that the process is reversible and higher values of ΔE were observed for the higher working electrode surface areas. In potassium hexacyanoferrate (III) probe higher ΔE separation values have been observed, which may come from the possible modifications of the surface of graphene electrodes causing not very good contact with the $Fe(CN)_6^{3-/4-}$ ions [313]. The ΔE values obtained were 75±4.8 mV and 150±5.6 mV and increased with the working area surface. The intensities of the anodic and cathodic peaks are also followed versus scanning rate. The peak current ratio of the reverse and the forward scans is equal to unity (I_{ox}/I_{red} = 1.0) and was independent of the scan rate for all the working areas (Figure 98). It was also found that the peak currents were essentially constant for several cycles. In order to compare the behavior of the different working areas of

graphene electrodes, the intensities were divided by the geometrical surface area and the evolution of the current densities versus the square root of the scanning rate has been plotted for all the cases and presented in Figure 98 for both electrochemical probes.

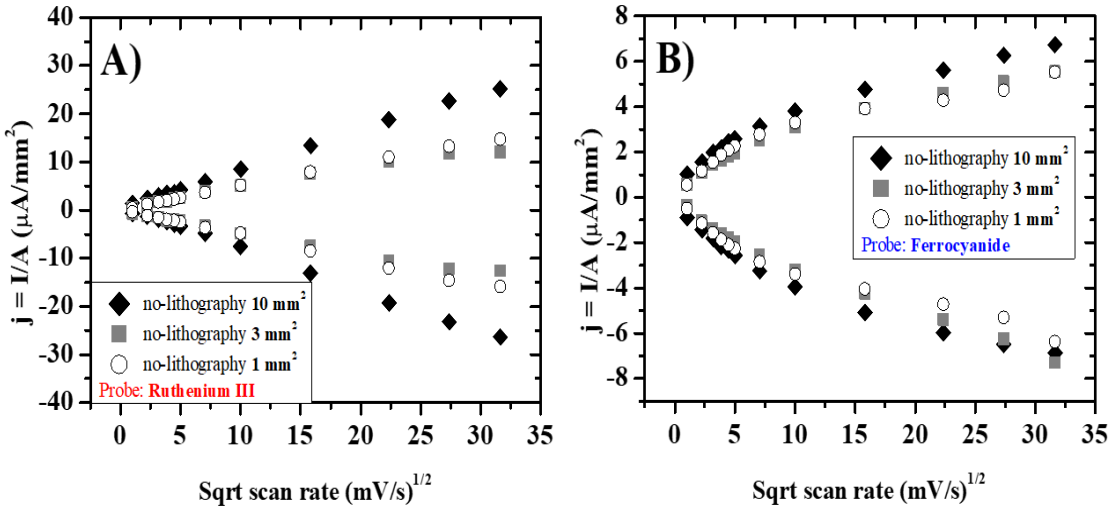

Figure 98. Evaluation of current densities versus the square root of the scanning rate for both electrochemical probes A) hexaammineruthenium (III) chloride, B) potassium hexacyanoferrate (III) obtained on graphene (-2.5 V)/PS electrodes fabricated with our own method at different values of working surface area.

Basically, for each electrochemical probe the two linear regions have been observed for the working surface area at 10 mm², whereas in the case of ruthenium (III) probe at 3 mm² and 1 mm² there was obtained linear range (Figure 98-A), and two linear ranges in hexacyanoferrate (III) probe (Figure 98-B) for the given surface areas. The slopes associated to the different working areas and different electrochemical probes are summarized in Table 7.

Table 7. Extracted data by plotting the slopes from the evaluation of current densities versus square root of the scanning rate for graphene (-2.5 V)/PS electrodes from the Figure. 98-A and 98-B.

Probe: Hexaammineruthenium (III) chloride in KCl					
Geometrical area	Active area	Slope of line equation		R^2	
10 mm²	7.9 mm²	4.357		0.9993	
3 mm²	2.7 mm²	1.2934		0.9951	
1 mm²	0.93 mm²	0.8203		0.999	
Probe: Potassium hexacyanoferrate (III) in KCl					
Geometrical area	Active area	Slope of line equation		R^2	
10 mm²	6.9 mm²	3.8307	0.7136	0.994	0.9856
3 mm²	2.01 mm²	1.0293	0.3758	0.9917	0.9843
1 mm²	0.89 mm²	0.3891	0.1441	0.9955	0.9914

These results highlight an important dependence of the reaction kinetics with the working area and with the electrochemical probes. Redox systems, such as $Fe(CN)_6^{3-/4-}$ are very sensitive to the modifications of the electrode surface and the electron transfer rates are strongly dependent on surface history [313]. That may be the reason why we haven't obtained the same behavior. Furthermore, when we used the graphene (-2.5 V)/PS photolithography electrodes at different working areas, it was impossible to obtain the anodic and cathodic peaks in potassium hexacyanoferrate (III) probe after the lithography step. Whereas in hexaammineruthenium (III) chloride probe the obtained cyclic voltammograms by graphene (-2.5 V)/PS photolithography electrodes are shown in Figure 99.

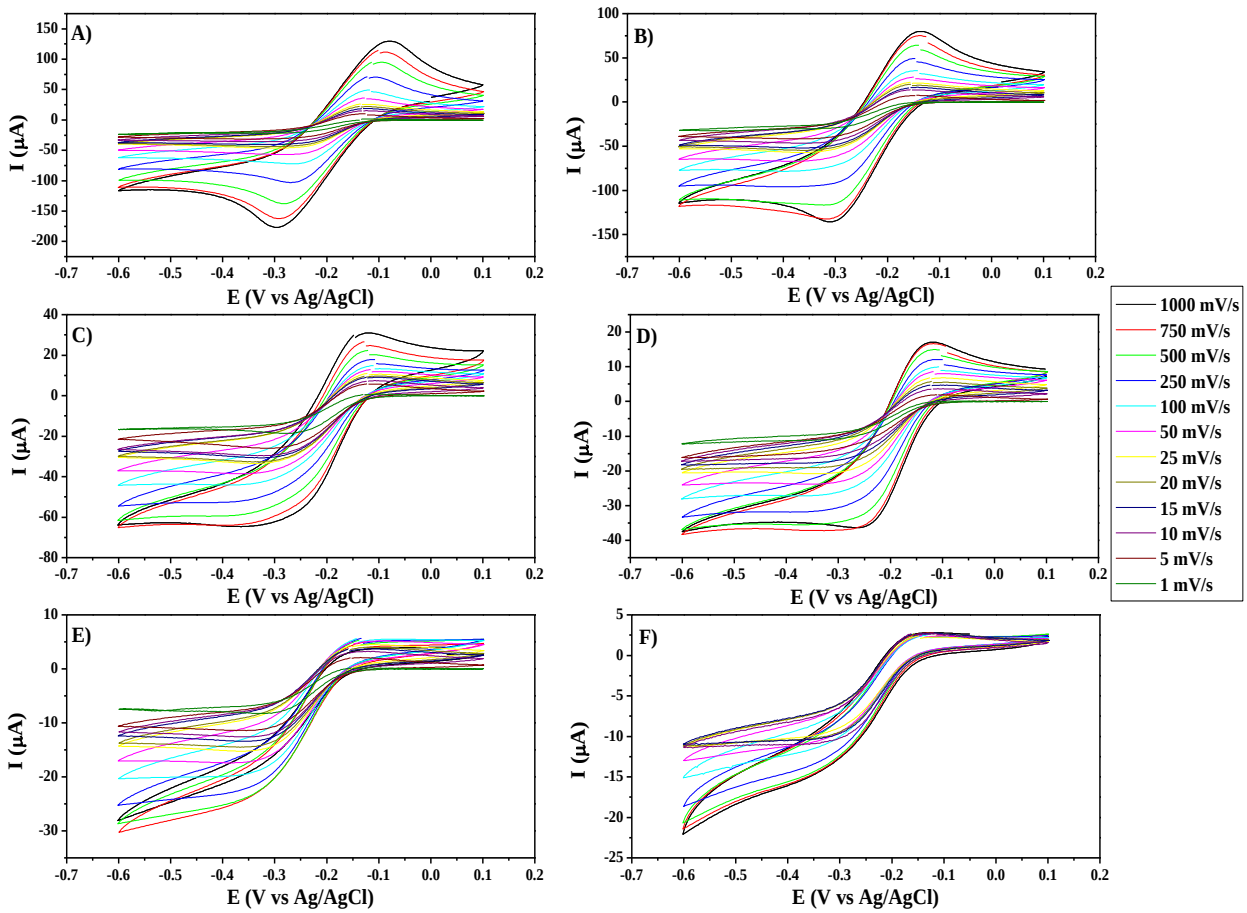

Figure 99. Cyclic voltammetry at different scanning rate on graphene (-2.5 V)/PS electrodes fabricated with photolithography using hexaammineruthenium (III) chloride (C = 2.5mM) in KCl 0.1M with different working electrode surface areas A) 10mm², B) 5mm², C) 1mm², D) 500µm², E) 200µm², and F) 100µm².

The electrochemical signal at higher working surface area, respectively at 10 mm², 5 mm², and 1 mm², show a I_{ox}/I_{red} ratio closed unit (see Figures 99-A, 99-B, 99-C) and a

higher ΔE separation value than in the case of electrodes fabricated without lithography, whereas at lower working electrode surface areas, respectively at 500 μm², 200 μm², and 100 μm² the cyclic voltammogram signal belongs to the microelectrode behavior [314] (see Figures 96D, 96E, 96F). The data are shown in Table 8.

Table 8. Variation of ΔE versus the scanning rate for both electrochemical probes hexaammineruthenium (III) chloride obtained on graphene (-2.5 V)/PS electrodes fabricated with photolithography method at different working surface areas.

Probe: Hexaammineruthenium (III) chloride in KCl						
Scan rate (mV/s)	ΔE (V) A = 10mm²	ΔE (V) A = 5mm²	ΔE (V) A = 1mm²	ΔE (V) A = 500μm²	ΔE (V) A = 200μm²	ΔE (V) A = 100μm²
1000	0.2	0.155	0.13	0.115	0.13	0.16
750	0.185	0.15	0.135	0.11	0.135	0.11
500	0.17	0.14	0.145	0.12	0.145	0.16
250	0.145	0.135	0.155	0.135	0.15	0.16
100	0.115	0.13	0.165	0.14	0.155	0.15
50	0.11	0.145	0.16	0.14	0.165	0.145
25	0.115	0.15	0.155	0.135	0.16	0.144
20	0.12	0.155	0.15	0.14	0.155	0.14
15	0.125	0.145	0.15	0.145	0.16	0.14
10	0.125	0.14	0.145	0.14	0.16	0.13
5	0.13	0.15	0.15	0.145	0.155	0.143
1	0.135	0.14	0.135	0.13	0.125	0.13

Here we will consider the reversible reaction of hexaammineruthenium (III) chloride and potassium hexacyanoferrate (III) for the calculation of the working electrode active area reversible reaction on all the surfaces for graphene (-2.5 V)/PS electrodes fabricated with our own method in the laboratory, whereas only hexaammineruthenium (III) chloride probe show reversible reaction at high working geometrical area for graphene (-2.5 V)/PS photolithography electrodes. The electrochemical active area of the graphene electrodes has been calculated using Randles-Sevick equation for totally reversible reactions presented in the previously parts [315]:

$$i_p = \pm 0.446\, nFAC\left(\frac{nFDv}{RT}\right)^{1/2} \ldots\ldots\ldots\ldots (5.4)$$

-where: n-number of electrons involved, υ - scanning rate (mV/s), F - Faraday's constant (A s mol^{-1}), T - temperature (K), A - electrode active area (cm²), R - perfect gas constant (J mol^{-1} K^{-1}), c - concentration of the electrochemical probe (mol dm^{-3}), and D - diffusion

coefficient of the electrochemical probe ($cm^2\ s^{-1}$). The calculated working active area (A) for all the cases were summarized in Table 9.

Table 9. Calculated active working surface area using Randles-Sevick equation for graphene (-2.5 V)/PS electrodes fabricated with our own method for both electrochemical probes.

Geometrical surface area (mm^2)	**$Ru(NH_3)_6^{3+/2+}$** Active surface area (mm^2)	**$Fe(CN)_6^{3-/4-}$** Active surface area (mm^2)
1	0.93 (93%)	0.89 (89%)
3	2.7 (90%)	2.01 (67%)
10	7.9 (79)%	6.9 (69%)

In general, the active area of the electrodes is lower to geometrical ones. Indeed, in the case of hexaammineruthenium (III) chloride probe, according to the error bars, the working active area are closed to the geometrical ones matching from 79% - 93% for graphene (-2.5 V)/PS electrodes fabricated with our own method in the laboratory and around 71% - 89% for the graphene (-2.5 V)/PS photolithography electrodes, whereas in the case of potassium hexacyanoferrate (III) probe, according to the error bars, the working active area are closed to the geometrical ones matching from 69% - 90% for graphene (-2.5 V)/PS electrodes fabricated with our own method in the laboratory.

5.4.2.3. Calculation of the kinetic constant (k_0)

In order to evaluate the electronic behavior of the two different probes, the different working surface areas, and the effect of photolithography, it is necessary to calculate the electronic transfer rate [313] by simulation using Digisim® software. The theoretical approach in the Digisim® software is based on a fast implicit finite difference method which is achieved by combining the exponentially expanding space model with the DuFort-Frankel algorithm [316]. By using this theoretical model, it is possible to evaluate homogenous or heterogeneous rate constant of any order of magnitude with potential steps of several millivolts. In Figure 100 are presented the simulated cyclic voltammograms by using Digisim® software as the theoretical approach and a superposition with the experimental cyclic voltammograms has been done for the case of graphene (-2.5 V)/PS electrodes fabricated with our own method with working surface area of 10 mm^2 in both hexaammineruthenium (III) chloride probe and in potassium hexacyanoferrate (III) probe (see Figure 100-A and 100-B), whereas for

graphene (-2.5 V/PS photolithography electrodes we observed results only in hexaammineruthenium (III) chloride probe (Figure 100-C).

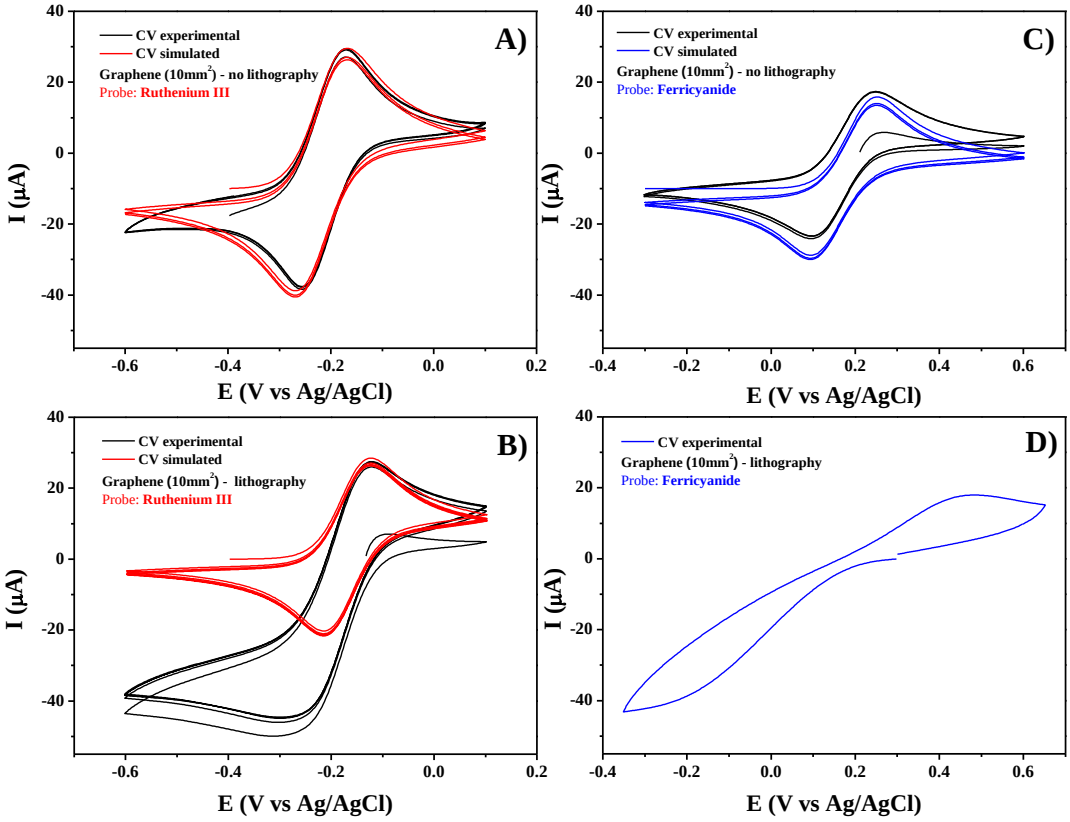

Figure 100. The superposition of the experimental cyclic voltammograms with the simulated ones obtained during the Digisim® simulation for two electrochemical probes with using graphene (-2.5 V)/PS electrode fabricated with our own method A), B), and with graphene (-2.5 V)/PS photolithography electrode C), D). Scan rate for the curves in this figure was 50 mV/s.

In Figure 100-D is presented the cyclic voltammogram obtained by graphene (-2.5 V)/PS photolithography electrode with working surface area 10 mm^2 in potassium hexacyanoferrate (III) probe, which provides not enough information for performing Digisim® simulation. The results obtained for all the working surface areas by using two kinds of graphene (-2.5 V)/PS electrodes are summarized in Tables 10 and 11. These results show that in the case of graphene (-2.5 V)/PS electrodes fabricated with our own methods in the laboratory, the simulated cyclic voltammogram obtained with Digisim® software is very closed to the experimental one, and it can be compared with the theoretical simulation which has been performed for the glassy carbon electrode and presented in Appendix 4. On the other hand, when the photolithography method has been used for the fabrication of graphene (-2.5 V)/PS electrodes with controlled working surface area has leading in some modifications on the surface of graphene electrode

appearing lots of errors during the theoretical simulation. However, the (k_0) values obtained with graphene (-2.5 V)/PS electrodes fabricated without photolithography are closed to those obtained in literature [313], [317].

Table 10. Simulated values of the heterogeneous electron transfer rate obtained by graphene (-2.5 V)/PS electrodes fabricated with our own method for the different working surface area at the different scanning rates in two electrochemical probes using Digisim® software.

Probe: Hexaammineruthenium (III) chloride in KCl			
Scan rate (mV/s)	A = 10 mm^2 k_0 (cm/s)	A = 3 mm^2 k_0 (cm/s)	A = 1 mm^2 k_0 (cm/s)
500	0.0041	0.004	0.002
100	0.0043	0.0041	0.00016
50	0.0044	0.0039	0.0015
25	0.0045	0.0038	0.0014
10	0.0045	0.0039	0.0015
Average k_0 (cm/s)	0.00436	0.00394	0.0016
Standard deviation	0.00017	0.00011	0.00023
Probe: Potassium hexacyanoferrate (III) in KCl			
Scan rate (mV/s)	A = 10 mm^2 k_0 (cm/s)	A = 3 mm^2 k_0 (cm/s)	A = 1 mm^2 k_0 (cm/s)
500	0.0015	0.0018	0.00145
100	0.0016	0.0012	0.0014
50	0.0015	0.0013	0.0013
25	0.0014	0.001	0.001
10	0.00092	0.0011	0.0008
Average k_0 (cm/s)	0.0014	0.0013	0.0012
Standard deviation	0.00027	0.0003	0.00028

Table 11. Simulated values of the heterogeneous electron transfer rate obtained by graphene (-2.5 V)/PS photolithography electrodes for the different working surface area at the different scanning rates in two electrochemical probes using Digisim® software.

Probe: Hexaammineruthenium (III) chloride in KCl				
Scan rate (mV/s)	A = 10 mm^2 k_0 (cm/s)	A = 3 mm^2 k_0 (cm/s)	A = 1 mm^2 k_0 (cm/s)	A = 500 μm^2 k_0 (cm/s)
500	0.005	0.0035	0.0029	0.0018
100	0.0041	0.0031	0.0031	0.0023
50	0.0045	0.0046	0.0038	0.0027
25	0.0038	0.0049	0.0037	0.0022
10	0.0048	0.0054	0.0041	0.002
Avg. k_0 (cm/s)	0.0044	0.0043	0.0035	0.0022
St. deviation	0.0005	0.0009	0.0005	0.00034

5.5. Correlation between crystallography structure of different graphene electrodes and their electrochemical behavior

Various methods for the characterization of the graphene electrode materials were presented in the previous sections. The aim of this part is to try to correlate the electrochemical activity of the electrodes with the crystallographic organization and surface chemistry of the graphene electrodes. Indeed in literature, it has been shown that the electrochemical behavior of carbon electrodes depends on the surface chemistry [313], [318], [319], and on the presence of defaults in carbon structure [320]–[322]. This correlation is not well understood in the literature, and the open question is: "In order to have a high electrochemical activity with high electron transfer rate constant, is-it better to have high or low degree of defaults in carbon structure?"

Two kinds of graphene electrodes have been compared, that one prepared by the electrochemical exfoliation of graphite electrodes in aqueous solvent and the other one in organic solvent media. According to the results obtained during the characterization of these kinds graphene electrodes it was observed a good correlation between the obtained results for their crystallography and their surface chemistry with the obtained results during the study of their electrochemical behavior.

The XPS results obtained during the characterization of graphene electrodes exfoliated in aqueous solvent showed a higher presence of carbon atoms bonded with oxygenic functional groups which can be seen as a contamination of the surface of the electrode. This contamination by oxygenic groups may be induced by the way of production of this graphene, i.e. by electrochemical exfoliation in aqueous media. These electrodes have also exhibited an higher D band in Raman spectra which is correlated with a higher density of defaults in their carbonic structure. On the Raman spectroscopic point of view the defaults can be the edge of the graphene layers, or vacancy in the sp^2 layer structure, which are in the two cases more chemically or electrochemically active site compared to the sp^2 layer, due to the free carbon present on these sites. Finally, higher density of defaults should be an advantage for electrochemistry, but also a disadvantage as the electrodes should be more sensitive to pollution due to the presence of free bonds on the default sites. This is highlighted by the results obtained with IR spectroscopy which have given a higher presence of oxygenic groups for the graphene electrodes exfoliated in aqueous solvents in comparison with that one exfoliated in organic solvent.

For the electrodes made by using graphene exfoliated in organic solvent, the XPS results highlighted a low degree of oxygenic groups on the electrodes surfaces, correlated with a low density of defaults highlighted by the Raman spectroscopy results. These results are confirmed by the IR spectra obtained on these electrodes.

Finally, the electrochemical exfoliation in organic solvent seems to be a more convenient way of exfoliation of graphene, as the obtained graphene present a low degree of surface contamination induced by the exfoliation step, and a low density of defaults, and then a low sensitivity to surface pollution.

On the electrochemical point of view, better electrochemical behavior was shown during the use of graphene electrodes which have been exfoliated in organic solvent, showing a larger potential range during the performing of the electrochemical window and higher transfer kinetic during the characterization with different redox probes. Finally, the exfoliated graphene in organic solvent has good electrochemical properties for testing it in sensors application.

In this context, the graphene electrodes prepared by CA electrochemical exfoliation of graphite electrodes at -2.5 V in organic solvent was chosen as the working electrode for the further usage with the aim of electrochemical polymerization of polypyrrole imprinted films dedicated to the detection of isoproturon. In the following sections we present the work which has been performed for the electrochemical preparation of Graphene (-2.5 V) – MIPPy sensors for the detection of isoproturon in water samples.

5.6. Electrochemical preparation of MIP films onto graphene/polystyrene electrodes

5.6.1. Electrochemical behavior of isoproturon on graphene/polystyrene electrodes

In order to study the behavior of isoproturon, as a targeted pollutant molecule on the graphene electrode surface, we used two working surface areas for the graphene (-2.5 V)/PS electrodes fabricated with our own method (10 mm^2 and 1 mm^2), and for the graphene (-2.5 V)/PS photolithography electrodes (10 mm^2 and 500 μm^2) respectively. The electrochemical study of isoproturon has been performed by cyclic voltammetry in an acidic solution of H_2SO_4 0.1M charged with 70% ethanol and 30% milli-Q water. In Figures 101-A and 101-B are presented the anodic oxidation of isoproturon on the graphene (-2.5 V)/PS electrode, the anodic oxidation of isoproturon appeared at +1.18 V vs ref. Ag/AgCl electrode: current density around 2 x 10^{-3} $\mu A/cm^2$ with working surface area 10 mm^2 for ISO 3 mM, and about 3 x 10^{-3} $\mu A/cm^2$ higher in the case of graphene electrode with 1 mm^2. If compared with the electrochemical oxidation of isoproturon on glassy carbon electrodes (peak position at +1.1 V) (see Figure 39 in Chapter III), here on graphene electrode the oxidation of isoproturon molecule occurs at more positive potentials showing an irreversible reaction, diffusion controlled, and two-electron transfer oxidation [17].

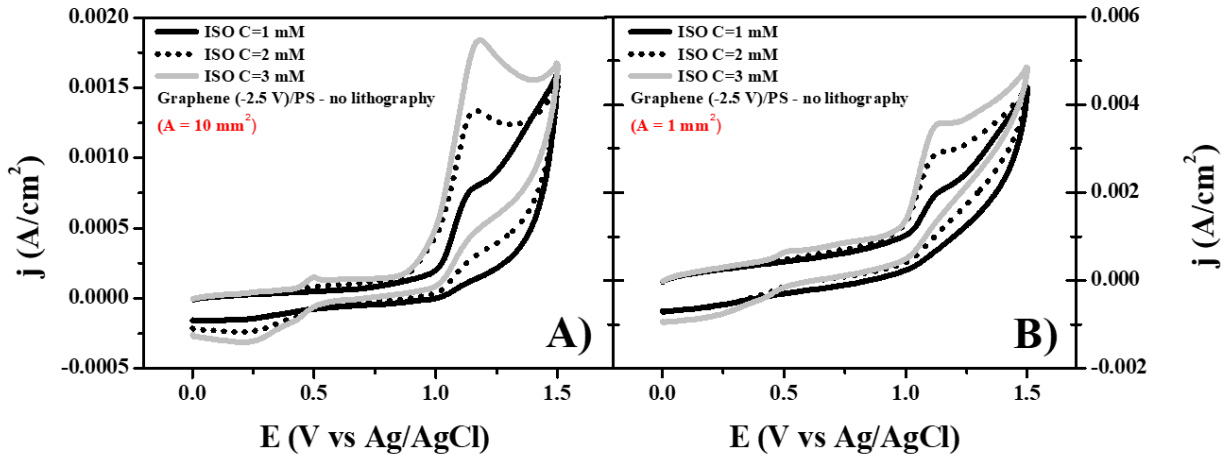

Figure 101. Voltammograms obtained on graphene (-2.5 V)/PS electrodes fabricated with our own method at working surface area A) 10 mm^2 and B) 1 mm^2 for ISO (1, 2 or 3 mM) in H_2SO_4 (0,1M) (70/30 ethanol/water v/v). Scan rate 100 mV/s.

At higher working surface areas some little peaks were appeared in the potential region around +0.2 V and +0.5 V, coming from some intermediates during the anodic oxidation of isoproturon on graphene electrode. In Figure 101 is also shown that the oxidation peak of isoproturon is well expressed due to high electrochemical activity of isoproturon molecule on the graphene (-2.5 V)/PS electrode surface. In the case of graphene (-2.5 V)/PS lithography electrode, the cyclic voltammogram curves were appeared with a larger capacitive current, and providing difficulties to analyze the anodic oxidation peak of isoproturon. That may come due to some modifications occur on the graphene (-2.5 V)/PS electrode surface during the photolithography procedure. Moreover, the oxidation of isoproturon on these graphene electrodes occurs at even more positive potentials, at around +1.25 V vs ref. Ag/AgCl electrode (see Figure 102).

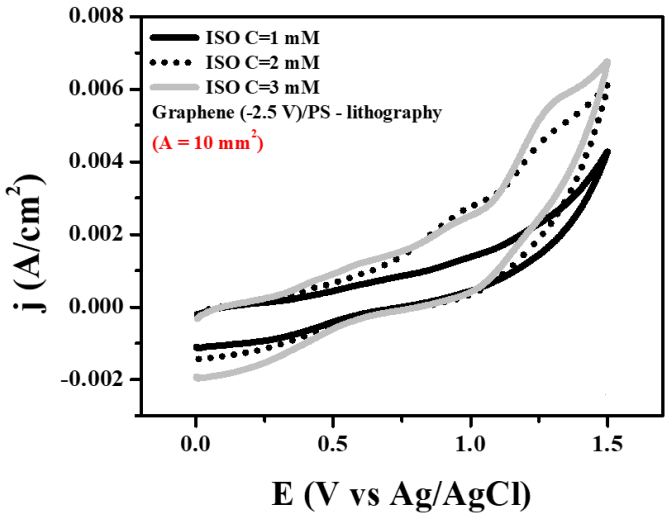

Figure 102. Voltammograms obtained on graphene (-2.5 V)/PS electrodes fabricated with photolithography at working surface area 10 mm^2 for ISO (1, 2 or 3 mM) in H_2SO_4 (0,1M) (70/30 ethanol/water v/v). Scan rate 100 mV/s.

5.6.2. Electropolymerization of isoproturon imprinted polypyrrole films onto graphene/polystyrene electrodes

The electrochemical polymerization of isoproturon imprinted polypyrrole films on graphene electrodes has been performed using the optimized conditions as in the Chapter III already published [165]. The whole process during the electrochemical fabrication of Graphene-MIP electrodes which can be used then for the detection of isoproturon includes three main steps: during the first one is the electrochemical

polymerization of the MIPs onto graphene electrodes, the second one is the process of the isoproturon extraction from the polymeric matrix, and the third step is the electrochemical determination of isoproturon. In Figure 103 was schematically shown the first and second step used for the preparation of the Graphene-MIP electrodes.

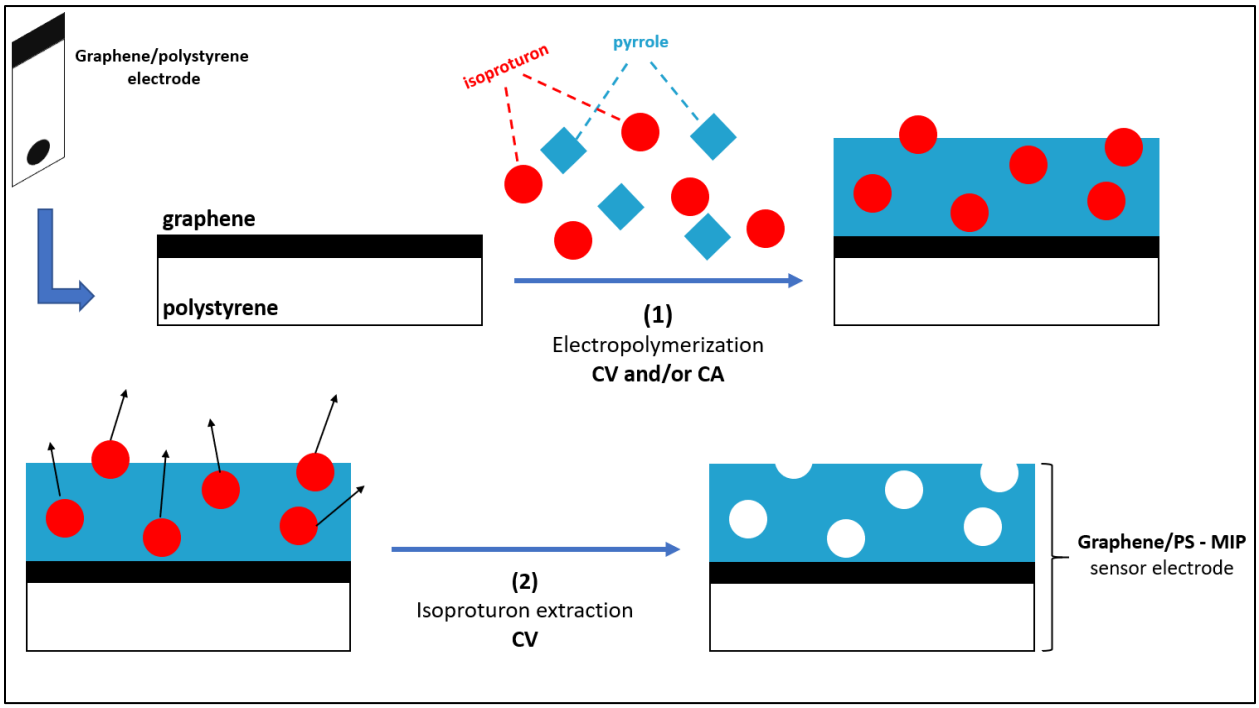

Figure 103. Schematic representation of the procedure used for the preparation of imprinted polypyrrole films onto Graphene (-2.5 V)/PS electrodes, including two main steps: 1) electropolymerization of MIPs by CV and/or CA, and 2) the CV extraction of isoproturon molecules.

The electropolymerization of isoproturon imprinted polypyrrole films on graphene electrodes has been performed using chronoamperometry electroanalytical method at the potential applied +1.1 V, duration time 600 sec, in a solution of $LiClO_4$ 0.1M dissolved in (20% ethanol + 80% milli-Q water) charged with pyrrole 10 mM and isoproturon 1 mM. This procedure has been employed for the graphene (-2.5 V)/PS electrodes fabricated with our own method at working surface areas 10 mm^2 and 1 mm^2, as well as for the graphene (-2.5 V)/PS photolithography electrodes at 10 mm^2 and 500 μm^2. The theoretical calculated thicknesses using Faraday's law [109], [178] for the MIP films fabricated varies from (420±15.2 nm) up to (630±37.4nm) and around three times thicker than the MIP films fabricated on the glassy carbon electrode. This may happen due to the presence of a larger active area of the graphene electrodes which show also higher rugosity on their surface.

5.6.3. Cyclic voltammetry extraction of isoproturon

The Graphene-MIP electrodes, once prepared, were rinsed with milli-Q water and immersed in an ethanol/water (70:30 v/v) solution of 0.1M sulfuric acid. They were biased to a potential excursion between −0.4 V and 1.5 V vs Ag/AgCl for several scans until complete extraction of the embedded isoproturon molecules. After extraction the Graphene-MIP electrode was used for isoproturon detection.

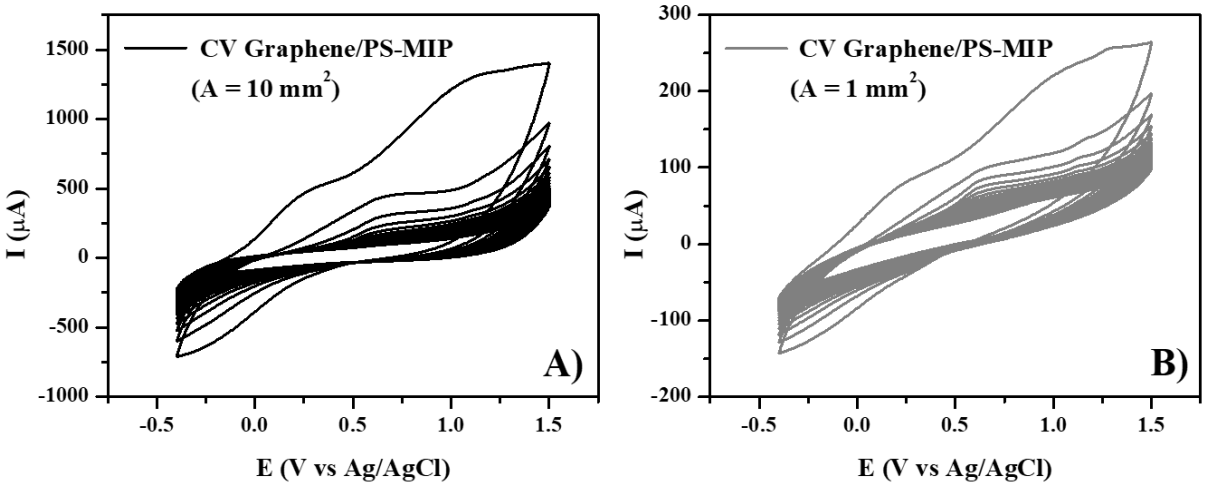

Figure 104. Isoproturon extraction from Graphene-MIP electrodes fabricated with our own method with different working surface area A) 10 mm^2, B) 1 mm^2, by cyclic voltammetry in an ethanol/water (70:30 v/v) solution of 0.1M H_2SO_4. Scan rate 100 mV/s.

In Figure 104 are presented the cyclic voltammograms observed during the isoproturon extraction process from the Graphene-MIP electrodes at 10 mm^2 (Figure 104-A) and at 1 mm^2 (Figure 104-B) in the case of graphene/PS electrodes fabricated with our own method. An oxidation peak of isoproturon has been observed at around +1.2 V, and disappeared with increasing of number of cycles until this peak was not observed anymore.

In Figure 105, is presented the cyclic voltammogram observed during the isoproturon extraction from the MIP films electropolymerized on graphene (-2.5 V)/PS lithography electrodes. As seen from the Figure 105, the isoproturon oxidation peak was not observed at all at any potential values during the CV extraction.

However, this process is a key step for the whole preparation procedure of the Graphene-MIP electrodes, where the isoproturon molecules after their extraction from the polymer matrix leave some cavities which are complementary shaped to the isoproturon molecules. At this stage the Graphene-MIP sensors were rinsed with milli-Q water and placed in a clean place before further use.

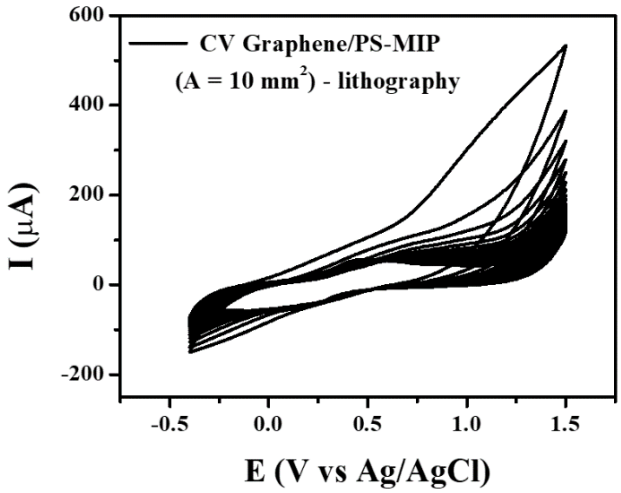

Figure 105. Isoproturon extraction from Graphene-MIP photolithography electrode with working surfacee area 10 mm^2 by cyclic voltammetry in an ethanol/water (70:30 v/v) solution of 0.1M H_2SO_4. Scan rate 100 mV/s.

5.6.4. Electrochemical detection of isoproturon by using graphene-MIP/polystyrene electrodes

The electrochemical detection of isoproturon by using Graphene-MIP electrode includes two different steps. The first step is the incubation or rebinding process, and the second one is the square wave voltammetry detection of isoproturon.

5.6.4.1. Incubation (rebinding) step

During this step the Graphene-MIP prepared electrodes were immersed in a milli-Q water sample contaminated with isoproturon molecules at low concentration, where the Graphene-MIP electrodes were incubated for an optimized time 15 minutes. A magnetic stirring was employed in order to provoke the filling process of the cavities with isoproturon molecules, see this process illustrated in Figure 106. Once the incubation has been finished, the Graphene-MIP electrodes were then tested for the isoproturon SWV detection.

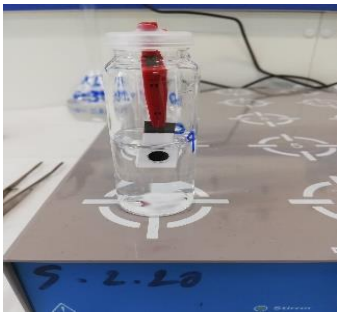

Figure 106. Incubation (rebinding) step

5.6.4.2. Calibration curve and determination of LOD/LOQ

In this subsection is presented the analytical performance of the Graphene-MIP electrodes under the optimal conditions to achieve the best sensitivity for isoproturon detection described previously. For obtaining the calibration plots, isoproturon detection is observed by square wave voltammetry in an ethanol/water (70:30 v/v) solution of 0.1M H_2SO_4, and the isoproturon concentration range for the calibration plots was chosen to be at 5 x 10^{-9} M – 5 x 10^{-6} M. For each electrode calibration, the measurements were repeated five times on four electrodes prepared under identical conditions.

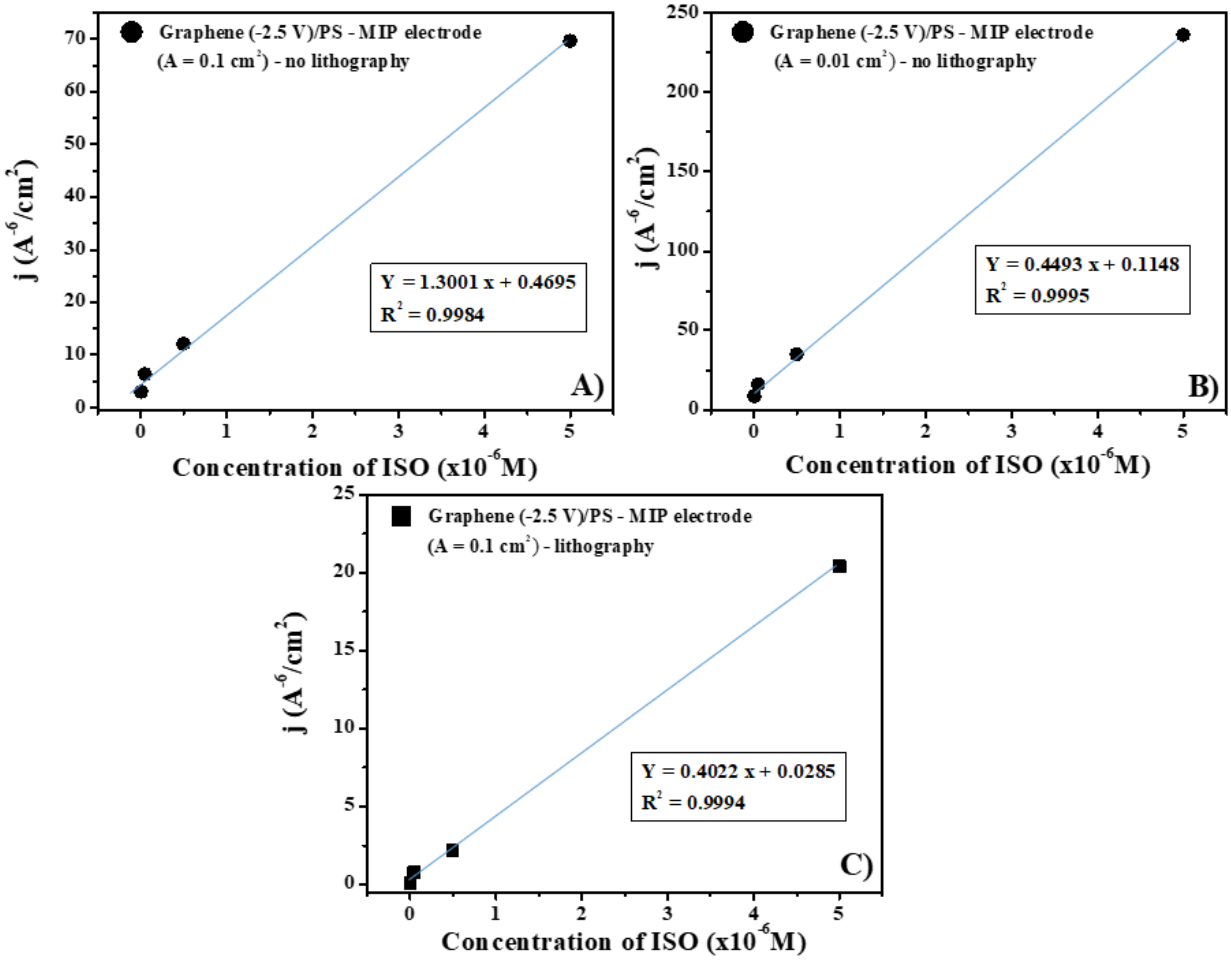

Figure 107. The calibration plots of isoproturon detection obtained at Graphene-MIP electrodes in milli-Q water samples, the electrode substrate was graphene (-2.5 V)/PS obtained by our own method at different working surface area A) 10 mm^2 and B) 1 mm^2, and on graphene (-2.5 V)/PS photolithography electrodes with working surface area 10 mm^2 C). The electrochemical analysis was performed by square wave voltammetry (SWV) in an ethanol/water (70:30 v/v) solution of 0.1M H_2SO_4.

In Figure 107 are presented the calibration plots for the different Graphene-MIP electrode. Also, it has been tested the detection of isoproturon for the calibration plot with Graphene-MIP electrodes prepared on graphene (-2.5 V)/PS photolithography electrodes with a working surface area 500 μm^2, but there was obtained any detection signal at all.

Table 12. Comparison of graphene electrodes sensitivity with that one of glassy carbon electrodes.

Electrode	Straight line equation	LOD	RSD
Graphene (-2.5 V)/PS - no lithography A = 10 mm^2	I (μA) = 1.3001 [Isoproturon] + 0.4695 (R^2 = 0.9984)	6.9 x 10^{-8} M (14.2 μg/L)	13.1%
Graphene (-2.5 V)/PS - no lithography A = 1 mm^2	I (μA) = 0.4493 [Isoproturon] + 0.1148 (R^2 = 0.9995)	6.6 x 10^{-8} M (13.6 μg/L)	9.56%
Graphene (-2.5 V)/PS - lithography A = 10 mm^2	I (μA) = 0.4022 [Isoproturon] + 0.0285 (R^2 = 0.9994)	8.9 x 10^{-8} M (18.4 μg/L)	17.2%
Glassy carbon electrode A = 10 mm^2	I (μA) = 4.8701 [Isoproturon] - 0.0043 (R^2 = 0.9959)	2.76 × 10^{-9} M (0.5 μg/L)	7.6%

In Table 12, are shown the data obtained during the SWV determination of isoproturon by using graphene electrodes with different working surface area. The calculated isoproturon LOD for graphene (-2.5 V)/PS no lithography electrode was found to be lower than in the case of graphene (-2.5 V)/PS lithography electrodes. The isoproturon LODs obtained by using graphene electrodes showed to be still higher than those obtained by using GCE (results presented in Chapter III). In addition, in the case of graphene (-2.5 V)/PS no lithography electrodes a well-voltammograms was observed in comparison with the graphene (-2.5 V)/PS lithography electrodes which did not show good reproducibility.

5.7. Conclusion and future perspectives

In this part, electrochemistry was used for the electrochemical exfoliation of graphite rod electrodes into graphene flakes. The graphene was then used for the fabrication of graphene/PS electrodes after transferring the graphene on polystyrene substrates. Furthermore, these graphene/PS electrodes were used for electropolymerization of MIP sensing thin films for the SWV determination of isoproturon in water samples.

Firstly, the electrochemical exfoliation of graphite rod electrodes has been performed in aqueous salts media, then the produced graphene oxide was further treated chemically with hydrazine hydrate at high temperature. According to the XPS, Raman, IR and electrochemical characterization results the quality of graphene fabricated through electrochemical exfoliation in aqueous media was not in good level, due to the high presence of oxygenated functional groups. In a second way, we developed a new method for exfoliation of graphite rod electrode in organic media with a single stage of exfoliation, no need to use voltage booster and also no need for chemically reduction of the final product with hydrazine hydrate. Hence, the second way of graphite exfoliation provides producing a high-quality graphene according to the XPS, Raman, IR and electrochemical characterization results, showing low presence of oxygenated functional groups in the structure of graphene. Furthermore, this kind of graphene was easy to be transferred mechanically on the polystyrene substrate.

Two methods have been used for the fabrication of graphene graphene/PS electrodes with controlled working surface area, the method developed manually in the laboratory and the photolithography method which was automatically one. However, photolithography caused some modifications on the graphene/PS electrode surface and leaded in decreasing the electrochemical signal according to the characterization results.

Electrochemical MIP sensors for the sensitive and selective SWV determination of isoproturon were also developed. These Graphene-MIP sensing devices showed to ultra-sensitive electrodes which can be prepared easily by CV or CA through various electro-analytical steps. The Graphene-MIP sensor was able to detect isoproturon in nano-molar concentration with good reproducibility and repeatability and shows good robustness during the seven successive analyzes. Low limits of detections (LOD) and quantifications (LOQ) have been reached in water samples contaminated with isoproturon, but higher if compared with results obtained on GC-MIP electrodes which were already presented in the Chapter III.

However, these first results obtained on MIP-graphene electrodes are very encouraging and an optimization of the electrode design should improve the detection limits of these graphene electrodes.

General conclusions and future perspectives

The overall objectives of this thesis were, first-to develop an electroanalytical method based on MIP modified glassy carbon electrode to detect isoproturon as micropollutant in water at nanomolar range, and secondly to elaborate pure graphene electrode then to evaluate its properties for the isoproturon electroanalyses by a similar way.

We have first started with the preparation of MIP electrochemical sensor on GC electrode. The electrochemical synthesis of polypyrrole polymer in the presence of isoproturon is performed by CV or CA while the determination of isoproturon concentration is made by SWV. Various key parameters for MIP electro-synthesis procedure have been optimized, such as electropolymerization time, number of scans, solvent ratio, and incubation (rebinding) time. The extraction of the template molecule was made electrochemically in aqueous acidic solutions thus avoiding the use of toxic organic solvents.

These developed GC-MIP sensors we have been able to detect isoproturon in nano-molar range of concentrations, have shown good reproducibility and repeatability, and robustness during several analysis. The performances of these sensors in terms of LOD, LOQ and selectivity were quite satisfactory, where for the contaminated natural waters LOD was shown to be 1,2 $\mu g\ L^{-1}$, whereas in the contaminated milli-Q water samples LOD was calculated to be 0,5 $\mu g\ L^{-1}$. However, these limits values of concentrations of isoproturon were still higher than the maximum allowed concentrations set by the WFD for isoproturon.

In order to increase the performance of these sensors we have made the investigations into the nanostructuration of the polypyrrole MIP film during the second part of this work. In this context by using different electro-analytical, microscopy and spectroscopy techniques, the correlation of several key parameters in terms of sensitivity and selectivity of these sensors was studied. MIP films prepared by CA and CV at lower anodic potentials provided higher conductivity than those prepared at higher positive potentials due to the overoxidation of PPy film. This parameter has directly influenced the performance of the sensor for the isoproturon detection. A good approach between the theoretical thicknesses film values and real thicknesses obtained under AFM scratching mode was observed.

The impact of overoxidation on the MIP behavior has also been studied by using EIS, where it shows that both NIP and MIP films prepared either by CA or CV their charge transfer resistance increase at higher anodic potentials and in particular during CV extraction of the template molecule. XPS and IR analysis have shown a higher presence

of oxygenic functional groups in the structure of NIPs and MIPs prepared at more positive potentials and after their overoxidation as well.

AFM images did not show any difference between CA and CV films, but higher roughness has been in all cases observed for MIP films after template molecule extraction. Moreover, the mechanism of the film growing onto different electrode substrates was investigated by electrochemical quartz crystal microbalance. Due to these optimized conditions, we were able to increase the isoproturon detection SWV signal for about 30%.

In the third part of this work, we reached to develop an original method for elaboration of 100% graphene electrodes by performing electrochemical exfoliation of graphite rod electrodes into graphene flakes. Electrochemical exfoliation of graphite electrode was firstly observed in aqueous salts media enables the formation of graphene oxide a material which needed for the further treatment. Its transformation to reduced graphene oxide has been performed with hydrazine hydrate at high temperatures for about 24 hours.

The electrochemical exfoliation process that provides 100 % graphene was observed by CA at negative potentials, at -2,5 V and at -5,0 V for about 6 hours. The graphene exfoliated at -2,5 V by CA was shown to have higher electrical conductivity than that one exfoliated at -5,0 V. Exfoliation process was much shorter in time and can be easily finished in a single stage because graphene flakes do not need further chemical treatment and the use of a voltage booster.

XPS, Raman, IR analysis of the final graphene flakes prepared by electrochemical reduction showed the absence of oxygenic groups on the graphene layers, providing a high-quality graphene.

The obtained graphene isolated in powder form was then transferred onto polystyrene substrate for the fabrication of graphene/PS electrodes.

Two ways for the defining the working electrode surface area were used, the first one which was performed in our laboratory and the second one which was performed in a clean room by using photolithography. The graphene (-2.5 V)/PS lithography electrodes showed to have higher I_D/I_G ratio values, and also lower electrical conductivity in comparison with graphene (-2,5 V)/PS not lithographed electrodes. Moreover, graphene (-2,5 V)/PS lithography electrodes gives CV signal only in presence of hexaammineruthenium (III) redox probe, but not in presence of potassium hexacyanoferrate (III) redox probe, whereas electrodes not made by lithography give good CV signal in both of redox probes. Overall graphene materials, graphene (-2,5 V)/PS electrodes showed larger electrochemical window and higher kinetic constant (k_0) according to the Digisim simulation analysis.

By using these electrodes, we were able to fabricate the MIP-Graphene sensors for the nanomolar SWV detection of isoproturon. LOD and LOQ calculated statistically was shown to be 14,2 μg/L and 47,4 μg/L for graphene (-2,5 V)/PS no lithography electrodes, whereas LOD and LOQ calculated statistically for graphene (-2,5 V)/PS lithography electrodes was shown to be 18,4 μg/L and 59 μg/L. These first results, obtained without optimizing the MIPs on graphene and the design of the electrodes, are therefore very promising for further applications of these 100% graphene electrodes for the development of electrochemical sensors.

Future perspectives

The future prospects of this category of MIP sensors that have shown promising results for isoproturon detection include:

- Further optimization of the modification procedure of GC electrodes to prepare MIP will be to explore a softer way for the template extraction, in order to limit the overoxidation of polypyrrole films during its electrochemical removal. This approach will help in improving the lifetime of the sensors.

- Further studies for the electrochemical exfoliation of graphite rod electrode into graphene flakes are needed in order to replace the NMP as organic solvent with another solvent which is more friendly for the environment.

- To improve the sensitivity of the electrochemical detection of the 100% graphene electrode will involve the optimization of the design and the procedure of the preparation of these electrodes. The elaboration of photolithography electrodes has to be exposed further: the non-reticulated resin in contact with the graphene modify its surface and then its electrochemical properties. Two ways would be following: the change of the resin and the use of a soft surface treatment as argon plasma for example. Methods based on the impression, inkjet impression for example, could be a solution to avoid the photolithography use.

- Improving the detection of isoproturon by the pure graphene electrodes requires optimizing the development of the MIP and electroanalytical method on these new electrodes because the change of the substrate nature changes the growth of the PPy layer and therefore its properties.

Concerning the environmental application, however effective sensors may be, there are still many locks, in particular the problems linked to the chemical complexity of the environment. The prioritarity micropollutants are numerous and their lists will still increase in the future. Selectivity is therefore a real problem, but it is also important to envisage a viable economic sensor solution as microsensors lab-on chip that would allow chemical detection a lot of these pollutants of water.

Currently, research on heavy analytical laboratory techniques as mass spectroscopy are emphasizing efforts to simplify devices and miniaturize them to allow the simultaneous detection of all the micropollutants. Other ways of research are also explored, such as solutions aimed not pollutants identification but the environment toxicity assessment using methods based on living organisms for example. So, the competition between these different approaches is important, driven by the suppression of the locks such as sensitivity, robustness, fiablitiy, adaptability, etc., but also by the economic viability of the proposed solutions.

Appendices

Appendix 1 – Analytical performances of volt-amperometric MIP-based sensors

In order to evaluate the performance of sensors, it is necessary to determine parameters characteristic of their sensitivity, selectivity, response time and robustness. This section presents the points usually studied to evaluate environmental sensors.

Limit of detection (LOD) and limit of quantification (LOQ)

MIP-based sensors are devices which show various analytical performances during their use. The limits of detection (LOD) and quantification (LOQ) are defined as the lowest concentration of the analyte that can be reliably detected and quantified, respectively. Usually, the LOD and LOQ refer to the limits associated with 95% probability of obtaining a correct result [323].

The LOD and LOQ can be calculated statistically with the following relations [323]:

$$LOD = \frac{3\ x\ standard\ deviation\ of\ the\ lowest\ concentration}{slope\ of\ the\ calibration\ line}$$

$$LOQ = \frac{10\ x\ standard\ deviation\ of\ the\ lowest\ concentration}{slope\ of\ the\ calibration\ line}$$

The attempt for reaching LOQ and LODs as low as possible, has been frequently reported to be one of the biggest challenges for the analytical applications of MIPs. That's why always has been tried to increase the number of imprinted sites per electrode surface or the concentration of imprinted sites in particle systems, in order to increase the ability of MIPs in catching the targeted template molecules. In general, for sensors it is therefore advisable to use the most sensitive types of transductions. In any case, the LOD is directly related to the combination of the type of transduction and features relating to the recognition phase. The interferent molecules can be other pollutants of the medium with some analogies in their form and their functions with the analyte. Their ability to be trapped by the MIP layer leads to a loss of the sensitivity of the sensors even if structurally related interferents can be sometimes identified by their electrochemical potential [53].

A loss of selectivity can appear during the measurements. In particular, the extraction step can lead to strong effects of unspecific adsorption on the electrode surface, particularly when carbon electrodes are used [324]. A unique feature of voltammetry is the possibility of improving detectability by separately optimizing the binding medium and the measurement medium. Other techniques of electrochemical transduction use the same medium for binding and detection.

Response time and long-term stability

Another important analytical performance that MIP sensors possess is the response time and long-term stability. In general, response times with sensors using MIP particles have been longer than with films, because of the difficulties associated with diffusion. MIP sensors, acrylic or vinyl, were reported to have good stability during prolonged storage (more than 6 months in many cases), as expected for a highly crosslinked polymer [53]. Good stability during the prolonged use was appeared also for the MIP sensors based on molecularly imprinted polypyrrole films [165], [325], [326].

Application for real samples

MIP sensors reported in literature to date are tested in standard solutions and in real samples, showing their response time and their life duration, mostly where the performance of the MIP-based electrochemical sensors was shown to be better in standard solutions than in natural water solutions or real samples [165]. However, some good results for the performance of MIPs in real samples have been reported in literature [138], [139], [141], [165], [327]–[329].

Appendix 2 – The real thickness of NIP and MIP films obtained by AFM – scratching mode

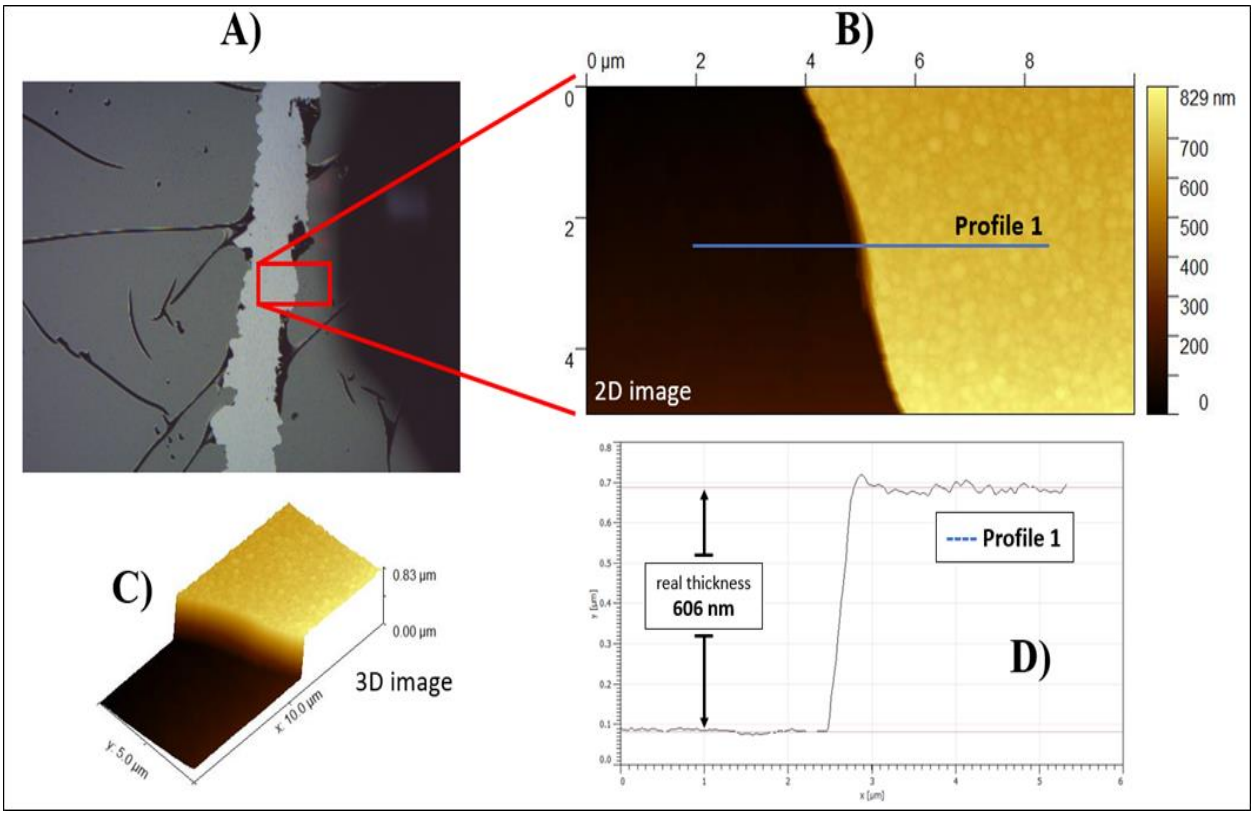

Figure. S-1.

In order to observe the real thickness of MIP and NIP films, AFM scratching mode has been employed as presented in Figure S-1. MIP and NIP films, once prepared electrochemically onto glassy carbon electrode wafers, they have been washed in an ethanol : milli-Q water (50:50 v/v) mixture for about 15 minutes and left to dry, then after a scratch on them has been drawn (Figure S-1A). The sample has been fixed inside the AFM microscope where the images were taken for each case (Figure S-1B). From the images presented in 3D view we have been able to see exactly where is the film and where is the electrode substrate. Moreover, on this region of image were extracted the profile lines which helped us to see the real thickness of the generated films (Figure S-1D).

The real thickness results obtained using this method were then compared with the theoretical ones calculated by Faraday's law.

Appendix 3 – Summary data obtained after the analysis of XPS results

From these tables we present the XPS data obtained during the characterization of different types of graphene materials.

C-C sp^2	Elemental composition (at. %)		Binding energy (eV)	
Electrodes	Atomic (%)	Std (%)	BE (eV)	Std (eV)
Graphite/PS	49,44	4,1	284,54	0
GOx/PS	36,6	4,1	284,52	0,02
rGOx/PS	31,9	2,37	284,51	0,02
rGOx-USA/PS	33,15	2,42	284,66	0,03
Gr. (-5.0 V)/PS	38,2	1,96	284,6	0,01
Gr. (-2.5 V)/PS	37,1	0,57	284,6	0,03
Gr. (-2.5 V)/PS–Lit.	16,45	4,4	284,56	0,01

C-C sp^3	Elemental composition (at. %)		Binding energy (eV)	
Electrodes	Atomic (%)	Std (%)	BE (eV)	Std (eV)
Graphite/PS	18,83	2,1	284,9	0
GOx/PS	20,08	5,7	285,11	0,2
rGOx/PS	22,5	1,66	284,9	0
rGOx-USA/PS	3,57	0,7	284,9	0,1
Gr. (-5.0 V)/PS	35,95	3,13	284,99	0,05
Gr. (-2.5 V)/PS	30,5	4,9	284,97	0,03
Gr. (-2.5 V)/PS–Lit.	19,8	3,5	285	0,19

C-O-	Elemental composition (at. %)		Binding energy (eV)	
Electrodes	Atomic (%)	Std (%)	BE (eV)	Std (eV)
Graphite/PS	18,19	0,5	286,03	0,065
GOx/PS	20,5	5,4	286,13	0,19
rGOx/PS	4,78	0,98	286,4	1,15
rGOx-USA/PS	3,22	0,6	286,15	1,1
Gr. (-5.0 V)/PS	3,96	1,6	286,32	0,15
Gr. (-2.5 V)/PS	6,84	0,78	286,2	0,2
Gr. (-2.5 V)/PS–Lit.	4,77	1,93	286,34	0,08

C=O	Elemental composition (at. %)		Binding energy (eV)	
Electrodes	Atomic (%)	Std (%)	BE (eV)	Std (eV)
Graphite/PS	0,06	0,12	287,48	0,145
GOx/PS	4,43	0,97	287,31	0,03
rGOx/PS	4,88	0,32	287,3	0
rGOx-USA/PS	18,52	1,3	285,77	0,83
Gr. (-5.0 V)/PS	4,46	0,9	286,76	0,71
Gr. (-2.5 V)/PS	2,56	0,87	287,3	0,077
Gr. (-2.5 V)/PS–Lit.	7,78	3,5	285,5	1

COO^-	Elemental composition (at. %)		Binding energy (eV)	
Electrodes	Atomic (%)	Std (%)	BE (eV)	Std (eV)
Graphite/PS	2,31	1,3	288,91	0,16
GOx/PS	1,3	0,44	288,93	0,08
rGOx/PS	1,84	0,16	288,82	0,03
rGOx-USA/PS	8,41	1,34	288,7	0,05
Gr. (-5.0 V)/PS	1,76	0,85	288,74	0,11
Gr. (-2.5 V)/PS	0,33	0,3	288,94	0,16
Gr. (-2.5 V)/PS–Lit.	10,29	1,72	288,92	0,21

π - π	Elemental composition (at. %)		Binding energy (eV)	
Electrodes	Atomic (%)	Std (%)	BE (eV)	Std (eV)
Graphite/PS	8,62	2,6	290,85	0,39
GOx/PS	1,04	0,36	290,4	0,2
rGOx/PS	1,2	0,33	290,32	0,21
rGOx-USA/PS	3,47	0,76	292,14	0,32
Gr. (-5.0 V)/PS	2,31	0,64	291,16	0,17
Gr. (-2.5 V)/PS	3,89	0,72	291,08	0,11
Gr. (-2.5 V)/PS–Lit.	1,3	0,1	292,2	1,1

C-OH	Elemental composition (at. %)		Binding energy (eV)	
Electrodes	Atomic (%)	Std (%)	BE (eV)	Std (eV)
Graphite/PS	2,54	0,81	532,3	0
GOx/PS	27,57	2,46	532,2	0,03
rGOx/PS	27,6	2,5	532,2	0,03
rGOx-USA/PS	13,09	1,2	531,5	0,04
Gr. (-5.0 V)/PS	4,9	0,84	532,16	0,13
Gr. (-2.5 V)/PS	4	0,35	521,95	0,12
Gr. (-2.5 V)/PS–Lit.	7,5	2,03	532,3	0,05

C-O-C	Elemental composition (at. %)		Binding energy (eV)	
Electrodes	Atomic (%)	Std (%)	BE (eV)	Std (eV)
Graphite/PS	3,2	1,2	533,24	0,19
GOx/PS	4,6	0,98	533,4	0,07
rGOx/PS	4,54	0,96	533,4	0,06
rGOx-USA/PS	16,11	2,1	533,5	0,23
Gr. (-5.0 V)/PS	2,4	0,97	533,23	0,18
Gr. (-2.5 V)/PS	3,36	0,39	533,13	0,11
Gr. (-2.5 V)/PS–Lit.	15,66	2	533,15	0,15

Appendix 4 – Simulated CV data on glassy carbon electrode

In Figure S-4, is presented the superposition of cyclic voltammogram, obtained experimentally using glassy carbon electrode in a solution of $K_4[Fe(CN)_6]$ 2.5 mM dissolved in KCl 0,1M, with the simulated one, and the values of k_0 parameter are presented in the table below.

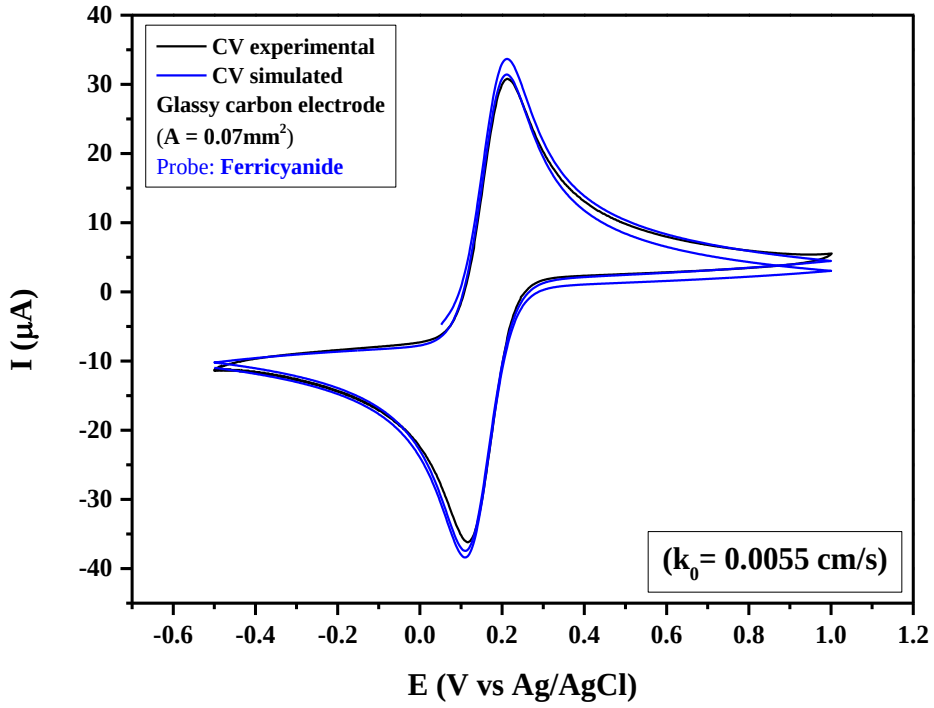

Figure S-4.

Glassy Carbon Electrode	
Scan rate (mV/s)	A = 7 mm², k_0 (cm/s)
500	0,0058
100	0,0055
50	0,00527
25	0,0052
10	0,0005
Average	0,004454
Standard deviation	0,0022

Appendix 5 – Simulated CV data on Graphene (-5.0 V)/PS – no lithography electrode

In Figure S-5, is presented the superposition of cyclic voltammogram, obtained experimentally by using Graphene (-5.0 V)/PS electrode in a solution of $K_4[Fe(CN)_6]$ 2.5 mM dissolved in KCl 0,1M, with the simulated one, and the values of k_0 parameter are presented in the table below.

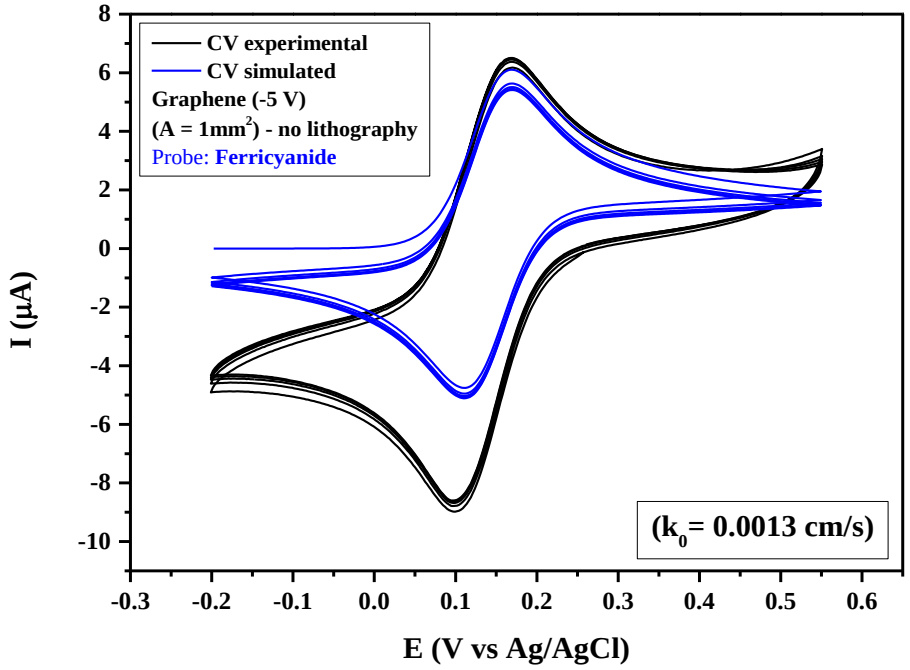

Figure S-5.

Graphene (-5.0 V)/PS – no lithography			
Scan rate (mV/s)	A = 10 mm², k_0 (cm/s)	A = 3 mm², k_0 (cm/s)	A = 1 mm², k_0 (cm/s)
500	0,0015	0,00138	0,00135
100	0,00123	0,0012	0,0013
50	0,0011	0,0012	0,00132
25	0,00122	0,00127	0,0012
10	0,00092	0,0011	0,0008
Average	0,0012	0,00123	0,001194
Standard deviation	0,00021	0,0001	0,00023

References

[1] Organizzazione mondiale della sanità, *Guidelines for drinking-water quality*. Geneva: World health organization, 2011.

[2] "Water Quality: Frequently Asked Questions," p. 2.

[3] "Directive 2013/39/EU of the European Parliament and of the Council of 12 August 2013 amending Directives 2000/60/EC and 2008/105/EC as regards priority substances in the field of water policyText with EEA relevance," p. 17.

[4] L. M. L. Nollet and H. S. Rathore, Eds., *Handbook of pesticides: methods of pesticide residues analysis*. Boca Raton, Fla.: CRC Press, 2010.

[5] M. Roser, "Pesticides," *Our World Data*, Oct. 2019, Accessed: Jan. 14, 2021. [Online]. Available: https://ourworldindata.org/pesticides

[6] H. M. G. van der Werf, "Assessing the impact of pesticides on the environment," *Agric. Ecosyst. Environ.*, vol. 60, no. 2–3, pp. 81–96, Dec. 1996, doi: 10.1016/S0167-8809(96)01096-1.

[7] "Pesticides and Water Pollution," *Safe Drinking Water Foundation*. https://www.safewater.org/fact-sheets-1/2017/1/23/pesticides (accessed May 06, 2021).

[8] J. S. Holt, "Herbicides," in *Encyclopedia of Biodiversity*, Elsevier, 2013, pp. 87–95. doi: 10.1016/B978-0-12-384719-5.00070-8.

[9] J. Liu, "Phenylurea Herbicides," *Handb. Pestic. Toxicol.*, p. 7.

[10] M. M. Nemat Alla and N. M. Hassan, "Alleviation of isoproturon toxicity to wheat by exogenous application of glutathione," *Pestic. Biochem. Physiol.*, vol. 112, pp. 56–62, Jun. 2014, doi: 10.1016/j.pestbp.2014.04.012.

[11] L. Liang, Y. L. Lu, and H. Yang, "Toxicology of isoproturon to the food crop wheat as affected by salicylic acid," *Environ. Sci. Pollut. Res.*, vol. 19, no. 6, pp. 2044–2054, Jul. 2012, doi: 10.1007/s11356-011-0698-7.

[12] World Health Organization and International Program on Chemical Safety, Eds., *Guidelines for drinking-water quality*, 2nd ed. Geneva: World Health Organization, 1993.

[13] World Health Organization, Ed., *Guidelines for drinking-water quality*, 4th ed. Geneva: World Health Organization, 2011.

[14] S. R. Ruberu, W. M. Draper, and S. K. Perera, "Multiresidue HPLC Methods for Phenyl Urea Herbicides in Water," *J. Agric. Food Chem.*, vol. 48, no. 9, pp. 4109–4115, Sep. 2000, doi: 10.1021/jf000266p.

[15] V. G. Amelin, D. K. Lavrukhin, and A. V. Tret'yakov, "Dispersive liquid-liquid microextraction for the determination of herbicides of urea derivatives family in natural waters by HPLC," *J. Anal. Chem.*, vol. 68, no. 9, pp. 822–830, Sep. 2013, doi: 10.1134/S1061934813070022.

[16] L. Rivoira, R. M. De Carlo, S. Cavalli, and M. C. Bruzzoniti, "Simple SPE–HPLC determination of some common drugs and herbicides of environmental concern by pulsed amperometry," *Talanta*, vol. 131, pp. 205–212, Jan. 2015, doi: 10.1016/j.talanta.2014.07.070.

[17] P. Manisankar, C. Vedhi, and G. Selvanathan, "Electrochemical studies of isoproturon," *Trans. SAEST Soc. Adv. Electrochem. Sci. Technol.*, vol. 37, pp. 135–140, Jul. 2002.

[18] W. E. Van der Linden and J. W. Dieker, "Glassy carbon as electrode material in electro- analytical chemistry," *Anal. Chim. Acta*, vol. 119, no. 1, pp. 1–24, Sep. 1980, doi: 10.1016/S0003-2670(00)00025-8.

[19] P. Noyrod, O. Chailapakul, W. Wonsawat, and S. Chuanuwatanakul, "The simultaneous determination of isoproturon and carbendazim pesticides by single drop analysis using a graphene-based electrochemical sensor," *J. Electroanal. Chem.*, vol. 719, Apr. 2014, doi: 10.1016/j.jelechem.2014.02.001.

[20] P. Manisankar, G. Selvanathan, S. Viswanathan, and H. Gurumallesh Prabu, "Electrochemical Determination of Some Organic Pollutants Using Wall-Jet Electrode," *Electroanalysis*, vol. 14, no. 24, pp. 1722–1727, Dec. 2002, doi: 10.1002/elan.200290016.

[21] K. Vytřas, I. Svancara, and R. Metelka, "Carbon paste electrodes in electroanalytical chemistry," *J. Serbian Chem. Soc.*, vol. 74, no. 10, pp. 1021–1033, 2009, doi: 10.2298/JSC0910021V.

[22] C. F. McFadden, P. Rossi. Melaragno, and J. A. Davis, "Fabrication of pyrolytic carbon film electrodes by pyrolysis of methane on a machinable glass ceramic," *Anal. Chem.*, vol. 62, no. 7, pp. 742–746, Apr. 1990, doi: 10.1021/ac00206a019.

[23] K. Pecková, J. Musilová, and J. Barek, "Boron-Doped Diamond Film Electrodes—New Tool for Voltammetric Determination of Organic Substances," *Crit. Rev. Anal. Chem.*, vol. 39, no. 3, pp. 148–172, Jul. 2009, doi: 10.1080/10408340903011812.

[24] P. Manisankar, PL. A. Sundari, R. Sasikumar, and SP. Palaniappan, "Electroanalysis of some common pesticides using conducting polymer/multiwalled carbon nanotubes modified glassy carbon electrode," *Talanta*, vol. 76, no. 5, pp. 1022–1028, Sep. 2008, doi: 10.1016/j.talanta.2008.04.056.

[25] S. Su, S. Chen, and C. Fan, "Recent advances in two-dimensional nanomaterials-based electrochemical sensors for environmental analysis," *Green Energy Environ.*, vol. 3, no. 2, pp. 97–106, Apr. 2018, doi: 10.1016/j.gee.2017.08.005.

[26] P. Manisankar, G. Selvanathan, and C. Vedhi, "Utilization of sodium montmorillonite clay-modified electrode for the determination of isoproturon and carbendazim in soil and water samples," *Appl. Clay Sci.*, vol. 29, no. 3, pp. 249–257, Jun. 2005, doi: 10.1016/j.clay.2005.01.006.

[27] P. Manisankar, G. Selvanathan, and C. Vedhi, "Determination of pesticides using heteropolyacid montmorillonite clay-modified electrode with surfactant," *Talanta*, vol. 68, no. 3, pp. 686–692, Jan. 2006, doi: 10.1016/j.talanta.2005.05.021.

[28] D. E. H. Baskeyfield, F. Davis, N. Magan, and I. E. Tothill, "A membrane-based immunosensor for the analysis of the herbicide isoproturon," *Anal. Chim. Acta*, vol. 699, no. 2, pp. 223–231, Aug. 2011, doi: 10.1016/j.aca.2011.05.036.

[29] M. Haddaoui and N. Raouafi, "Chlortoluron-induced enzymatic activity inhibition in tyrosinase/ZnO NPs/SPCE biosensor for the detection of ppb levels of herbicide," *Sens. Actuators B Chem.*, vol. 219, pp. 171–178, Nov. 2015, doi: 10.1016/j.snb.2015.05.023.

[30] X. Jiang *et al.*, "Immunosensors for detection of pesticide residues," *Biosens. Bioelectron.*, vol. 23, no. 11, pp. 1577–1587, Jun. 2008, doi: 10.1016/j.bios.2008.01.035.

[31] B. Liu, B. Xiao, L. Cui, and M. Wang, "Molecularly imprinted electrochemical sensor for the highly selective and sensitive determination of melamine," *Mater. Sci. Eng. C*, vol. 55, pp. 457–461, Oct. 2015, doi: 10.1016/j.msec.2015.05.080.

[32] B. Wu, Z. Wang, D. Zhao, and X. Lu, "A novel molecularly imprinted impedimetric sensor for melamine determination," *Talanta*, vol. 101, pp. 374–381, Nov. 2012, doi: 10.1016/j.talanta.2012.09.044.

[33] E. Pardieu *et al.*, "Molecularly imprinted conducting polymer based electrochemical sensor for detection of atrazine," *Anal. Chim. Acta*, vol. 649, no. 2, pp. 236–245, Sep. 2009, doi: 10.1016/j.aca.2009.07.029.

[34] M. L. Yola and N. Atar, "Electrochemical Detection of Atrazine by Platinum Nanoparticles/Carbon Nitride Nanotubes with Molecularly Imprinted Polymer," *Ind. Eng. Chem. Res.*, vol. 56, no. 27, pp. 7631–7639, Jul. 2017, doi: 10.1021/acs.iecr.7b01379.

[35] R. Elshafey and A.-E. Radi, "Electrochemical impedance sensor for herbicide alachlor based on imprinted polymer receptor," *J. Electroanal. Chem.*, vol. 813, pp. 171–177, Mar. 2018, doi: 10.1016/j.jelechem.2018.02.036.

[36] P. D. Marreto *et al.*, "Square-Wave Voltammetric Determination of Nanomolar Levels of Linuron in Environmental Water Samples Using a Glassy Carbon Electrode Modified with Platinum Nanoparticles within a Dihexadecyl Phosphate Film," *Aust. J. Chem.*, vol. 68, no. 5, pp. 800–805, Jun. 2015, doi: 10.1071/CH14393.

[37] J.-M. Zen, S.-H. Jeng, and H.-J. Chen, "Determination of Paraquat by Square-Wave Voltammetry at a Perfluorosulfonated Ionomer/Clay-Modified Electrode," *Anal. Chem.*, vol. 68, no. 3, pp. 498–502, Feb. 1996, doi: 10.1021/ac950590x.

[38] J. A. Ribeiro, C. A. Carreira, H. J. Lee, F. Silva, A. Martins, and C. M. Pereira, "Voltammetric determination of paraquat at DNA–gold nanoparticle composite electrodes," *Electrochimica Acta*, vol. 55, no. 27, pp. 7892–7896, Nov. 2010, doi: 10.1016/j.electacta.2010.03.058.

[39] L. M. Niu *et al.*, "Electrochemical Behavior of Paraquat on a Highly Ordered Biosensor Based on an Unmodified DNA-3D Gold Nanoparticle Composite and Its Application," *Electrochimica Acta*, vol. 153, pp. 190–199, Jan. 2015, doi: 10.1016/j.electacta.2014.11.191.

[40] M. A. E. Mhammedi, M. Bakasse, and A. Chtaini, "Electrochemical studies and square wave voltammetry of paraquat at natural phosphate modified carbon paste electrode," *J. Hazard. Mater.*, vol. 145, no. 1, pp. 1–7, Jun. 2007, doi: 10.1016/j.jhazmat.2007.02.054.

[41] T.-H. Lu and I.-W. Sun, "Electrocatalytic determination of paraquat using a nafion film coated glassy carbon electrode," *Talanta*, vol. 53, no. 2, pp. 443–451, Nov. 2000, doi: 10.1016/S0039-9140(00)00511-7.

[42] I. C. Lopes, D. De Souza, S. A. S. Machado, and A. A. Tanaka, "Voltammetric detection of paraquat pesticide on a phthalocyanine-based pyrolitic graphite electrode," *Anal. Bioanal. Chem.*, vol. 388, no. 8, pp. 1907–1914, Aug. 2007, doi: 10.1007/s00216-007-1397-6.

[43] C. Kalinke, A. S. Mangrich, L. H. Marcolino-Junior, and M. F. Bergamini, "Carbon Paste Electrode Modified with Biochar for Sensitive Electrochemical Determination of Paraquat," *Electroanalysis*, vol. 28, no. 4, pp. 764–769, 2016, doi: 10.1002/elan.201500640.

[44] A. Gevaerd, P. R. de Oliveira, A. S. Mangrich, M. F. Bergamini, and L. H. Marcolino-Junior, "Evaluation of antimony microparticles supported on biochar for application in the voltammetric determination of paraquat," *Mater. Sci. Eng. C*, vol. 62, pp. 123–129, May 2016, doi: 10.1016/j.msec.2016.01.020.

[45] A. Farahi, M. Achak, L. El Gaini, M. A. El Mhammedi, and M. Bakasse, "Electrochemical determination of paraquat in citric fruit based on electrodeposition of silver particles onto carbon paste electrode," *J. Food Drug Anal.*, vol. 23, no. 3, pp. 463–471, Sep. 2015, doi: 10.1016/j.jfda.2015.03.003.

[46] A. Wong, M. V. Foguel, S. Khan, F. M. de Oliveira, C. R. T. Tarley, and M. D. P. T. Sotomayor, "DEVELOPMENT OF AN ELECTROCHEMICAL SENSOR MODIFIED WITH MWCNT-COOH AND MIP FOR DETECTION OF DIURON," *Electrochimica Acta*, vol. 182, pp. 122–130, Nov. 2015, doi: 10.1016/j.electacta.2015.09.054.

[47] S. Li, H. Tao, and J. Li, "Molecularly Imprinted Electrochemical Luminescence Sensor Based on Enzymatic Amplification for Ultratrace Isoproturon Determination," *Electroanalysis*, vol. 24, Jul. 2012, doi: 10.1002/elan.201200088.

[48] A. Ramanavičius, A. Ramanavičienė, and A. Malinauskas, "Electrochemical sensors based on conducting polymer—polypyrrole," *Electrochimica Acta*, vol. 51, no. 27, pp. 6025–6037, Aug. 2006, doi: 10.1016/j.electacta.2005.11.052.

[49] D. Udomsap, C. Branger, G. Culioli, P. Dollet, and H. Brisset, "A versatile electrochemical sensing receptor based on a molecularly imprinted polymer," *Chem. Commun.*, vol. 50, no. 56, pp. 7488–7491, Jun. 2014, doi: 10.1039/C4CC02658F.

[50] K. Haupt and K. Mosbach, “Molecularly Imprinted Polymers and Their Use in Biomimetic Sensors,” *Chem. Rev.*, vol. 100, no. 7, pp. 2495–2504, Jul. 2000, doi: 10.1021/cr990099w.

[51] A. Hulanicki, S. Glab, and F. Ingman, “Chemical sensors: definitions and classification,” *Pure Appl. Chem.*, vol. 63, no. 9, pp. 1247–1250, Jan. 1991, doi: 10.1351/pac199163091247.

[52] D. Grieshaber, R. MacKenzie, J. Vörös, and E. Reimhult, “Electrochemical Biosensors - Sensor Principles and Architectures,” *Sensors*, vol. 8, no. 3, pp. 1400–1458, Mar. 2008.

[53] M. C. Blanco-López, M. J. Lobo-Castañón, A. J. Miranda-Ordieres, and P. Tuñón-Blanco, “Electrochemical sensors based on molecularly imprinted polymers,” *TrAC Trends Anal. Chem.*, vol. 23, no. 1, pp. 36–48, Jan. 2004, doi: 10.1016/S0165-9936(04)00102-5.

[54] A. Bratov, N. Abramova, and A. Ipatov, “Recent trends in potentiometric sensor arrays—A review,” *Anal. Chim. Acta*, vol. 678, no. 2, pp. 149–159, Sep. 2010, doi: 10.1016/j.aca.2010.08.035.

[55] N. Jaffrezic-Renault and S. V. Dzyadevych, “Conductometric Microbiosensors for Environmental Monitoring,” *Sensors*, vol. 8, no. 4, Art. no. 4, Apr. 2008, doi: 10.3390/s8042569.

[56] G. Korotcenkov and B. K. Cho, “Metal oxide composites in conductometric gas sensors: Achievements and challenges,” *Sens. Actuators B Chem.*, vol. 244, pp. 182–210, Jun. 2017, doi: 10.1016/j.snb.2016.12.117.

[57] A. J. Bard and L. R. Faulkner, *Electrochemical methods: fundamentals and applications*, 2nd ed. New York: Wiley, 2001.

[58] F. R. Simões, “6 - Electrochemical Sensors,” p. 24.

[59] E. Santos, R. Nazmutdinov, and W. Schmickler, “Electron transfer at different electrode materials: Metals, semiconductors, and graphene,” *Curr. Opin. Electrochem.*, vol. 19, pp. 106–112, Feb. 2020, doi: 10.1016/j.coelec.2019.11.003.

[60] P. Zuman, “Role of Mercury Electrodes in Contemporary Analytical Chemistry,” *Electroanalysis*, vol. 12, no. 15, pp. 1187–1194, 2000, doi: https://doi.org/10.1002/1521-4109(200010)12:15<1187::AID-ELAN1187>3.0.CO;2-S.

[61] T. Nasir, “Electrochemical sensors of environmental pollutants based on carbon electrodes modified by ordered mesoporous silica,” p. 187.

[62] K. S. Tulík, “Microelectrodes. Definitions, characterization, and applications,” *Pure Appl. Chem.*, p. 10, 2000.

[63] J. Janata, *Principles of chemical sensors*, 2nd ed. Dordrecht ; New York: Springer, 2009.

[64] G. Anantha-Iyengar *et al.*, “Functionalized conjugated polymers for sensing and molecular imprinting applications,” *Prog. Polym. Sci.*, vol. 88, pp. 1–129, Jan. 2019, doi: 10.1016/j.progpolymsci.2018.08.001.

[65] M. A. Najeeb, Z. Ahmad, and R. A. Shakoor, "Organic Thin-Film Capacitive and Resistive Humidity Sensors: A Focus Review," *Adv. Mater. Interfaces*, vol. 5, no. 21, p. 1800969, 2018, doi: https://doi.org/10.1002/admi.201800969.

[66] T.-H. Le, Y. Kim, and H. Yoon, "Electrical and Electrochemical Properties of Conducting Polymers," *Polymers*, vol. 9, no. 4, Art. no. 4, Apr. 2017, doi: 10.3390/polym9040150.

[67] J. Heinze, B. A. Frontana-Uribe, and S. Ludwigs, "Electrochemistry of Conducting Polymers—Persistent Models and New Concepts," *Chem. Rev.*, vol. 110, no. 8, pp. 4724–4771, Aug. 2010, doi: 10.1021/cr900226k.

[68] H. Letheby, "XXIX.—On the production of a blue substance by the electrolysis of sulphate of aniline," *J. Chem. Soc.*, vol. 15, no. 0, pp. 161–163, Jan. 1862, doi: 10.1039/JS8621500161.

[69] P.-H. Aubert and C. Plesse, "Les polymères conducteurs électroniques," p. 10.

[70] M. Zhou and J. Heinze, "Electropolymerization of Pyrrole and Electrochemical Study of Polypyrrole. 3. Nature of 'Water Effect' in Acetonitrile," *J. Phys. Chem. B*, vol. 103, no. 40, pp. 8451–8457, Oct. 1999, doi: 10.1021/jp990162l.

[71] A. de Leon and R. C. Advincula, "Chapter 11 - Conducting Polymers with Superhydrophobic Effects as Anticorrosion Coating," in *Intelligent Coatings for Corrosion Control*, A. Tiwari, J. Rawlins, and L. H. Hihara, Eds. Boston: Butterworth-Heinemann, 2015, pp. 409–430. doi: 10.1016/B978-0-12-411467-8.00011-8.

[72] R. D. McCullough, "The Chemistry of Conducting Polythiophenes," *Adv. Mater.*, vol. 10, no. 2, pp. 93–116, 1998, doi: https://doi.org/10.1002/(SICI)1521-4095(199801)10:2<93::AID-ADMA93>3.0.CO;2-F.

[73] "Properties of Conductive Polymers." https://polymerdatabase.com/polymer%20classes/Polyphenylene%20type.html (accessed May 07, 2021).

[74] A. L. Pang, A. Arsad, and M. Ahmadipour, "Synthesis and factor affecting on the conductivity of polypyrrole: a short review," *Polym. Adv. Technol.*, vol. 32, no. 4, pp. 1428–1454, 2021, doi: https://doi.org/10.1002/pat.5201.

[75] J. J. M. Halls *et al.*, "Efficient photodiodes from interpenetrating polymer networks," *Nature*, vol. 376, no. 6540, pp. 498–500, Aug. 1995, doi: 10.1038/376498a0.

[76] A. Kraft, A. C. Grimsdale, and A. B. Holmes, "Electroluminescent Conjugated Polymers-Seeing Polymers in a New Light," *Angew. Chem. Int. Ed Engl.*, vol. 37, no. 4, pp. 402–428, Mar. 1998, doi: 10.1002/(SICI)1521-3773(19980302)37:4<402::AID-ANIE402>3.0.CO;2-9.

[77] A. R. Hepburn, J. M. Marshall, and J. M. Maud, "Novel electrochromic films via anodic oxidation of carbazolyl substituted polysiloxanes," *Synth. Met.*, vol. 43, no. 1, pp. 2935–2938, Jun. 1991, doi: 10.1016/0379-6779(91)91210-2.

[78] J. C. Dubois, O. Sagnes, and F. Henry, "Polyheterocyclic conducting polymers and composites derivates," *Synth. Met.*, vol. 28, no. 1, pp. 871–878, Jan. 1989, doi: 10.1016/0379-6779(89)90616-4.

[79] A. Burke, "Ultracapacitors: why, how, and where is the technology," *J. Power Sources*, vol. 91, pp. 37–50, 2000, doi: 10.1016/S0378-7753(00)00485-7.

[80] C. A. Vincent, "Applications of electroactive polymers. Edited by B. Scrosati. Chapman and Hall, London, 1993. pp. 354 price £40.00. ISBN 0-412-41430-9," *Polym. Int.*, vol. 33, no. 3, pp. 343–343, 1994, doi: 10.1002/pi.1994.210330323.

[81] K. M. Vighnesha, Shruthi, Sandhya, D. N. Sangeetha, and M. Selvakumar, "Synthesis and characterization of activated carbon/conducting polymer composite electrode for supercapacitor applications," *J. Mater. Sci. Mater. Electron.*, vol. 29, no. 2, pp. 914–921, Jan. 2018, doi: 10.1007/s10854-017-7988-x.

[82] C. Peng, S. Zhang, D. Jewell, and G. Z. Chen, "Carbon nanotube and conducting polymer composites for supercapacitors," *Prog. Nat. Sci.*, vol. 18, no. 7, pp. 777–788, Jul. 2008, doi: 10.1016/j.pnsc.2008.03.002.

[83] H. da Silva, J. G. Pacheco, J. MCS Magalhães, S. Viswanathan, and C. Delerue-Matos, "MIP-graphene-modified glassy carbon electrode for the determination of trimethoprim," *Biosens. Bioelectron.*, vol. 52, pp. 56–61, Feb. 2014, doi: 10.1016/j.bios.2013.08.035.

[84] J. Janata and M. Josowicz, "Conducting polymers in electronic chemical sensors," *Nat. Mater.*, vol. 2, no. 1, Art. no. 1, Jan. 2003, doi: 10.1038/nmat768.

[85] X. Guo and A. Facchetti, "The journey of conducting polymers from discovery to application," *Nat. Mater.*, vol. 19, no. 9, Art. no. 9, Sep. 2020, doi: 10.1038/s41563-020-0778-5.

[86] A. Kahn, "Fermi level, work function and vacuum level," *Mater. Horiz.*, vol. 3, no. 1, pp. 7–10, 2016, doi: 10.1039/C5MH00160A.

[87] N. E. Kamchi, "Micro et Nano technologies, Acoustique et Télécommunications," p. 160, 2012.

[88] B. Wessling, "Dispersion as the link between basic research and commercial applications of conductive polymers (polyaniline)," *Synth. Met.*, vol. 93, no. 2, pp. 143–154, Mar. 1998, doi: 10.1016/S0379-6779(98)00017-4.

[89] M. Ates, T. Karazehir, and A. Sezai Sarac, "Conducting Polymers and their Applications," *Curr. Phys. Chem.*, vol. 2, no. 3, pp. 224–240, Aug. 2012.

[90] S. C. Rasmussen, "EARLY HISTORY OF POLYPYRROLE: THE FIRST CONDUCTING ORGANIC POLYMER," *Bull Hist Chem*, vol. 40, no. 1, p. 11, 2015.

[91] H. Dh, L. Hj, and P. Sm, "Electrochemistry of conductive polymers XXXV: Electrical and morphological characteristics of polypyrrole films prepared in aqueous media studied by current sensing atomic force microscopy," *Electrochimica Acta*, vol. 50, no. 15, pp. 3085–3092, 2005.

[92] U. Johanson, M. Marandi, T. Tamm, and J. Tamm, "Comparative study of the behavior of anions in polypyrrole films," *Electrochimica Acta*, vol. 50, no. 7, pp. 1523–1528, Feb. 2005, doi: 10.1016/j.electacta.2004.10.016.

[93] C. Weidlich, K.-M. Mangold, and K. Jüttner, "EQCM study of the ion exchange behaviour of polypyrrole with different counterions in different electrolytes," *Electrochimica Acta*, vol. 50, no. 7, pp. 1547–1552, Feb. 2005, doi: 10.1016/j.electacta.2004.10.032.

[94] E. Kriván, G. Peintler, and C. Visy, "Matrix rank analysis of spectral studies on the electropolymerisation and discharge process of conducting polypyrrole/dodecyl sulfate films," *Electrochimica Acta*, vol. 50, no. 7, pp. 1529–1535, Feb. 2005, doi: 10.1016/j.electacta.2004.10.031.

[95] S. Bousalem, A. Yassar, M. Chehimi, A. Ben Slimane, and A. Azioune, "Synthesis, Characterization, and Biomedical Applications of Conducting Polymer Particles," in *Colloidal Polymers*, vol. 20036129, A. Elaissari, Ed. CRC Press, 2003. doi: 10.1201/9780203911488.ch10.

[96] A. Azioune *et al.*, "Interactions and conformational changes of human serum albumin at the surface of electrochemically synthesized thin polypyrrole films.: Electrochimica Acta, 50 (2005) 1661¿1667," 2005, Accessed: Mar. 26, 2021. [Online]. Available: https://researchportal.unamur.be/fr/publications/interactions-and-conformational-changes-of-human-serum-albumin-at

[97] K. Arora *et al.*, "Application of electrochemically prepared polypyrrole–polyvinyl sulphonate films to DNA biosensor," *Biosens. Bioelectron.*, vol. 21, no. 9, pp. 1777–1783, Mar. 2006, doi: 10.1016/j.bios.2005.09.002.

[98] J.-B. Raoof, R. Ojani, and S. Rashid-Nadimi, "Preparation of polypyrrole/ferrocyanide films modified carbon paste electrode and its application on the electrocatalytic determination of ascorbic acid," *Electrochimica Acta*, vol. 49, no. 2, pp. 271–280, Jan. 2004, doi: 10.1016/j.electacta.2003.08.009.

[99] N. T. L. Hien, B. Garcia, A. Pailleret, and C. Deslouis, "Role of doping ions in the corrosion protection of iron by polypyrrole films," *Electrochimica Acta*, vol. 50, no. 7, pp. 1747–1755, Feb. 2005, doi: 10.1016/j.electacta.2004.10.072.

[100] R. McNeill and D. E. Weiss, "A Xanthene Polymer with Semiconducting Properties," *Aust. J. Chem.*, vol. 12, no. 4, pp. 643–656, 1959, doi: 10.1071/ch9590643.

[101] R. McNeill, R. Siudak, J. H. Wardlaw, and D. E. Weiss, "Electronic Conduction in Polymers. I. The Chemical Structure of Polypyrrole," *Aust. J. Chem.*, vol. 16, no. 6, pp. 1056–1075, 1963, doi: 10.1071/ch9631056.

[102] B. A. Bolto, R. McNeill, and D. E. Weiss, "Electronic Conduction in Polymers. III. Electronic Properties of Polypyrrole," *Aust. J. Chem.*, vol. 16, no. 6, pp. 1090–1103, 1963, doi: 10.1071/ch9631090.

[103] L. Chierici and G. P. Gardini, "The structure of the product of oxidation of pyrrole C8H10N2O," *Tetrahedron*, vol. 22, no. 1, pp. 53–56, Jan. 1966, doi: 10.1016/0040-4020(66)80100-X.

[104] M. A. Chougule, S. G. Pawar, P. R. Godse, R. N. Mulik, S. Sen, and V. B. Patil, "Synthesis and Characterization of Polypyrrole (PPy) Thin Films," *Soft Nanosci. Lett.*, vol. 01, no. 01, pp. 6–10, 2011, doi: 10.4236/snl.2011.11002.

[105] "Polypyrrole, a new possibility for covalent binding of oxidoreductases to electrode surfaces as a base for stable biosensors," *Sens. Actuators B Chem.*, vol. 1, no. 1–6, pp. 537–541, Jan. 1990, doi: 10.1016/0925-4005(90)80268-5.

[106] "New principles of amperometric enzyme electrodes and of reagentless oxidoreductase biosensors," *Sens. Actuators B Chem.*, vol. 13, no. 1–3, pp. 366–371, May 1993, doi: 10.1016/0925-4005(93)85403-W.

[107] S. Sadki, P. Schottland, N. Brodie, and G. Sabouraud, "The mechanisms of pyrrole electropolymerization," *Chem. Soc. Rev.*, vol. 29, no. 5, pp. 283–293, Jan. 2000, doi: 10.1039/A807124A.

[108] A. F. Diaz, K. K. Kanazawa, and G. P. Gardini, "Electrochemical polymerization of pyrrole," *J. Chem. Soc. Chem. Commun.*, vol. 0, no. 14, pp. 635–636, Jan. 1979, doi: 10.1039/C39790000635.

[109] T. Patois, B. Lakard, N. Martin, and P. Fievet, "Effect of various parameters on the conductivity of free standing electrosynthesized polypyrrole films," *Synth. Met.*, vol. 160, no. 19, pp. 2180–2185, Oct. 2010, doi: 10.1016/j.synthmet.2010.08.005.

[110] E. M. Genies, G. Bidan, and A. F. Diaz, "Spectroelectrochemical study of polypyrrole films," *J. Electroanal. Chem. Interfacial Electrochem.*, vol. 149, no. 1, pp. 101–113, Jul. 1983, doi: 10.1016/S0022-0728(83)80561-0.

[111] A. G. MacDiarmid *et al.*, "The Concept of `Doping' of Conducting Polymers: The Role of Reduction Potentials [and Discussion]," *Philos. Trans. R. Soc. Lond. Ser. Math. Phys. Sci.*, vol. 314, no. 1528, pp. 3–15, 1985.

[112] P. Camurlu, "Polypyrrole derivatives for electrochromic applications," *RSC Adv.*, vol. 4, no. 99, pp. 55832–55845, Oct. 2014, doi: 10.1039/C4RA11827H.

[113] J. L. Bredas and G. B. Street, "Polarons, bipolarons, and solitons in conducting polymers," *Acc. Chem. Res.*, vol. 18, no. 10, pp. 309–315, Oct. 1985, doi: 10.1021/ar00118a005.

[114] A. O. Patil, A. J. Heeger, and F. Wudl, "Optical properties of conducting polymers," *Chem. Rev.*, vol. 88, no. 1, pp. 183–200, Jan. 1988, doi: 10.1021/cr00083a009.

[115] T. Lewis, "A study of the overoxidation of the conducting polymer polypyrrole," *Univ. Wollongong Thesis Collect. 1954-2016*, Jan. 1998, [Online]. Available: https://ro.uow.edu.au/theses/1107

[116] I. Rodríguez, B. R. Scharifker, and J. Mostany, "In situ FTIR study of redox and overoxidation processes in polypyrrole films," *J. Electroanal. Chem.*, vol. 491, no. 1, pp. 117–125, Sep. 2000, doi: 10.1016/S0022-0728(00)00194-7.

[117] F. Beck, P. Braun, and M. Oberst, "Organic Electrochemistry in the Solid State-Overoxidation of Polypyrrole," *Berichte Bunsenges. Für Phys. Chem.*, vol. 91, no. 9, pp. 967–974, 1987, doi: https://doi.org/10.1002/bbpc.19870910927.

[118] S. P. Ozkorucuklu, Y. Sahin, and G. Alsancak, "Voltammetric Behaviour of Sulfamethoxazole on Electropolymerized-Molecularly Imprinted Overoxidized Polypyrrole," *Sensors*, vol. 8, no. 12, pp. 8463–8478, Dec. 2008, doi: 10.3390/s8128463.

[119] "Some aspects of the radiation processing of conducting polymers," *Radiat. Phys. Chem.*, vol. 45, no. 1, pp. 71–78, Jan. 1995, doi: 10.1016/0969-806X(94)E0025-E.

[120] M. Rahaman, A. Aldalbahi, M. Almoiqli, and S. Alzahly, "Chemical and Electrochemical Synthesis of Polypyrrole Using Carrageenan as a Dopant: Polypyrrole/Multi-Walled Carbon Nanotube Nanocomposites," *Polymers*, vol. 10, no. 6, Jun. 2018, doi: 10.3390/polym10060632.

[121] X. B. CHEN, J.-P. ISSI, J. DEVAUX, and D. BILLAUD, "The stability of polypyrrole and its composites," *J. Mater. Sci.*, vol. 32, no. 6, pp. 1515–1518, Mar. 1997, doi: 10.1023/A:1018570404693.

[122] J. Wen, Y. Tian, Z. Mei, W. Wu, and Y. Tian, "Synthesis of polypyrrole nanoparticles and their applications in electrically conductive adhesives for improving conductivity," *RSC Adv.*, vol. 7, no. 84, pp. 53219–53225, Nov. 2017, doi: 10.1039/C7RA09725E.

[123] Y. Li, P. Bober, M. Trchová, and J. Stejskal, "Polypyrrole prepared in the presence of methyl orange and ethyl orange: nanotubes versus globules in conductivity enhancement," *J. Mater. Chem. C*, vol. 5, no. 17, pp. 4236–4245, May 2017, doi: 10.1039/C7TC00206H.

[124] I. M. Minisy *et al.*, "Cationic dyes as morphology-guiding agents for one-dimensional polypyrrole with improved conductivity," *Polymer*, vol. 174, pp. 11–17, Jun. 2019, doi: 10.1016/j.polymer.2019.04.045.

[125] S. T. Navale, A. T. Mane, A. A. Ghanwat, A. R. Mulik, and V. B. Patil, "Camphor sulfonic acid (CSA) doped polypyrrole (PPy) films: Measurement of microstructural and optoelectronic properties," *Measurement*, vol. 50, pp. 363–369, Apr. 2014, doi: 10.1016/j.measurement.2014.01.012.

[126] B. Lakard *et al.*, "Effect of ultrasounds on the electrochemical synthesis of polypyrrole, application to the adhesion and growth of biological cells," *Bioelectrochemistry*, vol. 75, no. 2, pp. 148–157, Jun. 2009, doi: 10.1016/j.bioelechem.2009.03.010.

[127] Y. Fan *et al.*, "Conductively monolithic polypyrrole 3-D porous architecture with micron-sized channels as superior salt-resistant solar steam generators," *Sol. Energy Mater. Sol. Cells*, vol. 206, p. 110347, Mar. 2020, doi: 10.1016/j.solmat.2019.110347.

[128] B. Gowtham, V. Ponnuswamy, G. Pradeesh, R. Suresh, S. Ramanathan, and S. Ashokan, "Physical Investigations on Various Weight Percentage of Acetic Acid Doped Polypyrrole by Chemical Oxidative Polymerization," *J. Inorg. Organomet. Polym. Mater.*, Dec. 2019, doi: 10.1007/s10904-019-01408-5.

[129] N. Wang, H. Dai, D. Wang, H. Ma, and M. Lin, "Determination of copper ions using a phytic acid/polypyrrole nanowires modified glassy carbon electrode," *Mater. Sci. Eng. C*, vol. 76, pp. 139–143, Jul. 2017, doi: 10.1016/j.msec.2017.03.077.

[130] E. Smela, "Microfabrication of PPy microactuators and other conjugated polymer devices," *J. Micromechanics Microengineering*, vol. 9, no. 1, pp. 1–18, Jan. 1999, doi: 10.1088/0960-1317/9/1/001.

[131] A. Asan and M. Kabasakaloglu, "Electrochemical and Corrosion Behaviors of Mild Steel Coated with Polypyrrole," *Mater. Sci.*, vol. 39, no. 5, pp. 643–651, Sep. 2003, doi: 10.1023/B:MASC.0000023503.54062.be.

[132] G. K. Budnikov, "Biomedical aspects of electrochemical methods of analysis," *J. Anal. Chem.*, vol. 55, no. 11, pp. 1014–1023, Nov. 2000, doi: 10.1007/BF02757324.

[133] R. Jain, N. Jadon, and A. Pawaiya, "Polypyrrole based next generation electrochemical sensors and biosensors: A review," *TrAC Trends Anal. Chem.*, vol. 97, pp. 363–373, Dec. 2017, doi: 10.1016/j.trac.2017.10.009.

[134] A. Gümüş, G. Ersöz, İ. Yücedağ, S. Bayrakdar, and Ş. Altindal, "Comparative study of the temperature-dependent dielectric properties of Au/PPy/n-Si (MPS)-type Schottky barrier diodes," *J. Korean Phys. Soc.*, vol. 67, no. 5, pp. 889–895, Sep. 2015, doi: 10.3938/jkps.67.889.

[135] K. Malook, H. Khan, M. Shah, and Ihsan-Ul-Haque, "Synthesis, characterization and electrical properties of polypyrrole/V2O5 composites," *Korean J. Chem. Eng.*, vol. 35, no. 1, pp. 12–19, Jan. 2018, doi: 10.1007/s11814-017-0263-2.

[136] L. Özcan and Y. Şahin, "Determination of paracetamol based on electropolymerized-molecularly imprinted polypyrrole modified pencil graphite electrode," *Sens. Actuators B Chem.*, vol. 127, no. 2, pp. 362–369, Nov. 2007, doi: 10.1016/j.snb.2007.04.034.

[137] N. Maouche, M. Guergouri, S. Gam-Derouich, M. Jouini, B. Nessark, and M. M. Chehimi, "Molecularly imprinted polypyrrole films: Some key parameters for electrochemical picomolar detection of dopamine," *J. Electroanal. Chem.*, vol. 685, pp. 21–27, Oct. 2012, doi: 10.1016/j.jelechem.2012.08.020.

[138] A. Nezhadali, L. Mehri, and R. Shadmehri, "Determination of methimazole based on electropolymerized-molecularly imprinted polypyrrole modified pencil graphite sensor," *Mater. Sci. Eng. C*, vol. 85, pp. 225–232, Apr. 2018, doi: 10.1016/j.msec.2017.05.099.

[139] B. Qader, M. Baron, I. Hussain, and J. Gonzalez-Rodriguez, "Electrochemical determination of 2-isopropoxyphenol in glassy carbon and molecularly imprinted

poly-pyrrole electrodes," *J. Electroanal. Chem.*, Nov. 2017, doi: 10.1016/j.jelechem.2017.11.027.

[140] A. Turco, S. Corvaglia, and E. Mazzotta, "Electrochemical sensor for sulfadimethoxine based on molecularly imprinted polypyrrole: Study of imprinting parameters," *Biosens. Bioelectron.*, vol. 63, pp. 240–247, Jan. 2015, doi: 10.1016/j.bios.2014.07.045.

[141] C. Zhang *et al.*, "A highly selective electrochemical sensor based on molecularly imprinted polypyrrole-modified gold electrode for the determination of glyphosate in cucumber and tap water," *Anal. Bioanal. Chem.*, vol. 409, no. 30, pp. 7133–7144, Dec. 2017, doi: 10.1007/s00216-017-0671-5.

[142] C. Xie, S. Gao, Q. Guo, and K. Xu, "Electrochemical sensor for 2,4-dichlorophenoxy acetic acid using molecularly imprinted polypyrrole membrane as recognition element," *Microchim. Acta*, vol. 169, no. 1–2, pp. 145–152, Apr. 2010, doi: 10.1007/s00604-010-0303-7.

[143] S. Farooq *et al.*, "Molecularly imprinted polymers' application in pesticide residue detection," *Analyst*, vol. 143, no. 17, pp. 3971–3989, Aug. 2018, doi: 10.1039/C8AN00907D.

[144] H. da Silva, J. Pacheco, J. Silva, S. Viswanathan, and C. Delerue-Matos, "Molecularly imprinted sensor for voltammetric detection of norfloxacin," *Sens. Actuators B Chem.*, vol. 219, pp. 301–307, Nov. 2015, doi: 10.1016/j.snb.2015.04.125.

[145] L. Özcan, M. Sahin, and Y. Sahin, "Electrochemical Preparation of a Molecularly Imprinted Polypyrrole-modified Pencil Graphite Electrode for Determination of Ascorbic Acid," *Sensors*, vol. 8, no. 9, pp. 5792–5805, Sep. 2008, doi: 10.3390/s8095792.

[146] E. Mathieu-Scheers *et al.*, "Trace anthracene electrochemical detection based on electropolymerized-molecularly imprinted polypyrrole modified glassy carbon electrode," *J. Electroanal. Chem.*, vol. 848, p. 113253, Sep. 2019, doi: 10.1016/j.jelechem.2019.113253.

[147] V. K. Gupta, M. L. Yola, N. Özaltın, N. Atar, Z. Üstündağ, and L. Uzun, "Molecular imprinted polypyrrole modified glassy carbon electrode for the determination of tobramycin," *Electrochimica Acta*, vol. 112, pp. 37–43, Dec. 2013, doi: 10.1016/j.electacta.2013.08.132.

[148] H. Dai, N. Wang, D. Wang, H. Ma, and M. Lin, "An electrochemical sensor based on phytic acid functionalized polypyrrole/graphene oxide nanocomposites for simultaneous determination of Cd(II) and Pb(II)," *Chem. Eng. J.*, vol. 299, pp. 150–155, Sep. 2016, doi: 10.1016/j.cej.2016.04.083.

[149] Y. Wei, R. Yang, J.-H. Liu, and X.-J. Huang, "Selective detection toward Hg(II) and Pb(II) using polypyrrole/carbonaceous nanospheres modified screen-printed electrode," *Electrochimica Acta*, vol. 105, pp. 218–223, Aug. 2013, doi: 10.1016/j.electacta.2013.05.004.

[150] D. Ye, L. Luo, Y. Ding, Q. Chen, and X. Liu, "A novel nitrite sensor based on graphene/polypyrrole/chitosan nanocomposite modified glassy carbon electrode," *Analyst*, vol. 136, no. 21, pp. 4563–4569, Oct. 2011, doi: 10.1039/C1AN15486A.

[151] R. Ansari, A. F. Delavar, and A. Mohammad-khah, "Solid-state ion selective electrode based on polypyrrole conducting polymer nanofilm as a new potentiometric sensor for Zn2+ ion," *J. Solid State Electrochem.*, vol. 16, no. 10, pp. 3315–3322, Oct. 2012, doi: 10.1007/s10008-012-1759-7.

[152] M. Gholami, M. Rezayi, P. Moozarm Nia, I. Yusoff, and Y. Alias, "A novel method for fabricating Fe2+ ion selective sensor using polypyrrole and sodium dodecyl sulfate based on carbon screen-printed electrode," *Measurement*, vol. 69, pp. 115–125, Jun. 2015, doi: 10.1016/j.measurement.2015.03.030.

[153] J. Li, W. Lei, Y. Xu, Y. Zhang, M. Xia, and F. Wang, "Fabrication of polypyrrole-grafted nitrogen-doped graphene and its application for electrochemical detection of paraquat," *Electrochimica Acta*, vol. 174, pp. 464–471, Aug. 2015, doi: 10.1016/j.electacta.2015.06.028.

[154] L. Andersson, B. Sellergren, and K. Mosbach, "Imprinting of amino acid derivatives in macroporous polymers," *Tetrahedron Lett.*, vol. 25, no. 45, pp. 5211–5214, Jan. 1984, doi: 10.1016/S0040-4039(01)81566-5.

[155] P. A. G. Cormack and A. Z. Elorza, "Molecularly imprinted polymers: synthesis and characterisation," *J. Chromatogr. B Analyt. Technol. Biomed. Life. Sci.*, vol. 804, no. 1, pp. 173–182, May 2004, doi: 10.1016/j.jchromb.2004.02.013.

[156] J. J. BelBruno, "Molecularly Imprinted Polymers," *Chem. Rev.*, vol. 119, no. 1, pp. 94–119, Jan. 2019, doi: 10.1021/acs.chemrev.8b00171.

[157] L. Chen, X. Wang, W. Lu, X. Wu, and J. Li, "Molecular imprinting: perspectives and applications," *Chem. Soc. Rev.*, vol. 45, no. 8, pp. 2137–2211, 2016, doi: 10.1039/C6CS00061D.

[158] P. Rebelo *et al.*, "Molecularly imprinted polymer-based electrochemical sensors for environmental analysis," *Biosens. Bioelectron.*, vol. 172, p. 112719, Jan. 2021, doi: 10.1016/j.bios.2020.112719.

[159] M. T. Jafari, B. Rezaei, and B. Zaker, "Ion Mobility Spectrometry as a Detector for Molecular Imprinted Polymer Separation and Metronidazole Determination in Pharmaceutical and Human Serum Samples," *Anal. Chem.*, vol. 81, no. 9, pp. 3585–3591, May 2009, doi: 10.1021/ac802557t.

[160] A.-M. Poller, E. Spieker, P. A. Lieberzeit, and C. Preininger, "Surface Imprints: Advantageous Application of Ready2use Materials for Bacterial Quartz-Crystal Microbalance Sensors," *ACS Appl. Mater. Interfaces*, vol. 9, no. 1, pp. 1129–1135, Jan. 2017, doi: 10.1021/acsami.6b13888.

[161] Y. Cheng and X. Dong, "Preparation of a molecularly imprinted fluorescent chemosensor using quinoline modified vinyl-β-cyclodextrin and acrylamide as

monomers for the selective recognition of spermidine," *Anal. Methods*, vol. 8, no. 29, pp. 5838–5842, Jul. 2016, doi: 10.1039/C6AY00984K.

[162] K. K. Reddy and K. V. Gobi, "Artificial molecular recognition material based biosensor for creatinine by electrochemical impedance analysis," *Sens. Actuators B Chem.*, vol. 183, pp. 356–363, Jul. 2013, doi: 10.1016/j.snb.2013.04.015.

[163] Z. Xu, G. Fang, and S. Wang, "Molecularly imprinted solid phase extraction coupled to high-performance liquid chromatography for determination of trace dichlorvos residues in vegetables," *Food Chem.*, vol. 119, no. 2, pp. 845–850, Mar. 2010, doi: 10.1016/j.foodchem.2009.08.047.

[164] A. Florea, C. Cristea, F. Vocanson, R. Săndulescu, and N. Jaffrezic-Renault, "Electrochemical sensor for the detection of estradiol based on electropolymerized molecularly imprinted polythioaniline film with signal amplification using gold nanoparticles," *Electrochem. Commun.*, vol. 59, pp. 36–39, Oct. 2015, doi: 10.1016/j.elecom.2015.06.021.

[165] I. Sadriu *et al.*, "Molecularly imprinted polymer modified glassy carbon electrodes for the electrochemical analysis of isoproturon in water," *Talanta*, vol. 207, p. 120222, Jan. 2020, doi: 10.1016/j.talanta.2019.120222.

[166] J. Ashley *et al.*, "Molecularly imprinted polymers for sample preparation and biosensing in food analysis: Progress and perspectives," *Biosens. Bioelectron.*, vol. 91, pp. 606–615, May 2017, doi: 10.1016/j.bios.2017.01.018.

[167] A. Speltini, A. Scalabrini, F. Maraschi, M. Sturini, and A. Profumo, "Newest applications of molecularly imprinted polymers for extraction of contaminants from environmental and food matrices: A review," *Anal. Chim. Acta*, vol. 974, pp. 1–26, 29 2017, doi: 10.1016/j.aca.2017.04.042.

[168] A. G. Mayes and K. Mosbach, "Molecularly Imprinted Polymer Beads: Suspension Polymerization Using a Liquid Perfluorocarbon as the Dispersing Phase," *Anal. Chem.*, vol. 68, no. 21, pp. 3769–3774, Nov. 1996, doi: 10.1021/ac960363a.

[169] V. Pichon and F. Chapuis-Hugon, "Role of molecularly imprinted polymers for selective determination of environmental pollutants--a review," *Anal. Chim. Acta*, vol. 622, no. 1–2, pp. 48–61, Aug. 2008, doi: 10.1016/j.aca.2008.05.057.

[170] V.-P. Vu *et al.*, "Possible detection of antibiotic residue using molecularly imprinted polyaniline-based sensor," *Vietnam J. Chem.*, p. 6.

[171] P. S. Sharma, A. Pietrzyk-Le, F. D'Souza, and W. Kutner, "Electrochemically synthesized polymers in molecular imprinting for chemical sensing," *Anal. Bioanal. Chem.*, vol. 402, no. 10, pp. 3177–3204, Apr. 2012, doi: 10.1007/s00216-011-5696-6.

[172] O. S. Ahmad, T. S. Bedwell, C. Esen, A. Garcia-Cruz, and S. A. Piletsky, "Molecularly Imprinted Polymers in Electrochemical and Optical Sensors," *Trends Biotechnol.*, vol. 37, no. 3, pp. 294–309, Mar. 2019, doi: 10.1016/j.tibtech.2018.08.009.

[173] J. W. Lowdon *et al.*, "MIPs for commercial application in low-cost sensors and assays – An overview of the current status quo," *Sens. Actuators B Chem.*, vol. 325, p. 128973, Dec. 2020, doi: 10.1016/j.snb.2020.128973.

[174] R. Suedee, C. Jantarat, W. Lindner, H. Viernstein, S. Songkro, and T. Srichana, "Development of a pH-responsive drug delivery system for enantioselective-controlled delivery of racemic drugs," *J. Controlled Release*, vol. 142, no. 1, pp. 122–131, Feb. 2010, doi: 10.1016/j.jconrel.2009.10.011.

[175] C. Warwick *et al.*, "Conductance based sensing and analysis of soluble phosphates in wastewater," *Biosens. Bioelectron.*, vol. 52, pp. 173–179, Feb. 2014, doi: 10.1016/j.bios.2013.08.048.

[176] S. Bruckenstein and M. Shay, "Experimental aspects of use of the quartz crystal microbalance in solution," *Electrochimica Acta*, vol. 30, no. 10, pp. 1295–1300, Oct. 1985, doi: 10.1016/0013-4686(85)85005-2.

[177] J. Cheng *et al.*, "Molecularly imprinted electrochemical sensor based on biomass carbon decorated with MOF-derived Cr2O3 and silver nanoparticles for selective and sensitive detection of nitrofurazone," *Chem. Eng. J.*, vol. 398, p. 125664, Oct. 2020, doi: 10.1016/j.cej.2020.125664.

[178] J. Dejeu, A. E. Taouil, P. Rougeot, S. Lakard, F. Lallemand, and B. Lakard, "Morphological and adhesive properties of polypyrrole films synthesized by sonoelectrochemical technique," *Synth. Met.*, vol. 160, no. 23, pp. 2540–2545, Dec. 2010, doi: 10.1016/j.synthmet.2010.10.002.

[179] Z. Guo *et al.*, "Molecularly Imprinted Polymer/Metal Organic Framework Based Chemical Sensors," *Coatings*, vol. 6, no. 4, p. 42, Dec. 2016, doi: 10.3390/coatings6040042.

[180] D. Capoferri *et al.*, "MIP-MEPS based sensing strategy for the selective assay of dimethoate. Application to wheat flour samples," *Talanta*, vol. 174, pp. 599–604, Nov. 2017, doi: 10.1016/j.talanta.2017.06.062.

[181] A. Ramanaviciene and A. Ramanavicius, "Molecularly imprinted polypyrrole-based synthetic receptor for direct detection of bovine leukemia virus glycoproteins," *Biosens. Bioelectron.*, vol. 20, no. 6, pp. 1076–1082, Dec. 2004, doi: 10.1016/j.bios.2004.05.014.

[182] A. Nezhadali, Z. Rouki, and M. Nezhadali, "Electrochemical preparation of a molecularly imprinted polypyrrole modified pencil graphite electrode for the determination of phenothiazine in model and real biological samples," *Talanta*, vol. 144, pp. 456–465, Nov. 2015, doi: 10.1016/j.talanta.2015.06.082.

[183] Y. Zhao *et al.*, "An electrochemical sensor for selective determination of sulfamethoxazole in surface water using a molecularly imprinted polymer modified BDD electrode," *Anal. Methods*, vol. 7, no. 6, pp. 2693–2698, Mar. 2015, doi: 10.1039/C4AY03055A.

[184] "Basic Overview of The Working Principle...," *EEWeb Community*. https://www.eeweb.com/app-notes/basic-overview-of-the-working-principle-of-a-potentiostat-galvanostat-pgstat-electrochemical-cell-setup (accessed Mar. 20, 2020).

[185] T. Shigemitsu, G. Matsumoto, and S. Tsukahara, "Electrical properties of glassy-carbon electrodes," *Med. Biol. Eng. Comput.*, vol. 17, no. 4, pp. 465–470, Jul. 1979, doi: 10.1007/BF02447059.

[186] G. A. Mabbott, "An introduction to cyclic voltammetry," *J. Chem. Educ.*, vol. 60, no. 9, p. 697, Sep. 1983, doi: 10.1021/ed060p697.

[187] G. A. M. Mersal, "Electrochemical Sensor for Voltammetric Determination of Catechol Based on Screen Printed Graphite Electrode," *Int J Electrochem Sci*, vol. 4, p. 11, 2009.

[188] V. Mirceski, R. Gulaboski, M. Lovric, I. Bogeski, R. Kappl, and M. Hoth, "Square-Wave Voltammetry: A Review on the Recent Progress," *Electroanalysis*, vol. 25, no. 11, pp. 2411–2422, Nov. 2013, doi: 10.1002/elan.201300369.

[189] A. Lasia, "Electrochemical Impedance Spectroscopy and its Applications," in *Modern Aspects of Electrochemistry*, B. E. Conway, J. O. Bockris, and R. E. White, Eds. Boston, MA: Springer US, 2002, pp. 143–248. doi: 10.1007/0-306-46916-2_2.

[190] X. Kan *et al.*, "Molecularly imprinted polymers based electrochemical sensor for bovine hemoglobin recognition," *Sens. Actuators B Chem.*, vol. 168, pp. 395–401, Jun. 2012, doi: 10.1016/j.snb.2012.04.043.

[191] H.-H. Li *et al.*, "A novel electrochemical sensor for epinephrine based on three dimensional molecularly imprinted polymer arrays," *Sens. Actuators B Chem.*, vol. 222, pp. 1127–1133, Jan. 2016, doi: 10.1016/j.snb.2015.08.018.

[192] J. Shen, T. Gan, Y. Jin, J. Wang, and K. Wu, "Electrochemical sensor based on electropolymerized dopamine molecularly imprinted film for tetrabromobisphenol A," *J. Electroanal. Chem.*, vol. 826, pp. 10–15, Oct. 2018, doi: 10.1016/j.jelechem.2018.08.019.

[193] G. Marrazza, "Piezoelectric biosensors for organophosphate and carbamate pesticides: a review," *Biosensors*, vol. 4, no. 3, pp. 301–317, Sep. 2014, doi: 10.3390/bios4030301.

[194] V. Syritski, J. Reut, A. Öpik, and K. Idla, "Environmental QCM sensors coated with polypyrrole," *Synth. Met.*, vol. 102, no. 1, pp. 1326–1327, Jun. 1999, doi: 10.1016/S0379-6779(98)01047-9.

[195] V. Ratautaite, D. Plausinaitis, I. Baleviciute, L. Mikoliunaite, A. Ramanaviciene, and A. Ramanavicius, "Characterization of caffeine-imprinted polypyrrole by a quartz crystal microbalance and electrochemical impedance spectroscopy," *Sens. Actuators B Chem.*, vol. 212, pp. 63–71, Jun. 2015, doi: 10.1016/j.snb.2015.01.109.

[196] L. F. Q. P. Marchesi, F. R. Simões, L. A. Pocrifka, and E. C. Pereira, "Investigation of Polypyrrole Degradation Using Electrochemical Impedance Spectroscopy," *J. Phys. Chem. B*, vol. 115, no. 31, pp. 9570–9575, Aug. 2011, doi: 10.1021/jp2041263.

[197] P. A. Topart, M. A. M. Noël, and H.-D. Liess, "High frequency impedance analysis of quartz crystal microbalances coated with conducting polymers," *Thin Solid Films*, vol. 239, no. 2, pp. 196–204, Mar. 1994, doi: 10.1016/0040-6090(94)90851-6.

[198] Z. Jusys, H. Massong, and H. Baltruschat, "A New Approach for Simultaneous DEMS and EQCM: Electro-oxidation of Adsorbed CO on Pt and Pt-Ru," *J. Electrochem. Soc.*, vol. 146, no. 3, pp. 1093–1098, Mar. 1999, doi: 10.1149/1.1391726.

[199] T.-R. Ling, Y. Z. Syu, Y.-C. Tasi, T.-C. Chou, and C.-C. Liu, "Size-selective recognition of catecholamines by molecular imprinting on silica–alumina gel," *Biosens. Bioelectron.*, vol. 21, no. 6, pp. 901–907, Dec. 2005, doi: 10.1016/j.bios.2005.02.009.

[200] K. Kotova, M. Hussain, G. Mustafa, and P. A. Lieberzeit, "MIP sensors on the way to biotech applications: Targeting selectivity," *Sens. Actuators B Chem.*, vol. 189, pp. 199–202, Dec. 2013, doi: 10.1016/j.snb.2013.03.040.

[201] S. Stankovich *et al.*, "Synthesis of graphene-based nanosheets via chemical reduction of exfoliated graphite oxide," *Carbon*, vol. 45, no. 7, pp. 1558–1565, Jun. 2007, doi: 10.1016/j.carbon.2007.02.034.

[202] L. Viau, J. Y. Hihn, S. Lakard, V. Moutarlier, V. Flaud, and B. Lakard, "Full characterization of polypyrrole thin films electrosynthesized in room temperature ionic liquids, water or acetonitrile," *Electrochimica Acta*, vol. 137, pp. 298–310, Aug. 2014, doi: 10.1016/j.electacta.2014.05.143.

[203] S. Golczak, A. Kanciurzewska, M. Fahlman, K. Langer, and J. J. Langer, "Comparative XPS surface study of polyaniline thin films," *Solid State Ion.*, vol. 179, no. 39, pp. 2234–2239, Dec. 2008, doi: 10.1016/j.ssi.2008.08.004.

[204] E. Beelen, J. Riga, and J. J. Verbist, "Electrochemical doping of polypyrrole: XPS study," *Synth. Met.*, vol. 41, no. 1, pp. 449–454, Apr. 1991, doi: 10.1016/0379-6779(91)91105-J.

[205] E. T. Kang, K. G. Neoh, Y. K. Ong, K. L. Tan, and B. T. G. Tan, "XPS studies of proton modification and some anion exchange processes in polypyrrole," *Synth. Met.*, vol. 39, no. 1, pp. 69–80, Oct. 1990, doi: 10.1016/0379-6779(90)90199-U.

[206] P. Manisankar, G. Selvanathan, and C. Vedhi, "Utilisation of polypyrrole modified electrode for the determination of pesticides," *Int. J. Environ. Anal. Chem.*, vol. 85, no. 6, pp. 409–422, May 2005, doi: 10.1080/03067310500050726.

[207] H. Hrichi, L. Monser, and N. Adhoum, "A novel electrochemical sensor based on electropolymerized molecularly imprinted poly(aniline-co-anthranilic acid) for sensitive detection of amlodipine," *J. Electroanal. Chem.*, vol. 805, pp. 133–145, Nov. 2017, doi: 10.1016/j.jelechem.2017.10.019.

[208] J. Luo, J. Huang, Y. Wu, J. Sun, W. Wei, and X. Liu, "Synthesis of hydrophilic and conductive molecularly imprinted polyaniline particles for the sensitive and selective protein detection," *Biosens. Bioelectron.*, vol. 94, pp. 39–46, Aug. 2017, doi: 10.1016/j.bios.2017.02.035.

[209] B. Schweiger, J. Kim, Y. J. Kim, and M. Ulbricht, "Electropolymerized molecularly imprinted polypyrrole film for sensing of clofibric acid," *Sensors*, vol. 15, no. 3, pp. 4870–4889, Feb. 2015, doi: 10.3390/s150304870.

[210] V. Suryanarayanan, C.-T. Wu, and K.-C. Ho, "Molecularly Imprinted Electrochemical Sensors," *Electroanalysis*, vol. 22, no. 16, pp. 1795–1811, 2010, doi: 10.1002/elan.200900616.

[211] K. P. Singh, R. K. Prajapati, S. Ahlawat, S. Ahlawat, M. Mungali, and S. Kumar, "Use of Isoproturon Imprinted Polymer Membranes as a Selective Recognition Platform in a Resistance Based Electrochemical Sensor," *Open J. Appl. Biosens.*, vol. 02, no. 01, pp. 20–28, 2013, doi: 10.4236/ojab.2013.21003.

[212] A. Fakhry, F. Pillier, and C. Debiemme-Chouvy, "Templateless electrogeneration of polypyrrole nanostructures: impact of the anionic composition and pH of the monomer solution," *J. Mater. Chem. A*, vol. 2, no. 25, pp. 9859–9865, Jun. 2014, doi: 10.1039/C4TA01360C.

[213] L. A. Tom, N. A. Schneck, and C. Walter, "Improving the imprinting effect by optimizing template:monomer:cross-linker ratios in a molecularly imprinted polymer for sulfadimethoxine," *J. Chromatogr. B*, vol. 909, pp. 61–64, Nov. 2012, doi: 10.1016/j.jchromb.2012.10.020.

[214] Z. Guo, S. Du, M. Li, and W. Zhao, "Exploring GIS knowledge to improve building extraction and change detection from VHR imagery in urban areas," *Int. J. Image Data Fusion*, vol. 7, no. 1, pp. 42–62, Jan. 2016, doi: 10.1080/19479832.2015.1051138.

[215] Y. Li, *Organic Optoelectronic Materials*. Springer, 2015.

[216] R. Ansari, "Polypyrrole Conducting Electroactive Polymers: Synthesis and Stability Studies," *E-Journal of Chemistry*, 3. https://www.hindawi.com/journals/jchem/2006/860413/ (accessed Apr. 15, 2020).

[217] A. J. Downard and D. Pletcher, "The influence of water on the electrodeposition of polypyrrole in acetonitrile," *J. Electroanal. Chem. Interfacial Electrochem.*, vol. 206, no. 1, pp. 139–145, Jul. 1986, doi: 10.1016/0022-0728(86)90263-9.

[218] R. Loos *et al.*, "EU-wide monitoring survey on emerging polar organic contaminants in wastewater treatment plant effluents," *Water Res.*, vol. 47, no. 17, pp. 6475–6487, Nov. 2013, doi: 10.1016/j.watres.2013.08.024.

[219] A. Orlikowska, K. Fisch, and D. E. Schulz-Bull, "Organic polar pollutants in surface waters of inland seas," *Mar. Pollut. Bull.*, vol. 101, no. 2, pp. 860–866, Dec. 2015, doi: 10.1016/j.marpolbul.2015.11.018.

[220] A. Ramanavičius, A. Ramanavičienė, and A. Malinauskas, "Electrochemical sensors based on conducting polymer—polypyrrole," *Electrochimica Acta*, vol. 51, no. 27, pp. 6025–6037, Aug. 2006, doi: 10.1016/j.electacta.2005.11.052.

[221] N. Maouche, M. Guergouri, S. Gam-Derouich, M. Jouini, B. Nessark, and M. M. Chehimi, "Molecularly imprinted polypyrrole films: Some key parameters for

electrochemical picomolar detection of dopamine," *J. Electroanal. Chem.*, vol. 685, pp. 21–27, Oct. 2012, doi: 10.1016/j.jelechem.2012.08.020.

[222] J. Xu, Y. Zhang, K. Wu, L. Zhang, S. Ge, and J. Yu, "A molecularly imprinted polypyrrole for ultrasensitive voltammetric determination of glyphosate," *Microchim. Acta*, vol. 184, no. 7, pp. 1959–1967, Jul. 2017, doi: 10.1007/s00604-017-2200-9.

[223] N. M. Bergmann and N. A. Peppas, "Molecularly imprinted polymers with specific recognition for macromolecules and proteins," *Prog. Polym. Sci.*, vol. 33, no. 3, pp. 271–288, Mar. 2008, doi: 10.1016/j.progpolymsci.2007.09.004.

[224] Z. Yang, X. Liu, Y. Wu, and C. Zhang, "Modification of carbon aerogel electrode with molecularly imprinted polypyrrole for electrochemical determination of dopamine," *Sens. Actuators B Chem.*, vol. 212, pp. 457–463, Jun. 2015, doi: 10.1016/j.snb.2015.02.057.

[225] C.-J. Zhao, X.-H. Ma, and J.-P. Li, "An Insulin Molecularly Imprinted Electrochemical Sensor Based on Epitope Imprinting," *Chin. J. Anal. Chem.*, vol. 45, no. 9, pp. 1360–1366, Sep. 2017, doi: 10.1016/S1872-2040(17)61039-9.

[226] X. Kan *et al.*, "Molecularly imprinted polymers based electrochemical sensor for bovine hemoglobin recognition," *Sens. Actuators B Chem.*, vol. 168, pp. 395–401, Jun. 2012, doi: 10.1016/j.snb.2012.04.043.

[227] J. Tabačiarová, M. Mičušík, P. Fedorko, and M. Omastová, "Study of polypyrrole aging by XPS, FTIR and conductivity measurements," *Polym. Degrad. Stab.*, vol. C, no. 120, pp. 392–401, 2015, doi: 10.1016/j.polymdegradstab.2015.07.021.

[228] P. Pfluger and G. B. Street, "Chemical, electronic, and structural properties of conducting heterocyclic polymers: A view by XPS," *J. Chem. Phys.*, vol. 80, no. 1, pp. 544–553, Jan. 1984, doi: 10.1063/1.446428.

[229] D. Yang *et al.*, "Chemical analysis of graphene oxide films after heat and chemical treatments by X-ray photoelectron and Micro-Raman spectroscopy," *Carbon*, vol. 47, no. 1, pp. 145–152, Jan. 2009, doi: 10.1016/j.carbon.2008.09.045.

[230] M. J. Allen, V. C. Tung, and R. B. Kaner, "Honeycomb Carbon: A Review of Graphene," *Chem. Rev.*, vol. 110, no. 1, pp. 132–145, Jan. 2010, doi: 10.1021/cr900070d.

[231] J. C. Slonczewski and P. R. Weiss, "Band Structure of Graphite," *Phys. Rev.*, vol. 109, no. 2, pp. 272–279, Jan. 1958, doi: 10.1103/PhysRev.109.272.

[232] R. Lakshmanan and N. Maulik, "Graphene-based drug delivery systems in tissue engineering and nanomedicine," *Can. J. Physiol. Pharmacol.*, vol. 96, no. 9, pp. 869–878, Sep. 2018, doi: 10.1139/cjpp-2018-0225.

[233] K. S. Novoselov, "Electric Field Effect in Atomically Thin Carbon Films," *Science*, vol. 306, no. 5696, pp. 666–669, Oct. 2004, doi: 10.1126/science.1102896.

[234] W. Ren and H.-M. Cheng, "The global growth of graphene," *Nat. Nanotechnol.*, vol. 9, no. 10, Art. no. 10, Oct. 2014, doi: 10.1038/nnano.2014.229.

[235] A. K. Geim and K. S. Novoselov, "The rise of graphene," *Nat. Mater.*, vol. 6, no. 3, Art. no. 3, Mar. 2007, doi: 10.1038/nmat1849.

[236] J. Zhu, D. Yang, Z. Yin, Q. Yan, and H. Zhang, "Graphene and Graphene-Based Materials for Energy Storage Applications," *Small*, vol. 10, no. 17, pp. 3480–3498, 2014, doi: https://doi.org/10.1002/smll.201303202.

[237] G. R. Bhimanapati *et al.*, "Recent Advances in Two-Dimensional Materials beyond Graphene," *ACS Nano*, vol. 9, no. 12, pp. 11509–11539, Dec. 2015, doi: 10.1021/acsnano.5b05556.

[238] S. Gilje, S. Han, M. Wang, K. L. Wang, and R. B. Kaner, "A chemical route to graphene for device applications," *Nano Lett.*, vol. 7, no. 11, pp. 3394–3398, Nov. 2007, doi: 10.1021/nl0717715.

[239] C. Mattevi *et al.*, "Evolution of Electrical, Chemical, and Structural Properties of Transparent and Conducting Chemically Derived Graphene Thin Films," *Adv. Funct. Mater.*, vol. 19, no. 16, pp. 2577–2583, 2009, doi: https://doi.org/10.1002/adfm.200900166.

[240] G. Eda and M. Chhowalla, "Chemically Derived Graphene Oxide: Towards Large-Area Thin-Film Electronics and Optoelectronics," *Adv. Mater.*, vol. 22, no. 22, pp. 2392–2415, 2010, doi: https://doi.org/10.1002/adma.200903689.

[241] V. Georgakilas *et al.*, "Functionalization of Graphene: Covalent and Non-Covalent Approaches, Derivatives and Applications," *Chem. Rev.*, vol. 112, no. 11, pp. 6156–6214, Nov. 2012, doi: 10.1021/cr3000412.

[242] D. Krishnan *et al.*, "Energetic graphene oxide: Challenges and opportunities," *Nano Today*, vol. 7, no. 2, pp. 137–152, Apr. 2012, doi: 10.1016/j.nantod.2012.02.003.

[243] Y. L. Zhong, Z. Tian, G. P. Simon, and D. Li, "Scalable production of graphene via wet chemistry: progress and challenges," *Mater. Today*, vol. 18, no. 2, pp. 73–78, Mar. 2015, doi: 10.1016/j.mattod.2014.08.019.

[244] A. Catheline *et al.*, "Graphene solutions," *Chem. Commun.*, vol. 47, no. 19, p. 5470, 2011, doi: 10.1039/c1cc11100k.

[245] W. S. Hummers and R. E. Offeman, "Preparation of Graphitic Oxide," *J. Am. Chem. Soc.*, vol. 80, no. 6, pp. 1339–1339, Mar. 1958, doi: 10.1021/ja01539a017.

[246] C. Gómez-Navarro *et al.*, "Electronic Transport Properties of Individual Chemically Reduced Graphene Oxide Sheets," *Nano Lett.*, vol. 7, no. 11, pp. 3499–3503, Nov. 2007, doi: 10.1021/nl072090c.

[247] J. Wang, K. K. Manga, Q. Bao, and K. P. Loh, "High-Yield Synthesis of Few-Layer Graphene Flakes through Electrochemical Expansion of Graphite in Propylene Carbonate Electrolyte," *J. Am. Chem. Soc.*, vol. 133, no. 23, pp. 8888–8891, Jun. 2011, doi: 10.1021/ja203725d.

[248] D. Wei *et al.*, "Graphene from electrochemical exfoliation and its direct applications in enhanced energy storage devices," *Chem. Commun.*, vol. 48, no. 9, pp. 1239–1241, Jan. 2012, doi: 10.1039/C2CC16859F.

[249] Y. Shang, D. Zhang, Y. Liu, and Y. Liu, "Simultaneous synthesis of diverse graphene via electrochemical reduction of graphene oxide," *J. Appl. Electrochem.*, vol. 45, no. 5, pp. 453–462, May 2015, doi: 10.1007/s10800-015-0818-z.

[250] J. Lu, J. Yang, J. Wang, A. Lim, S. Wang, and K. P. Loh, "One-Pot Synthesis of Fluorescent Carbon Nanoribbons, Nanoparticles, and Graphene by the Exfoliation of Graphite in Ionic Liquids," *ACS Nano*, vol. 3, no. 8, pp. 2367–2375, Aug. 2009, doi: 10.1021/nn900546b.

[251] Y. Hernandez *et al.*, "High-yield production of graphene by liquid-phase exfoliation of graphite," *Nat. Nanotechnol.*, vol. 3, no. 9, pp. 563–568, Sep. 2008, doi: 10.1038/nnano.2008.215.

[252] P. K. Ang, S. Wang, Q. Bao, J. T. L. Thong, and K. P. Loh, "High-Throughput Synthesis of Graphene by Intercalation−Exfoliation of Graphite Oxide and Study of Ionic Screening in Graphene Transistor," *ACS Nano*, vol. 3, no. 11, pp. 3587–3594, Nov. 2009, doi: 10.1021/nn901111s.

[253] W. W. Liu and J. N. Wang, "Direct exfoliation of graphene in organic solvents with addition of NaOH," *Chem. Commun.*, vol. 47, no. 24, pp. 6888–6890, Jun. 2011, doi: 10.1039/C1CC11933H.

[254] X. Wang *et al.*, "Direct exfoliation of natural graphite into micrometre size few layers graphene sheets using ionic liquids," *Chem. Commun.*, vol. 46, no. 25, pp. 4487–4489, Jun. 2010, doi: 10.1039/C0CC00799D.

[255] G. M. Morales *et al.*, "High-quality few layer graphene produced by electrochemical intercalation and microwave-assisted expansion of graphite," *Carbon*, vol. 49, no. 8, pp. 2809–2816, Jul. 2011, doi: 10.1016/j.carbon.2011.03.008.

[256] M. Zhou, J. Tang, Q. Cheng, G. Xu, P. Cui, and L.-C. Qin, "Few-layer graphene obtained by electrochemical exfoliation of graphite cathode," *Chem. Phys. Lett.*, vol. 572, pp. 61–65, May 2013, doi: 10.1016/j.cplett.2013.04.013.

[257] N. Liu, F. Luo, H. Wu, Y. Liu, C. Zhang, and J. Chen, "One-Step Ionic-Liquid-Assisted Electrochemical Synthesis of Ionic-Liquid-Functionalized Graphene Sheets Directly from Graphite," *Adv. Funct. Mater.*, vol. 18, no. 10, pp. 1518–1525, May 2008, doi: 10.1002/adfm.200700797.

[258] W. Sirisaksoontorn, A. A. Adenuga, V. T. Remcho, and M. M. Lerner, "Preparation and Characterization of a Tetrabutylammonium Graphite Intercalation Compound," *J. Am. Chem. Soc.*, vol. 133, no. 32, pp. 12436–12438, Aug. 2011, doi: 10.1021/ja2053539.

[259] G. Bernard and J. Simonet, "Irreversible cathodic behavior of graphite in the presence of some mixtures of onium salts," *J. Electroanal. Chem. Interfacial Electrochem.*, vol. 96, no. 2, pp. 249–253, Feb. 1979, doi: 10.1016/S0022-0728(79)80383-6.

[260] J. Simonet and H. Lund, "Electrochemical behaviour of graphite cathodes in the presence of tetraalkylammonium cations," *J. Electroanal. Chem. Interfacial*

Electrochem., vol. 75, no. 2, pp. 719–730, Jan. 1977, doi: 10.1016/S0022-0728(77)80211-8.

[261] J. O. Besenhard and H. P. Fritz, "Cathodic reduction of graphite in organic solutions of alkali and NR4+ salts," *J. Electroanal. Chem. Interfacial Electrochem.*, vol. 53, no. 2, pp. 329–333, Jun. 1974, doi: 10.1016/S0022-0728(74)80146-4.

[262] J. O. Besenhard, "The electrochemical preparation and properties of ionic alkali metal-and NR4-graphite intercalation compounds in organic electrolytes," *Carbon*, vol. 14, no. 2, pp. 111–115, Jan. 1976, doi: 10.1016/0008-6223(76)90119-6.

[263] J. O. Besenhard, H. Möhwald, and J. J. Nickl, "Electronic conductivity and structure of DMSO-solvated A+ - and NR4+-graphite intercalation compounds," *Carbon*, vol. 18, no. 6, pp. 399–405, Jan. 1980, doi: 10.1016/0008-6223(80)90031-7.

[264] D. C. Marcano *et al.*, "Improved Synthesis of Graphene Oxide," *ACS Nano*, vol. 4, no. 8, pp. 4806–4814, Aug. 2010, doi: 10.1021/nn1006368.

[265] I. Jung *et al.*, "Simple Approach for High-Contrast Optical Imaging and Characterization of Graphene-Based Sheets," *Nano Lett.*, vol. 7, no. 12, pp. 3569–3575, Dec. 2007, doi: 10.1021/nl0714177.

[266] Z. Wang, X. Zhou, J. Zhang, F. Boey, and H. Zhang, "Direct Electrochemical Reduction of Single-Layer Graphene Oxide and Subsequent Functionalization with Glucose Oxidase," *J. Phys. Chem. C*, vol. 113, no. 32, pp. 14071–14075, Aug. 2009, doi: 10.1021/jp906348x.

[267] L. Gomez De Arco, Y. Zhang, C. W. Schlenker, K. Ryu, M. E. Thompson, and C. Zhou, "Continuous, Highly Flexible, and Transparent Graphene Films by Chemical Vapor Deposition for Organic Photovoltaics," *ACS Nano*, vol. 4, no. 5, pp. 2865–2873, May 2010, doi: 10.1021/nn901587x.

[268] J. Kim, F. Kim, and J. Huang, "Seeing graphene-based sheets," *Mater. Today*, vol. 13, no. 3, pp. 28–38, Mar. 2010, doi: 10.1016/S1369-7021(10)70031-6.

[269] S. Pei and H.-M. Cheng, "The reduction of graphene oxide," *Carbon*, vol. 50, no. 9, pp. 3210–3228, Aug. 2012, doi: 10.1016/j.carbon.2011.11.010.

[270] J. Liu *et al.*, "Fabrication of Flexible, All-Reduced Graphene Oxide Non-Volatile Memory Devices," *Adv. Mater.*, vol. 25, no. 2, pp. 233–238, 2013, doi: https://doi.org/10.1002/adma.201203349.

[271] J.-Y. Kim *et al.*, "Chlorination of Reduced Graphene Oxide Enhances the Dielectric Constant of Reduced Graphene Oxide/Polymer Composites," *Adv. Mater.*, vol. 25, no. 16, pp. 2308–2313, 2013, doi: https://doi.org/10.1002/adma.201300385.

[272] L. Liu *et al.*, "Electrochemically 'Writing' Graphene from Graphene Oxide," *Small*, vol. 10, no. 17, pp. 3555–3559, 2014, doi: https://doi.org/10.1002/smll.201301953.

[273] K. Parvez *et al.*, "Exfoliation of Graphite into Graphene in Aqueous Solutions of Inorganic Salts," *J. Am. Chem. Soc.*, vol. 136, no. 16, pp. 6083–6091, Apr. 2014, doi: 10.1021/ja5017156.

[274] A. J. Cooper, N. R. Wilson, I. A. Kinloch, and R. A. W. Dryfe, "Single stage electrochemical exfoliation method for the production of few-layer graphene via intercalation of tetraalkylammonium cations," *Carbon*, vol. 66, pp. 340–350, Jan. 2014, doi: 10.1016/j.carbon.2013.09.009.

[275] A. M. Abdelkader, I. A. Kinloch, and R. A. W. Dryfe, "Continuous Electrochemical Exfoliation of Micrometer-Sized Graphene Using Synergistic Ion Intercalations and Organic Solvents," *ACS Appl. Mater. Interfaces*, vol. 6, no. 3, pp. 1632–1639, Feb. 2014, doi: 10.1021/am404497n.

[276] Md. S. A. Bhuyan, Md. N. Uddin, Md. M. Islam, F. A. Bipasha, and S. S. Hossain, "Synthesis of graphene," *Int. Nano Lett.*, vol. 6, no. 2, pp. 65–83, Jun. 2016, doi: 10.1007/s40089-015-0176-1.

[277] V. C. Tung, M. J. Allen, Y. Yang, and R. B. Kaner, "High-throughput solution processing of large-scale graphene," *Nat. Nanotechnol.*, vol. 4, no. 1, Art. no. 1, Jan. 2009, doi: 10.1038/nnano.2008.329.

[278] M. C. Kim, G. S. Hwang, and R. S. Ruoff, "Epoxide reduction with hydrazine on graphene: A first principles study," *J. Chem. Phys.*, vol. 131, no. 6, p. 064704, 2009, doi: 10.1063/1.3197007.

[279] X. Miao *et al.*, "High Efficiency Graphene Solar Cells by Chemical Doping," *Nano Lett.*, vol. 12, no. 6, pp. 2745–2750, Jun. 2012, doi: 10.1021/nl204414u.

[280] S. Pang, Y. Hernandez, X. Feng, and K. Müllen, "Graphene as Transparent Electrode Material for Organic Electronics," *Adv. Mater.*, vol. 23, no. 25, pp. 2779–2795, Jul. 2011, doi: 10.1002/adma.201100304.

[281] T. O. Wehling *et al.*, "Molecular Doping of Graphene," *Nano Lett.*, vol. 8, no. 1, pp. 173–177, Jan. 2008, doi: 10.1021/nl072364w.

[282] C. J. Raj, R. Manikandan, W.-G. Lee, W.-J. Cho, K. H. Yu, and B. C. Kim, "Polypyrrole thin film on electrochemically modified graphite surface for mechanically stable and high-performance supercapacitor electrodes," *Electrochimica Acta*, vol. 283, pp. 1543–1550, Sep. 2018, doi: 10.1016/j.electacta.2018.07.091.

[283] F. Beck, H. Junge, and H. Krohn, "Graphite intercalation compounds as positive electrodes in galvanic cells," *Electrochimica Acta*, vol. 26, no. 7, pp. 799–809, Jul. 1981, doi: 10.1016/0013-4686(81)85038-4.

[284] F. Beck, J. Jiang, and H. Krohn, "Potential oscillations during galvanostatic overoxidation of graphite in aqueous sulphuric acids," *J. Electroanal. Chem.*, vol. 389, no. 1, pp. 161–165, Jun. 1995, doi: 10.1016/0022-0728(95)03870-M.

[285] C. A. Goss, J. C. Brumfield, E. A. Irene, and R. W. Murray, "Imaging the incipient electrochemical oxidation of highly oriented pyrolytic graphite," *Anal. Chem.*, vol. 65, no. 10, pp. 1378–1389, May 1993, doi: 10.1021/ac00058a014.

[286] S. Park, J. An, J. R. Potts, A. Velamakanni, S. Murali, and R. S. Ruoff, "Hydrazine-reduction of graphite- and graphene oxide," *Carbon*, vol. 49, no. 9, pp. 3019–3023, Aug. 2011, doi: 10.1016/j.carbon.2011.02.071.

[287] D. Li, M. B. Müller, S. Gilje, R. B. Kaner, and G. G. Wallace, "Processable aqueous dispersions of graphene nanosheets," *Nat. Nanotechnol.*, vol. 3, no. 2, pp. 101–105, Feb. 2008, doi: 10.1038/nnano.2007.451.

[288] G. Eda, G. Fanchini, and M. Chhowalla, "Large-area ultrathin films of reduced graphene oxide as a transparent and flexible electronic material," *Nat. Nanotechnol.*, vol. 3, no. 5, pp. 270–274, May 2008, doi: 10.1038/nnano.2008.83.

[289] X. Fan *et al.*, "Deoxygenation of Exfoliated Graphite Oxide under Alkaline Conditions: A Green Route to Graphene Preparation," *Adv. Mater.*, vol. 20, no. 23, pp. 4490–4493, 2008, doi: https://doi.org/10.1002/adma.200801306.

[290] Z. Sun, Z. Yan, J. Yao, E. Beitler, Y. Zhu, and J. M. Tour, "Growth of graphene from solid carbon sources," *Nature*, vol. 468, no. 7323, pp. 549–552, Nov. 2010, doi: 10.1038/nature09579.

[291] Q. Yu *et al.*, "Control and characterization of individual grains and grain boundaries in graphene grown by chemical vapour deposition," *Nat. Mater.*, vol. 10, no. 6, pp. 443–449, Jun. 2011, doi: 10.1038/nmat3010.

[292] M. Zhou *et al.*, "Controlled Synthesis of Large-Area and Patterned Electrochemically Reduced Graphene Oxide Films," *Chem. – Eur. J.*, vol. 15, no. 25, pp. 6116–6120, Jun. 2009, doi: 10.1002/chem.200900596.

[293] M. Hakimi and P. Alimard, "Graphene: Synthesis and Applications in Biotechnology - A Review," *World Appl. Program.*, p. 13.

[294] S. Stankovich, R. D. Piner, X. Chen, N. Wu, S. T. Nguyen, and R. S. Ruoff, "Stable aqueous dispersions of graphitic nanoplatelets via the reduction of exfoliated graphite oxide in the presence of poly(sodium 4-styrenesulfonate)," *J Mater Chem*, vol. 16, no. 2, pp. 155–158, 2006, doi: 10.1039/B512799H.

[295] A. B. Bourlinos, D. Gournis, D. Petridis, T. Szabó, A. Szeri, and I. Dékány, "Graphite Oxide: Chemical Reduction to Graphite and Surface Modification with Primary Aliphatic Amines and Amino Acids," *Langmuir*, vol. 19, no. 15, pp. 6050–6055, Jul. 2003, doi: 10.1021/la026525h.

[296] S. Wang *et al.*, "Band-like Transport in Surface-Functionalized Highly Solution-Processable Graphene Nanosheets," *Adv. Mater.*, vol. 20, no. 18, pp. 3440–3446, 2008, doi: https://doi.org/10.1002/adma.200800279.

[297] Z.-S. Wu, W. Ren, L. Gao, B. Liu, C. Jiang, and H.-M. Cheng, "Synthesis of high-quality graphene with a pre-determined number of layers," *Carbon*, vol. 47, no. 2, pp. 493–499, Feb. 2009, doi: 10.1016/j.carbon.2008.10.031.

[298] M. J. McAllister *et al.*, "Single Sheet Functionalized Graphene by Oxidation and Thermal Expansion of Graphite," *Chem. Mater.*, vol. 19, no. 18, pp. 4396–4404, Sep. 2007, doi: 10.1021/cm0630800.

[299] C. Vallés *et al.*, "Solutions of Negatively Charged Graphene Sheets and Ribbons," *J. Am. Chem. Soc.*, vol. 130, no. 47, pp. 15802–15804, Nov. 2008, doi: 10.1021/ja808001a.

[300] S. Giordani *et al.*, "Debundling of Single-Walled Nanotubes by Dilution: Observation of Large Populations of Individual Nanotubes in Amide Solvent Dispersions," *J. Phys. Chem. B*, vol. 110, no. 32, pp. 15708–15718, Aug. 2006, doi: 10.1021/jp0626216.

[301] B. J. Landi, H. J. Ruf, J. J. Worman, and R. P. Raffaelle, "Effects of Alkyl Amide Solvents on the Dispersion of Single-Wall Carbon Nanotubes," *J. Phys. Chem. B*, vol. 108, no. 44, pp. 17089–17095, Nov. 2004, doi: 10.1021/jp047521j.

[302] T. Hasan, V. Scardaci, P. Tan, A. G. Rozhin, W. I. Milne, and A. C. Ferrari, "Stabilization and 'Debundling' of Single-Wall Carbon Nanotube Dispersions in N-Methyl-2-pyrrolidone (NMP) by Polyvinylpyrrolidone (PVP)," *J. Phys. Chem. C*, vol. 111, no. 34, pp. 12594–12602, Aug. 2007, doi: 10.1021/jp0723012.

[303] S. D. Bergin *et al.*, "Exfoliation in ecstasy: liquid crystal formation and concentration-dependent debundling observed for single-wall nanotubes dispersed in the liquid drug γ-butyrolactone," *Nanotechnology*, vol. 18, no. 45, p. 455705, Nov. 2007, doi: 10.1088/0957-4484/18/45/455705.

[304] K. Krishnamoorthy, M. Veerapandian, K. Yun, and S.-J. Kim, "The chemical and structural analysis of graphene oxide with different degrees of oxidation," *Carbon*, vol. 53, pp. 38–49, Mar. 2013, doi: 10.1016/j.carbon.2012.10.013.

[305] H. Ago *et al.*, "Work Functions and Surface Functional Groups of Multiwall Carbon Nanotubes," *J. Phys. Chem. B*, vol. 103, no. 38, pp. 8116–8121, Sep. 1999, doi: 10.1021/jp991659y.

[306] D. W. Lee and J. W. Seo, "sp2/sp3 Carbon Ratio in Graphite Oxide with Different Preparation Times," *J. Phys. Chem. C*, vol. 115, no. 6, pp. 2705–2708, Feb. 2011, doi: 10.1021/jp107906u.

[307] T. Livneh, T. L. Haslett, and M. Moskovits, "Distinguishing disorder-induced bands from allowed Raman bands in graphite," *Phys. Rev. B*, vol. 66, no. 19, p. 195110, Nov. 2002, doi: 10.1103/PhysRevB.66.195110.

[308] M. S. Dresselhaus, A. Jorio, M. Hofmann, G. Dresselhaus, and R. Saito, "Perspectives on Carbon Nanotubes and Graphene Raman Spectroscopy," *Nano Lett.*, vol. 10, no. 3, pp. 751–758, Mar. 2010, doi: 10.1021/nl904286r.

[309] K. Krishnamoorthy, U. Navaneethaiyer, R. Mohan, J. Lee, and S.-J. Kim, "Graphene oxide nanostructures modified multifunctional cotton fabrics," *Appl. Nanosci.*, vol. 2, no. 2, pp. 119–126, Jun. 2012, doi: 10.1007/s13204-011-0045-9.

[310] G. Venugopal, K. Krishnamoorthy, R. Mohan, and S.-J. Kim, "An investigation of the electrical transport properties of graphene-oxide thin films," *Mater. Chem. Phys.*, vol. 132, no. 1, pp. 29–33, Jan. 2012, doi: 10.1016/j.matchemphys.2011.10.040.

[311] K. Parvez *et al.*, "Electrochemically Exfoliated Graphene as Solution-Processable, Highly Conductive Electrodes for Organic Electronics," *ACS Nano*, vol. 7, no. 4, pp. 3598–3606, Apr. 2013, doi: 10.1021/nn400576v.

[312] F. Shi, Z. Song, P. N. Ross, G. A. Somorjai, R. O. Ritchie, and K. Komvopoulos, "Failure mechanisms of single-crystal silicon electrodes in lithium-ion batteries," *Nat. Commun.*, vol. 7, no. 1, Art. no. 1, Jun. 2016, doi: 10.1038/ncomms11886.

[313] Piehong. Chen, M. A. Fryling, and R. L. McCreery, "Electron Transfer Kinetics at Modified Carbon Electrode Surfaces: The Role of Specific Surface Sites," *Anal. Chem.*, vol. 67, no. 18, pp. 3115–3122, Sep. 1995, doi: 10.1021/ac00114a004.

[314] N. A. Choudhry, R. O. Kadara, and C. E. Banks, "'Cosmetic electrochemistry': the facile production of graphite microelectrode ensembles," *Phys. Chem. Chem. Phys.*, vol. 12, no. 10, pp. 2285–2287, Feb. 2010, doi: 10.1039/B923246J.

[315] K. Ngamchuea, S. Eloul, K. Tschulik, and R. G. Compton, "Planar diffusion to macro disc electrodes—what electrode size is required for the Cottrell and Randles-Sevcik equations to apply quantitatively?," *J. Solid State Electrochem.*, vol. 18, no. 12, pp. 3251–3257, Dec. 2014, doi: 10.1007/s10008-014-2664-z.

[316] A. W. Bott, "Fitting Experimental Cyclic Voltammetry Data with Theoretical Simulations Using DigiSim® 2.," *Curr. Sep.*, p. 5, 1996.

[317] S. Ranganathan and R. L. McCreery, "Electroanalytical Performance of Carbon Films with Near-Atomic Flatness," *Anal. Chem.*, vol. 73, no. 5, pp. 893–900, Mar. 2001, doi: 10.1021/ac0007534.

[318] P. Chen and R. L. McCreery, "Control of Electron Transfer Kinetics at Glassy Carbon Electrodes by Specific Surface Modification," *Anal. Chem.*, vol. 68, no. 22, pp. 3958–3965, Jan. 1996, doi: 10.1021/ac960492r.

[319] S. H. DuVall and R. L. McCreery, "Self-catalysis by Catechols and Quinones during Heterogeneous Electron Transfer at Carbon Electrodes," *J. Am. Chem. Soc.*, vol. 122, no. 28, pp. 6759–6764, Jul. 2000, doi: 10.1021/ja000227u.

[320] C. E. Banks, T. J. Davies, G. G. Wildgoose, and R. G. Compton, "Electrocatalysis at graphite and carbon nanotube modified electrodes: edge-plane sites and tube ends are the reactive sites," *Chem. Commun.*, vol. 0, no. 7, pp. 829–841, 2005, doi: 10.1039/B413177K.

[321] R. Sharma, J. H. Baik, C. J. Perera, and M. S. Strano, "Anomalously Large Reactivity of Single Graphene Layers and Edges toward Electron Transfer Chemistries," *Nano Lett.*, vol. 10, no. 2, pp. 398–405, Feb. 2010, doi: 10.1021/nl902741x.

[322] J.-H. Zhong *et al.*, "Quantitative Correlation between Defect Density and Heterogeneous Electron Transfer Rate of Single Layer Graphene," *J. Am. Chem. Soc.*, vol. 136, no. 47, pp. 16609–16617, Nov. 2014, doi: 10.1021/ja508965w.

[323] A. Shrivastava and V. Gupta, "Methods for the determination of limit of detection and limit of quantitation of the analytical methods," *Chron. Young Sci.*, vol. 2, no. 1, pp. 21–21, Jan. 2011.

[324] S. Kröger, A. P. F. Turner, K. Mosbach, and K. Haupt, "Imprinted Polymer-Based Sensor System for Herbicides Using Differential-Pulse Voltammetry on Screen-

Printed Electrodes," *Anal. Chem.*, vol. 71, no. 17, pp. 3698–3702, Sep. 1999, doi: 10.1021/ac9811827.

[325] B. Lu, M. Liu, H. Shi, X. Huang, and G. Zhao, "A Novel Photoelectrochemical Sensor for Bisphenol A with High Sensitivity and Selectivity Based on Surface Molecularly Imprinted Polypyrrole Modified TiO2 Nanotubes," *Electroanalysis*, vol. 25, no. 3, pp. 771–779, 2013, doi: https://doi.org/10.1002/elan.201200585.

[326] B. Rezaei, M. Khalili Boroujeni, and A. A. Ensafi, "Caffeine electrochemical sensor using imprinted film as recognition element based on polypyrrole, sol-gel, and gold nanoparticles hybrid nanocomposite modified pencil graphite electrode," *Biosens. Bioelectron.*, vol. 60, pp. 77–83, Oct. 2014, doi: 10.1016/j.bios.2014.03.028.

[327] M. Khadem *et al.*, "Modification of Carbon Paste Electrode Based on Molecularly Imprinted Polymer for Electrochemical Determination of Diazinon in Biological and Environmental Samples," *Electroanalysis*, vol. 29, no. 3, pp. 708–715, 2017, doi: https://doi.org/10.1002/elan.201600293.

[328] S. J. Shahtaheri, F. Faridbod, and M. Khadem, "Highly Selective Voltammetric Sensor Based on Molecularly Imprinted Polymer and Carbon Nanotubes to Determine the Dicloran Pesticide in Biological and Environmental Samples," *Procedia Technol.*, vol. 27, pp. 96–97, Jan. 2017, doi: 10.1016/j.protcy.2017.04.041.

[329] M. E. Khalifa and A. B. Abdallah, "Molecular imprinted polymer based sensor for recognition and determination of profenofos organophosphorous insecticide," *Biosens. Bioelectron. X*, p. 100027, Aug. 2019, doi: 10.1016/j.biosx.2019.100027.

Imer SADRIU

Elaboration de capteurs environnementaux à base de graphène fonctionnalisé par des polymères à empreintes moléculaires permettant la détection de pesticides dans les eaux

Résumé

Dans cette thèse, nous avons développé des électrodes de carbone vitreux modifiées par des films minces de polypyrrole à empreinte moléculaire (MIP-PPy) dédiées à l'analyse électrochimique d'un herbicide, l'isoproturon. Les limites de détection obtenues en condition de laboratoire sont de l'ordre des seuils imposés pour ce micropolluant dans la directive cadre européenne sur l'eau. Enfin une méthode de préparation de nouvelles électrodes constituées de 100% de graphène électrochimique a été mise au point. Ces électrodes graphène ont été modifiées par électropolymérisation de MIP-PPYR avec succès et les premiers résultats portant sur leur application à l'analyse de l'isoproturon sont très prometteurs pour leur intégration dans des capteurs environnementaux.

Mots clés: Capteurs Électrochimiques, Polymères à Empreinte Moléculaire (MIP), Électropolymérisation du Polypyrrole, Détection électrochimique de l'Isoproturon, électrodes en Graphène électrochimique

Development of environmental sensors based on MIP/graphene electrode allowing the detection of pesticides in waters

Summary

In this PhD thesis, we developed modified glassy carbon electrodes by molecularly imprinted polypyrrole (MIP-PPy) film dedicated to the electrochemical analysis of a herbicide, isoproturon. The detection limits obtained under the laboratory conditions are in the range of the thresholds imposed for this micropollutant in the European Water Framework Directive. Finally, a method for the preparation of new electrodes made up of 100% electrochemical graphene has been developed. These graphene electrodes have been successfully modified by electropolymerization of MIP-PPy and the first results obtained for their application to the isoproturon analysis have given a great promise for their integration into environmental sensors.

Key words: Electrochemical sensors, Molecularly Imprinted Polymers (MIP), Electropolymerization of Polypyrrole, Electrochemical Detection of Isoproturon, Electrochemical Graphene Electrodes

ICMN - Interfaces, Confinement, Matériaux et Nanostructures
Address: 1 Rue de la Ferollerie, 45100 Orléans, France

Department of Chemistry, FMNS - University of Prishtina
Address: m9 Eqrem Çabej, Prishtinë 10000, Kosovo